STUDY ON CATION EXCHANGE OF A LEAD COORDINATION POLYMER TARGETING DYNAMIC MIXED CATION DOPED AND MIXED-VALENT COORDINATION POLYMERS

HAMISU ALIYU MOHAMMED

DEPARTMENT OF CHEMISTRY
FACULTY OF SCIENCE
UNIVERSITI MALAYA
KUALA LUMPUR

2020

STUDY ON CATION EXCHANGE OF A LEAD COORDINATION POLYMER TARGETING DYNAMIC MIXED CATION DOPED AND MIXED-VALENT COORDINATION POLYMERS

HAMISU ALIYU MOHAMMED

THESIS SUBMITTED IN FULFILMENT OF THE REQUIREMENTS FOR THE DEGREE DOCTOR OF PHILOSOPHY

DEPARTMENT OF CHEMISTRY
FACULTY OF SCIENCE
UNIVERSITI MALAYA
KUALA LUMPUR

2020

UNIVERSITI MALAYA

ORIGINAL LITERARY WORK DECLARATION

Name of Candidate: **HAMISU ALIYU MOHAMMED**

Matric No: **SCH150079**

Name of Degree: **DOCTOR OF PHILOSOPHY**

Title of Thesis ("this Work"):

STUDY ON CATION EXCHANGE OF A LEAD COORDINATION POLYMER TARGETING DYNAMIC MIXED CATION DOPED AND MIXED-VALENT COORDINATION POLYMERS

Field of Study:

MATERIAL CHEMISTRY

I do solemnly and sincerely declare that:

(1) I am the sole author/writer of this Work;
(2) This Work is original;
(3) Any use of any work in which copyright exists was done by way of fair dealing and for permitted purposes and any excerpt or extract from, or reference to or reproduction of any copyright work has been disclosed expressly and sufficiently and the title of the Work and its authorship have been acknowledged in this Work;
(4) I do not have any actual knowledge nor do I ought reasonably to know that the making of this work constitutes an infringement of any copyright work;
(5) I hereby assign all and every rights in the copyright to this Work to the University of Malaya ("UM"), who henceforth shall be owner of the copyright in this Work and that any reproduction or use in any form or by any means whatsoever is prohibited without the written consent of UM having been first had and obtained;
(6) I am fully aware that if in the course of making this Work I have infringed any copyright whether intentionally or otherwise, I may be subject to legal action or any other action as may be determined by UM.

Candidate's Signature Date: 23rd November, 2020

Subscribed and solemnly declared before,

Witness's Signature Date: 23rd November, 2020

Name:

Designation:

STUDY ON CATION EXCHANGE OF A LEAD COORDINATION POLYMER TARGETING DYNAMIC MIXED CATION DOPED AND MIXED-VALENT COORDINATION POLYMERS

ABSTRACT

Solid solution in Metal-Organic Coordination Polymers (MOCPs) is an emerging synthetic pathway for modifying chemical compositions and has been expansively investigated. It has been demonstrated to be an important tool for engineering novel functional materials that otherwise have not been synthesized via the conventional technique. Although stable solid material with variable functionalities and intriguing structural motifs could be engineered by judicious selection of multivariate metal centers and multifunctional ligands. However, solid solution featuring mixed valence in MOCP is rare. Motivated by the ability of Pb^{2+} to adopt range of coordination numbers (CN) and chemical environments (CE), in addition to its flexibility to readily undergo cation exchange owing to its low electronegativity, we opted for solid solution in Pb-based MOCP. Herein, we exploited a dynamic 3D, Pb-based MOCPs that contain 1D moiety featuring 3 distinctive Pb^{2+} sites each with different CN and CE that can potentially undergo cation exchange with exogenous divalent and aliovalent including mono- or trivalent cations. Under optimized condition, we achieved to our knowledge the first, hetero-valent, single and multiple valent substituted MOCP featuring cation vacancy. In addition to this, under the guidance of Pearson's Hard-Soft Acid-Base (HSAB) principle, we gained the control of the process and tune the % of cations exchange under appropriate conditions. A tunable photoluminescent (PL) emission exhibiting good antenna effect and retention of the original 3D MOCP was observed when doped with as little as 6 wt% of Eu^{3+}. Remarkably, the PL intensity of the Eu^{3+} substituted MOCP increases as the amount of Eu^{3+} increases even up to 80 wt. %, which is also a rather rare case and the first, to the best of our knowledge in MOCP solid solution. 10 wt. % Eu^{3+} substituted MOCP was

found to have a significant conductivity improvement at 25 ^{o}C. Fe^{2+} substituted MOCP was also found to have some magnetic hysteresis at room temperature, another very rare case of mononuclear or cluster Fe^{2+} doped to show some hysteresis at RT. The formation of solid solution and phase purity of these compounds were confirmed by single crystal and powder X-ray diffractions, SEM-EDX, ICP-OES as well as XPS.

Keywords: Solid solution; HSAB principle; Photoluminescence; Structural transformation; Conductivity.

LARUTAN PEPEJAL DALAM POLIMER KOORDINATAN LOGAM-ORGANIK (MOCP): MENYASARKAN MOCP DINAMIK UNTUK APLIKASI PENDOPAN PELBAGAI, VALEN BERCAMPUR DAN ANGKUTAN CAS

ABSTRAK

Larutan pepejal dalam Polimer Koordinatan Logam-Organik (MOCP) ialah satu tapak jalan sintesis yang sedang membangun untuk mengubah suai komposisi kimia dan telah dikaji secara meluas. Ia telah diperlihatkan sebagai satu alat yang penting untuk kejuruteraan bahan berfungsi baharu yang tidak boleh disintesis melalui kaedah konvensional. Namun, bahan pepejal stabil dengan pelbagai kumpulan berfungsi dan motif struktur yang menarik boleh direka melalui pemilihan pusat logam berbilang dan ligan pelbagai fungsi secara bijaksana. Walaubagaimanapun, larutan pepejal yang menampilkan valen bercampur dalam MOCP jarang berlaku. Sifat Pb^{2+} yang mampu untuk mengguna pakai berbagai-bagai nombor koordinatan (CN) dan persekitaran kimia (CE), serta sifatnya yang mudah untuk menjalani pemindahan kation akibat daripada kelektonegatifannya yang rendah telah menyebabkan kami tertarik untuk menggunakannya dalam larutan pepejal MOCP berasaskan Pb. Dalam tesis ini, kami telah melakukan pengkajian mendalam terhadap MOCP berasaskan Pb yang bersifat dinamik 3D, mengandungi bahagian 1D yang memaparkan 3 tapak Pb^{2+} tersendiri, mempunyai CN dan CE yang berbeza serta mampu menjalani proses pemindahan kation dengan eksogen monovalen dan aliovalen termasuk kation monovalen dan trivalen. Berdasarkan pengetahuan kami, bawah keadaan yang optimum, kami telah menghasilkan MOCP pertama yang digantikan dengan heterovalen, valen tunggal dan valen pelbagai yang memperlihatkan kekosongan tapak kation. Tambahan pula, berlandaskan prinsip Asid-Bes Keras-Lembut (HSAB) Pearson, kami memperoleh kawalan terhadap proses dan menyelaraskan % pemindahan kation bawah keadaan yang bersesuaian. Satu pembebasan fotoluminesen (PL) yang boleh diselaraskan mempunyai kesan antena yang

baik dan pengekalan luminesen daripada hos 3D asal telah diperhatikan walaupun didopkan dengan Eu^{3+} dalam kuantiti serendah 6%bt. Intensiti PL yang dibebaskan oleh MOCP yang ditukar ganti dengan Eu^{3+} menunjukkan peningkatan luar biasa apabila muatan Eu^{3+} ditingkatkan sehingga 80%bt., merupakan satu kes yang jarang berlaku dan berdasarkan pengetahuan kami, kes yang pertama berlaku dalam larutan pepejal MOCP. MOCP yang ditukar ganti dengan 10%bt. Eu^{3+} juga menunjukkan kekonduksian yang ketara pada suhu 25˚C. MOCP yang ditukar ganti dengan Fe^{2+} menunjukkan sifat histeresis magnet pada suhu bilik, satu kes yang sangat jarang berlaku untuk mononuklear atau kluster terdop Fe^{2+} untuk menujukkan sifat histeresis pada suhu bilik. Pembentukan larutan pepejal dan ketulenan fasa sebatian-sebatian disahkan melalui kaedah pembelauan sinar-X hablur tunggal dan serbuk, SEM-EDX, ICP-OES dan XPS.

Katakunci: Larutan pepejal; Prinsip HSAB; Fotoluminesen; Penjelmaan struktur; Kekonduksian

ACKNOWLEDGEMENTS

In the name of Allah, the Most Gracious and the Most Merciful. All praises be to Him for giving me the ability, strength and good health to carry out this research work and to witness the end of my Ph.D. journey.

I would like to thank and acknowledge my well-informed supervisors; Assistant Professor Dr. Arief C. Wibowo and Professor Dr. Azhar Bin Ariffin, for giving me all the indispensable opportunities, guidance and excellent supervision to train myself over the course of my Ph.D. period. Although the journey was rough and exciting, your uprightness and meticulousness has prepared me to be a better researcher, this is an invaluable asset to me, I thank you for this.

To my adorable wife (Salima Abubakar) and our kids (Rahma, Abdussalam and Safiyyah), I don't know how to thank you enough for your patience, encouragement, endurance, and trust in me throughout my Ph.D. journey, it wasn't easy for you guys, you have missed my companionship and attention most of the time throughout these years, may Allah reward you abundantly and continue to bless you and our home. To my brothers, especially Bashir Ali and Nuraddeen Ali for your constant encouragement and supporting my home affairs during my stay overseas, I really appreciate your kindness. Special thanks to Baba Ayye, you are more than just a brother but a father, thank you for all your fatherly advice and support, may Allah continue to give you good health.

To my labmates, especially Fendi Y. Wardana and Mesoun A. A. Al-Nubi, it has been really incredible to work with. To my mentors, Dr. Isah Baba Koki and Dr. Ibrahim Isah Fagge, for your encouragements and guidance at the beginning of the journey, thank you so much. I would also like to appreciate En. Fauzan and En. Shukri for wonderful job on PXRD and FESEM measurements.

Finally, my sincere appreciation to my friends, especially Lee Mei Koon, without you I wonder how my life in Malaysia would have been, I thank you for all the cares, generosity, support and kindness during the trying times of my life, you are always there reinforcing me and encouraging me to keep going. To my Nigerian friends, Mujitapha Ilyas, Abubakar Ibrahim, Mustapha Muhammad and many more.. You really deserve my acknowledgement for your companionship.

TABLE OF CONTENTS

LIST OF FIGURES

LIST OF TABLES

LIST OF SCHEMES

CHAPTER 1: INTRODUCTION

Conventional MOMs are important class of solids assembled from the supramolecular and coordination interactions of organic building blocks (such as neutral, anionic or cationic ligands) and metal moieties, such as metal ions or inorganic clusters. They are primarily built through coordination bonding, hydrogen bonding, π–π stacking or other electrostatic interactions. As a result, they have the potential to be assembled as modular and adjustable structures with tailorable compositions and properties. With multitude of organic and inorganic building blocks, it provides endless possible combinations to prepare MOMs. Intended properties can be easily engineered using the intrinsic properties of either metal moiety or the organic ligands or both. For instance, photophysical properties of metal ions such as lanthanides and their interaction with phonons and electrons endows them with excellent luminescence and magneto-optical properties suitable for use as functional materials in devices. (Binnemans, 2009; Carlos et al., 2011; Eliseeva & Bünzli, 2010) On the other hand, the intrinsic functionalities of the organic components such as organic chromophores, bioorganic molecules or radicals are very important components for synthesizing optical, (Binnemans, 2009) biocompatible (Ge et al., 2017; Grall et al., 2015) and magnetic (Shaozhou Li & Huo, 2015) MOMs. Novel properties may therefore arise from the synergistic interactions and association of the component building blocks. As such, they display very exciting and promising applications in gas storage/separation, solid state emissions, drug encapsulation and delivery, catalysis, medical diagnostics, sensing, ion exchange/separation, conductivity, magnetism and host of other potential applications. (Canivet et al., 2014; Czaja et al., 2009; Hiroyasu Furukawa et al., 2013; Shaozhou Li & Huo, 2015; H. Wang et al., 2017)

MOMs are generally classified into; discrete material (zero dimensional materials) which includes; metal-organic polygons, metal organic polyhedra or nanoballs, and

polymeric materials (coordination polymers), including 1 dimensional coordination polymers (CPs) that can form chains, ladders or tapes, or 2 dimensional CPs built into sheets, bilayers or 3 dimensional porous coordination polymers also known as metal organic frameworks (PCPs/MOFs) and non-porous 3D CPs, Figure 1.1.

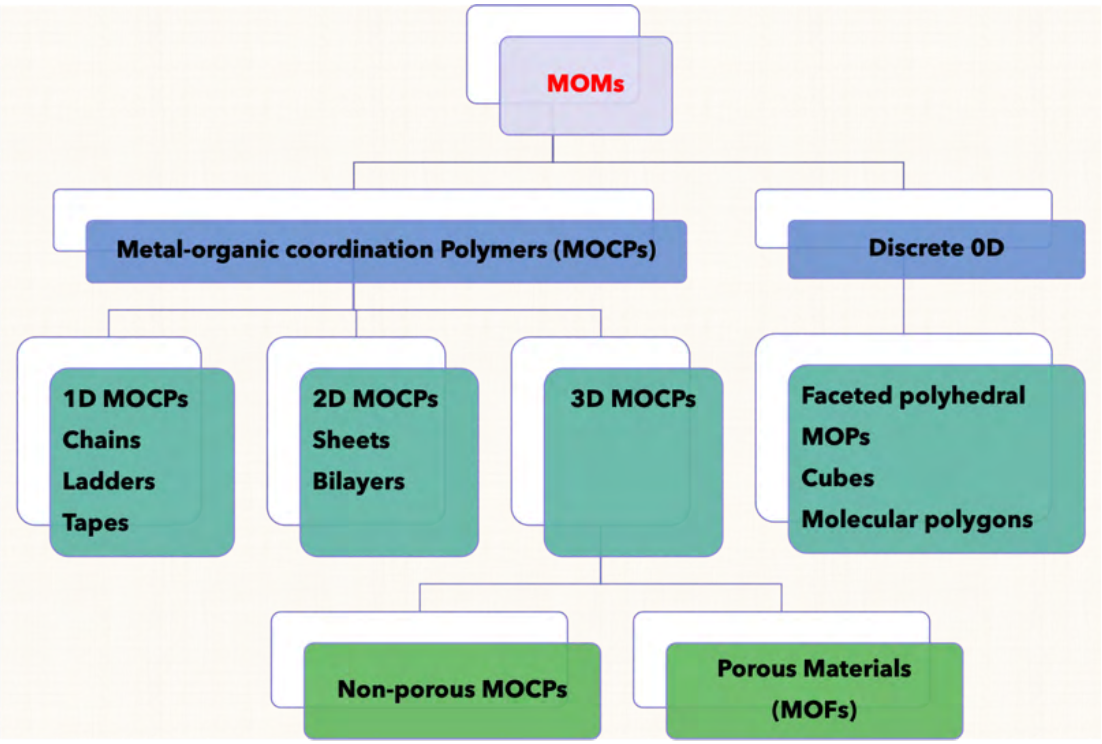

Figure 1.1: Classification of metal organic materials (MOMs) based on periodicity.

1.1 Metal-organic coordination polymers (MOCPs)

MOCPs are hybrid materials originating from interdisciplinary fields of chemistry namely; organic and inorganic (coordination) chemistry. These materials gained a lot of attention from the scientific world and industries in the last couple of decades and rapidly growing (Czaja et al., 2009; Perry et al., 2009; Zaworotko, 2007) owing to their intriguing properties and the potential applications.

According to IUPAC recommendations, (Stuart R. Batten et al.) MOCPs are materials constituted of macromolecules with an infinite recurring coordination units extended in one, two or three dimensions. They are generally crystalline solids build by self-assembly

of metallic cations with multi-dentate organic ligands. The metal center can be single metal ions or group of metal cations, otherwise known as secondary building units (SBUs), and these ions/clusters act as Lewis acids by accepting electron pairs from the Lewis bases' organic linkers. In the first generation of coordination polymers, transition metal cation moieties function as nodes that is linked by multifunctional organic ligands such as bipyridine and carboxylates acting as a spacer ligand in the structure. MOCPs are highly modular due to the nature of their building blocks and therefore it is used as a blueprints and prototypal for a variety of structures suitable for crystal engineering strategies. (Perry et al., 2009; Zaworotko, 2007) The coordinative association of the metal moieties and the organic ligands may extend in different periods, each with unique atomic arrangements. For instance, in 1D periodic extension, chains ladders, tapes, zigzag single and double chains, ribbon, twisted ribbon, knotted string, or box-pleated chains are formed. (Slabbert & Rademeyer, 2015) However, bilayers, square grid and sheets are formed for 2D extensions. While in the 3D extension, numerous architectures such as diamondoid or octahedral nets are formed, including those with potential void, the so-called "metal-organic frameworks (MOFs)". (Cohen, 2010; Hiroyasu Furukawa et al., 2013; Kalmutzki et al., 2018; Susumu Kitagawa, 2014)

Metal cation play a vital role in the crystal structure formation, with different metal having distinctive attributes such as geometrical and coordination number preference; for example pentagonal-bipyramidal, trigonal-bipyramidal, trigonal-prismatic, octahedral, square pyramidal, square-planar, tetrahedral, T-shaped, trigonal planar or linear geometry. Cation size and its sub-lattice ratios, charge matching, defect structuring, ligand-field stabilization energy and hardness/softness also defines the crystal structure formation (L. Soderholm & J. F. Mitchell, 2016; Robin & Fromm, 2006). Vast majority of the reported MOCP structures are however, composed of a primary building units (PBUs) as the metals center. PBUs are single ion metal centers connected by the organic

ligands to form the extended structure. Unlike PBUs, the secondary building units (SBUs) are discrete molecular clusters with simple geometrical shape such as squares, triangles, tetrahedra and octahedra metal containing units, further linked by multitopic linkers into polymeric structures. The use of SBUs to for building periodic structures is the so-called Reticular Chemistry (Helal et al., 2017; M. Li et al., 2014; O'Keeffe et al., 2008; O. M. Yaghi et al., 2003). Prominent MOFs such as MOF-5 is built of tetra nuclear cluster (Zn_4O-$(CO_2))_6$ SBUs with octahedral shape having six vertexes as a point of extension (carboxylate C-atoms) linked further by a ditopic 1,6-benzene dicarboxylate rod like linker assembled into a ***pcu*** net. While HKUST-1 is assembled into a ***tbo*** net by linking bimetallic paddlewheel cluster ($Cu_2(-CO_2)_4$) with a square geometry and tritopic linker (benzene tricarboxylate). (M. Li et al., 2014)

Combination of different metal moieties and large number of spacer ligands have been utilized to engineer several intriguing structures with fascinating properties. Design and synthesis of metal organic coordination polymer is receiving tremendous attention by scientist due to their modular nature, ease of preparation, diverse structural motifs, appealing properties and impending applications such as gas storage, gas separation, sensors, magnetism, catalysis, electrical conductivity and photoluminescence (Janiak, 2003; C. Wang et al., 2016; S. Yuan et al., 2018).

Various synthesis methods and strategies have been developed to engineer crystalline MOCP materials. However, in each case, the onset of crystallization is when the concentration of the substance in solvent is greater than its solubility product. This is because, crystals only grows from meta-stable supersaturated solutions due to kinetic hindrance of crystallization (Muller, 2009). To achieve the aforementioned supersaturation, several methods were used, summarized by Muller, Figure 1.2. (Muller, 2009) The simplest method is *slow evaporation*, also called saturation method, this

method involves dissolving the reactants in a suitable solvent and slowly evaporating the solvent through which the concentration of the reactants increases until the onset of crystallization. Another popular method is *slow cooling*, in which the solubility at elevated temperature is exploited. Generally, compounds tends to be more soluble in hot solvent than in cold solvents, hence compounds are dissolved to make an almost super-saturated solution in hot solvent and allowed to cool down yielding crystals at room temperature. Other ways to obtain crystalline materials is use of *binary solvents* method, the so-called liquid-liquid or solvent-liquid diffusion, where two immiscible liquids (solvent and precipitant) are utilized, in which the starting materials are soluble only in one of the solvents and other serve as precipitant. Similar to binary solvent method, *slow diffusion of reactants,* also involves dissolving the reactants in a separate solvents and a permeable/semipermeable barrier or solution layer is placed in between the solutions to slow down diffusion and subsequent precipitations. This technique is so far one of the best strategy to obtain quality crystals suitable for single crystal measurements (Muller, 2009; Robin & Fromm, 2006).

On the other hand, *hydro/solvothermal* technique is also one the most powerful and highly utilized approach, (X. J. Cui et al., 2009; Jensen et al., 2014; S. C. King et al., 2017; Y. C. Liang et al., 2002; McKinstry et al., 2016; F. X. Wei et al., 2016) where reactions are carried out at an elevated temperature and autogenous pressure. These conditions, highly favored the crystal growth of highly insoluble materials. This can be attributed to the increase in the solute solubility and decrease in solvent viscosity and hence, enhances the diffusion process and crystallization speed. Other strategies include; *sonochemical synthesis* (where reactions are carried out by application of high ultrasound radiation), *mechanochemical* (involving the use of mechanical grinding, no single crystal is obtain using this technique), *microwave* and *electrochemical* method (Askarinejad &

Morsali, 2009; Kumar et al., 2015; Masoomi et al., 2014; Masoomi et al., 2015; Safarifard & Morsali, 2012; Soltanzadeh & Morsali, 2010).

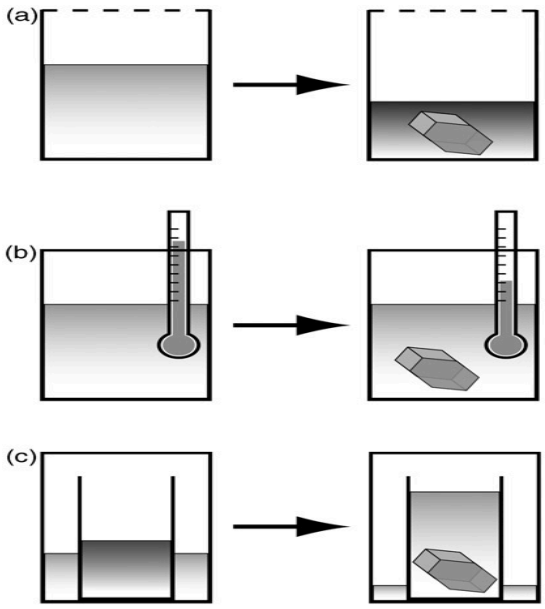

Figure 1.2: Graphical representations of some popular crystal growth methods. (a) slow evaporation technique, (b) slow cooling method and (c) gas-phase diffusion strategy. (Muller, 2009)

On a different note, compared to the *d* or *f*-block metals, *p*-block metals such as lead (Pb) are generally less explored despite their impressive potential applications such as in photovoltaic conversion, electroluminescence, organic light-emitting diodes (OLEDs) or fluorescent sensors (Tsuboi & Silfsten, 1991; J. Yang et al., 2007). Several materials of technological interest are observed to have an asymmetric electronic densities (Walsh & Watson, 2005) associated typically with the main group metals owing to the presence of nonbonding electron pair. In particular, large number of Pb^{2+} based MOCPs was reported and majority are amenable to structural transformation and other molecular adjustments. (Leila Aboutorabi & Ali Morsali, 2016; Akhbari & Morsali, 2013, 2015; Al-Nubi et al., 2019; Cimen et al., 2018) Pb^{2+} ion with its $6s^2$ nonbonding lone pair of electrons has an interesting stereochemistry, as it can associate with coordinated ligands in both symmetric and asymmetric passion. The steric activity of the $6s^2$ electrons cause the Pb^{2+} coordination environment to direct ligands either perfectly distributed in the coordination

sphere or distorted sideways with a visible empty space, in the so-called holo- or hemi-directed alignment respectively, Figure 4.1. The holodirected polyhedra has a symmetric distribution where the $6s^2$ nonbonding electron pair is said to be sterically inactive while the asymmetric distribution in the hemidirected arrangement has a sterically active lone pair. However, certain factors influences the steric activity of Pb^{2+} $6s^2$ lone pair of electrons; such as the coordination number (high, medium or low), ligands type (hard or soft), ligand-ligand interaction (repulsive or attractive), hybridization of 6s and 6p atomic orbitals (presence or absence of *p* character), the nature of donating ligands (high or low electron donation) (M. L. Hu et al., 2011). Therefore, being a borderline Lewis acid, metal cation and its large ionic radius, based on the HSAB concept it possessed a unique advantage to adopt different CE and variety of flexible CN (2 to 12). The chemistry of the CE and CN can afford Pb^{2+} complexes and the related compounds with numerous configurations which is of great scientific interest (Ding et al., 2008; M. L. Hu et al., 2011; J. Yang et al., 2007).

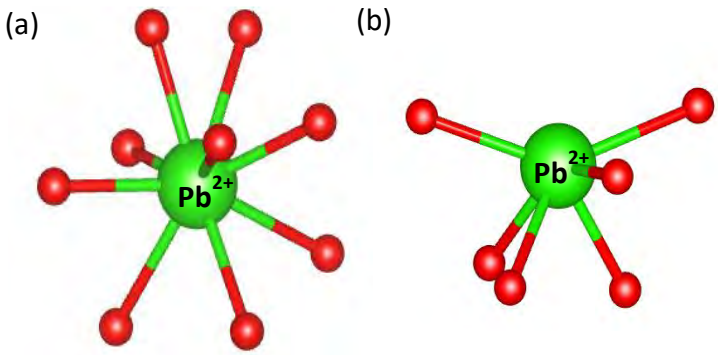

Figure 1.3: Effect of lone pair activity (a) Symmetric distribution (Holodirected) (b) Asymmetric distribution (Hemidirected)

On the other hand, Che et. al. (2009) reports that pyrazine-2,3-dicarboxylic acid (2,3-H_2pzdc) can be fully or partially deprotonated as a function of pH and it can adopt several coordination modes depending on the cation chemistry, (Fendi Y. Wardana et al., 2015; L.-R. Yang et al., 2011) Figure 4.2. H_2pzdc can be considered as both N-donor and O-

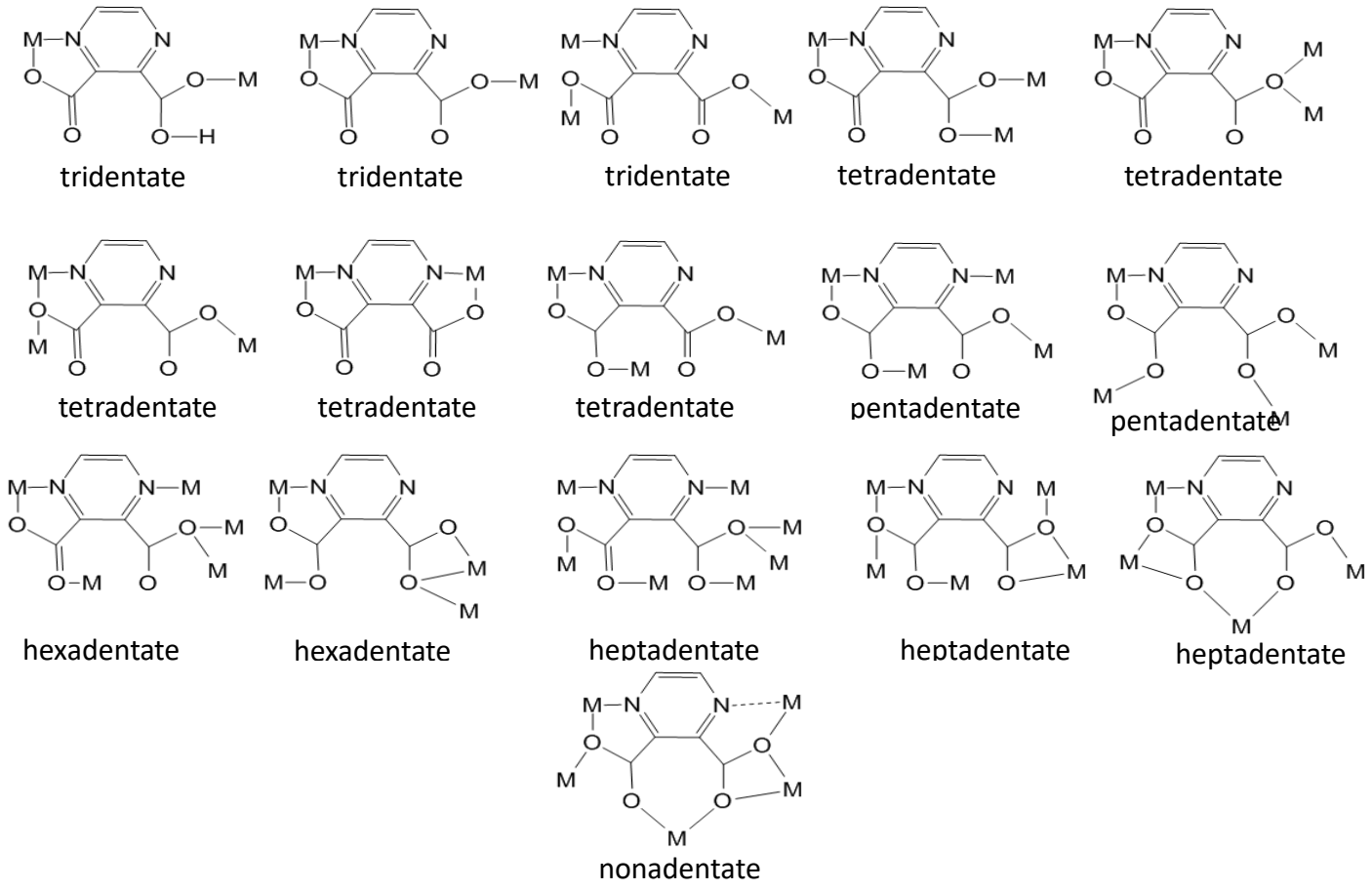

Figure 1.4: Typical coordination modes of 2,3-pyrazinedicaboxylic acid in MOCPs.

donor ligand making it more like borderline Lewis base combining both soft N-donor groups and hard O-donor groups that can bind well with hard, soft and borderline Lewis acids. We envisaged combining the flexibility of Pb^{2+} in terms of CN and CE, the fascinating coordination modes of 2,3-pzdc and the variable hard and soft donor groups, to synthesize dynamic extended network of MOCP that could pave a way to engineer material amenable to molecular adjustment and substitutional defects such as multiple doping and mixed valent incorporation.

1.2 Solid solution in MOCPs

The basis of which the material design and engineering was built is believe to be the ability to modify or tune the materials' molecular compositions or the atomic arrangements. Tunable physical or chemical functionalities in MOCPs, can be ascribed largely to its tailorable chemical composition, flexibility, modularity, high porosity or surface area. The tunable properties enables targeted functionalities to be designed for specific applications, such as tunable light emission, (Emam et al., 2018; X. Mi et al., 2019; C.-Y. Sun et al., 2013; X.-P. Zhang et al., 2013) luminescence sensors, (R. An et al., 2016; Kempahanumakkagari et al., 2018; X.-Y. Xu & Yan, 2015) energy, (H. L. Wang et al., 2017) decontamination of pollutants via adsorption interactions. (Abdelhameed et al., 2016; Abdelhameed, el-deib, et al., 2018; Abdelhameed & Emam, 2019; Abdelhameed et al., 2017; Abdelhameed, Rehan, et al., 2018; Emam et al., 2019) In addition to this, presence of defects either intrinsic or extrinsic in MOCPs and systematically understanding their nature yields impressive benefits in controlling and manipulating materials properties. (Cheetham et al., 2016; Z. Fang et al., 2015; W. Liang et al., 2016; Shearer et al., 2016; Taylor et al., 2015; Trickett et al., 2015) For example, Richard P. Feynman, (1960) once envisaged in his classic talk 'There is plenty of room at the bottom' in 1959; *"....What would the properties of materials be if we could really arrange the atoms the way we want them? ... I can hardly doubt that when we have some*

control of the arrangement of things on a small scale we will get an enormously greater range of possible properties that substances can have, and of different things that we can do".

Going down to the atomic level and gaining control over the composition and the spatial arrangements of atoms has always been projected to yield materials of unprecedented properties and functionalities. (Barth et al., 2010; Ci et al., 2010; Peng & Yang, 2009; Van Aert et al., 2011) This is because, properties and functionalities are strongly related to the atomic arrangements and the molecular compositions that make up the material. (A. Y. Liu & Cohen, 1990; Siegel, 1994; Suyetin et al., 2020; T. Xu et al., 2019) Typically, crystal structures and the chemical compositions are the two fundamental attributes that define MOCPs. The chemical composition comprises the elements that made up the MOCPs and their relative compositions. While the crystal structure, is the arrangements of constituent atoms or ions in 1, 2 or 3 dimensional space.

Inspired by the complexity of nature generally, and in particular biological systems such as DNA, RNA or enzymes, much time and resources has been devoted by chemist, scientist and engineers to develop strategies for the synthesis of materials with predesigned compositions and controllable building block arrangements and dispositions that can mimic biological systems in terms of complexities, defects and functionalities for the desired applications. (J. Brown, 2011; J. W. Brown et al., 2015; Cadman et al., 2016; H. X. Deng & Yaghi, 2011; Dong et al., 2017; Fischer, 2013; Helal et al., 2017; Kim, 2014; S. Li et al., 2017; Q. Liu et al., 2016; Xia et al., 2017; O. M. Yaghi, 2014; S. Yuan et al., 2015; Y. B. Zhang et al., 2015) These properties can be judiciously introduced through solid solution approach using multiple and multivariate building blocks in the same MOCP crystal structure.

Complex materials especially those comprising more than one type of cation or ligand (multivariate) in the structure offered improved properties and exceptional applications. For instance, extensive use of mixed metal oxides and salt composite as anode in batteries (Goodenough & Park, 2013); pnictides and oxides of multinary metal family composed of combination of several cations has been shown to possessed superconductivity (Farrell et al., 1987; Z. W. Jin et al., 2001; C. Z. Yuan et al., 2014); heterogeneous materials are often used in optical devises due to the charge transfer between different proximal cations; and magneto-resistant materials (diluted magnet) are engineered by doping paramagnetic transition metals into framework of titanium or zinc oxide (de la Cruz et al., 2008; Lin et al., 2013); solid solution in metal oxides also demonstrate a promising catalytic activity in important chemical conversions (Donkova et al., 2010).

Defect engineering, through judicious control of structural defects and any related heterogeneity, is of unparalleled importance in solid state electronic materials, such as silicon, Group III/V semiconductor and its derivatives. (Capper, 2005; Singh, 2003) Application of such concept in metal-organic frameworks (MOFs) or MOCP in general, (Aguirre-Diaz et al., 2015; Chaemchuem et al., 2016; Chuan Tan & Chun Zeng, 2016; Z. Fang et al., 2014; H. Furukawa et al., 2015; Horike et al., 2013; S. Kitagawa et al., 2004; O. Kozachuk et al., 2014; Olesia Kozachuk et al., 2013; W. Liang et al., 2016; Y. Liu et al., 2016; Ramaswamy et al., 2014; Shearer et al., 2016; L. Sun et al., 2016; Taylor et al., 2015; Trickett et al., 2015; H. C. Zhou & Kitagawa, 2014) would realize MOCP material with tunable properties. (Z. Fang et al., 2015; Hendon et al., 2012) Despite being an exciting concept to manipulate the structure and the resulting electronic properties, defect engineering by design in MOCP remains elusive. (Gul-E-Noor et al., 2012; Jiao et al., 2015; O. Kozachuk et al., 2012; Nikas et al., 2015; Parkes et al., 2015; B. Tu et al., 2014; Vuong et al., 2013; W. Zhang et al., 2016) In fact, based on recent reviews, it is reported that there is no well-documented report on MOCP with fully characterized cation vacancy

due to partial replacement of cationic host by aliovalent cationic guest. (Cheetham et al., 2016; Z. Fang et al., 2015; H. Furukawa et al., 2015) It will be very exciting if the dynamics of MOCP in terms modularity, tunability and flexibility can be combined with the concept of defect engineering. Such synergy between the two processes may allow a plethora of functional materials to be engineered that may not be obtainable using each process separately.

On the other hand, compounds that contain main group element with lone pair are reported to be tolerant to defects, (Brandt et al., 2017; Fabini et al., 2016; Laurita et al., 2017) and can also be easily ion exchanged. Amongst the frequently used cations for ion exchange in MOCP, Pb^{2+} possesses lowest electronegativity that gives labile ionic bonds, which in turn allowing it to be exchanged faster. (Brozek & Dinca, 2014) In addition, Pb^{2+} is one of the cations that are in borderline of Hard-Soft-Acid-Base (HSAB) concept, (Briand & Burford, 2000; Ralph G. Pearson, 1963a) hence can adopt a variety of CE, (K. P. Rao et al., 2007; A. Thirumurugan et al., 2008) in addition to having flexible CN (2-10) due to its large size. (Fan & Zhu, 2007; J. Yang et al., 2007; J. Yang et al., 2009; Y. H. Zhao et al., 2008) Such features prompt us to explore a dynamic 1D Pb MOCP system that can undergoes structural transformation into 3D MOCP with more than one distinctive Pb^{2+} crystallographic sites each with different CN and CE which can undergo aliovalent cationic substitution to realize mixed valent, hence cation vacancy creation, and multiple doping. (Fendi Y. Wardana et al., 2015) Under the guidance of the principle of HSAB, we envisage to device a method to tune the cation exchange with mono, di or trivalent cations including multiple and mixed valent exchange, which may paves a way towards defect engineering by design.

1.3 Research Question

What would happen if heterogeneity, defects and/or complexity (in terms of multiple doping, mixed valent or cation vacancy) are introduced within ordered MOCP structures in a designed fashion? What new property could be imparted onto the material and what added benefits can we harness upon introduction of such heterogeneity? Can integrity of the structure and the crystallinity be maintained after such introduction? Can we tune properties in a designed fashion as a function of introduced complexities? Herein, we make use of dynamic MOCP built from flexible building blocks that can undergo structural transformation, to higher dimension forming more than one metal ion crystallographic sites each with unique CE and CN. Using the proposed system, we envisioned to judiciously engineer facile solid solution through concurrent structural transformation and cation exchange via dissolution recrystallization process.

1.4 The Hypothesis

To approach these questions, the following hypothesis has been proposed to be tested; multiple doping and mixed valent could be engineered judiciously through concurrent structural transformation and cation exchange via dissolution recrystallization process. The suitable MOCP must be dynamic and built from flexible building blocks, and upon transformation, the MOCP must have more than crystallographic sites each with unique chemical environment (CE) and coordination number (CN) suitable for facile solid solution.

1.5 Aims of the Study

To judiciously design a new synthetic approach for multiple doping and mixed valent using a dynamic and robust MOCP, through structural transformation and simultaneous cation exchange via dissolution recrystallization technique.

1.6 Objectives of the Study

1.6.1 Part one

a. To synthesize or adopt a dynamic and robust 1D coordination polymer featuring structural properties amenable to structural transformation and made of flexible cation that can adopt different CE and CN.
b. To carefully transform the 1D coordination polymer into a 3D featuring crystallographically unique sites, each with distinctive CN and CE that can permit potential insertion of an exogenous cation of different sizes, valency, and properties.
c. To characterize the resulting 1D and subsequently the 3D MOCP.

1.6.2 Part two

a. To prudently conduct solid solution strategy to insert and incorporate different exogenous cations of different sizes and chemistry from *s, p, d* and *f*-block of the periodic table.
b. To carry out a facile but judicious mixed valent and multiple doping (including *3d-4f* mixed orbital strategy)
c. To characterize the resultant doped material in terms of their structures and their photo-physical properties and charge transport application.

1.6.3 Part three

a. To strategically tune properties as function of the percentage dopants, under the guidance of HSAB principle. Focusing especially on tunable color emissions and magnetism and/or conductivity.
b. To measure photo-physical, magnetic and/or conductivity properties.

CHAPTER 2: LITERATURE REVIEW

The foundation upon which research is built depends on how critically literature was reviewed and evaluated, for it helps provides proper understanding of the previously related works, the emerging trends therein and identification of possible research gap in terms of synthesis method, applications, or characterization technique of interest that requires some further understanding, development or other contributions. Herein, the extent to which the previously related literature work goes in trying to answer the research questions in this thesis would be evaluated, discussed and analyzed and subsequently the whole research project would focus on bridging some of the identified shortfalls in the reported literature, or at least partially.

2.1 Metal-Organic Coordination Polymers (MOCPs)

The emergence of a new class of organic-inorganic hybrid material popularly referred to as coordination polymers encompassing both the non-porous (1, 2 or 3D coordination polymers (CPs)) and porous CPs otherwise known as Metal Organic Frameworks (MOFs) or Porous Coordination Polymers (PCPs) some decades ago (Hoskins & Robson, 1990; S. Kitagawa et al., 1992; O. M. Yaghi et al., 1995), has continued to gain tremendous prominence in chemistry, material science, medical and engineering fields (Dang et al., 2017; Isaeva & Kustov, 2010; H. L. Wang et al., 2017; H. B. Zhang et al., 2017). MOCPs are generally designed through self-assembly of inorganic cations and organic ligands via coordination bonds under appropriate conditions (X. J. Cui et al., 2009; Guillerm et al., 2014; Jensen et al., 2014; Kirchon et al., 2018; McKinstry et al., 2016; Muller, 2009; J. Park et al., 2014; Robin & Fromm, 2006). The metal center can be single metal ions or group of metal cations, otherwise known as secondary building units (SBUs); these ions/clusters act as Lewis acids by accepting electron pairs from the Lewis bases' organic linkers. Several factors contribute to the final framework design; such as ligand geometry

and functionality, number of open metal sites on the SBUs, binding affinity, moiety symmetry and the strength of the coordination bonds between the building blocks. The inherent high porosity and surface area (Eddaoudi et al., 2002), structural modularity (Dolgopolova et al., 2017), flexibility (Mon et al., 2018; Schneemann et al., 2014; Wieme et al., 2018), and tailored compositions in some MOCPs endowed them with exceptional potentials for chemical manipulations geared toward functionalization for specific applications (Demuynck et al., 2018; Guillerm et al., 2014; W. Lu et al., 2014; Mon et al., 2018; Ogiwara et al., 2019; Rogacka et al., 2019; L. J. Wang et al., 2014; Wieme et al., 2018; H. B. Zhang et al., 2017).

Unlike other rigid porous materials such as active carbons, aluminophosphates, mesoporous silica or aluminosilicate (zeolites), the modular nature of the molecular building units in MOCPs especially MOFs, is the key attribute that endow them with the ability to undergo complete or partial exchange of any of the structural components; including cations, anions, ligands, coordinated or uncoordinated solvents and guest ions/molecules (Brozek & Dinca, 2014; X. J. Cui et al., 2009; Dinca & Long, 2007; W. Lu et al., 2014; Lisa J. Wang et al., 2014; S. Yuan et al., 2015). The exchange may proceed in a single crystal-to-single crystal (SC-SC), crystal-to-crystal or crystal-to-amorphous or crystal-to-less crystalline (J. Liu et al., 2012; M. Liu et al., 2015; J. J. Zhang et al., 2008; X. F. Zhang et al., 2018). The lability of the coordinative bonds and the flexibilities of the MOFs frameworks structure account mostly for the required defect tolerance for the substitution of virtually all the building blocks and the potential introduction of the required properties and functionalities after the assembly through the so-called post-synthetic modifications (PSM). Certain functionalities can be engineered via one-pot synthesis, well-known as Reticular Chemistry, before the assembly process of the framework by judiciously selecting the appropriate building blocks possessing the required functionalities, structural and geometrical properties that define the underlying

framework, otherwise known as molecular building blocks (MBBs) (Guillerm et al., 2014; O'Keeffe et al., 2008; O. M. Yaghi et al., 2003).

Solid solution especially cation exchange, has been expansively investigated and has been shown to be an emerging synthetic pathway for modifying the chemical composition of MOCPs. It also has already been proven to be an important tool for engineering novel functional materials that otherwise have not been synthesized via the conventional technique. (Brozek & Dinca, 2014; M. Kim et al., 2012). It is a synthetic procedure in which an exogenous cation substitutes a specific cation into the predefined environments at the SBUs of the host. This technique provides typically milder means of getting materials especially when the conventional design fails (M. Kim et al., 2012). Although the metal centers are an integral part of the MOCP framework, the cations can be exchanged entirely or partially as a function of time with a small or no effect on structural integrity. New materials have been designed using cation exchange, making it a potentially powerful tool for modifying SBUs of MOCPs.

Complexities as a result of structural heterogeneity in MOCPs allow tunable functionalities to be tailored, making them suitable for far-reaching applications, such as gas storage. For example, when pyrimidine group was introduced into NOTT-101, a new MOF (UTSA-76) was found to have the most efficient methane storage capacity of 257 cm^3 (STP) cm^{-3} at 65 bar and 298K (B. Li et al., 2014). Introducing exogenous cation with open metal sites and open-shell electronic structure dramatically increases the gas uptake by efficiently improving the host-guest interactions (Y. Kim et al., 2012; Xiaokai Song, Seok Jeong, et al., 2012; Sumida et al., 2013; C.-Y. Sun et al., 2013; X.-J. Wang et al., 2012). Mixed metals $Zn_3(BDC)_3[Cu(Salpycy)]9.(G)_x$ and $Zn_3(CDC)_3[Cu(Salpycy)].(G)_x$ have shown a very remarkable and efficient selective separation of C_2H_2/C_2H_4 (Xiang et al., 2011). Mixed-metal MOFs have also displayed

remarkable enantioselective separations of alcohols. (Das et al., 2012; Xiang et al., 2011) Mixed-lanthanides MOFs on the other hand, have also been efficiently used as ratiometric luminescent thermometers. (X. Rao et al., 2012; X. Rao et al., 2013) $Eu_{0.0069}Tb_{0.9931}$-DMBDC, (Y. Cui, H. Xu, et al., 2012; Das et al., 2012; Xiang et al., 2011) have also great potential as a heterogenous catalyst (Horcajada et al., 2012; Kreno et al., 2012; J.-R. Li et al., 2012; Suh et al., 2012; Sumida et al., 2012; Yoon et al., 2012).

2.2 Solid solution in MOCPs and the concept of Hard-Soft Acid-Base (HSAB)

The last few decades have recorded an increasingly remarkable development on MOCPs, witnessed by a plethora of new structures and molecular modification of the previously reported structures, enriching the scope of research and applications of MOCPs especially MOFs. One of the success stories in MOPCs is their ability to undergo solid solution, especially via the postsynthetic cation or ligand exchange as a targeted approach to engineer functionalities into a preformed MOCP under mild conditions with or without altering the structural integrity of the framework. Isomorphous cation exchange should be feasible in the MOCP's SBUs, since MOCPs can be considered basically as the conjugate base of a weak acid. (Tranchemontagne et al., 2009) The extent to which solid solution can be used as a synthetic tool depends on the appropriate understanding of governing factors that influence the process especially the chemistry of the metal ions and organic linkers in terms of their hardness or softness, how they interact and in what way it affects their stabilities.

Some decades ago, Pearson (1963b) through his HSAB principle, put forward a unifying concept by which chemical dynamics, stabilities, reactivities, and selectivities may be readily assessed and rationalized. This generalized principle has been and continues to be a very useful approach to guide the design of stable MOCPs, (S. Yuan et al., 2018) rationalize large diversity of experimental results in multifarious fields of

chemistry. (Ahrland et al., 1958; Paul W Ayers & Cárdenas, 2013; Breugst & Mayr, 2010; Chemaly et al., 2011; M. Kim et al., 2012; Yazaki et al., 2010) As a guide, HSAB is often used to predict the effect of chemical reactivities (Akiba & Inamoto, 1975; Alfarra et al., 2004; Ho, 1975; Woodward, 2002) including cation exchange. Although the concept of HSAB does not explain chemical facts, it correlates most of them efficiently. In the HSAB principle, soft bases prefer and bind well with soft acids and hard bases prefer and bind well with hard acids (P. W. Ayers et al., 2006; R. G. Pearson, 1980, 1986a, 1986b, 1987, 1990). Hence, the metal-ligand (M–L) strength and stability of any compound partly depend on the softness or hardness of the components' Lewis acids and bases. However, chemical hardness or softness is not the only contributor to the strength of acid-base interaction, other factors such as steric effects, intrinsic strength, ion-pairing, medium effects, thermodynamic or kinetic control, may also play an important role.

The notion of which the principle of HSAB was built upon is fundamentally a concise interpretation and restatement of the available experimental observations, in which Lewis acids and bases are categorized into soft and hard, on the basis of their size, polarizability, electronegativity, ionization potentials, and orbital energy. The principle states that; there is a preference for hard acids to bind with hard bases and soft bases with soft acids. (Ralph G. Pearson, 1963b) The preference, however only provide additional stability in terms of bond dissociation energy amongst hard-hard or soft-soft pairs and destabilization between mismatched pairs. The extra energy of the interaction preferences being as much as 130 kcal mol^{-1} for simple anionic bases (Reed, 2012). This, however, indicates the presence of other factors that are equally important, including the solvation effect or the intrinsic strength of acids and bases. (Ralph G. Pearson, 1995)

Generally, cations are categorized as Lewis acids and anions as Lewis bases; Table 2.1 and Table 2.2 contains some example of categorization of Lewis acids and bases

respectively. In principle, typical MOCP is an example of Lewis acid-base adduct, considering its two major building blocks are the metal center (Lewis acid/electron-acceptor) and ligands/linkers (Lewis base/electron-donor). With the proper understanding of the trends in Lewis acids and bases in the order of decreasing or increasing their strength, it is possible to predict with certain confidence the solid solution possibilities in MOFs and the stability of the modified MOCP products, in the aftermath of the solid solution process.

Table 2.1: Categorization of Lewis acids (metal cations) based on the HSAB principle

Hard	Borderline	Soft
H^+, Li^+, Na^+, K^+ Rb^+, Cs^+ Be^{2+}, Mg^{2+}, Ca^{2+}, Sr^{2+}, Al^{3+}, Sc^{3+}, Ga^{3+}, In^{3+}, La^{3+} Gd^{3+}, Lu^{3+}, Y^{3+}, Ti^{3+}, V^{3+}, Cr^{3+}, Fe^{3+}, As^{3+}, Sn^{3+}, Co^{3+}, Ni^{3+}, Mo^{3+}, Ru^{3+}, Tb^{3+}, Eu^{3+}, Sm^{3+}, Si^{4+}, Ti^{4+}, Zr^{4+}, Th^{4+}, U^{4+}, Pu^{4+}, Ce^{3+}, Hf^{4+}, WO^{4+}, UO_2^{2+}	Cu^{2+},Fe^{2+}, Co^{2+}, Ni^{2+}, Zn^{2+}, Pb^{2+}, Sn^{2+}, Sb^{3+}, Bi^{3+}, Rh^{3+}, Ir^{3+}, Ru^{2+}, Os^{2+}, Mn^{2+}, Fe^{2+}, Sc^{2+}, Ti^{2+}, V^{2+}, Cr^{2+}, Ge^{2+}, Y^{2+}, Zr^{2+}, Nb^{2+}, Mo^{2+}, W^{2+}, Mn^{3+}	Cu^+, Ag^+, Au^+, Tl^+, Hg^+ Pd^{2+}, Cd^{2+}, Pt^{2+}, Hg^{2+}, Co^+, Pt^{4+}, Te^{4+}, Rh^+, Ir^+, Rh^{2+}, Pd^{2+}, Cd^{2+}, Ag^{2+}, Hf^{2+}, Tl^{3+}, $Tl(CH_3)_3$, BH_3, $Ga(CH_3)_3$ $GaCl_3$, GaI_3, $InCl_3$ Metal atoms (M^0) Bulk metals

Table 2.2: Categorization of some selected Lewis bases (ligands) based on the HSAB principle

Hard	Borderline	Soft
BDC, BDC-Br, BDC-NH_2, DOBDC, TMBDC, 1,3-BDC, BTC, NDC, BTB, [1,1':3',1''-terphenyl]-4,4'',5'-tricarboxylate, 1,3,5-tris(3,5-dicarboxylphenylethynyl)-benzene, N_3-BTB, TATB, BPT, HETT, TCPP, BPBTTBA, DCPP,TMBDI, TMQPTC, Me_3-MPBA, BDCPPI, $FcphSO_3$, py-PTP, OX, succinate, MTBC, BTBA, BPTA, 1,3-ADC	Aniline, pyridine, 3,4-PYDC, bIM, PZDC, DCBPY, nIM, methionine, ICA, histidine, FTZB, BTDC, AB, BPPCOO, L_{16}	DABCO, 4,4'-BPY, BBTA, BTDD, 4-ABPT, MIM, DCIM, (R, R)-N,N'-bis(3-tert-butyl-5-(4-pyridyl)salicylidene)-1,2-diphenyldiamine nickel (II), BTT, BTX, 4-(2-pyrazinyl)-1,2,3-triazole, BPBA, F-BPBA, BTP, benzene-1,3,5-triyltriisonicotinate. BPEE, BPE, Adenine, HMTA

Table 2.2, continued.

BTP = 1,3,5-tris(1*H*-pyrazol-4-yl)benzene, bIM = benzimidazolate, DCBPY = 2,2'-bipyridine-5,5'-dicarboxylate, BPEE = 1,2-bipyridylethene, BPE = *trans*-bis(4-pyridyl)ethylene, nIM = 2-nitroimidazolate, ICA = imidazolate-2-carboxyaldehyde, FTZB = 2-fluoro-4-(tetrazol-5-yl)benzoate, BTDC = 2,2'-(bithiphene-ethynyl)benzoate, AB = 4-aminobenzoate, HMTA = hexamethyleneteramine, OX = oxalate, py-PTP = 4,4',4'',4'''-((pyrene-1,3,6,8-tetryltetrakis(benzene-4,1-dilyl)tetrakis(ethyne-2,1-dily)tetrabenzoate, MTBC = 4,4',4'',4'''-methanetetrayl-tetrabiphenyl-benzoate, BTBA = 4,4',4'',4'''-(biphenyl-3,3',5,5'-tetrakis(ethyne2,1-diyl)tetrabenzoate, BPTA = biphenyl-3,3',5,5'-tetracarboxylate, 1,3-ADC = adamantanedicarbozylate, L_{16} = 2-[4-[[4-methyl-6-(1-methylbenzimidazol-2-yl)-2-propylbenzimidazol-1-yl]methyl]phenyl]benzoic acid.

Generally, chemical reactivities are fundamentally adjustment of valence electrons between the reactant orbitals in terms of highest occupied molecular orbital (HOMO) and LUMO based on the frontier orbital theory (FOT) proposed by Fukui. (Fukui, 1970) Since the operational definition of soft species generally are large in size with low charge whereas hard species are small species with high charge, it is expected for soft–soft reaction to be predominated by the covalent bond character while ionic bond character predominates the hard–hard interaction. (Klopman, 1974; Kostyk & Whitehead, 1991) Hence, in the soft–soft interaction, the two soft species will mainly interact through frontier orbitals because the nuclear charge is effectively screened by the core electrons. However, in the case of hard–hard interaction, the core electrons are not screened. Soft–soft interaction are follow "through-bond" interactions (frontier orbital-controlled) while that of hard–hard interactions are follow "through space" interactions (charge-controlled). (Klopman, 1974) While it is possible for all MOCPs to undergo some molecular adjustments, it is obvious those made of matched pairs (soft-soft or hard-hard interaction) would be more difficult to modification than those of mismatched pairs (soft-hard, borderline-hard or hard-soft). This can be attributed to the strength of the M–L bonds, with matched pairs having strong bond with high dissociation energy, while the mismatched pairs having a labile bonds with low dissociation energy and readily modifiable.

On the other hand, MOCPs are fundamentally composed of repeating coordination entities forming the framework in some cases with potential voids (such as in MOFs) (Stuart R. Batten et al., 2013). The metal ions and the organic linkers are the two major building blocks that coordinatively form the framework. The stability or lability in MOCPs can be affected by several factors including; the chemistry of the metal ions and the organic linkers which defined the strength of the M–L bonds, the coordination geometry, pore surface properties or the operating condition (Burtch et al., 2014; Canivet et al., 2014; C. Wang et al., 2016). However, the strength of the coordination bonds that support the structural framework between the metal ions and the organic linkers is believed to be the most important factor for the stability or lability of MOCP under different conditions (Howarth et al., 2016). Based on the quantum mechanical calculations on MOF clusters, the labile Zn–O bond strength in MOF-5 is 365 kJ mol^{-1} while that of relatively stable Al–O in MIL-53 is approximately 520 kJ mol^{-1} (Low et al., 2009). Such differences in M–L bond strength between different metal ions and the organic ligands can be rationally explained using the HSAB concept and can be applied to efficiently predict the stability or lability of MOCPs, and its ability to undergo solid solution.

Generally, high valent cations such as Zr^{4+}, Ti^{4+}, Cr^{3+}, Fe^{3+} or Al^{3+} are regarded as hard acids, Table 2.1, that can form stable MOCPs featuring strong M–L bonds with hard Lewis bases such as carboxylate (e.g. terephthalic acid or BDC; trimesic acid or BTC) or phosphonates such as (*S* or *R*)-3,3'-di-*tert*-butyl-5,5'-dicarboxyphenyl-6,6'-dimethylbiphenyl-2,2'-dihydrogen phosphonate Table 2.2. Example of these kinds of MOCPs was first prepared by Férey and coworkers, in the well-known MIL-series using Al^{3+}, Cr^{3+} or Fe^{3+} (Gerard Férey et al., 2005; Gérard Férey et al., 2004; Serre et al., 2002; Vaesen et al., 2013). Zr-based MOCPs, constructed from a hard Zr^{4+} and hard carboxylate

linker also exhibited very outstanding stability in aqueous and acidic conditions (Cavka et al., 2008).

Zeolitic Imidazolate Frameworks (ZIFs) are the typical example of MOCPs with soft-soft interaction, having very strong metal-ligand bonds between borderline divalent TM such as Co^{2+}, Cu^{2+}, Zn^{2+}, or Ni^{2+} Table 2.1 and soft N-donor ligands such as azolates Table 2.2. (B. L. Chen et al., 2014; S. Yuan et al., 2018) A family of 12 ZIFs was first introduced by Yaghi and coworkers in 2006, (K. S. Park et al., 2006) with outstanding thermal and chemical stabilities especially ZIF-8. Its exceptional hydrothermal stability at 350 ^{o}C in 50% steam and ligand displacement activation energy of 58.5 KJ mol^{-1} is higher than those of other archetypal MOFs. (Low et al., 2009) In fact it is expected for MOCPs constructed using soft-soft Lewis acid-base, to have an increased stability largely due to greater charge transfer between soft acids and soft bases and increased correlation energy in the framework (Ralph G. Pearson, 1995).

Early MOCPs, however, are constructed mostly from the borderline first-row divalent transition metals such as Cu^{2+}, Co^{2+}, Ni^{2+}, Cd^{2+} or Zn^{2+} and hard carboxylate linkers, (Chui et al., 1999; Sunirban Das et al., 2009; S. Huang et al., 2010; Yonghwi Kim et al., 2012; H. Li et al., 1999; Xiaokai Song, Tae Kyung Kim, et al., 2012) although some of them have demonstrated an exceptional porosity and very promising applications, yet, their instability in harsh or even mild conditions limits their potential applications. A notable example, includes MOF-5 or HKUST-1, which tend to degrade on exposure to moisture in the air or flue gas (Al-Janabi et al., 2015; H. Li et al., 1999; Schoenecker et al., 2012). This instability can be attributed to the lability of M–O bonds that can be qualitatively rationalized based on the HSAB principle. The borderline Lewis acid, Zn^{2+} and hard Lewis base, BDC in MOF-5 or borderline Lewis acid, Cu^{2+} and hard Lewis base, BTC in HKUST-1 form labile coordination bonds due to a mismatch between borderline

Zn^{2+} or Cu^{2+} and hard oxygen-anion terminated BDC or BTC. These weak M–O coordination bonds render them unfit for certain industrial applications. (Morris & Brammer, 2017) Hydrolytic and thermal stabilities are paramount to industrial applications such as water desalination, ion exchange, gas separation, proton conduction or biomedical applications and a large number of heterogenous catalytic processes carried out at a varying temperature, pH or in the presence of water vapor. (J. Y. Lee et al., 2009; J.-R. Li et al., 2009; X. Liu et al., 2015; Sumida et al., 2011; X. Zhao et al., 2013)

2.2.1 Solvents and the solvation effects on cation exchange

Cation exchange in MOCPs typically involves the substitution of endogenous cations in the framework with exogenous cations from the proximate solution. The summary of all the reviewed MOCPs that undergoes cation exchange is provided in Table 2.3. The process normally involves the exchange of solvents and ligands between endogenous and exogenous cations. Evidently, based on reported investigations, solvents take part actively during cation exchange process and as such when investigating cation exchange process, it cannot be treated as a homogenous dielectric continuum (Brozek et al., 2014b). The equilibrium of cation exchange is strongly influenced by the solvent type and the identity of both the incoming and outgoing cations and the ligand or linker type. Generally, there is no universal condition through which cation can be exchanged, it is very specific to different MOCP chemistry, type of solvent used and the identity of the cations and ligands. For an exchange to proceed however, the bond dissociation energy between the solvent and the incoming cation must be lower than that of the outgoing cation and solvents. Meaning, the solvated exogenous cation must be able to easily get desolvated and interact more with the linker in the framework, while the interactions between the endogenous cations and the solvent must be more favorable. With this, once the cation is exchanged, the outgoing cation will be readily solvated with high bond dissociation energy, making the exchange reaction more thermodynamically feasible. The

type of solvent used influences the kinetics and thermodynamics of cation exchange, however systematic studies on the effect of solvents are very rare. (Brozek et al., 2014a; Brozek & Dinca, 2015; X. J. Cui et al., 2009)

An excellent work by Dinca and coworker explored the effects of solvents and thermodynamic parameters in cation exchange, including Gibbs free energy ($\Delta G^{o}_{P,T}$), entropy (ΔS), and enthalpy (ΔH) for the exchange of Zn^{2+} by Ni^{2+} or Co^{2+} into MOF-5 and exchange of Zn^{2+} by Co^{2+} into MFU-4*l*. Their findings concluded that, the process is endergonic with solvent and cation identity having strong influence to the thermodynamics of the cation exchange. (Brozek et al., 2014a; Brozek & Dinca, 2015) According to their study, the extent of Ni^{2+} ions substituting Zn^{2+} in MOF-5 in range of solvents from π-donors to π-acceptors, such as DMF, DMSO, NMP, NMF, THF, and MeCN were mapped against several solvent parameters that are expected to influence the exchange process, including solvent dielectric constant, the ligand field parameter of the corresponding solvated $[Ni(solvent)_x]^{2+}$ species (Dq), Hansen solubility parameter δ_H, Synder polarity index and Gutmann donor number. However, only the Dq parameter shows some trends. Ni/Zn ratio increases with increasing Dq values, Figure 2.1. That is, Ni^{2+} exchanged more Zn^{2+} using solvent(s) that interact less strongly with Ni^{2+} ions in solution and more strongly with Zn^{2+} once exchanged. This trend is also in agreement with DFT calculation for metal-solvent bond strengths of Ni and Zn, which shows a good correlation of low Dq with strong metal-solvent interactions. The $O^{\delta-}$ filled π-donating orbitals on DMSO lead to small Dq while the empty π* orbitals of MeCN lead to large Dq. Thus, the extent of Ni substituting Zn increases for solvent with high Dq value (weaker metal-solvent bonds), Figure 2.2.

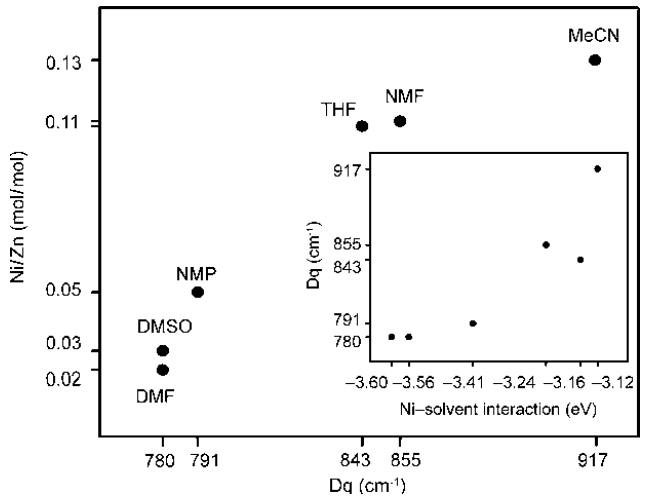

Figure 2.1: Ni/Zn molar ratio vs. Dq value. Inset: Dq value determined from UV-Vis analysis of $[Ni(solv)_6]^{2+}$ complexes against calc. Ni–Solv. bond strength. Reprinted with the consent of ref. (Brozek et al., 2014b). Copyright 2014 Wiley-VCH.

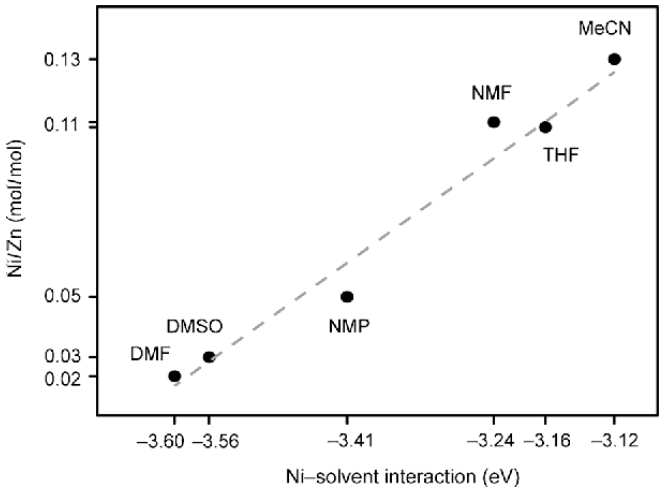

Figure 2.2: Ni/Zn ratio vs. calculated Ni–solv. interaction. Reprinted with the consent of ref. (Brozek et al., 2014b). Copyright 2014 Wiley-VCH.

In this example, the exogenous Ni^{2+} ions exchanged the Zn^{2+} ions after immersion of MOF-5 into different solutions of Ni^{2+} ions. Based on the HSAB principle, there are two borderline acids (Ni^{2+} and Zn^{2+}) and two bases; hard anionic carboxylate O base and solvents competing with each other to attain more stable products with Ni^{2+} or Zn^{2+} based on their preference in terms of relative hardness and stability. Normally, cation exchange proceeds in a way so as to produce the hardest possible products, and the average value of the hardness of the new products must be more than that of the reactants average. Both

Zn^{2+} and Ni^{2+} are borderline acids and form a labile bond with hard carboxylate O and the lability of the metal-ligand bonds allowed them to be substituted for one another. However, the exchange of Zn^{2+} depends on two factors, i.e. its interaction with solvent molecules and their ability to subsequently get solvated; and the ability of the Ni^{2+} to interact less strongly with solvents and get desolvated and form a stable product with the framework. The hydration energy of Zn^{2+} is significantly less than that of Ni^{2+} due to its negligible ligand field stabilization energy (Smith, 1977). Zn^{2+} could be favorably more solvated than Ni^{2+} ions in a suitable solvent which makes it easier for Ni^{2+} to replace Zn^{2+} especially with the large excess of Ni^{2+} ions in solution to push the exchange based on Le Chatelier's principle. (Le Chatelier & Boudouard, 1898) Complete cation exchange could not be achieved, however since Ni^{2+} is relatively softer than Zn^{2+} and may form more labile bonds with hard carboxylate O.

MFU-4*l,* $[Zn_5Cl_4(BTDD)_3]$ was also investigated for the exchange of Zn^{2+} with Co^{2+} at room temperature for 7 d. Unlike in MOF-5, in which the exchange of Zn^{2+} with Ni^{2+} increases with an increase in Dq value, the exchange of Zn^{2+} with Co^{2+} in MFU-4*l* has an inverse correlation with Dq, that is Co^{2+} exchange increases in solvent of lower Dq value. It was also found that, the exchange extent of Zn^{2+} by Co^{2+} correlates well with Gutmann donor numbers. This in essence shows that, for MFU-4*l*, the exchange rate increases with more basic solvents, Figure 2.3, unlike in the case of MOF-5. This inverse relationship could be simply attributed to the different types of ligands and the nature of the interactions between the ligands and the cations. For instance, while in MFU-4*l* it involves soft-soft M–L interaction, in MOF-5 however involves a labile borderline-hard M–L interaction. Although cation-solvent interaction strongly influences the exchange of cations, the solubility of ligands equally plays an important role, and each of this could be the rate limiting step. In this example, the exchange of Zn^{2+} by Co^{2+} in MFU-*4l* increases as the solvent basicity increases from MeCN to DMSO, Figure 2.3 and this

correlates well with fact that, the solubility of soft BTDD also increases as the solvent basicity increases from MeCN to DMSO. The inverse relationship is expected for the exchange of Zn^{2+} by Ni^{2+} ions in MOF-5 having a hard BDC linker. In another example, the exchange of Zn^{2+} by Cu^{2+} in isomorphous Zn-HKUST-1 and Zn-PMOF-2 in MeOH, was limited partly by the solubility of the two organic ligands. In MeOH, 1,3,5-tris(3,5-dicarboxylphenylethynyl)-benzene is more soluble and more flexible than BTC. This may account for the fact that Cu^{2+} was able to exchange Zn^{2+} completely in Zn-PMOF-2 having more soluble linker but only partially exchanged in Zn-HKUST-1 with a less soluble BTC linker (Xiaokai Song, Seok Jeong, et al., 2012).

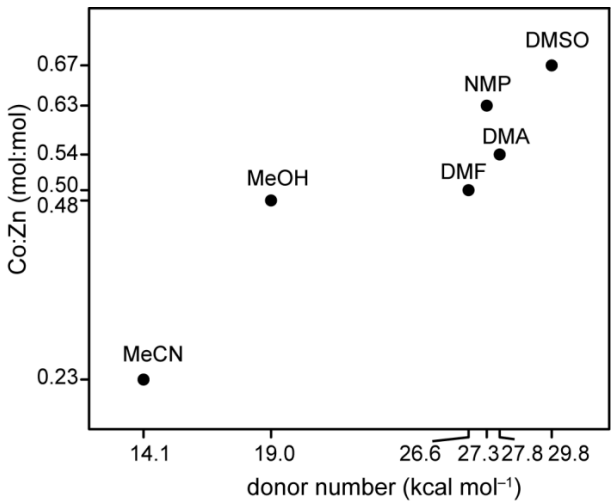

Figure 2.3: Co/Zn exchange mole ratio in MFU-4*l* vs Gutmann donor numbers of different solvents. Reprinted with the consent of ref. (Brozek et al., 2014b). Copyright 2014 Wiley-VCH.

2.2.2 Cation exchange in MOCPs

Most MOCPs are inherently labile when in contact with suitable condition, which may reveal dynamics that are not initially obvious. Majority of the reported cation-exchanged MOCPs are predominantly those with labile M–L bonds. However, MOCPs that are perceived stable and robust with stronger M–L bonds, due to their high thermal and chemical stabilities were also demonstrated to readily undergo an exchange of their central metal ions. Cohen and coworkers reported one of the earliest cation and ligand

exchanges in MOFs that are believed to be inert, stable and robust to resist any structural change (M. Kim et al., 2012). However, their findings on the ligand and/or cation exchange, both in solid-solid and solid-liquid phase, on several perceived stable MOFs, including MIL or UiO or ZIFs series, implies that the stability and strength of the M–L bonds was overly estimated (M. Kim et al., 2012).

Demonstrating the susceptibility of stable MOCPs to undergo cation exchange, here immersing stable UiO-66(Zr) into DMF solutions of different Ti^{4+} salts, for 5 d at room temperature and at 85 °C, afforded a mixed-metal UiO-66(Zr/Ti). Although Ti^{4+} is harder than Zr^{4+} based on the HSAB principle, the magnitude of exchange depends on the Ti^{4+} precursor used. The highest exchange was observed using $TiCl_4(THF)_2$ as the cation precursor, with 93% at 85 °C and 54% at room temperature. $TiBr_4$ however, exchanged 73% at 85 °C and 57% at room temperature, Figure 2.4. Based on the HSAB principle, the hardness or softness of species in solution is influenced by the chemistry of surrounding ligands. For instance, Ti^{4+} in $TiBr_4$ is less hard than Ti^{4+} in $TiCl_4(THF)_2$ due to the differences in the donor atoms. Molecule with hard donor atoms such as F^-, or Cl^- becomes harder resulting from large negative values of the electron affinity. The hardness drops with softer donor atoms such as Br^- or I^- (Ralph G Pearson, 1988).

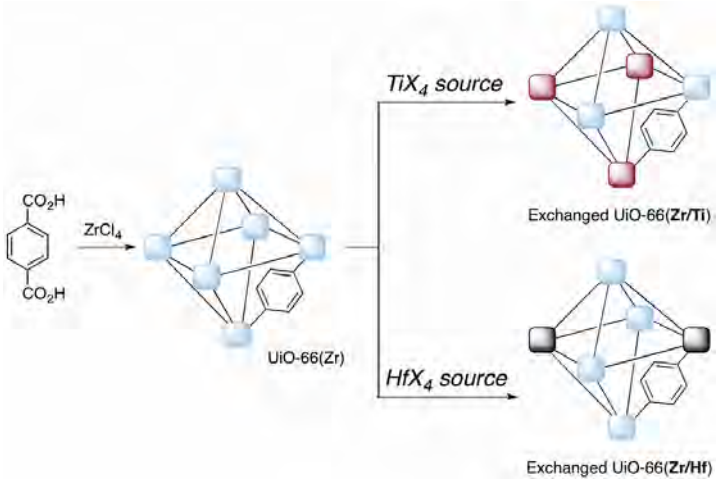

Figure 2.4: Schematics of cation exchange in UiO-66 with Ti^{4+} and Hf^{4+}. Reprinted with the consent of ref. (M. Kim et al., 2012). Copyright 2012, American Chemical Society.

The slight differences in the exchange behavior could be explained as follows, the Ti^{4+} in $TiCl_4(THF)_2$ is relatively harder and can interact well and compete with Zr^{4+} for the hard carboxylate O. Whereas, the Ti^{4+} in $TiBr_4$ may not be as hard to compete and substitute Zr^{4+} due to the slight softening effect by the surrounding bromide-donor atoms. The strength of the Zr–O bond may also prevent the complete exchange of Zr^{4+}, however, increasing the temperature could help to overcome the bond dissociation energy of Zr–O, making the exchange feasible. Analogous experiment was also conducted using Hf^{4+} salt. However, the exchange was only about 10% at room temperature and about 18% at an elevated temperature. Nonetheless, Hf^{4+} is relatively lower in hardness compared to both Zr^{4+} and Ti^{4+}, hence its inability to substitutes appreciably the harder Zr^{4+}, even at elevated temperature.

A similar study on exchange of Zr^{4+} with Ti^{4+} in UiO-66 was also conducted by Hill and coworkers (Lau et al., 2013) for a dramatic CO_2 uptake. Immersing UiO-66 in a DMF solution of $TiCl_4(THF)_2$ for 1, 5, and 15 d, at 95 ^oC resulted in a mixed metal UiO-66(Zr/Ti) with 32, 44 and 56% yield for 1, 5, and 15 d, respectively. Although Ti^{4+} is harder than Zr^{4+} and is expected to exchange it readily in the typical hard O-donor environment, but the exchange does not proceeds to completion even at 95 ^oC for 15 d, signifying the strength of M–L bond due to hard-hard interactions.

Generally, it is difficult to construct MOCPs using high valence metal cations largely because of the kinetic inertness of the metal–ligand bonds. In most cases, crystalline powders were formed in which characterization was done not in a straightforward manner. To circumvent this problem, Zhou group introduced a very robust concept of post synthetic metathesis and oxidation (PSMO). (T.-F. Liu et al., 2014) In PSMO, a template MOF with labile M–L bond is selected then exchanged with oxidizable cation, then oxidized to higher oxidation state. For instance, PCN-426-Mg, Figure 2.5, was

selected as the template MOF, due to its very labile Mg–O bond and high ligand exchange rate of Mg^{2+}. Subsequently, Mg^{2+} was successfully exchanged with cations of low exchange rate, and high relative stability constant, Fe^{2+} and Cr^{2+}, to PCN-426-Fe(II) and PCN-426-Cr(II) intermediates in a single crystal manner. Both Fe^{2+} and Cr^{2+} are softer Lewis acids, having a higher ligand exchange kinetics and lower hydrolysis equilibrium constant compared to their higher oxidation state versions, Fe^{3+} and Cr^{3+}. Ultrahigh water stable PCN-426-Fe(III) and PCN-426-Cr(III) were obtained after air oxidation of the metal nodes of the intermediate MOFs, Figure 2.6, featuring hard acids of Fe^{3+} and Cr^{3+} expected to form a very stable bond with carboxylate O. In this work, the weak Mg–O bonds have been strategically exchanged and altered to relatively inert Fe^{3+}–O or Cr^{3+}–O through oxidation which significantly improved the resulting product stability owing to the hard-hard M–L interactions.

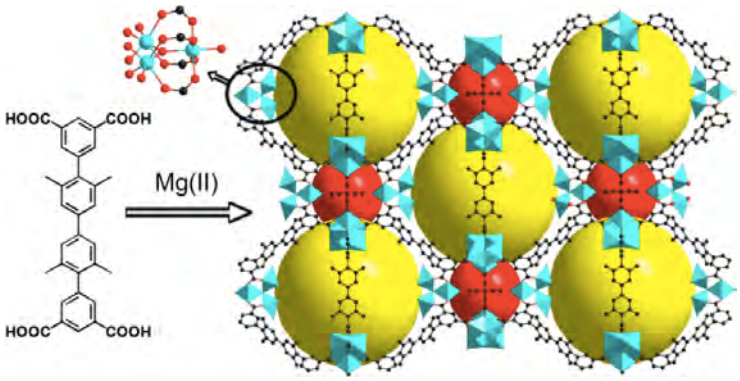

Figure 2.5: The structure of PCN-426-Mg, showing the oxo-trinuclear cluster. Reprinted with the consent of ref. (T.-F. Liu et al., 2014). Copyright 2014, American Chemical Society.

Following their success in the above strategy, same group also devised another effective synthetic strategy to engineer series of Ti^{4+}-based MOFs, including, MIL-100(Sc), PCN-333(Sc), MOF-74(Zn) and MOF-74(Mg), which all have a common tri-nuclear oxo-clusters $M_3O(COO)_6$, via a method called high valence exchange and oxidation. (Zou et al., 2016) Through carefully selecting MOF templates, they

successfully synthesized Ti^{4+} containing MIL-100(Sc)-Ti, PCN-333(Sc)-Ti, MOF-74(Zn)-Ti, and MOF-74(Mg)-Ti. To accomplish this, they first exchanged the parent Sc^{3+}, Zn^{2+}, or Mg^{2+} in the template with Ti^{3+} followed by oxidation of Ti^{3+} to Ti^{4+} under mild conditions, Figure 2.7.

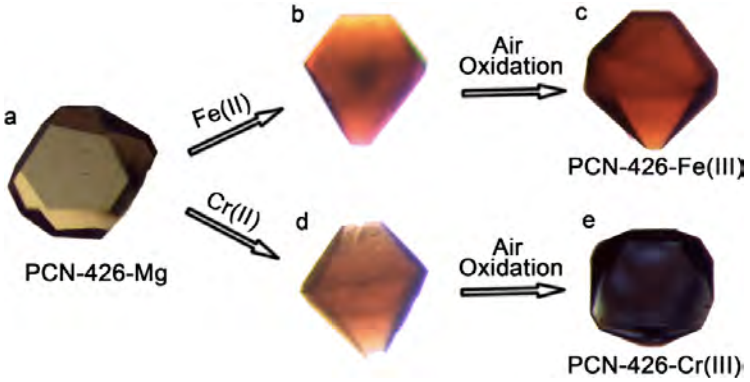

Figure 2.6: Digital images of: PCN-426-Mg (a), the intermediate PCN-426-Fe(II) (b), PCN-426-Cr(II) (d), and PCN-426-Fe(III) (c), PCN-426-Cr(III) (e). Reprinted with the consent of ref. (T.-F. Liu et al., 2014). Copyright 2014, American Chemical Society.

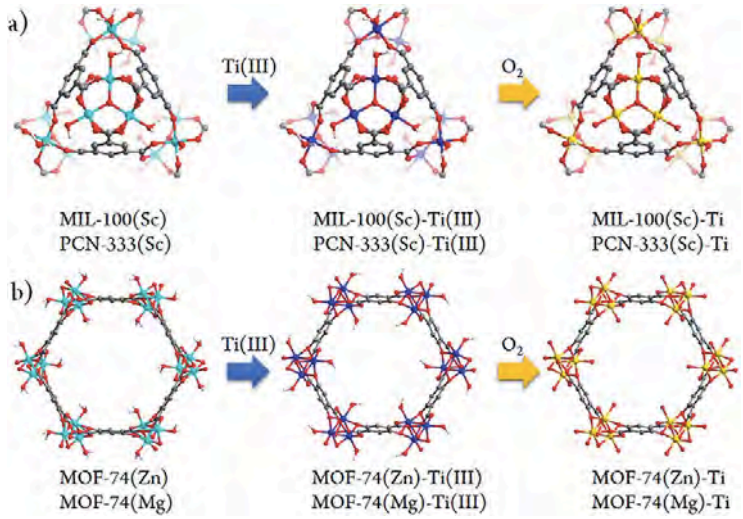

Figure 2.7: Summary of the high valence cation exchange and oxidation procedure for the selected template MOFs. First exchange with Ti^{3+} followed by oxidation to Ti^{4+} (Zou et al., 2016). Copyright 2016, Royal Society of Chemistry.

Immersing MIL-100(Sc), PCN-333(Sc), MOF-74(Zn) or MOF-74(Mg), into a DMF solution of $TiCl_3(THF)_3$, for 1 d, at 120 ºC while replenishing the Ti^{3+} solution every 6 hours, and then subsequent air oxidation, afforded the corresponding Ti^{4+} substituted MOFs. Though both PCN-333 and MIL-100 are isostructural, 85.9% of Sc^{3+} was substituted in PCN-333, whereas, only 52.0% of Sc^{3+} was exchanged in MIL-100. Similarly for isostructural MOF-74(Zn) and MOF-74(Mg), 100% Zn was substituted in MOF-74(Zn) and only 35.1% of Mg^{2+} was exchanged in MOF-74(Mg). In PCN-333, the ligand TATB is less hard and more flexible than BTC of MIL-100. Therefore, the Sc–BTC bond strength is higher than Sc–TATB, making it easier to substitute more Sc^{3+} in PCN-333(Sc) than in MIL-100(Sc). Similarly, the 2,5-dihydroxyterephthalate (L) in MOF-74 is hard, making Zn–L bonds more labile due to the soft nature of Zn^{2+},while the harder Mg^{2+} will bind relatively stronger with the hard L. In addition to this, harder Mg^{2+} may not be favorably solvated by the relatively soft DMF compared to the case of softer Zn^{2+}, which justifies why Zn^{2+} was 100% exchanged while only 35.1% of Mg^{2+} was exchanged.

The success of the method developed by Zhou group inspired Wang and coworkers to devise a more viable method to engineer many Cr-based MOCPs under mild conditions. Several synthetically demanding Cr-based MOFs including Cr-MIL-100, Cr-MIL-142A/C, Cr-PCN-600 and Cr-PCN-333, were synthesized together with a new Cr-SXU-1 by using relatively labile Fe(III)-MOFs as precursor. (J. H. Wang et al., 2017) Their strategy involved solvent-assisted metal exchange exploring different solvents with different coordination abilities. When a freshly prepared Fe-SXU-1 [$Fe_3O(BPBTTBA)_2$], Figure 2.8, featuring similar $Fe_3O(COO)_6$ SBUs found in most Cr-based MOFs, was immersed in DMF, DEF (N,N-diethyl-formamide), DMA (N,N-dimethyl-acetamide), NMP (N-methyl-pyrrolidine), MPEA (1-(4-methylphenyl)-ethanone), CA (cyclohexanone), TFAP (2,2,2,4'-tetrafluoroaceto-phenone), or acetone solution of

$CrCl_3.6H_2O$, at a temperature between 60–100 °C, the harder Cr^{3+} substituted Fe^{3+} to varying degrees depending on the solvent used. When in DMF solution, very negligible amount of Fe^{3+} was exchanged, similar to the case when DEF was used, even at 178 °C. However, when the solvent was changed to DMA or NMP or acetone, Fe-SXU-1 underwent a complete exchange of Fe^{3+} to an isostructural Cr-SXU-1. The exchange, remarkably, occurred at a relatively lower temperatures, 80 °C, and with a much lower concentration and a shorter duration especially when using acetone.

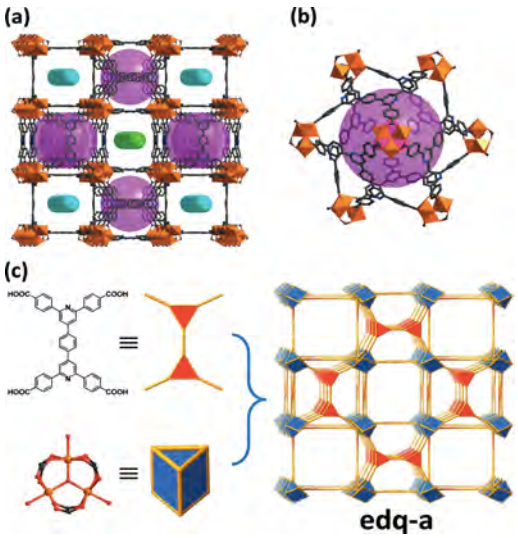

Figure 2.8: The general structure of Fe-SXU-1 (a), the cubic cage showing 8 SBUs (b), and the underline net by deconstructing Fe-SXU-1 (c). Reprinted with the consent of ref. (J. H. Wang et al., 2017). Copyright 2017 Wiley-VCH.

To rationalize this experiment using the HSAB principle, it is important to understand the relative hardness of all the species, including the exogenous and the endogenous cations, the coordinating donor groups in the framework and the solvents used. Both Fe^{3+} and Cr^{3+} are hard acids, but Cr^{3+} is much inert and harder than Fe^{3+}, while carboxylate O is considered a hard base. The kinetic inertness of Cr^{3+} can be seen in its very low ligand (water) exchange rate constant of 10^{-6} (k, s^{-1}) compared to Fe^{3+} having 10^{2} (k, s^{-1}) (Eigen, 1963). The solvents used can be categorized into two types, those with aldehydes carbonyl group (DMF, DEF), and those with ketones carbonyl group (DMA, NMP, or acetone).

Generally, ketones are more strongly basic than aldehydes, for e.g. pKa of DMF and acetone is -0.3 and 20, respectively. (Sejeant & Dempsey, 1979) All successful exchange was recorded in ketonic solvents especially acetone, while using aldehydes solvents failed to yield a positive result. Thus, we can relate this observation as follows; the increase in temperature and higher ligand exchange constant help to overcome the Fe–O bond dissociation energy. Further, the acetone is hard enough to bind strongly and solvate Fe^{3+} which paves a way for harder, more oxophillic and more kinetically inert Cr^{3+} to substitutes Fe^{3+}.

The exchange failed in DMF because of the fact that DMF is a very weak base and is expected to interact weakly with Fe^{3+}, not strong enough to displace carboxylate O through solvation, therefore giving no room for Cr^{3+} to substitute it. Henceforth, many other Cr-based MOFs from their Fe^{3+}-based precursor was successfully synthesized using acetone as solvent, at a much lower concentration, milder condition, and less duration, including Cr-MIL-100, Cr-MIL-142A/C, Cr-PCN-600 and Cr-PCN-333, Figure 2.9.

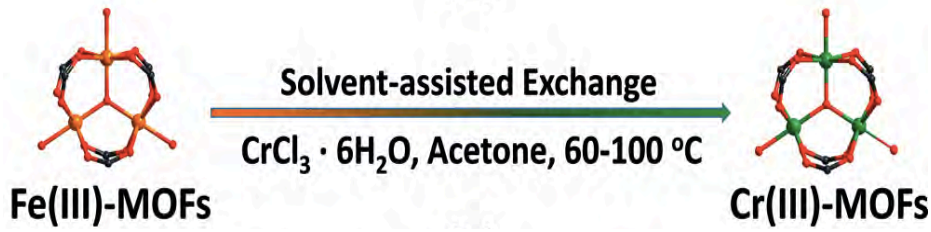

Figure 2.9: Solvent-assisted metal exchange using acetone under mild conditions. Reprinted with the consent of ref. (J. H. Wang et al., 2017). Copyright 2017 Wiley-VCH.

Another subset of stable porous MOCPs called metal-azolates frameworks (MAFs), are synthesized using soft low valent TMs and soft azolates linkers. They form a very formidable M–L bond, very high thermal and chemical stability with high performance functionality. Cation exchange in MAFs are very rare owing to their high stability. Denysenko and coworkers (2012) reported one of the earliest cation exchange in Zn^{2+} or

Co^{2+} and benzotriazolate, BTDD, based framework (MFU-4*l*). It is a pentanuclear framework with two types of crystallographic sites, in which one Zn center adopts an octahedral geometry surrounded by six N atoms from BTDD and the remaining four Zn centers adopt tetrahedral coordination geometry with three N atoms from BTDD and an axial Cl ion. Immersing MFU-4*l* in a concentrated DMF solution of $CoCl_2$ and heated at 140 ^oC led to Co^{2+} exchanged all the tetrahedral Zn^{2+} sites without exchanging the octahedral Zn^{2+} sites to form an isostructural Co-MFU-4*l* [$ZnCo_4Cl_4(BTDD)_3$]. With the use of soft linker BTDD, it is expected for relatively softer cation to form more stable MOF. Both Zn^{2+} and Co^{2+} are borderline acids, but Zn^{2+} is slightly harder than Co^{2+} and it is expected for relatively softer Co^{2+} to exchange Zn^{2+} and forms a relatively more stable exchanged product, though it proceeded at a high temperature. Whereas, immersing an isomorphous MFU-4, $Zn_5Cl_4(BBTA)_3$, with a smaller BBTA linker in a similar condition, no exchange was recorded. BBTA with a higher basicity than BTDD is expected to form more stable, soft-soft M–L bonds. In addition to the smaller pore size that can limit diffusion in MFU-4, the higher M–L bond dissociation energy can also prevent the exchange of Zn^{2+} with Co^{2+}.

Zeolitic Imidazolate Frameworks (ZIFs) are subclass of Metal-Azolate-Frameworks (MAFs) that are very stable. They combined the organic functionalities and inorganic zeotype topologies. (B. Chen et al., 2014) They are known to have a very high thermal and chemical stabilities, manifested by their ability to withstands boiling and highly basic solutions. (K. S. Park et al., 2006) Structural modifications in ZIFs are not very common especially cation exchange, which is attributed to their formidable M–L bond dissociation energy. However, the first example of cation exchange in ZIFs was reported by Cohen group, (Fei et al., 2013) using ZIF-71 [$Zn(dcim)_2$] (dcim = 4,5-dichloroimidazolate) and ZIF-8 [$Zn(mim)_2$] (Hmim = 2-methylimidazole) with ***rho*** and ***sod*** topology respectively. Immersing ZIF-71 or ZIF-8 in a methanolic solution of $Mn(acac)_2$ (acac =

acetylacetonate) and incubated at 55 °C for 24 h, 12 % of the tetrahedral Zn^{2+} in ZIF-71 and 10 % in ZIF-8 was exchanged by Mn^{2+}, Figure 2.10. As expected, high stability of the M–L bonds may prevent the exchange to proceed appreciably since ZIF-71 and ZIF-8 involved a borderline–soft Lewis acid-base interactions (Zn–dcim or Zn-mim; dcim = dichloro-imidazolate, mim = dimethyl imidazolate). Hence, Mn^{2+} was only able to exchange 12 and 10 % of Zn^{2+} in ZIF-74 and ZIF-8 respectively, signifying their stabilities. This difference however, may also be attributed to the types of ligands used, dcim is more basic (softer) than mim and Mn^{2+} is slightly softer than Zn^{2+}.

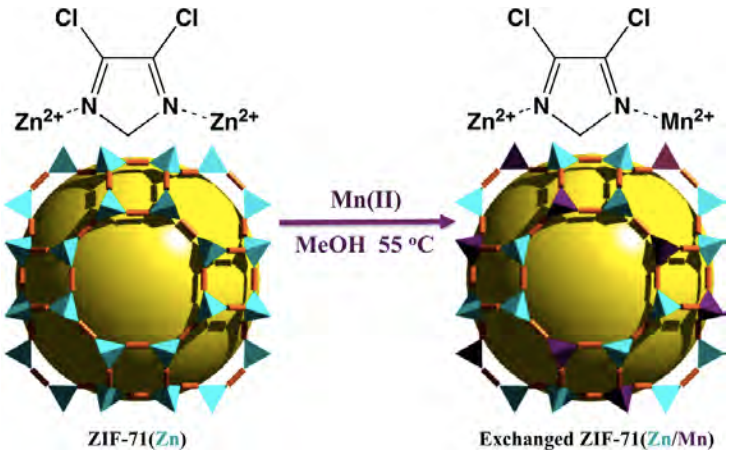

Figure 2.10: cation exchange in ZIF-71. Reprinted with the consent of ref. (Fei et al., 2013). Copyright 2013, American Chemical Society.

Large number of MOCPs reported are labile and amenable to solid solution including structural transformation, anion/cation or ligand exchange. Such MOCPs are predominantly made of borderline first row TMs and hard carboxylate O-donor linkers. They are more susceptible to degradation compared to those constructed from hard high valence metals and hard carboxylate O-donor linkers.

Kim and coworkers reported the first example of complete and reversible cation exchange in labile MOF, $[Cd_{1.5}(H_3O)_3[(Cd_4O)_3(hett)_8].6H_2O$ (POST-65(Cd), in a SC-SC manner (S. Das et al., 2009). POST-65(Cd) is air stable and stable up to 350 °C after

activation. However, it underwent a rapid and facile cation exchange of Cd^{2+} with Pb^{2+} with 98 % of Cd^{2+} exchanged from the parent MOCP in aqueous solution within 2 hours and subsequently completed within 2 days, to isomorphous POST-65(Pb) Figure 2.11. While Pb^{2+} is a borderline ion, Cd^{2+} is soft ion and the bases are hard O-donor ligands and water. Both Cd^{2+} and Pb^{2+} are expected to form labile M–L bonds with hard hett carboxylate O. This lability paves a way for exchange with each other in the framework. And since hard solvent (water) is used, both cations may have large values with Pb^{2+} expected to have larger value being a borderline acid. The exchange proceeded readily however, because borderline Pb^{2+} is harder than soft Cd^{2+} and would form more stable bonds with hard carboxylate O-donor. 98% of Cd^{2+} was exchanged within 2 h, and completed within 2 d. However, the reverse exchange of Pb^{2+} with Cd^{2+} took almost three weeks with several replenishments of Cd^{2+} solution, indicating the higher stability of POST-65(Pb) compared to POST-65(Cd). This also vindicates the fact that borderline-hard interaction is more stable than soft-hard interaction.

Further, the exchange process was extended to trivalent lanthanide (Ln) ions (Dy^{3+} or Nd^{3+}). However, methanol was used as the solvent, instead of water. Ln^{3+} are generally hard acids and are expected to interact and form a stronger bond with hard carboxylate O-donors. Hence, they are expected to readily exchange Cd^{2+} due to the lability of the Cd–L bonds. In addition to this, Dy^{3+} or Nd^{3+} may also interact less with MeOH solvent and have a relatively large Dq value, paving a way for the exchange. The faster rate of exchange of Cd^{2+} with the Ln's in methanolic solution compared with the exchange of Pb^{2+} with Cd^{2+} in aqueous solution also corroborate the above arguments. The authors further explored the cation exchange of Mn^{2+} in POST-65(Mn) with other TMs (Fe, Co, Ni, or Cu), (Y. Kim et al., 2012) using DMF solution of the chloride salts of these metals. 99% exchange of Mn^{2+} was achieved in 12 days for Fe^{3+}, Co^{2+}, and Ni^{2+}, while Cu^{2+} exchanged only 66%. In addition to this, POST-65(Co or Ni) was completely reversible

to POST-65(Mn), with much longer duration (more than 1 month); whereas POST-65(Cu) was only partially exchanged and POST-65(Fe) could not be exchanged at all even after 1 month process, Figure 2.11. These cation exchange processes can be rationalized as follows; the stability of first row divalent TM complexes increases from left to right of the periodic table. This can be attributed to the general decrease in the ionic radius which slightly increases the hardness due to increase in the charge to radius ratio and hence the stability of their complexes from Mn^{2+} to a maximum at Cu^{2+} (Ralph G Pearson, 1988), this also corroborate with the Irving-Williams series, in which the crystal field stabilization energy goes from maximum at Ni^{2+} to zero at Mn^{2+} in TMs complexes. (Irving & Williams, 1953) The differences in hardness allowed them to substitute softer Mn^{2+} having a relatively more labile bonds with harder carboxylate O.

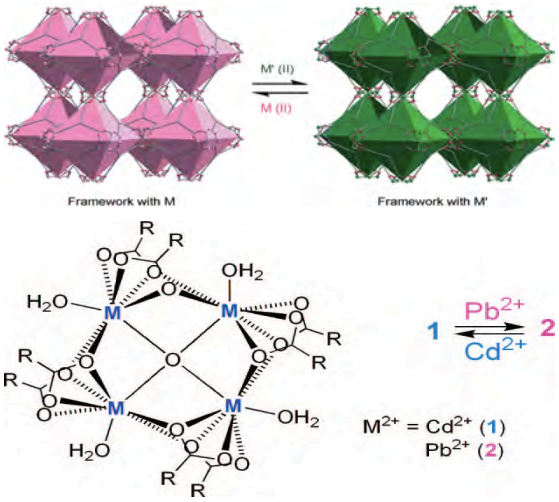

Figure 2.11: Reversible isomorphous metal-ion exchange in POST-65 (top). POST-65, the SBU (bottom) Reprinted with the consent of ref. (S. Das et al., 2009). Copyright 2009, American Chemical Society.

The exchange kinetics also bolster this notion. The time required to substitutes 50% ($t_{1/2}$, h) of Mn^{2+} by Co^{2+}, Ni^{2+}, Fe^{3+} and Cu^{2+} was 96, 75, 64 and 39 hours, Figure 2.12. Cu^{2+} have the fastest and Co^{2+} the slowest exchange rate. This also justified their relative hardness in preference for the harder O. However, Cu^{2+} was only able to exchange 66% of Mn^{2+}, which may be attributed to the stability of its complexes, either in solvated (in

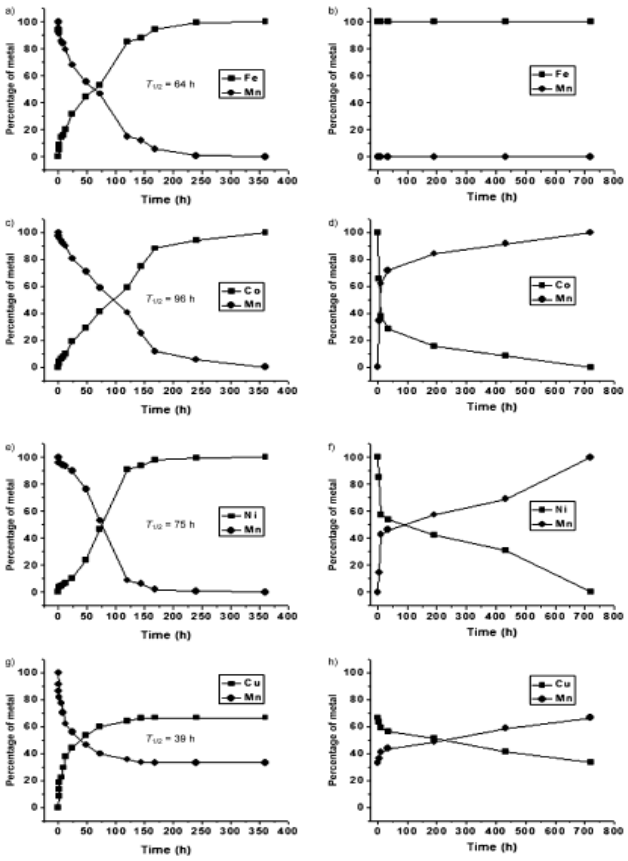

Figure 2.12: Kinetic profiles of the cation exchange in POST-65(Mn) into POST-65(Fe/Co/Ni/Cu) (left) and the corresponding reversal exchange to POST-65(Mn) (right). Reprinted with the consent of ref. (Y. Kim et al., 2012). Copyright 2012 Wiley-VCH.

this case) or in the framework related to the Jahn-Teller effect for its octahedral geometry complexes. The exchanged POST-65(Fe/Co/Ni or Cu) shows higher stability compared with the parent POST-65(Mn), as expected due to better hard-hard interactions. Such facts were validated by further observations. For instance, the reverse exchange required much longer time for Co^{2+} and Ni^{2+}, Figure 2.12. Notably, the Cu^{2+} exchanged POST-65(Mn/Cu) was only partially reversed (66%). Further, harder Fe^{3+}, compared to any other divalent TM, have readily and preferentially exchanged Mn^{2+} and the process was irreversible. This is also attributed to the hard-hard M–L interaction preference of hard Fe^{3+} and hard carboxylate O-donor forming more stronger M–O bonds that endows higher stability into the substituted POST-65(Fe).

Table 2.3: Summary of the reviewed MOCPs that undergo cation exchange at the SBUs.

Common name	Molecular formula	Inserted cation(s)	Exchange condition	% exchanged	M-L Interaction type	Ref.
MIL-53(Fe)-Br	Fe(OH)(BDC-Br)	Al^{3+}	85 °C, 5 d, H_2O	unspecified	Hard-hard	(M. Kim et al., 2012)
MIL-53(Al)-Br	Al(OH)(BDC-Br)	Fe^{3+}	85 °C, 5 d, H_2O	unspecified	Hard-hard	(M. Kim et al., 2012)
UiO-66(Zr)	$Zr_6O_4(OH)_4(BDC)_{12}$	Ti^{4+} or Hf^{4+}	85 °C, 5 d, DMF	Ti^{4+}(93) Hf^{4+}(18)	Hard-hard	(M. Kim et al., 2012)
UiO-66(Zr)	$Zr_6O_4(OH)_4(BDC)_{12}$	Ti^{4+}	95 °C, 1, 5 & 15 d, DMF	32, 44 & 56	Hard-hard	(Lau et al., 2013)
NH_2UiO-66(Zr)	$Zr_6O_4(OH)_4(BDC\text{-}NH_2)_{12}$	Ti^{4+}	100 °C, 4 d, DMF	34.2	Hard-hard	(D. Sun et al., 2015)
NH_2UiO-66(Zr)	$Zr_6O_4(OH)_4(BDC\text{-}NH_2)_{12}$	Ti^{4+}	120 °C, 4 d, DMF	53.4	Hard-hard	(D. Sun et al., 2015)
NH_2UiO-66(Zr)	$Zr_6O_4(OH)_4(BDC\text{-}NH_2)_{12}$	Ti^{4+}	120 °C, 16 d, DMF	57	Hard-hard	(D. Sun et al., 2015)
PCN-426-Mg	$Mg_3(\mu_3\text{-}O)(TMQPTC)_6$	Fe^{3+} or Cr^{3+}	RT, 3 h, DMF, from Fe^{2+} or Cr^{2+} under nitrogen	complete	Hard-hard	(T.-F. Liu et al., 2014)
MIL-100(Sc)	$Sc_3(\mu_3\text{-}O)(OH)(BTC)_2$	Ti^{4+}	120 °C, 1 d, DMF, from Ti^{3+}	85.9	Hard-hard	(Zou et al., 2016)

Table 2.3: continued..

Common name	Molecular formula	Inserted cation(s)	Exchange condition	% exchanged	M-L Interaction type	Ref.
PCN-333(Sc)	$Sc_3(\mu_3\text{-}O)(TATB)_2$	Ti^{4+}	120 °C, 1 d, DMF, from Ti^{3+}	52.0	Hard-hard	(Zou et al., 2016)
MOF-74(Zn)	$Zn_2(DOBDC)(DMF)_2$	Ti^{4+}	120 °C, 1 d, DMF, from Ti^{3+}	complete	Hard-hard	(Zou et al., 2016)
MOF-74(Mg)	$Mg_2(DOBDC)(DMF)_2$	Ti^{4+}	120 °C, 1 d, DMF, from Ti^{3+}	35.1	Hard-hard	(Zou et al., 2016)
Fe-SXU-1	$Fe_3O(BPBTTBA)_2$	Cr^{3+}	60 – 100 °C, DMA, NMP or acetone	99.14	Hard-hard	(J. H. Wang et al., 2017)
Fe-SXU-1	$Fe_3O(BPBTTBA)_2$	Cr^{3+}	178 °C, DMF or DEF	partial/zero	Hard-hard	(J. H. Wang et al., 2017)
PCN-333(Fe)	$Fe_3(\mu_3\text{-}O)(TATB)_2$	Cr^{3+}	60 °C, acetone	98.03	Hard-hard	(Zou et al., 2016)
MIL-100(Fe)	$Fe_3(\mu_3\text{-}O)(OH)(BTC)_2$	Cr^{3+}	60 °C, acetone	97.63	Hard-hard	(J. H. Wang et al., 2017)
MIL-142A	$Fe_3O(H_2O)_2(Cl^-)(BDC)(BTB)_{4/3}$	Cr^{3+}	60 °C, acetone	98.24	Hard-hard	(J. H. Wang et al., 2017)

Table 2.3: continued..

Common name	Molecular formula	Inserted cation(s)	Exchange condition	% exchanged	M-L Interaction type	Ref.
MIL-142C	$Fe_3O(H_2O)_2(Cl^-)(NDC)(BTB)_{4/3}$	Cr^{3+}	60 °C, acetone	98.34	Hard-hard	(J. H. Wang et al., 2017)
Fe-PCN-600	$(Fe_3O)_2(TCPP)_3$	Cr^{3+}	60 °C, acetone	Partial	Hard-hard	(J. H. Wang et al., 2017)
UiO-66(Zr)	$Zr_6O_4(OH)_4(BDC)_{12}$	Ti^{4+}	Microwave assisted, 120 °C, 4 h, DMF	50	Hard-hard	(J. Tu et al., 2017)
PCN-333(Fe)	$Fe_3(\mu_3\text{-}O)(N_3\text{-}BTB)_2$	Cr^{3+}	150 °C, 1 h, DMF	complete	Hard-hard	(Jihye Park et al., 2015)
MIL-53(Al)	Al(OH)(BDC)	Fe^{3+}	RT, 30 minutes, H_2O	unspecified	Hard-hard	(C.-X. Yang et al., 2013)
MFU-4*l*	$Zn_5Cl_4(BTDD)_3$	Co^{2+}	140 °C, DMF	80	Borderline-soft	(Denysenko et al., 2012)
MFU-4	$Zn_5Cl_4(BBTA)_3$	Co^{2+},	140 °C, DMF	no exchange	Borderline-soft	(Denysenko et al., 2012)
	$Cd_3[(Cd_4Cl)_3(BTT)_8(H_2O)_{12}]_2$	Co^{2+} or Ni^{2+}	RT, 2 month, MeOH	complete	Soft-soft	(Liao et al., 2013)

Table 2.3: continued..

Common name	Molecular formula	Inserted cation(s)	Exchange condition	% exchanged	M-L Interaction type	Ref.
MFU-4*l*	$Zn_5Cl_4(BTDD)_3$	Co^{2+},	RT, 7 d, range of solvents	67	Borderline-soft	(Brozek et al., 2014b)
ZIF-8	$Zn(mim)_2$	Mn^{2+}	55 ^oC, 24 h, MeOH	12	Borderline-soft	(Fei et al., 2013)
ZIF-71	$Zn(dcim)_2$	Mn^{2+}	55 ^oC, 24 h, MeOH	10	Borderline-soft	(Fei et al., 2013)
MOF-5	$Zn_4O(BDC)_3$	Ni^{2+}	RT, 7 d, range of solvents	13	Borderline-hard	(Brozek et al., 2014b)
POST-65(Cd)	$[Cd_{1.5}(H_3O)_3[(Cd_4O)_3(hett)_8]•6H_2O$	Pb^{2+}	RT, 2 d, H_2O	complete	Soft-hard	(S. Das et al., 2009)
POST-65(Cd)	$[Cd_{1.5}(H_3O)_3[(Cd_4O)_3(hett)_8]•6H_2O$	Dy^{3+} or Nd^{3+}	RT, 12 d, MeOH	unspecified	Soft-hard	(S. Das et al., 2009)
POST-65(Mn)	$Mn(H_3O)[(Mn_4Cl)_3(hmtt)_8]•55DMF•40H_2O$	Fe^{3+}, Co^{2+}, Ni^{2+}, Cu^{2+}	RT, 12 d, DMF	Fe^{2+}, Co^{2+}, Ni^{2+}, complete. Cu^{2+}, 66	Borderline-hard	(Y. Kim et al., 2012)
POST-65(Co)	$Co(H_3O)[(Co_4Cl)_3(hmtt)_8]•55DMF•40H_2O$	Mn^{2+}	RT, 1 month, DMF	complete	Borderline-hard	(Y. Kim et al., 2012)
POST-65(Ni)	$Ni(H_3O)[(Ni_4Cl)_3(hmtt)_8]•55DMF•40H_2O$	Mn^{2+}	RT, 1 month, DMF	complete	Borderline-hard	(Y. Kim et al., 2012)

Table 2.3: continued..

Common name	Molecular formula	Inserted cation(s)	Exchange condition	% exchanged	M-L Interaction type	Ref.
POST-65(Cu)	$Cu(H_3O)[(Cu_4Cl)_3(hmtt)_8]$•55DMF•40$H_2O$	Mn^{2+}	RT, 1 month, DMF	Partial	Borderline-hard	(Y. Kim et al., 2012)
POST-65(Fe)	$Fe[(FeOH)_3O_6(hmtt)_8]$	Mn^{2+}	RT, 1 month, DMF	Partial	Borderline-hard	(Y. Kim et al., 2012)
ITHD-Zn	$Zn_6(BTB)_4(4,4'\text{-}BIPY)_3(DMF)_{55}(H_2O)_{32}$	Co^{2+}, Cu^{2+}	RT, 48 h, DMF	complete	Borderline-hard	(X. Song et al., 2012)
ITHD-Co	$Co_6(BTB)_4(4,4'\text{-}BIPY)_3(DMF)_{55}(H_2O)_{32}$	Zn^{2+}, Cu^{2+}	RT, 24 h, DMF	complete	Borderline-hard	(X. Song et al., 2012)
ITHD-Ni	$Ni_6(BTB)_4(4,4'\text{-}BIPY)_3(DMF)_{55}(H_2O)_{32}$	Cu^{2+}	RT, 2 w, DMF	complete	Borderline-hard	(X. Song et al., 2012)
ITHD-Cu	$Cu_6(BTB)_4(4,4'\text{-}BIPY)_3(DMF)_{55}(H_2O)_{32}$	Zn^{2+}, Co^{2+}, Ni^{2+}	RT, 24 h, DMF	No exchange	Borderline-hard	(X. Song et al., 2012)
	$\{[Cd_2(btx)_2(tp)_2Cl_2]$•$H_2O\}_n$	Cu^{2+}	RT, 7 d, H2O	complete	Soft-hard/soft	(S. Huang et al., 2010)
	$[Co_3(btx)_4(tp)_3$•$(H_2O)_4]_n$	Cd^{2+}	RT, 7d, H_2O	complete	Borderline-hard/soft	(S. Huang et al., 2010)

Table 2.3: continued..

Common name	Molecular formula	Inserted cation(s)	Exchange condition	% exchanged	M-L Interaction type	Ref.
SUMOF-1	$[Zn_6(BTB)_4(Bpy)_3]\bullet(Sol)_x$	Cu^{2+}	RT, 3 months, DMF	complete and partially reversible	Borderline-hard/soft	(Yao et al., 2012)
SUMOF-1	$[Zn_6(BTB)_4(Bpy)_3]\bullet(Sol)_x$	Co^{2+}, Ni^{2+}	RT, 3 months, DMF	Co^{2+} 35%, Ni^{2+} 38% and reversible	Borderline-hard/soft	(Yao et al., 2012)
P11-Cd	$([Cd_4(BPT)_4]\bullet[Cd(C_{44}H_{36}N_8)(S)]\bullet[S]$	Cu^{2+}	RT, 10 d, MeOH	Complete and reversible	Soft-hard	(Z. Zhang et al., 2013)
	$[Zn_4(DCPP)_2(DMF)_3(H_2O)_2]_n$	Cu^{2+}	80 °C, 4 h, ACN	Complete and reversible	Borderline-hard	(Meng et al., 2014)
	$\{[Zn(L)_2(H_2O)_2]\bullet2(PF_6)\bullet pyrene\bullet2(H_2O)\}_n$	Cu^{2+}	RT, 6 h, MeOH	Complete and irreversible	Borderline-hard	(Mukherjee & Biradha, 2012)
	$\{[Cd(L)_2(H_2O)_2]\bullet2(PF_6)\bullet pyrene\bullet2(H_2O)\}_n$	Cu^{2+}	RT, 6 h, MeOH	Complete and partially reversible	Soft-hard	(Mukherjee & Biradha, 2012)
UPC-6	$\{Zn_2(TMBDI)(H_2O)_2]\bullet2.5DMF\bullet2(1,4dioxane)\bullet6H_2O\}_2$	Cu^{2+}	RT, 7 d, MeOH	complete	Borderline-hard	(Xiao et al., 2017)
UPC-8	$\{[Co_2(TMBDI)(DMA)_2]\bullet2DMA\bullet5EtOH\}_n$	Cu^{2+}	RT, 7 d, MeOH	complete	Borderline-hard	(Xiao et al., 2017)

Table 2.3: continued..

Common name	Molecular formula	Inserted cation(s)	Exchange condition	% exchanged	M-L Interaction type	Ref.
	$\{[Zn_2(4ABPT)(3,4\text{-}PYDC)_2]\bullet 2DMAc\bullet 3MeOH.H_2O\}_n$	Cu^{2+}	RT, 10 d, DMAc	complete	Borderline-hard	(L.-W. Lee et al., 2019)
	$\{[Zn_2(4ABPT)(3,4\text{-}PYDC)_2]\bullet 2DMAc\bullet 3MeOH\bullet H_2O\}_n$	Co^{2+}, Ni^{2+}	RT, 30 d, DMAc	Co^{2+} 12, Ni^{2+} 51	Borderline-hard	(L.-W. Lee et al., 2019)
	$\{[Zn_3(L)_2(DABCO)\ (H_2O)]\bullet 9DMF\}$	Cu^{2+}	RT, 4 d, DMF	33	Borderline-hard	(P.-P. Cui et al., 2017)
	$\{[Cu_3(L)_2(DABCO)(H_2O)]\bullet 9DMF\}$	Zn^{2+}	RT, 5 d, DMF	33	Borderline-hard	(P.-P. Cui et al., 2017)
	$\{Zn(BPPCOO)_2\}_n$	Cu^{2+}	RT, 2 d, DMF	complete	Borderline-hard	(Bommakanti et al., 2018)
	$\{Zn(BPPCOO)_2\}_n$	Mn^{2+}, Fe^{2+}, Co^{2+} or Ni^{2+}	RT, 2 d, DMF	partial	Borderline-hard	(Bommakanti et al., 2018)
	$Zn_2(TMBDC)_2(bpy)$	Ni^{2+}	80 °C, 72h DMF	75	Borderline-hard	(Y. Xu et al., 2016)
	$Mg_2\{Mg_4[Cu^{2+}{}_2\text{-}(Me_3MPBA)_2]_3\}\bullet nH_2O$	Co^{2+} or Ni^{2+}	RT, 7 d, H_2O	complete	Hard-hard	(Grancha et al., 2015)
Ps-CMOF-1	$[Cd_2(NiL^1)(CdL^2)][Cd_2(NiL^1)(H_2L^2)]\bullet 6DMF\bullet 5MeOH$	Cu^{2+}, Zn^{2+}, Co^{2+} or Ni^{2+}	RT, 7 d, DMF	partial	Soft-hard	(J. Li et al., 2018)

Table 2.3: continued..

Common name	Molecular formula	Inserted cation(s)	Exchange condition	% exchanged	M-L Interaction type	Ref.
porph@MOM-10	$[Cd_6(BPT)_4Cl_4(H_2O)_4]$	Mn^{2+}	RT, 1 month, MeOH	complete	Soft-hard	(Z. Zhang et al., 2011)
porph@MOM-10	$[Cd_6(BPT)_4Cl_4(H_2O)_4]$	Cu^{2+}	RT, 1 month, MeOH	76	Soft-hard	(Z. Zhang et al., 2011)
MOF-74(Zn)	$Zn_2(DOBDC)(DMF)_2$	Ca^{2+}	100, 75 or 50 °C, 7 d, DMF	68, 33 or 20	Borderline-hard	(Z. Zhang et al., 2019)
	$[Zn(4,4'\text{-}bpy)_2(FcphSO_3)_2]_n$	Cd^{2+} or Cu^{2+}	RT, 1 month, MeOH	Cd^{2+} 62.82 or Cu^{2+} 49.87	Borderline-hard	(L. W. Mi et al., 2008)
	$[Zn(4,4'\text{-}bpy)_2(FcphSO_3)_2]_n$	Pb^{2+}	RT, 1 month, H_2O	23.57	Borderline-hard	(L. W. Mi et al., 2008)
Zn-HKUST-1	$Zn_3(BTC)_2(H_2O)_3$	Cu^{2+}	RT, 3 month, MeOH	56	Borderline-hard	(Xiaokai Song, Seok Jeong, et al., 2012)
Zn-PMOF-2	$Zn_{24}L_8(H_2O)_{12}$	Cu^{2+}	RT, 3 d, MeOH	Complete and irreversible	Borderline-hard	(Xiaokai Song, Seok Jeong, et al., 2012)

Table 2.3: continued..

Common name	Molecular formula	Inserted cation(s)	Exchange condition	% exchanged	M-L Interaction type	Ref.
HKUST-1	$Cu_3(BTC)_2(H_2O)_3$	Mn^{2+}, Fe^{2+} or Co^{2+}	90 °C, 1 d, DMF	Mn^{2+} 6, Fe^{2+} 13.5 or Co^{2+} 25.5	Borderline-hard	(Sava Gallis et al., 2015)
	$[Cu_8L_{16}]$	Zn^{2+} or Co^{2+}	RT, 5 d, H_2O	Zn^{2+} 20.8 or Co^{2+} 14.97	Borderline-hard	(J. a. Zhao et al., 2008)
MnMnBTT	$Mn_3[(Mn_4Cl)_3(BTT)_8]_2$	Fe^{2+}, Cu^{2+}, or Zn^{2+}	RT, 7 d, MeOH	Fe^{2+} 3.2, Cu^{2+} 88.8, Zn^{2+} 74	Soft-soft	(Brozek et al., 2013)
PUM210	$[Zn_4(BPBA)_{1.5}(NDC)_4(H_2O)]_n$	Cu^{2+}	60 °C, 3 d, DMF	28	Borderline-soft/hard	(Balestri et al., 2018)
PUM210F	$[Zn_3(BPBA)(NDC)_3(DMF)]_n$	Cu^{2+}	60 °C, 7 d, DMF	32	Borderline-soft/hard	(Balestri et al., 2018)
SNU-51	$\{Zn_2(BDCPPI)(dmf)_3]\bullet 6DMF\bullet 4H_2O\}_n$	Cu^{2+}	RT, 5 d, MeOH	complete	Borderline-hard	(Prasad et al., 2010)
	$\{[Zn(OOCClH_3C_6Fc)_2(H_2O)_3](CH_3OH)\}_n$	Cd^{2+} or Pb^{2+}	RT, 5 d, H_2O	Cd^{2+} 18.11 or Pb^{2+} 26.66	Borderline-hard	(J. Li et al., 2009)
	$\{[Cu^{2+}{}_5Cu^{+}{}_4L_6]\bullet(NO_3)_2\}\bullet 15H_2O$	Ag^+	RT, 1 month, EtOH/ H_2O	45	Borderline/Soft-soft	(Han et al., 2013)
	$[Zn(4,4'\text{-bpy})(NO_3)_2]_\infty$	Ag^+ or Cd^{2+}	RT, 10 d, ACN	Complete and reversible	Borderline-soft	(X. Cui et al., 2009)

Table 2.3: continued..

Common name	Molecular formula	Inserted cation(s)	Exchange condition	% exchanged	M-L Interaction type	Ref.
	$[M(4,4'\text{-bpy})(NO_3)_2]_\infty$ M = Zn^{2+}, Ag^+ or Cd^{2+}	Hg^{2+}	RT, 10 d, ACN	Complete and irreversible	Soft-soft Borderline-soft	(X. Cui et al., 2009)
	$[Zn^{2+}(4,4'\text{-bpy})(NO_3)_2]_\infty$	Ag^+, Cd^{2+} or Hg^{2+}	RT, 10 d, MeOH	Complete and irreversible	Borderline-soft	(X. Cui et al., 2009)
	$[Cd^{2+}(4,4'\text{-bpy})(NO_3)_2]_\infty$	Ag^+ or Hg^{2+}	RT, 10 d, MeOH	Complete and irreversible	Soft-soft	(X. Cui et al., 2009)
	$[Ag^+(4,4'\text{-bpy})(NO_3)_2]_\infty$	Hg^{2+}	RT, 10 d, MeOH	Complete and irreversible	Soft-soft	(X. Cui et al., 2009)

BDC = 1,4-benzene-dicarboxylate, BDC-Br = 2-bromo-1,4-benzene-dicarboxylate, BDC-NH2 = 2-amino-1,4-benzene-dicarboxylate, DOBDC = 2,5-dihydroxy-1,4-benzene-dicarboxylate, BTC = Benzene-1,3,5-tricarboxylate, TATB = 4,4',4''-s-triazine-2,4,6-triyl-tribenzoate, TMQPTC = 2',3'',5'',6'-tetramethyl-[I,I':4',I'':4'',1'''-quaterphenyl]-3,3''',5,5'''-tetracarboxylate, BPBTTBA = 4,4',4'',4'''-(1,4-phenylenebis(pyridine-4,2,6-triyl))tetrabenzoate, 2,6-NDC = 2,6-naphthalenedicarboxylate, TCPP = Meso-tetrakis(4-carboxylatephenyl)porphyrin, BTB = 1,3,5-Tris(4-carboxyphenyl)benzene, N_3-BTB = 2'-(2-azidoethoxy)-5'-(4-carboxyphenyl)-[1,1':3',1"-terphenyl]-4,4"-dicarboxylate, BTDD = Bis-(1,2,3-triazolo-[4,5,-b],[4',5'-i])dibenzo-[1,4]-dioxin, BBTA = 1H,5H-benzo(1,2-d:4,5-d')bistriazole, BTT = 1,3,5-tris(tetrazol-5-yl)benzene, HETT = 5,5',10,10',15,15'-hexaethyltruzene-2,7,12-caboxylate, 4,4'-BPY = 4,4'-Bipyridine, BTX = 1,4-bis(triazol-1-ylmethyl)benzene, BPT = biphenyl-3,4',5-tricarboxylate, DCPP = 4,5-bis(4'-carboxylphenyl)-phthalate, L1 = benzene-1,3,5-triyltriisonicotinate, TMBDI = 2,3,5,6- tetramethyl-1,4-benzene-diisophthalate, 4-ABPT = 4-amino-3,5-bis(5-pyridyl)-1,2,4-triazole, 3,4-PYDC = 3,4-pyridnedicarboxylate, L2 = [1,1':3',1''-terphenyl]-4,4'',5'-tricarboxylate, DABCO = 1,4-diazabicyclo[2.2.2]octane, BPPCOO = 2,6-bis(pyrazol-1-yl)pyridine-4-carboxylate, TMBDC = tetramethylterephthalate, Me_3MPBA = N,N'-2,4,6-trimethyl-1,3-phenylenebis(oxamate), NiL^1 = (R, R)-N,N'-bis(3-tert-butyl-5-(4-pyridyl)salicylidene)-1,2-diphenyldiamine nickel (II), H_6L^2 = tetra-(4-carboxyphenyl)porphyrin, FcphSO$_3$ = m-ferrocenyl benzene-sulfonate, L_8 = 1,3,5-tris(3,5-dicarboxylphenyl)-benzene, L_{16} = 2-[4-[[4-methyl-6-(1-methylbenzimidazol-2-yl)-2-propylbenzimidazol-1-yl]methyl]phenyl]benzoic acid, BPBA = N,N'-(1,1'-biphenyl)-4,4'-diylbis-4-pyridinecarboxamide, F-BPBA = N,N'-(perfluoro-1,1'-biphenyl)-4,4'-diylbis-4-pyridinecarboxamide, BDCPPI = N,N-bis(3,5-dicarboxyphenyl) pyromellitic diimide, L_6 = 4-(2-pyrazinyl)-1,2,3-triazole, pzdc = 2,3-pyrazine dicarboxylate, mim = 2-methylimidazalate, dcim = dichloroimidazolate.

Generally, TMs with coordination sphere surrounded by both O and some N-donor ligands, are more stable than those with all O-donors. N-donor ligands tend to increase the stabilities of divalent TMs, due to the decreased bond lability between the TMs and N-donor ligands. A large number of N-based or N and O mixed ligand-based stable MOFs with divalent TMs was reported. (Burd et al., 2012; Cadiau et al., 2016; Cadiau et al., 2017; Gao et al., 2016; Heering et al., 2013; Y. Hu et al., 2016; Masciocchi et al., 2010; Montoro et al., 2011; Nugent et al., 2013; Shekhah et al., 2014; Tan et al., 2012; Tonigold et al., 2009; X. Wang et al., 2016) The effect of N-donor ligands presence in TM's coordination sphere can be observed in large number of relatively stable TM-based MOCPs, featuring slow exchange kinetics or in some cases not proceeding to completion. A family of $[Zn_6(BTB)_4(Bpy)_3].(Sol)_x$, (SUMOF-1) (Yao et al., 2012), exhibited a complete cation exchange of Zn^{2+} with Cu^{2+}. Soaking SUMOF-1-Zn in DMF solution of $Cu(NO_3)_2$ for 3 months resulted in Cu^{2+} exchanged Zn^{2+} completely, with about 50% replaced within 1 h and 95% within 3 d. However, other divalent Co^{2+} or Ni^{2+} only partially exchanged Zn^{2+} (Co^{2+} 35%; Ni^{2+} 38%) even after 3 months. However, the Co^{2+} or Ni^{2+} exchanged SUMOF-1 are readily reversible to original SUMOF-1-Zn within 7 d. However, the reverse exchange of Cu^{2+} substituted SUMOF-1 with Zn^{2+} was only partial, Figure 2.13.

The presence of soft N-donor atoms from the bpy increases the stability due to the increased bond strength with the borderline Zn^{2+}. This is obvious, while Cu^{2+} can substitutes Zn^{2+} after long period, Co^{2+} and Ni^{2+} only partially substitute Zn^{2+} even after 3 months. The exchanged SUMOF-1-Co or SUMOF-1-Ni are readily reversible to the original SUMOF-1-Zn as expected, because Zn^{2+} is relatively harder than both Co^{2+} and Ni^{2+} and is expected to forms comparably more stable SUMOF. Unsurprisingly, SUMOF-1-Cu could not be reversed to SUMOF-1-Zn, this is due to higher stability of Cu-exchanged MOF. Accordingly, the stability of these materials increases from $Co^{2+} < Ni^{2+}$

< Zn^{2+} < Cu^{2+} in line with the decreasing ionic radius (increasing relative hardness) and also in agreement with the Irving-Williams series.

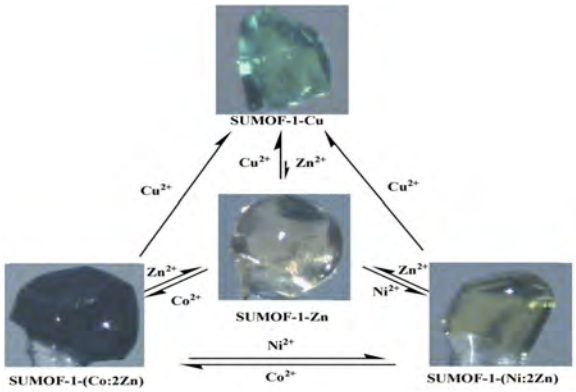

Figure 2.13: Detail cation exchange at the paddlewheel cluster of SUMOF-1. Reprinted with the consent of ref. (Yao et al., 2012). Copyright 2012 Royal Society of Chemistry.

2.2.3 Structural transformation in MOCPs

Application of crystal engineering principles allow for a facile design of reactive solids and subsequent transformation in solid state with much ease than ever before (Biradha et al., 2009). Multidirectional bond breakages and formations triggered by response to stimuli causes some reactive solids to undergo solid state structural transformation. This may involve several coordination bonds, covalent bonds, hydrogen, electrostatic or π-π interactions to be broken and remake in the process. The stimuli causing structural transformation can be due to uptake/removal of uncoordinated or coordinated solvents, gas-solid reaction, heat, photochemical reactions, mechanochemical grinding, metal-ion exchange, ligand exchange, and ligand addition/elimination (L. Aboutorabi & A. Morsali, 2016; Kole & Vittal, 2013). Response to these stimuli may obviously causes a notable change in dimensionality, coordination number/environment, chirality, interpenetration and other structural modifications.

Structural transformation and property tuning in MOCP materials is of great importance since it can furnish further understanding in to the structure-property

relationship in these materials and this may open up other opportunities for realizing new applications such as sensors, (Q. Zhang et al., 2014) magnetism, (Xiaoju Li et al., 2015; T.-H. Yang et al., 2009) adsorption and separation. (Chaemchuen et al., 2016) Several MOCPs have been reported to undergo structural transformations either reversibly or irreversibly upon respond to internal or external stimulus. For instance, a dimeric $[Hg_2(\mu\text{-}bpdb)I_4]$ (bpdb = 1,4-bis(2-pyridyl)-2,3-diaza-1,3-butadiene) was irreversibly polymerized after heating the dimeric cluster $[Hg_2(\mu\text{-}bpdb)I_4]$, to 2D coordination polymer $[Hg_2(\mu\text{-}bpdb)(\mu\text{-}I)_2I_2]_n$ (Mahmoudi & Morsali, 2008).

Another discrete zero dimensional monomer, $[Cu\text{-}(tzbc)_2(H_2O)_4]$ (Htzbc = 4-(1H-1,2,4-triazol-1-yl)) can be transformed reversibly in to a 3D 4-fold interpenetrated diamondoid MOCP, $[Cu\text{-}(tzbc)_2]$ by exposure to methanol or ethanol in a SCSC manner. The 3D MOCP can also be depolymerized to the corresponding monomers by exposure to air for 3 months (M. Liu et al., 2015) Figure 2.14.

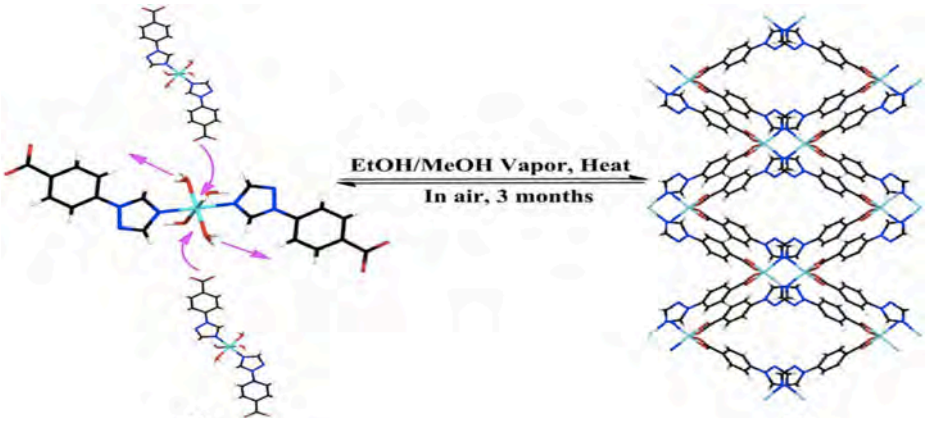

Figure 2.14: SCSC transformation of discrete monomer, $[Cu\text{-}(tzbc)_2(H_2O)_4]$ to 3D-network. (M. Liu et al., 2015)

Pan and co-workers reported a 3D condensed Er-based coordination polymer $Er_4\text{-}(bdc)_6.6H_2O$ that can be transformed to $Er_4\text{-}(bdc)_6$ and $Er_2\text{-}(bdc)_3.4H_2O$ upon desorption and reabsorption of water respectively (Pan et al., 2001). In a similar example of

absorption/reabsorption, a tetranuclear $[Fe(tpa)\{N(CN)_2\}]_4\cdot(BF_4)_4$ $(H_2O)_2$ (tpa = tris(2-pyridylmethyl)amine) was transformed to $[Fe(tpa)\{N(CN)_2\}]_4\cdot(BF_4)_4$ by removal and reinsertion of the guest water in a single-crystal to single crystal fashion (Noshiranzadeh et al., 2007; R. Wei et al., 2011). In another SCSC transformation reported by Sundberg and coworkers, on heating at 80 ^oC, an oxygenated complex $[\{(bpbp)Co_2(O_2)\}_2(NH_2bdc)]$-$(NO_3)_4\cdot 7H_2O$ (bpbp = 2,6-bis(N,N-bis(2-pyridylmethyl)-aminomethyl)-4-tert -butylphenolato; NH_2bdc = 2-amino-1,4-benzenedicarboxylato) transformed to the deoxygenated form $[\{(bpbp)Co_2(NO_3)\}_2(NH_2bdc)]$-$(NO_3)_2\cdot 2H_2O$ accompanied by translational movements of two nitrate ions. This transformation can be reversed back to the oxygenated form upon stoichiometric uptake of O_2 (Sundberg et al., 2014). In a related case of SCSC transformation, upon hydration and dehydration of, $[Dy_2(phen)_2(L)_6]\cdot 2H_2O$, (phen = 1,10-phenanthroline; L =(−)-4,5 bis(pinene)-2,2-bipyridine). (O'Keeffe et al., 2008; Y. M. Song et al., 2012) On heating $[Dy_2(phen)_2(L)_6]\cdot 2H_2O$ at 160 ^oC, the two water molecules were lost to form $[Dy_2(phen)_2(L)_6]$ and regenerated upon immersing the dehydrated form in water with retention of single crystallinity. In another remarkable transformation involving chiral Dy^{3+}-based compound $[Dy(L)_2\ (acac)_2]\cdot NO_3\cdot CH_3OH\cdot H_2O$ (L = (−)-4,5-bis(pinene)-2,2-bipyridine), Figure 2.15, also on desorption/reabsorption of solvent molecules, it underwent structural transformation to different structure by subjecting it to heat or pressure. Here, not only does the structure changed in a SCSC manner, but also the magnetic, ferroelectric and non-linear optics properties (NLO) changed (J. Liu et al., 2012).

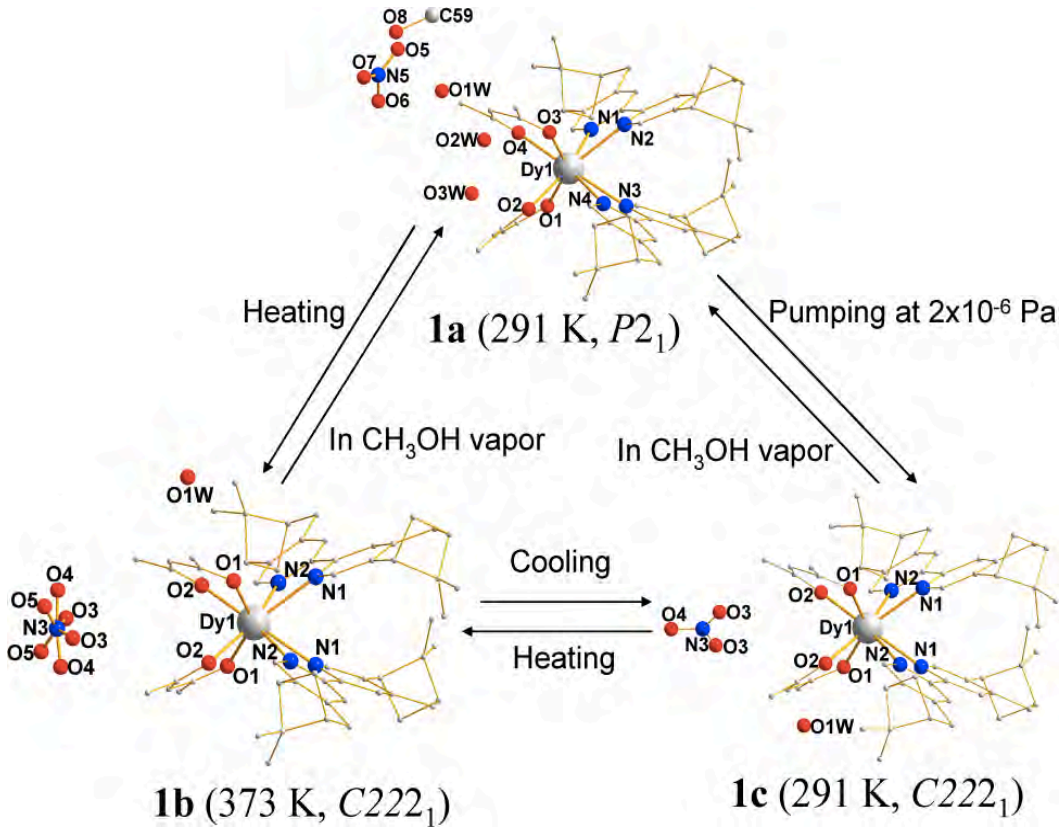

Figure 2.15: SCSC reversible transformation of $[Dy(L)_2(acac)_2]\cdot NO_3\cdot CH_3OH\cdot H_2O$ under different conditions. (J. Liu et al., 2012)

2.2.4 Solvent mediated simultaneous structural transformation and cation exchange in MOCPs via dissolution-recrystallization process

Recently, the dynamics of MOCPs in solvent mediated technique has garnered considerable interest owing to their potential applications for ion exchange, adsorption, sensor technology, drug delivery and lots more. (Akhbari & Morsali, 2013; Kang et al., 2015; Peedikakkal & Vittal, 2011; A Thirumurugan & Rao, 2005) It served as a novel approach to adjust molecular structures through either solid-state diffusion method with a non-homogenous phase exchange in which the structure remained intact (X. J. Cui et al., 2009; S. Das et al., 2009) or solvent mediated exchange mechanism with a homogenous phase reaction mechanism. The later approach involved simultaneous dissolution-recrystallization to an entirely new structure. (X. J. Cui et al., 2009; C. Y. Xu et al., 2011).

Ion exchange and structural transformation in solid state are some of the most exciting properties of hybrid metal organic coordination polymers and hence widely investigated (Brozek & Dinca, 2014; X. J. Cui et al., 2009; Fu et al., 2011; Fukushima et al., 2010; S. Furukawa et al., 2009; Kawano & Fujita, 2007; Khlobystov et al., 2002; Kole & Vittal, 2013; Schubert et al., 2008; C. Y. Xu et al., 2011). In particular, solid to solid phase transformations triggered by solvent that facilitates cation exchange has been one of the important area of investigation by material and solid state chemist (X. J. Cui et al., 2009; Fu et al., 2011; Khlobystov et al., 2002; Kole & Vittal, 2013; C. Y. Xu et al., 2011). Generally, ion exchange proceeded in one of the two common mechanisms often observed, solvent induced/mediated or solid state diffusion. In the former, the mechanism involved partial but instantaneous dissolution of the original MOCP followed by immediate recrystallization of new MOCP from the solution phase, in this case, mostly the single crystallinity is not maintained, the polymer becomes polycrystalline and often not suitable for single crystal measurements (Cametti et al., 2016; X. J. Cui et al., 2009; Fu et al., 2011; C. Huang et al., 2013; Khlobystov et al., 2002; C. Y. Xu et al., 2011; J. J. Zhang et al., 2008). In the later mechanism, it is considered to be through solid-state diffusion process reflecting true single crystal to single crystal phase transformation, here the single crystallinity is maintained at the end of the exchange and this process is usually accompanied by little or no structural transformation (Chaudhary et al., 2017; Kawano & Fujita, 2007; Kole & Vittal, 2013; P. Wang et al., 2007).

Typically, MOCPs are perceived to be insoluble due to their low solubility in common solvents. (Min & Suh, 2000; Noro et al., 2002; O. M. Yaghi & Li, 1996) In some cases, although the crystals morphology, size and shape may be preserved during ion exchange mediated by solvent, it is commonly reported to lose its transparency and subsequently turned opaque in which the single crystal integrity is compromised (Cametti et al., 2016; X. J. Cui et al., 2009; Fu et al., 2011; C. Huang et al., 2013; Khlobystov et al., 2002; C.

Y. Xu et al., 2011), which does not conform with the proposed solid-state mechanism. The observed phenomena above however, signifies substantial structural rearrangement and the accompanied change in crystal symmetry which could only be explained by dissolution recrystallization process. In addition to this, even obviously "insoluble" MOCPs may still in principle undergo solvent mediated ligand or ion exchange over long period of time due to the localized solubilization at the exterior of the crystal in suitable solvent, even though visually or spectroscopically may appears to be insoluble.

Cui and coworker (2009), argue that, the common perception that ion exchange proceeded via diffusion of free ions through the channel of the MOCPs by "solid-state mechanism" is a misconception of fact. According to them, there is no clear evidence to prove such assignment and therefore ascribed such mechanism to solvent mediated ion exchange reactions (K. J. Cui et al., 2017; X. J. Cui et al., 2009). They proceeded to prove the mechanism is purely solvent mediated and not solid state phase transformation. Series of Ag^{+}, Zn^{2+}, Cd^{2+}, and Hg^{2+} based MOCPs were synthesized and exploited for solvent mediated exchange with different anions (NO_3^{-}, $CF_2SO_3^{-}$, Bf_4^{-} or ClO_4^{-}), cations and even ligands reversibly or irreversibly through solvent mediated mechanism which involved dissolution and precipitation of the new MOCPs (X. J. Cui et al., 2009). They further examined the solubilities the MOCPs in different solvents, and found out that the solubility of the MOCP is one of the important key to its dynamic behavior. Based on their report, exchange proceeds only if the initial MOCP has appreciable solubility in a particular solvent and the expected product of exchange must be more stable than the host in equilibrium. Initial and final MOCP solubility in a particular solvent is the determining factor for the exchange and its reversibility (X. J. Cui et al., 2009). According to their results, solvents of high polarity and higher dielectric constant dissolve MOCPs more readily because, the dissolution of building block constituents can be expedited by proper

solvation of the metal cations in the framework. They conducted an interconversion of MOCPs via cation exchange exploring N- and O-donor solvents, Figure 2.16.

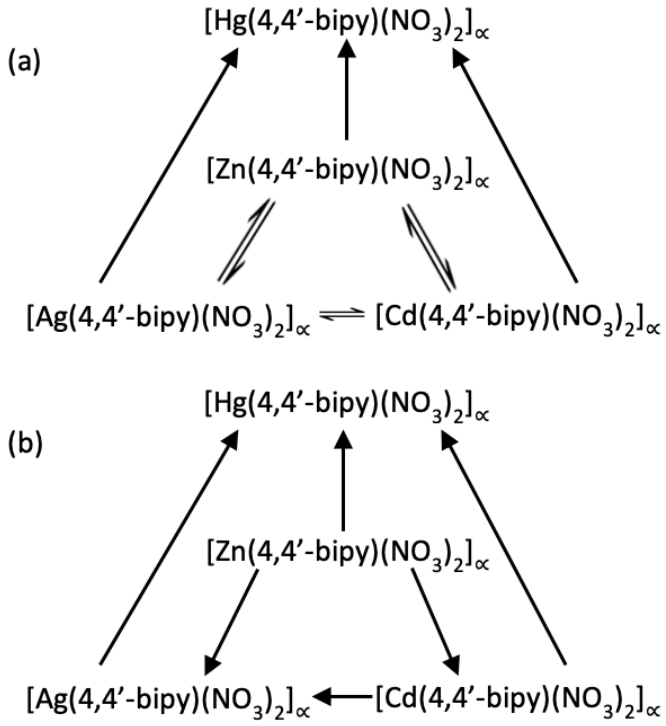

Figure 2.16: Cation exchange and interconversion summary in $[M(4,4'\text{-bipy})(NO_3)_2]_\propto$ in (a) ACN (b) MeOH. Reprinted with the consent of ref. (X. Cui et al., 2009). Copyright 2009 Wiley-VCH.

To visually monitor the evolution of the crystal morphology, environmental AFM was used after immersion into a 0.2 M solution of $NaCF_3SO_3$ or $NaBF_4$, Figure 2.17. The initial layered morphology of the pristine $[Ag(4,4'\text{-bipy})NO_3]_\propto$ changed drastically after exposure and gradually disappeared with appearance of a morphologically new phase on the surface of the former. This clearly indicate an epitaxial growth of the daughter $[Ag(4,4'\text{-bipy})CF_3SO_3]_\propto$ on the surface of the pristine Figure 2.12. (X. J. Cui et al., 2009)

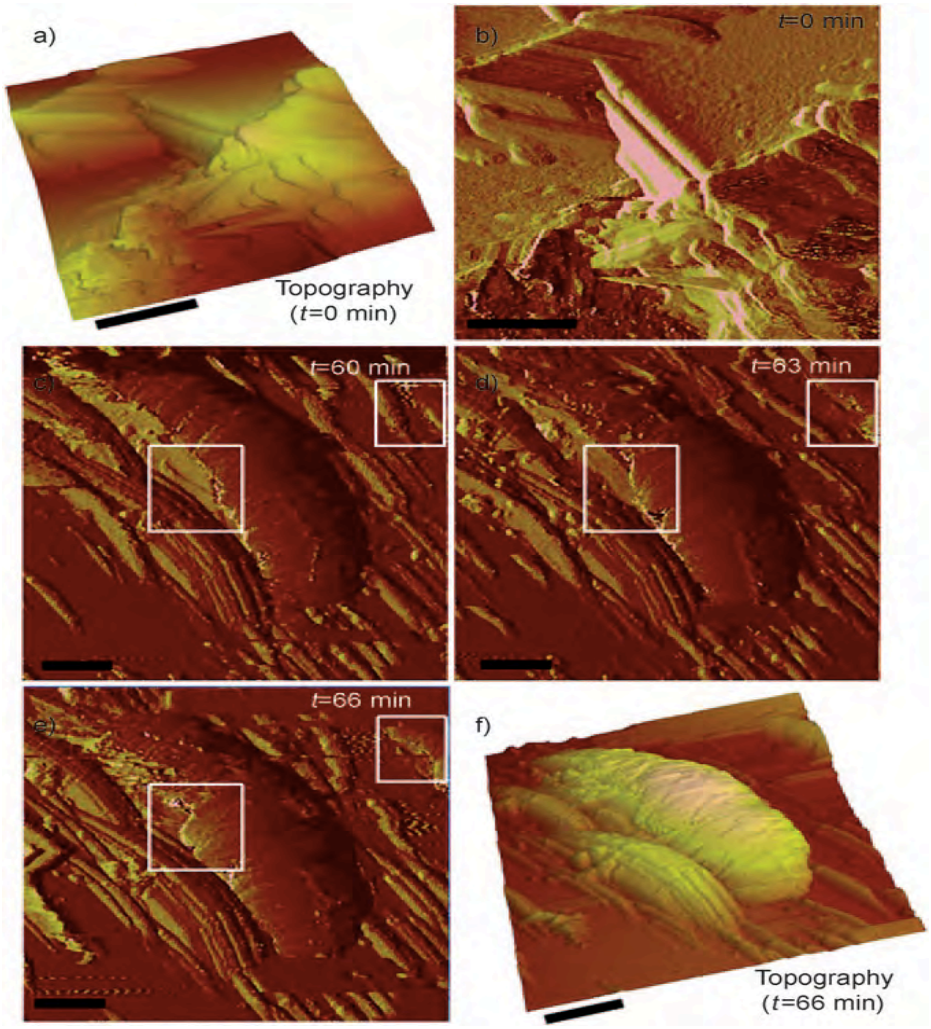

Figure 2.17: 3D topography and amplitude AFM images of the surface after immersion of $[Ag(4,4'\text{-bipy})NO_3]_\infty$ in aqueous solution of $NaCF_3SO_3$ for (a,b) t=0 mins, amplitude images at (c) t=60 mins, (d) t=63 mins (e) t=66 mins (f) the final 3D topographic view after 66 mins. (X. J. Cui et al., 2009)

In another example of solvent mediated dissolution recrystallization and exchange technique, a 1D meso-helical chain $[CdL(Ac)_2]_n$ (L = 1,4-bis(2-methylbenzimidazole-1yl-methyl)benzene, was transformed simultaneously with cation exchange upon immersion into a methanolic solution of $Hg(Ac)_2$ to another 1D zigzag chain, in which the Hg^{2+} adopt an unprecedented six-coordinated in a binuclear unit Figure 2.18, (C. Y. Xu et al., 2011).

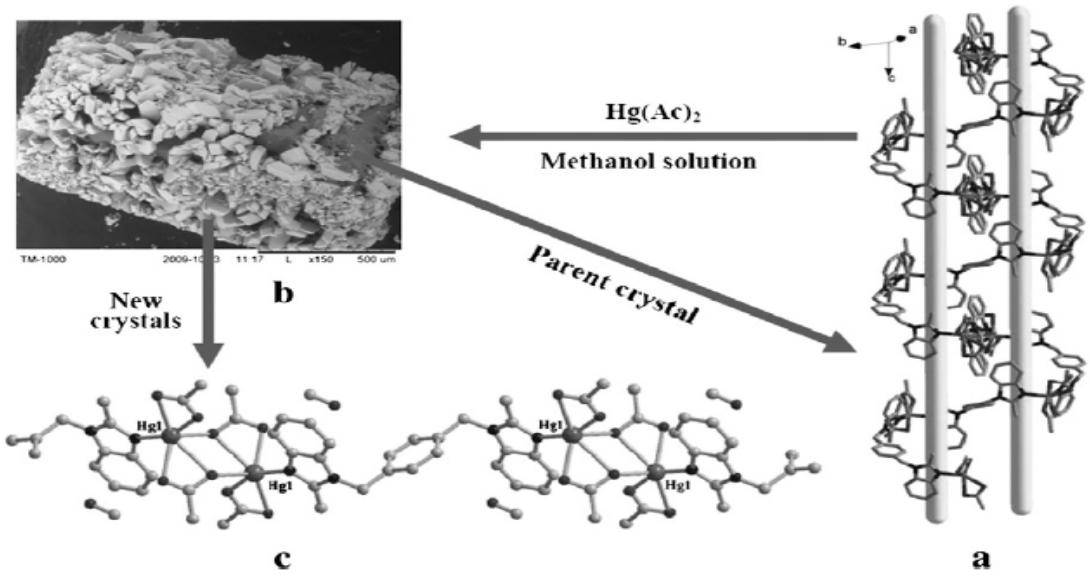

Figure 2.18: Dissolution-exchange-recrystallization process in $[CdL(Ac)_2]_n$ (a) pristine meso-helical chain (b) SEM image of the pristine with the newly recrystallized product (c) newly formed 1D zig-zag chain of Hg^{2+} exchanged. (C. Y. Xu et al., 2011)

2.2.5 Photoluminescence in MOCPs.

The process through which light is emitted by absorption of energy is known as the luminescence. Luminescence can be in two forms; fluorescence and phosphorescence which basically differs in the radiative relaxation process, depending on the spin state. While in fluorescence light is emitted between energy state of the same spin state and the process last up to 10 ns, in phosphorescence however, the light emission is between states having distinctive spin multiplicities and may last up to several seconds. (Demas, 1983; Frackowiak, 1988; IUPAC, 1997) Conventional organic and inorganic materials have been increasingly synthesized and explored owing to their exceptional properties and promising applications in optical devices, lighting, sensing or in display devices. (Binnemans, 2009; Carlos et al., 2011; Eliseeva & Bünzli, 2010; Hwang et al., 2008; Wibowo et al., 2010) Therefore, synergistic assembly of organic-inorganic components into a MOCPs is very promising strategy to build multifunctional luminescence materials, since both the component organic and inorganic can be exploited as a platform to produce

luminescence emissions. Further, the charge transfer between the components in form of ligand-to-metal or metal-to-ligand charge-transfer (LMCT or MLCT) within the MOCP can add extra dimensional luminescence emission functionalities. (Allendorf et al., 2009; Gérard Férey, 2008; Janiak, 2003; Silva et al., 2010; Suh et al., 2008) The origin of the emission can be from organic ligands especially highly conjugated ligands excitation, (Q. Fang et al., 2006; Xing Li et al., 2008) metal-centered luminescence, typically seen in lanthanides based MOCPs via the so-called lanthanide sensitization (antenna effect), (Binnemans, 2009; Moore et al., 2009) charge-transfer emissions including metal-to-ligand or ligand-to-metal charge transfer (MLCT or LMCT) (Feng et al., 2009; M.-X. Li et al., 2009; G.-H. Wang et al., 2009; Y. Wei et al., 2008) and guest induced charge-transfer. (J. An et al., 2011; Q. R. Fang et al., 2007; Luo & Batten, 2010)

Lanthanide ions (Ln^{3+}) have an intricate optical properties connected to their electronic configurations. For instance, from $4f^0$ for La^{3+} to $4f^{14}$ for Lu^{3+}, there is a gradual filling of 4f orbitals and as such, generates several energy levels. (Moore et al., 2009) With the exception of La^{3+} and Lu^{3+} with zero and filled f-orbital respectively, all other Ln^{3+} can emits typical *f–f* luminescence emissions at different region of the spectrum, from UV to Vis and NIR range. (Pieterson et al., 2001) (Moore et al., 2009) For instance, Sm^{3+}, Eu^{3+}, Tb^{3+} and Tm^{3+} luminesces orange, red, green and blue UV emissions respectively, on the other hand, Er^{3+}, Nd^{3+} and Yb^{3+} emits in the NIR region. Although Ln^{3+} exhibits an exciting optical properties, however, direct excitation is very inefficient because they are weak light absorbers owing to the forbidden f–f transitions according to the Laporte selection rule. (Steemers et al., 1995) To increase the efficiency of light absorption, Ln^{3+} are typically sensitized by incorporation into a system that can facilitate in the energy transfer process, known as the antenna effect, Figure 2.19. (Binnemans, 2009; Moore et al., 2009) This process normally involves energy migrations paths; from ligand-centered absorptions, then intersystem crossing $S_1 \rightarrow T_1$, $T_1 \rightarrow Ln^{3+}$ transition and then metal

centered emission. (Y. Cui, Y. Yue, et al., 2012) It is therefore important to judiciously design an organic linker with an appropriate energy level to generate luminescent MOCPs. This is because, for the organic ligand to act as a sensitizer it is essential that its lowest triplet state is localized at an energy level nearly the same or above the resonance level of the Ln^{3+} ions.

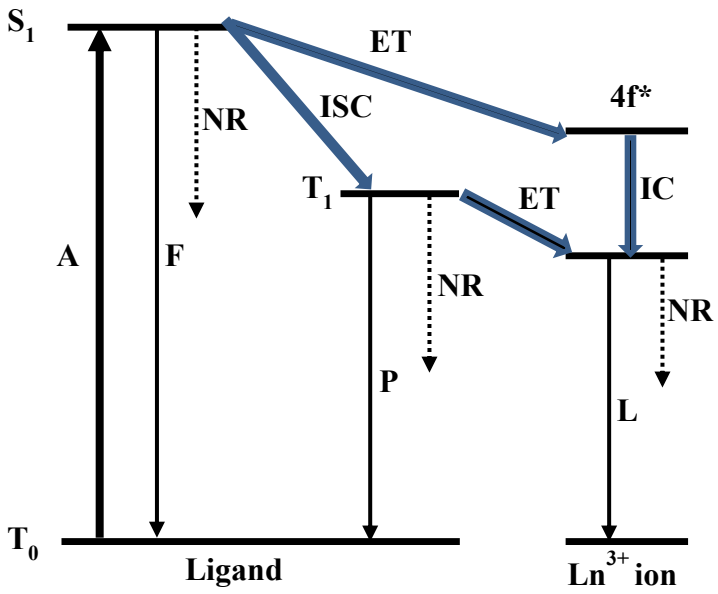

Figure 2.19: Jablonski diagram schematics of energy absorption, transfer, emission and process in MOCPs. Where S, T, A, F, P, L, ET, NR, ISC and IC are singlet, triplet, absorption, fluorescence, phosphorescence, lanthanide centered luminescence, energy transfer, non-radiative transition, intersystem crossing, and internal conversion respectively.

Modularity, heterogeneity, diverse and intriguing structures coupled with tunable optical emissions endows MOCPs with huge potentials to be an excellent materials for light-emitting devices. Several MOCPs featuring tunable photoluminescence have been engineered and explored. (Allendorf et al., 2009; Mahata et al., 2017; Meyer et al., 2014) (Heine & Müller-Buschbaum, 2013; Z. Hu et al., 2014; Luo & Batten, 2010; Y. Zhang et al., 2018)

In an example of a heterometallic MOCP luminescence displaying an antenna effect, (Y.-Q. Sun et al., 2006) $[LnCd(imdc)(SO_4)(H_2O)_3]\cdot 0.5H_2O$ (Ln = Nd, Eu, Tb, Er, Yb,

Gd, Dy or Pr, imdc = 4,5-imidazoledicaboxylate), the Dy–Cd, Eu–Cd and Tb–Cd heterometal MOCPs exhibit the typical *f–f* character emission of Ln^{3+} ions. Gd–Cd however, shows 3 broad peaks, which may be ascribed to the ligand phosphorescence, ligand centered fluorescence and LMCT transitions, while, Pr–Cd and Nd–Cd MOCPs do not display the expected NIR emission, indicating that there is no efficient energy transfer by the ligand to Pr^{3+} or Nd^{3+} to emits the NIR luminescence. In a related example of heterometallic luminescing Ln-Ag MOCPs, (X.-Q. Zhao et al., 2009) $[LnAg(PDA)_2(H_2O)_3]\cdot 3H_2O$, $[PrAg(PDA)_2(H_2O)_3]\cdot 2.5H_2O$ and $[CeAg_2(PDA)_2(py)_4]\cdot H_2O$ (Ln = Eu^{3+}, Sm^{3+}, Tb^{3+}, Ce^{3+}, Nd^{3+}, Dy^{3+}, PDC = pyridine-2,6-dicaboxylate, py = pyridine), the Eu–Ag, Dy–Ag, Tb–Ag and Sm–Ag MOCPs displayed the typical Ln^{3+} character interestingly in both solid state and in DMF solvent. Further, the on addition of Mg^{2+} in DMF solution, the luminescence intensity of Eu–Ag decreases, while that of Dy–Ag increases significantly compared to that of Tb–Ag that increases slightly.

A series of NIR emitting multi-cation Ln–Ag MOCPs was also reported by Jin and coworkers, (J. Jin et al., 2010) $LnAg_5(1,2\text{-BDC})_4$, (1,2-BDC = 1,2-benzenedicaboxylate, Ln = Er, Ho, Yb). The Yb–Ag displayed a broad luminescence band from 950 to 1050 nm which was assigned to the $^2F_{5/2} \rightarrow {}^2F_{7/2}$ transition typical of Yb^{3+} ion. In Ho–Ag however, a peak emission at 995 nm was ascribed to $^5F_5 \rightarrow {}^5I_7$ and a band at 1400 to 1600 attributed to the splitting of $^5F_5 \rightarrow {}^5I_6$ transition and the Er–Ag displayed a broad peak between 1450 and 1650 nm assigned to the $^4I_{13/2} \rightarrow {}^4I_{15/2}$ transition of Er^{3+}. Compared to the isolated Ln^{3+} emission bands, in these MOCPs shifting, broadening and splitting emission spectra was observed and this could be ascribed to the influence and interaction of 4d and 4f orbitals. Number of examples of heterometallic Ln^{3+}–Cu^{+} MOCP was reported by Bo and coworkers. The heterometals assembled into an MOCP using mixed ligands to form $Ln(pydc)_3Cu_3(bipy)_3\cdot m(H_2O)$ (Ln = Eu, Tb, Gd, Sm, Yb, Er, m = 4; Ln =

Nd, Pr, *m* = 5, pydc = 2,6-pyridinedicarboxylate, bipy = 4,4'-bipyridine). (Bo et al., 2010) Here the multi metals are linked by mixed ligands into a spindle-like shaped multimetal rings SBUs, $[Ln_6(pydc)_6Cu_{12}(bipy)_6]$ which is further pillared by bipy ligands into a 3D Ln–Cu MOCP, Figure 2.20.

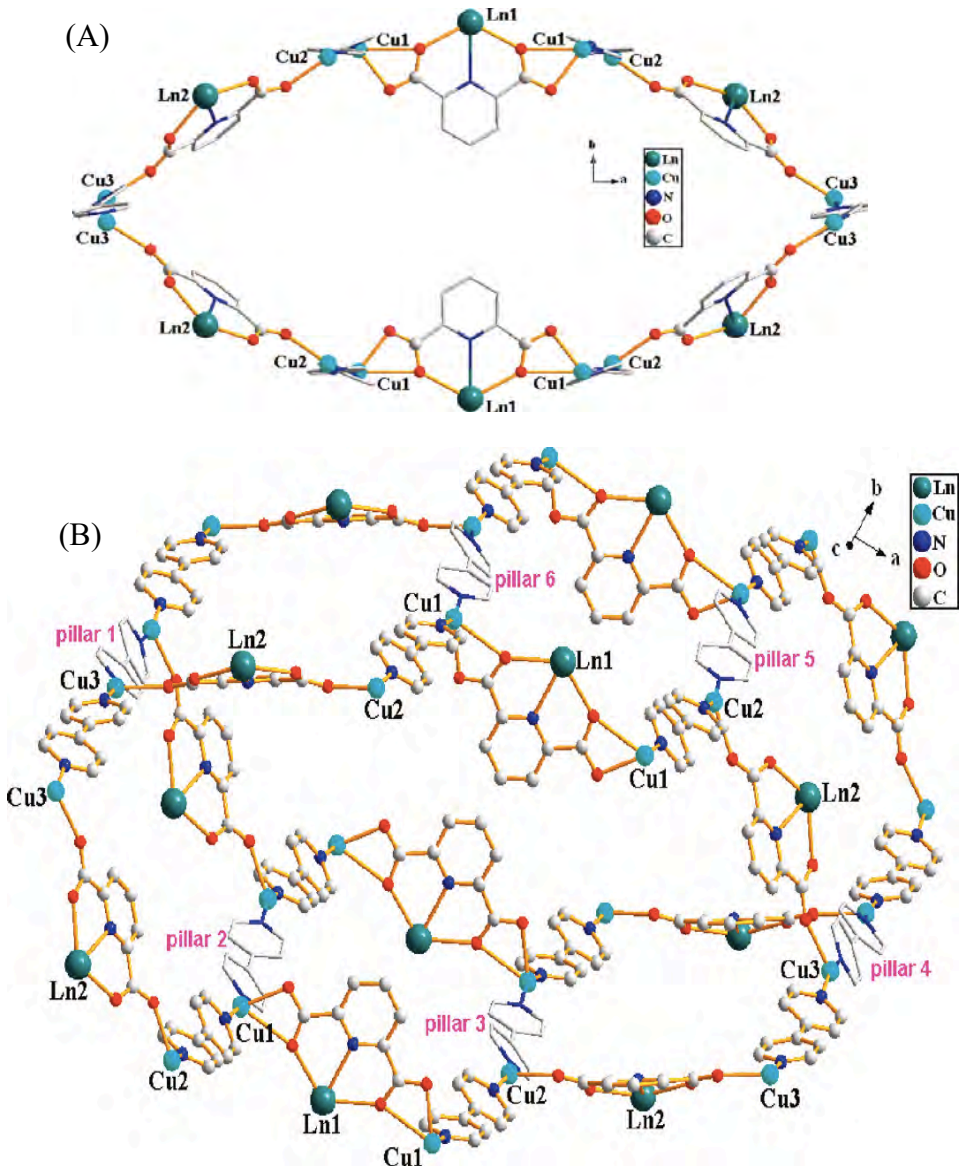

Figure 2.20: (A) Spindle-like shaped multimetal rings SBUs, $[Ln_6(pydc)_6Cu_{12}(bipy)_6]$ and (B) pillared layer structure with bipy pillar incorporated between the 2 layers forming $Ln(pydc)_3Cu_3(bipy)_3 \cdot m(H_2O)$. (Bo et al., 2010)

The Nd–Cu shows the strongest emission peak at 1062 nm assigned to $^4F_{3/2} \rightarrow {}^4I_{11/2}$ transition typical to Nd^{3+} ion, while a broad peak at 895 nm is ascribed to $^4F_{3/2} \rightarrow {}^4I_{9/2}$

transition in addition to a sharp weak emission band at 1345 nm assigned to $^4F_{3/2} \rightarrow {}^4I_{13/2}$ transition. Yb–Cu MOCP shows a strong emission at 980 nm, assigned to $^2F_{5/2} \rightarrow {}^2F_{7/2}$ transition in the NIR region typical to Yb^{3+} ion. However, all others, Eu–Cu, Sm–Cu, and Tb–Cu MOCPs displayed their corresponding characteristic emissions, while Er–Cu, Pr–Cu and Gd–Cu two intense emission bands located at 532 and 488 nm were observed, which is comparable to those observed in Cu(I) complexes that are associated with MLCT transition, Figure 2.21.

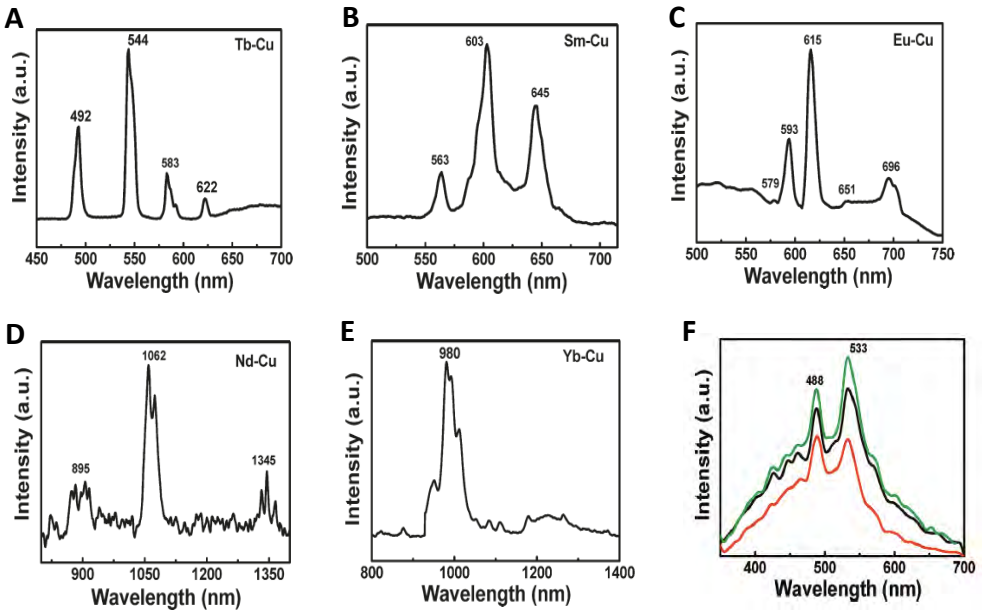

Figure 2.21: Room temperature solid state photoluminescence emission spectra of (A) Tb–Cu at 275 nm, (B) Sm–Cu at 275 nm, (C) Eu–Cu at 275 nm, (D) Nd–Cu at 280 nm, (E) Yb–Cu at 275 nm, (F) Pr–Cu (red), Gd–Cu (black) and Er–Cu (green) excited at 240 nm. (Bo et al., 2010)

Several strategies have been developed to tune the photoluminescence emission as a function of Ln^{3+} concentration. For instance, the emission property of $Eu_{1-x}Tb_x(BTC)(H_2O)$, can be tuned by gradually changing the Tb/Eu ratio (2.75, 2.44, 1.95, 1.46, 1.02, 0.40, and 0.26). (Guo et al., 2010) The compiled PL emission spectra, Figure 2.16, shows that, the spectral band located in the green region at 540 nm, assigned to $^5D_4 \rightarrow {}^7F_5$ transition is typical to Tb^{3+}. Two main transition bands $^5D_0 \rightarrow {}^7F_1$ and $^5D_0 \rightarrow {}^7F_2$

located at 589 and 615 nm are typical to Eu^{3+}. It was observed that, the intensity of band located at 540 nm assigned to Tb^{3+} emission changes as a function of Tb/Eu ratio indicating energy transfer and gradually the characteristic emission peaks of Tb^{3+} disappear at a Tb/Eu, ratio equal to 1, Figure 2.22 (e), suggesting efficient energy transfer from Tb^{3+} to Eu^{3+}.

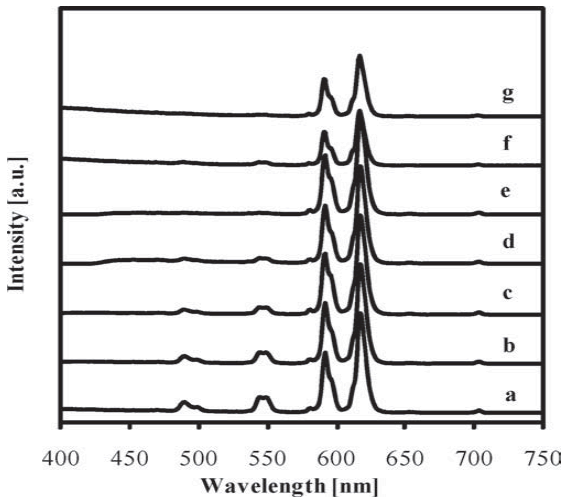

Figure 2.22: Solid state emission spectra of $Eu_{1-x}Tb_x(BTC)(H_2O)$; Tb/Eu mole ratio (a) 2.75, (b) 2.44, (c) 1.95, (d) 1.46, (e) 1.02, (f) 0.40 and (g) 0.30. (Guo et al., 2010)

On another example of tuning luminescence emission, the photoluminescence emission of Tb-based MOCP, $Tb(BTC)(H_2O)\cdot 3H_2O$ can be tuned from green, to green-yellow, yellow, orange, red-orange by doping with variable amounts of Eu^{3+}. The pristine $Tb(BTC)(H_2O)\cdot 3H_2O$ displayed four spectral peaks approximately at 487,543, 580 and 620 nm assigned to $^5D_4 \rightarrow {}^7F_J$ where J = 6, 5, 4, and 3, respectively, Figure 2.17 (a). On doping with Eu^{3+} (0.1, 0.3, 0.5, 1, 5, and 10 mole %), the emission character of Tb^{3+} gradually decreases while the emission character of Eu^{3+} increases, however, the luminescence of Eu^{3+} increases until maximum at 1 mole % and gradually decreases with increase of Eu^{3+}, which can be attributed to the concentration quenching effect, Figure 2.23(a). The CIE coordinates of the Eu^{3+} doped MOCP changes from (0.264, 0.620) to (0.596, 0.370) as a function of increasing dopant amount, Figure 2.23 (b)

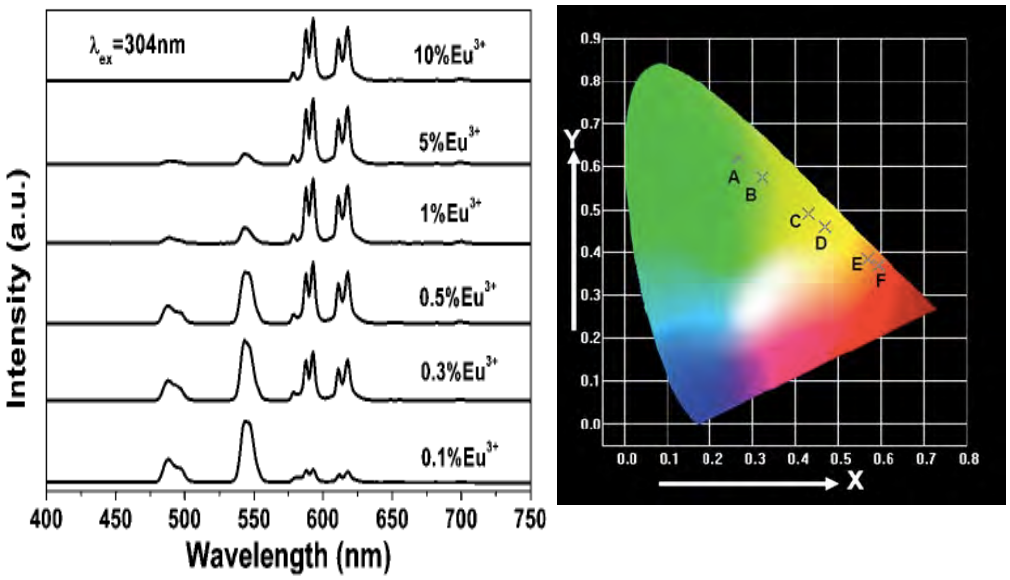

(A) (B)

Figure 2.23: Solid state emission spectra of $Eu_{1-x}Tb_x(BTC)(H_2O)\cdot 3H_2O$; Tb/Eu mole ratio ($x = 0.1 – 10$ mole %) excited at 304 nm (A), and the corresponding CIE chromaticity diagram (B).

Guest exchange or modification in the pores of porous MOCPs can also generate exceptional optical emission properties. For example, when Tb^{3+}, Eu^{3+}, or Nd^{3+} hydrates are inserted into the framework of Pb_2L_2 (L = 1,5-bis(*m*-carboxyphenoxy)-3-oxapentane) which is a crown-ether like MOCP, the incorporated guest can be reversibly exchanged that endows the MOCP with dual and bimodal photoluminescence, the emission bands and intensities can also be tuned by manipulating the Ln^{3+} ions exchange. (Jiang et al., 2009) For example, upon immersion of Pb_2L_2 MOCP into an aqueous solution of $Tb(ClO_4)_3$ a typical characteristic peaks of Tb^{3+} was observed in the solid state spectrum. When $Tb@Pb_2L_2$ was immersed in $Eu(ClO_4)_3$ solution, hydrated Tb^{3+} was partially exchanged by hydrated Eu^{3+} generating multi-metal guest system. The solid state dual emission intensities is produced from both the Ln^{3+} ions and can be tuned by controlling the Eu/Tb exchange ratio. The $Tb@Pb_2L_2$ can also be partially exchange by NIR emitting Nd^{3+}, and a similar photoluminescence emission tuning was observed. In another example of ion exchange tunable photoluminescence, Gd_2L (L = 3,3'-(4-amino-4H-1,2,4-triazole-

3,5-diyl)dibenzoate) with a cage like pore that can be used to encapsulate $[Mn(H_2O)_6]^{2+}$ cations, Figure 2.24. (Peng Wang et al., 2007) The MOCP containing the encapsulated cation $[Gd_2LMn(H_2O)_6]\cdot 0.5H_2O$ displayed a blue shifted emission band at 428 nm due to MLCT.

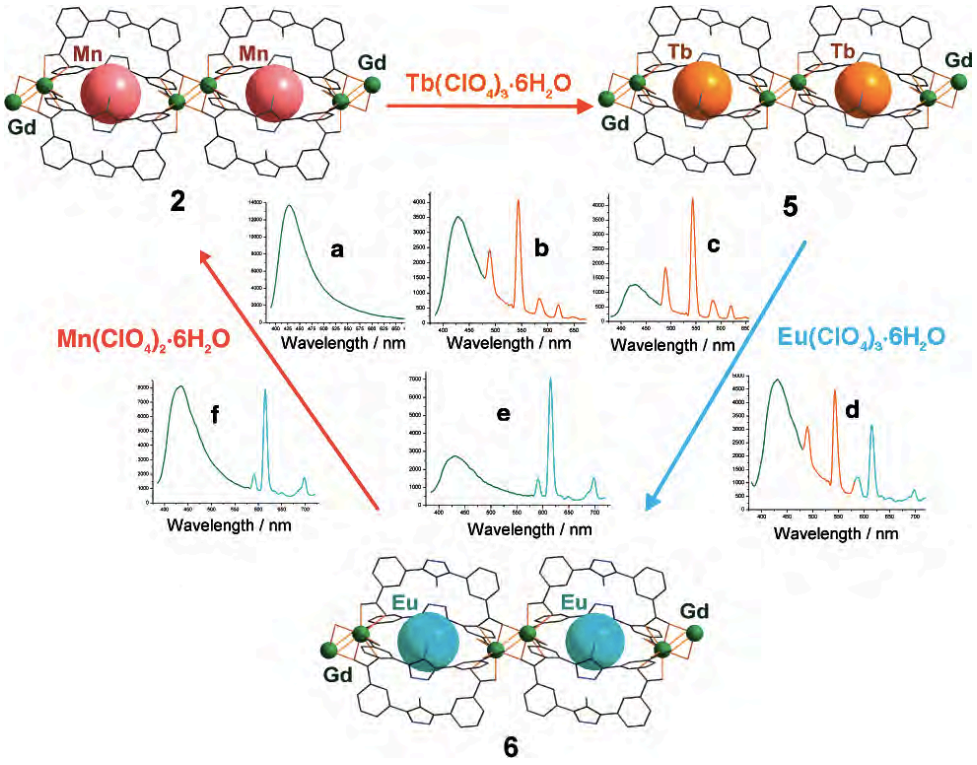

Figure 2.24: Process of guest cation exchange in of $[Gd_2LMn(H_2O)_6]\cdot 0.5H_2O$ and the solid state luminescence emission spectra excited at 386 nm; (a–c) after soaking $[Gd_2LMn(H_2O)_6]\cdot 0.5H_2O$ in aqueous solution of $Tb(ClO_4)_3$ to give $[Gd_2L_4Tb(H_2O)_8ClO_4]\cdot 0.5H_2O$, for 0, 2 and 7 days respectively, (c–e) after soaking $[Gd_2L_4Tb(H_2O)_8ClO_4]\cdot 0.5H_2O$ in $Eu(ClO_4)_3$ for 0, 2 and 7 days respectively, and (e–a) after soaking $\{[(Gd_2L_4)Eu(H_2O)_8ClO_4]\cdot 0.5H_2O\}_n$ in $Mn(ClO_4)_3$ back to for 0, 2 and 7 days respectively. (Peng Wang et al., 2007)

Interestingly, $[Gd_2LMn(H_2O)_6]\cdot 0.5H_2O$ can reversibly cation substituted with $[Eu(H_2O)_8]^{3+}$ or $[Tb(H_2O)_8]^{3+}$ to $\{[(Gd_2L_4)Eu(H_2O)_8ClO_4]\cdot 0.5H_2O\}_n$ or $[Gd_2L_4Tb(H_2O)_8ClO_4]\cdot 0.5H_2O$ in a SC-SC manner respectively. The exchanged product emits a typical Eu^{3+} or Tb^{3+} characteristic peaks with decrease in emission intensity of $[Gd_2LMn(H_2O)_6]\cdot 0.5H_2O$.

2.2.6 Magnetic susceptibility

Magnetic susceptibility in materials is principally dependent on the magnetic dipole moment associated with the spin or intrinsic angular momentum of its electrons. Magnetism in materials can be characterized as diamagnetic, paramagnetic, ferromagnetic or antiferromagnetic depending on the response to the external magnetic field applied. (Buschow & Boer, 2003; Jiles, 2015) Judicious choice of metal cation and functional organic linker and their synergistic interaction in the framework of the solid material can be used to incorporate some electronic properties. Several MOCPs exhibiting magnetic properties such as cooperative spin crossover, magnetic ordering and those exhibiting molecular properties such as single-molecule magnetism. Majority of magnetic MOCPs has been reported as high temperature magnets, for instance, the molecule-based magnetic MOCPs with spontaneous magnetization above room temperature. (Manriquez et al., 1991) Large number of MOCPs were reported to have different magnetic functionalities; such as ferromagnetic, (Duan et al., 2009) single chain magnet, (Z.-X. Li et al., 2010) antiferromagnetic, (E.-C. Yang et al., 2010) metamagnetic, (X. H. Zhang et al., 2011) spin canting (Z.-X. Li et al., 2009) and spin-glass behavior, (Tran & Świątek-Tran, 2008). In addition to this, different coordination modes of carboxylate ligands that can adopt *syn* or *anti* configuration that have influence on the magnetic exchange between the proximal cations, and paramagnetic cations produce an interesting structures which allows the study of the magnetic and structure relationship. (Kato & Muto, 1988; P. King et al., 2003)

CHAPTER 3: MATERIALS AND METHODS

All reagents were purchased from Sigma-Aldrich and used without further purification. Quantitative analyses (atomic percentage of elements) were performed using Hitachi SU8220 Scanning Electron Microscope-Energy Dispersive Spectrometry (SEM-EDS). Li/Pb stoichiometric ratio, in particular, was determined using an analytikjena PlasmaQuant PQ 9000 Inductively Coupled Plasma-Optical Emission Spectroscopy (ICP-OES) spectrometry.

3.1 Materials

3.1.1 Inorganic salts

PbO, $Ln(NO_3)_3.5H_2O$ (Ln = Sm, Eu, Gd, Tb and Er), $Fe(OAc_2)_2$, $FeCl_2$, $Co(NO_3)_2.6H_2O$, $CoCl_2.6H_2O$ $Cd(NO_3)_2$ $Hg(NO_3)_2.H_2O$, $Zn(NO_3)_2.6H_2O$, $Ni(NO_3)_2.6H_2O$, $Cu(NO_3)_2.3H_2O$, $Cu(OAc_2)_2.H_2O$, $CuCl_2.2H_2O$, $Cd(NO_3)_2$, $Ag(NO_3)$, $Ce(OAc_2)_3.xH_2O$, $Li(NO_3)$, $Li(OAc_2)$, LiOH, $LiPF_6$, LiI, NaOH and KOH.

3.1.2 Organic reagents

Pyrazine-2,3-dicarboxylic acid, Piperazine, pyridine, pyradazine, imidazole, ethylenediamine, and diethylamine.

3.1.3 Solvents

Distilled water, DMF, dioxane, DMSO, THF, ACN, acetone and ethanol.

3.1.4 Glass and non-glassware

250 mL beakers, glass tube, test tube, glass vials with screws, 30 mL specimen bottles, 10 mL measuring cylinders, glass funnel, thermometers, spatulas, weighing paper, filter paper, spatula, aspirating bottles, wipes and hand towel.

3.1.5 Equipment and Instruments

Weighing balance, hot plate magnetic stirrer, vacuum pump, sonicator, programmable electric oven, optical microscope, optical camera, UV box, powder and single crystal X-ray diffractometer (P/SC-XRD), Steady-state and time-resolved photoluminescence (TRPL) spectrometer equipped with xenon lamp and a TCSPC module, FESEM-EDX, ATR-FTIR, ICP-MS, XPS, VSM, and Solartron Impedance Analyzer.

3.2 Experimental Methods

3.2.1 Synthesis of precursor 1D MOCP ($Pb_2Cl_2(Hpzdc)_2(H_2O)_2$)

A similar synthesis procedure reported by us (Fendi Y. Wardana et al., 2015; S. Zhang et al., 2012) with further optimizations was adopted. Based on the new optimized method, the onset of the crystal formation time was greatly reduced to almost immediately, the clear solution was filtered and crystallization proceeded to completion within two to three hours. A mixture of PbO (0.089 g, 0.4 mmol), H_2pzdc (0.067 g, 0.4 mmol), and piperazine (0.0215 g, 0.25 mmol) in DI water (20 ml) was heated and stirred at 70 ˚C. Subsequently, 10 drops of conc. HCl was added dropwise into the mixture resulting in a clear solution. The stirring and heating were continued for 5 mins. Large, colorless, ribbon crystals were obtained in a quantitative yield after 2-3 hours of slow evaporation. The final products were isolated by vacuum filtration, and dried at room temperature, with 75 – 90 % yields based on the PbO.

3.2.2 Synthesis of Li^+/Pb doped MOCP

Precursor 1D MOCP (0.03 g, 0.035 mmol) was immersed into a ~7 ml aqueous solution of different Li(I)X precursor, X = NO_3, OAc, OH, I, and PF_6 (0.066 mmol). The dissolution-recrystallization progress was examined in-situ under an optical microscope as a function of soaking time at room temperature. The obtained products (after 3d of soaking) were then washed thoroughly with fresh DI water and dried at room temperature

prior to further characterizations. Yield of circa. 80 % based on the 1D MOCP. A quantitative analysis was performed by ICP-OES on some selected compounds.

3.2.3 Synthesis of M^{2+}/Pb doped MOCPs

Precursor 1D MOCP (0.03 g, 0.035 mmol) was immersed into a ~7 ml aqueous solution of either nitrate and/or chloride precursor of M^{2+}, M = Co, Ni, Zn, or Cd (0.066 mmol). Washing and characterizations procedures were done similar to those of monovalent soaking. A semi-quantitative analysis was performed by SEM-EDS. The products were collected after 3d of soaking. Yield of circa. 75 - 80 % based on the 1D MOCP.

3.2.4 Synthesis of M^{3+}/Pb doped MOCPs

Precursor 1D MOCP (0.03 g, 0.035 mmol) was immersed into a ~7 ml aqueous solution of nitrate precursor of Ln^{3+}, Ln = La, Eu, Gd, Tb, or Er (0.066 mmol). Washing and characterizations procedures were done similar to those of divalent soaking. The products were collected in quantitative yields after 3d of soaking. Yield of circa. 60 - 80 % based on the 1D MOCP.

3.2.5 Synthesis of M^{3+}/Pb (M = Eu, Tb) MOCPs with dopant variations under guidance of HSAB principle

Precursor 1D MOCP (0.03 g, 0.035 mmol) was immersed into a: ~7 ml aqueous solution, for condition (1) or ~7 ml H_2O/Dioxane/DMF mixture with the addition of 2 drops of pyridine, for condition (2) or same as (2) but with heating at 60 ^oC for 24 h, for condition (3), of nitrate precursor of Ln^{3+}, Ln = Eu or Tb (0.066 mmol). Washing and characterizations procedures were done similar to those of divalent soaking. The products were collected in yield of circa. 60 - 80 % based on the 1D MOCP after 3d of soaking, except for condition (3).

3.2.6 Synthesis of M^{3+}/M^{2+}/Pb doped MOCPs

Precursor 1D MOCP (0.03 g, 0.035 mmol) was immersed into a ~7 ml aqueous solution of nitrate precursors of a mixture of Eu^{3+} (0.035 mmol) and Zn^{2+} (0.035 mmol). Washing and characterizations procedures were done similar to those of divalent soaking. The products were collected in yield of circa. 60 - 80 % based on the 1D MOCP after 3d of soaking.

3.2.7 Synthesis of M^{n+}/M^{n+}/Pb double doped MOCPs

Precursor 1D MOCP (0.03 g, 0.035 mmol) was immersed into a ~7 ml aqueous solution of nitrate precursors of a mixture of M^{n+} (0.035 mmol) and M^{n+} (0.035 mmol). To vary the dopant we use the same mole rations, but a mixture of solvents DMF:dioxane:H_2O with 2 drops of pyridine was also used. Washing and characterizations procedures were done similar to those of divalent soaking. The products were collected in yield of circa. 50 - 80 % based on the 1D MOCP after 3d of soaking. (M = TMs or Lns and n = 2 or 3)

3.2.8 Synthesis of $M^{n+}/M^{n+}/M^{n+}$/Pb triple doped MOCPs

Precursor 1D MOCP (0.03 g, 0.035 mmol) was immersed into a ~7 ml aqueous solution of nitrate precursors of a mixture of M^{2+} (0.035 mmol) and M^{2+} (0.035 mmol). To vary the dopant we use the same mole rations, but a mixture of solvents DMF:dioxane:H_2O with 2 drops of pyridine was also used. Washing and characterizations procedures were done similar to those of divalent soaking. The products were collected in yield of circa. 50 – 80 % based on the 1D MOCP after 3d of soaking.

3.2.9 Rendering cation-exchanged product into a doped MOCP

Cation-exchanged product was produced when the precursor 1D MOCP (0.03 g, 0.035 mmol) was immersed into a ~7 ml aqueous solution of $FeCl_2$ or $CuCl_2$ (0.066 mmol). Rendering this into a doped product was successfully done by soaking the precursor 1D

MOCP (0.03 g, 0.035 mmol) into a ~7 ml DMF/H_2O (1:1) solution of $FeCl_2$ (0.066 mmol) or a ~7 ml DMF/H_2O/1,4-dioxane (1:1:1) solution of Copper (II) acetate (0.066 mmol). Washing and characterizations procedures were done similar to those of divalent soaking. The products were collected in yield of circa. 50 - 80 % based on the 1D MOCP after 3d of soaking.

3.2.10 Soaking 3D Pb MOCP in a solution of divalent cation precursor at room temperature

The 3D Pb MOCP, $Pb_3(pzdc)_3(H_2O)$, was synthesized according to the literature. (S. Zhang et al., 2012) The resulting product (0.03 g, 0.035 mmol) was immersed into a ~7 ml aqueous solution of either nitrate and/or chloride precursor of Co^{2+} (0.066 mmol). The dissolution-recrystallization progress was examined in-situ under an optical microscope as a function of soaking time at room temperature. Two batches of products (after 3d and nearly 1 month of soaking) were then washed thoroughly with fresh DI water and dried at room temperature prior to further characterizations. A semi-quantitative analysis was performed by SEM-EDS.

3.3 Measurement Procedures

3.3.1 X-ray Crystallography

Single crystal X-ray diffraction was performed on a Bruker Kappa APEX2 diffractometer with a MoKα (λ = 0.71073 Å) IμS microfocus source at 100 K. Prior to data collections, the single crystal samples were stored in a small amount of corresponding mother liquor in which each dissolution-recrystallization occurred. Data collection, cell refinement, and data reduction were carried out using the program APEX3. (Bruker, 2002) Numerical absorption corrections were performed with the program SADABS. Using Olex2, (Dolomanov et al., 2009) the structure was solved with the ShelXS (Sheldrick, 2008) structure solution program using Direct Methods and

refined with the XL (Sheldrick, 2008) refinement package using Least Squares minimization.

3.3.1.1 Cation vacancy refinements

Most of the crystallographic contrast between the substituent and the Pb atoms sharing the same site comes from the refinement of the partial occupancy factor of the Pb atoms. Since the atomic structure factor of Pb is very large, determination of the partial occupancy of Pb is very sensitive to the amount of substitution. As the substituted members are semiconductors, all crystallographic refinements were performed assuming charge balance. Therefore, a soft constrain (SUMP command) was used for imposing charge balance for all atoms that occupy partially the Pb sites. Because the valence state of most substituents is different (aliovalent) than that of Pb^{2+}, as confirmed by X-ray Photoemission measurements, a small amount of vacancies must be utilized in order to have charge balance.

3.3.2 Powder X-ray Diffraction

Ground single crystals of the samples were used to collect powder X-ray diffraction patterns using a PanAlytical X'Pert Pro Powder Diffractometer (Cu Kα radiation λ = 1.5418 Å) over the 2 range of 5 - 50^0, with a step size of 0.02° and a scan speed of 0.25°/min. The measured patterns were compared to the simulated diffraction patterns using the respective single crystal data.

3.3.3 X-ray Photoelectron Spectroscopy (XPS)

X-ray photoelectron studies were performed using a Thermo Scientific ESCALAB 250 Xi spectrometer equipped with a monochromatic Al Kα X-ray source (1486.6 eV) and operated at 300 W. Samples were analysed under vacuum ($P < 10^{-8}$ mbar), whereas survey scans and high-resolution scans were collected using pass energy of 50 eV. Binding energies were referred to the C 1s binding energy at 284.6 eV. A low-energy

electron flood gun was employed for charge neutralization and ion beam etching for surface cleaning. Prior to XPS measurements, ground crystals of each sample attached on copper foil and mounted on stubs and successively put into the entry-load chamber to pump.

3.3.4 Solid state photoluminescence measurements

Solid state photoluminescence measurements were performed using a Horiba LabRam Evolution high-resolution confocal Raman microscope spectrometer (600 g/mm diffraction grating) equipped with a diode continuous wave laser (473 nm, 25 mW) and a Synapse charge-coupled device camera. The maximum power output of the laser source was filtered to 1% of the maximum power output. While the variation of dopant amounts for the tunable PL emission was conducted using FLS920, Edinburgh Instrument with steady-state time resolved PL measurement capability, 50ps to ns time range. Equipped with 450W xenon lamp excitation source for the emission analysis and TCSPC module for time resolved.

3.3.5 Solid state UV-Vis-NIR measurements

Solid state UV-Vis was carried out using diffuse reflectance Perkin Elmer Lambda 950, equipped with an integrating sphere.

3.3.6 Conductivity measurements

Dried crystals were crushed into powder and pellets were formed using Specac manual hydraulic press instrument that can deliver up to 25 ton. About 1.8 ton was used to form all the pellets for the conductivity measurement. All pellets has 13 mm diameter and variable thicknesses were measured using AICEYI portable digital display plastic film thickness measuring instrument. Nicely formed pellets were sandwiched between two copper electrodes and wires were connected to each disc. Impedance measurements was conducted using Solartron 1620A frequency response analyzer/impedance/gain-phase

analyzer and all data were determined at amplitude 0 V DC and 250 mV AC bias with frequency range 1 MHz to 1 Hz, in some cases at 10 MHz to 1 KHz. The conductivity σ, was calculated using equation 1. Resistance was obtained by circle fittings.

$$\sigma = \frac{L}{R.A} \quad \text{.....(3.1)}$$

Where L, R and A are thickness (m), Resistance (Ω) and area (m^2).

3.3.7 Magnetic susceptibility measurement

The magnetic susceptibility of the dried crystalline powder samples of pristine and Fe^{2+}, Tb^{3+}, Eu^{3+}, Co^{2+}, Fe^{3+}-doped 3D MOCPs were analyzed using Lake Shore, 7400 series Vibrating Sample Magnetometry (VSM) system, with a field maximum of 8000 Oe. The DC magnetic properties of the samples was characterized as a function of magnetic field at room temperature with the field sweeping from -8000 to 8000 Oe. The hysteresis was analyzed using the Lake Shore software version 4.6.0.

CHAPTER 4: RESULTS AND DISCUSSION

4.1 Justification for the selection of 1D ($Pb_2Cl_2(Hpzdc)_2(H_2O)_2$

The dynamics of hybrid MOCPs has been of interest due to their potential applications such as ion-exchange, chemical and physical adsorption, sensors, magnetism, conductivity, drug delivery, catalytic and solid state lighting (Janiak, 2003).

A Pb^{2+}-based 1D coordination polymer ($Pb_2Cl_2(Hpzdc)_2(H_2O)_2$) reported by Wardana and co-workers (2015), containing ladder-like centro-symmetric Pb_2Cl_2 dimers forming a chain by connecting to the mono-protonated carboxylic ($Hpzdc^-$), and a chlorine bridging was identified and selected for facile solid solution. The Pb^{2+} ion center is 7 coordinated with O and N-donors from $Hpzdc^-$, O-donor atom from H_2O and Cl ions completing the coordination sphere, Figure 4.3.

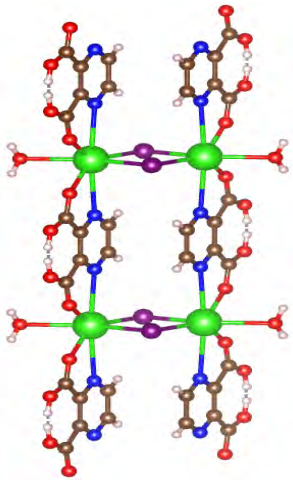

Figure 4.1: Ladder-like dimers connected by $Hpzdc^-$ chain forming 1D-MOCP along b-axis. Green, blue, red, purple, brown and white spheres are Pb, N, O, Cl, C and H respectively.

Several structural features that makes the selected 1D MOCP amenable to molecular modifications were identified. Below are justifications for our selection of this 1D MOCP as the best candidate for solid-solution and structural adjustments;

- presence of reactive protonated carboxylic group through which can render the structure unstable in a suitable solvent(s) that can cause structural rearrangements and transformation.
- the flexibility of Pb^{2+} metal center in terms CN (typical 2 – 10) owing to its ionic size. Pb^{2+} also based on the concept of HSAB principle is categorized as a borderline acid, that can adopt both soft and hard CE.
- presence of labile Cl bridging and the coordinated water which makes the Pb^{2+} as an easy target for cation exchange and transformation.
- presence of both soft N- and hard O-donor atoms that coordinate with hard, soft or borderline Lewis acids.
- Pb^{2+} is known to be defect tolerant, it can allows distortions, deformations or bond formations and breakages in the structure.

4.2 Structural description of *$Pb_2Cl_2(Hpzdc)_2(H_2O)_2$ (precursor 1D MOCP)*

Following the synthesis strategy reported by Wardana and coworkers (2015), with some modifications, air stable, large, colorless ribbon single crystals of precursor 1D MOCP was synthesized. It crystallizes in the $C_{2/m}$ space group (a = 11.561(1) Å, b = 8.4327(7) Å, a = 11.561(1) Å, a = 11.792(1) Å. Å,β = 126.3070(8)°). The structure was confirmed using single crystal X-ray diffractometry (SC-XRD) and CHN elemental analysis. The phase purity and crystallinity of the bulk material was further confirmed using powder X-ray diffractometry (PXRD).

The crystal structure of the precursor 1D MOCP is a one dimensional framework containing centrosymmetric Pb-dimers (Pb_2Cl_2) bridged by chloride atoms and further connected by mono protonated 2,3-pzdc ($Hpzcd^-$) forming a 1D ladder-like chain extended along the b-axis Figure 4.3 (A). In the precursor 1D MOCP structure, the $Hpzdc^-$ adopt a simple coordination mode where Pb^{2+} ions are *N,O*-chelated by the pzdc and the

other O-donor of the dicarboxylate are monoprotonated, Figure 4.4 (C). (Fendi Y. Wardana et al., 2015)

The whole 1D structure is composed of repetitions of AA' chains in which A' relates to A by glide plane along the b-axis, Figure 4.5 (A). The chemical environment surrounding the lead cations comprises N and O-atoms of the ligand, independent chloride atoms and coordinated O-atom from water molecule completes the coordination sphere, Figure 4.5 (B), forming a slightly distorted pentagonal pyramid geometry ($PbCl_2N_2O_3$) Figure 4.5 (C). (Fendi Y. Wardana et al., 2015)

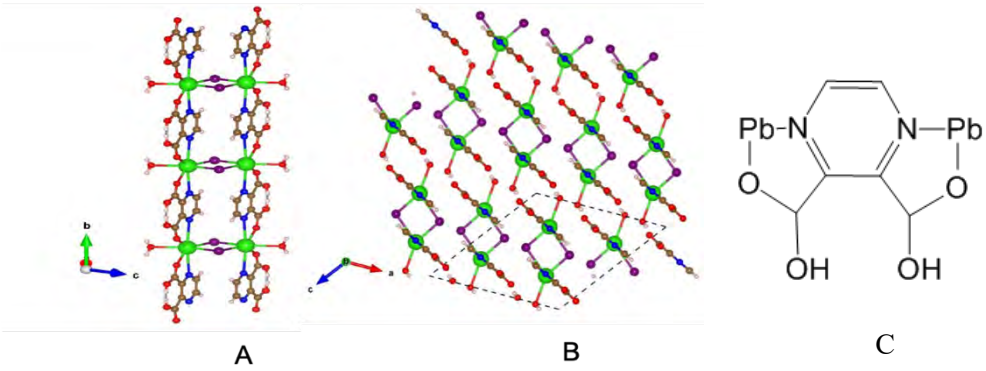

Figure 4.2: (A) ladder-like precursor 1D MOCP (B) precursor 1D MOCP viewing along b-axis, (C) coordination mode of pzdc ligand in the precursor 1D MOCP. Green, blue, red, purple, brown and white spheres are Pb, N, O, Cl, C and H respectively. (Fendi Y. Wardana et al., 2015)

The presence of monoprotonated dicarboxylic acid with Lewis base O atoms is confirmed using ATR FT-IR (attenuated total reflectance Fourier-Transform infrared) spectroscopy. Compared to the free O–H group stretch in MOCP which is normally observed as a sharp peak at 3600 cm^{-1}. (Karagiaridi et al., 2014) The existence of weakly H-bonded hydroxyl groups as observed in the crystal structure was also confirmed using IR analysis as relatively sharp peak around 340 and 3550 cm^{-1}. The long H-bond decreases the proton exchange, which resulted in sharp O–H stretch, Figure 4.6.

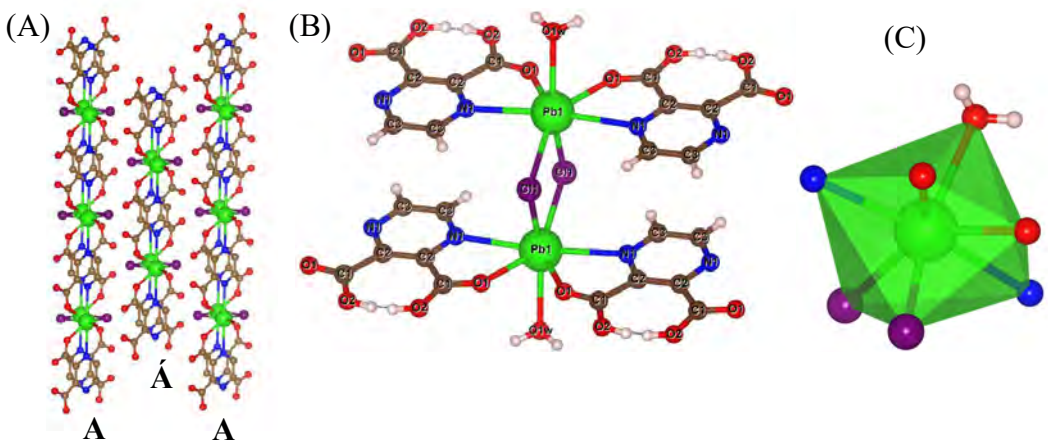

Figure 4.3: The precursor 1D MOCP showing A and A' related by a glide plane along b-axis, (A) labelled Pb coordination sphere, (B) and Pb-polyhedra (C) (Fendi Y. Wardana et al., 2015)

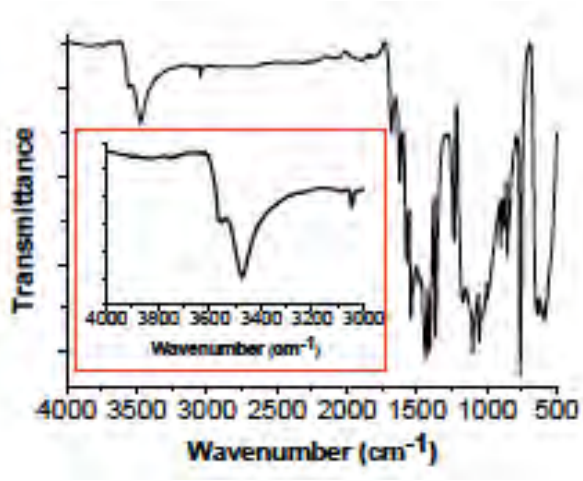

Figure 4.4: ATR-FT-IR spectra of the precursor 1D MOCP displaying sharp peaks of weakly H-bonded O–H stretch (3000–4000 cm^{-1}). (Fendi Y. Wardana et al., 2015)

The ladder-like chains of the precursor 1D MOCP are packed via extensive hydrogen bonding between the coordinated water molecules and two carboxylate O (O1 and O2) in adjacent chain Figure 4.7. The simplified chains can be topologically classified as uninodal 3-connected net with point symbol of (4^2.6). However, when the hydrogen bond was taken in to account is becomes 3,4-connected, 2-nodal net, Figure 4.8. (Fendi Y. Wardana et al., 2015)

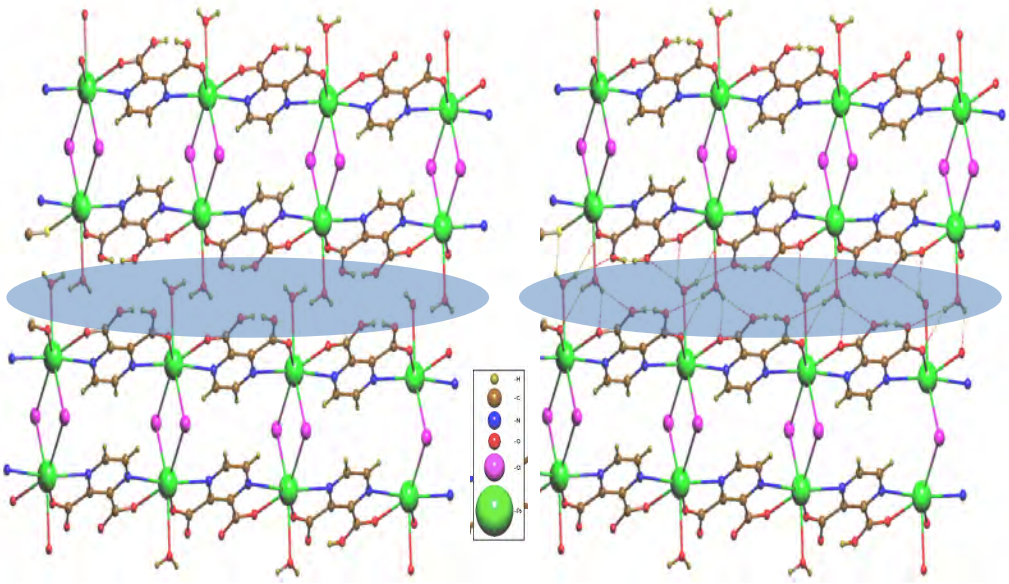

Figure 4.5: The precursor 1D MOCP crystal packing (A) showing H-bonding between 1D chains (B). (Fendi Y. Wardana et al., 2015)

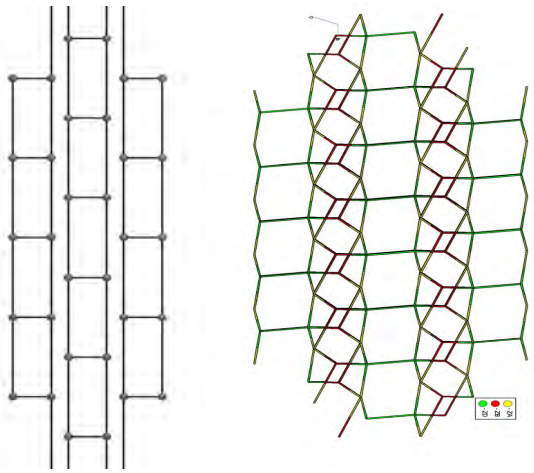

Figure 4.6: Topological analysis of the precursor 1D MOCP crystal packing showing simplified structures (A) simplified ladder like structure uninodal 3-connected net, without H-bonding, (B) simplified ladder like structure with H-bonding having 2-nodal 3,4-connected nodes; ligands (yellow), water (red) and Pb^{2+} (green). (Fendi Y. Wardana et al., 2015)

The phase purity of the ground single crystals was ascertained using powdered X-ray diffraction. The powdered X-ray diffractogram Figure 4.9, revealed the observed patterns of the bulk precursor 1D MOCP as pure without any extra peaks of polymorphs which matched well with the simulated pattern from the single crystal data.

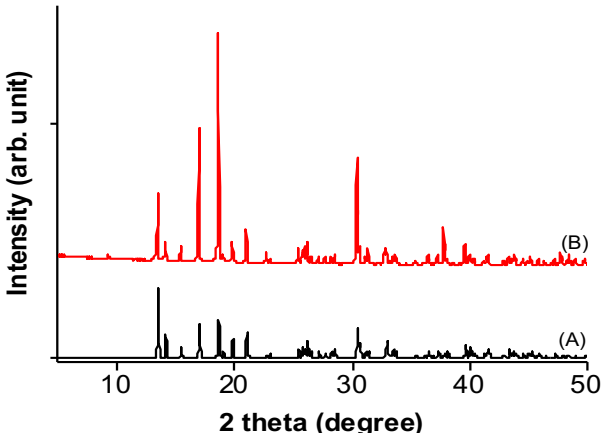

Figure 4.7: Powdered X-ray diffraction pattern of simulated (A) and observed (B). (Fendi Y. Wardana et al., 2015)

4.3 The dynamics of $Pb_2Cl_2(Hpzdc)_2(H_2O)_2$, (precursor 1D MOCP)

Since the precursor 1D MOCP has a flexible Pb^{2+} ions, presence of labile chloride bridging and reactive monoprotonated pzdc with a weakly H-bonded OH group, we purposely exploited the lability and dynamics of the precursor 1D MOCP by soaking in various solvents at room temperature. These features makes the precursor 1D MOCP amenable to solvent mediated simultaneous structural transformation and cation exchange upon simple soaking in aqueous solution. Reported from our lab, (F. Y. Wardana et al., 2015) it has shown that, upon simple soaking in aqueous solution, the precursor 1D MOCP can transform simultaneously with cation exchange to another 1D, $[Cu(pzdc)(H_2O)_2]_x.2_xH_2O$ or 2D, $(Pb(pzdc)(H_2O))$ or 3D, $(Pb_3(pzdc)_3(H_2O))$, Figure 4.10. The structural transformation was accompanied by loss of dichloride bridging, deprotonation of the -OH group and some changes and rearrangements in the coordination modes of pzdc. For instance while in precursor 1D MOCP, Pb^{2+} ions are *N,O*-chelated by pzdc, similar coordination mode was also observed in addition to *O,O*-chelation, O-bridging and uncoordinated O-atoms in the 2D MOCP. However, in the 3D, pzdc ligands adopts several unique coordination modes such as regular and weakly coordinated *N,O*-

chelation, monodendate, *O,O*-chelation, O-bridging, dioxo bridging, uncoordinated N-atoms Figure 4.4(C) and Figure 4.11. (Fendi Y. Wardana et al., 2015)

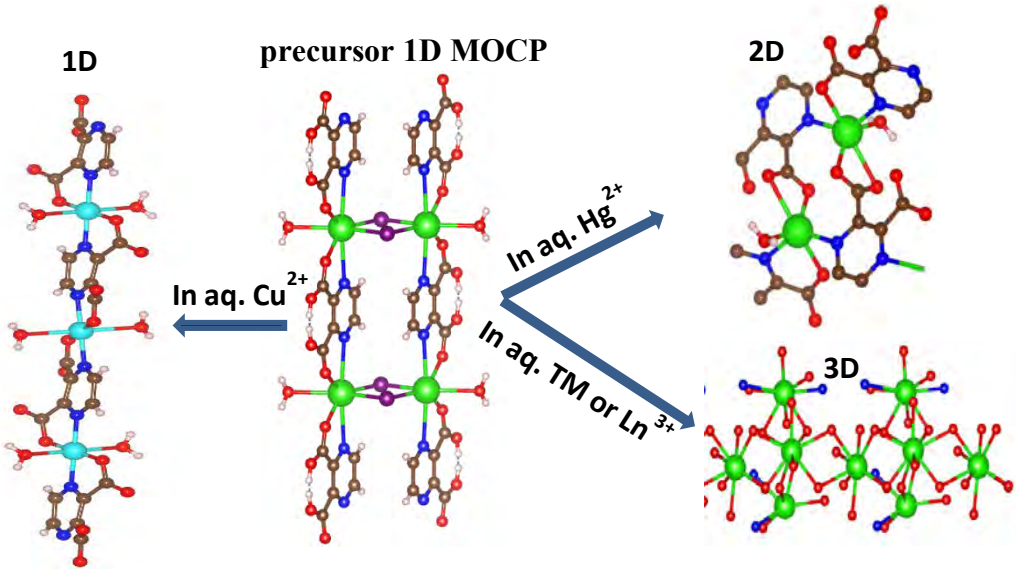

Figure 4.8: The dynamics of the precursor 1D MOCP to 1D, 2D or 3D MOCP. Green, cyan, purple, red, blue, brown and gray spheres are Pb, Cu, Cl, O, N, C and H respectively. (Fendi Y. Wardana et al., 2015)

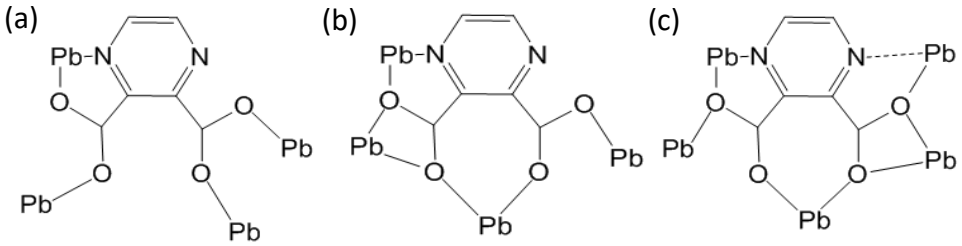

Figure 4.9: pzdc coordination modes observed in 3D MOCP, (a) pentadentate, (b) heptadentate and (c) nonadentate. The dashed line indicates a weak coordination bond.

4.4 The chemistry and structural description 3D MOCP, *$Pb_3(pzdc)_3(H_2O)$*

When the precursor 1D MOCP was soaked in an aqueous solution at room temperature, the colorless block crystals of the precursor 1D MOCP starts to lose transparency within 5 minutes and new plate-like crystals started to sprout on the surface of the precursor 1D MOCP visible with 10 minutes and continue to grow reaching

completion within 24 hours. (Fendi Y. Wardana et al., 2015) Examining the new plate crystals using X-ray diffraction, it was confirmed that the precursor 1D MOCP underwent a complete structural transformation from 1D structure to 3D structure with a molecular formula *$Pb_3(pzdc)_3(H_2O)$*. The loss transparency of precursor 1D MOCP upon soaking in aqueous solution and the subsequent growth of new crystals on the surface of the precursor 1D MOCP is a typical of dissolution recrystallization mechanism (X. Cui et al., 2009; X. J. Cui et al., 2009; C. Y. Xu et al., 2011) which is also confirmed by in situ visual observation using optical polarizing microscope and morphological electronic image by FESEM, Figure 4.12. Although the structural transformation was fast, it yields relatively good crystals suitable for single crystal X-ray diffraction in some cases.

The single crystal refinement of the 3D MOCP structure revealed that, the structure is made of trinuclear independent Pb^{2+} atoms, three pzdc and one coordinated H_2O per unit formula [*$Pb_3(pzdc)_3(H_2O)$*]. (Fendi Y. Wardana et al., 2015) The 3 Pb^{2+} atoms are crystallographically occupying unique sites each with different CN and CE. These three independent sites are further linked by O-atoms from the carboxylate ligands to form an infinite rod like SBUs which are further connected to three periodic structure, Figure 4.13. Pb(1) sites are 6-coordinated, distorted octahedron with one of the axis occupied by an active lone pair of electrons giving an asymmetric distribution of the coordinated ligands, the so-called hemi-directed distribution of ligands.

The coordination sphere Pb(1) site is surrounded by two N-atoms, three O-atoms from $pzdc^{2-}$ and one O-atom from coordinated H_2O completing the coordination sphere. Whereas the Pb(2) site, is 7-coordinated with somewhat distorted monocapped trigonal prism bounded by two N-atoms and five O-atoms all from the $pzdc^{2-}$ ligands. Pb(2) also exhibits a hemi-directed geometry with an detectable gap in the coordination sphere. Such is reflected in relatively large bond angle of 146.9º between O8–Pb(2)–O9 compared to

other O–Pb(2)–O bond angles. Pb(3) site, on the other hand, is 9-coordinated tricapped trigonal prism with nine O-atoms surrounding the coordination sphere, all from the $pzdc^{2-}$ ligands, Figure 4.14 (A). Pb(3) site exhibited a holo-directed coordination sphere evident by the uniform distribution of the ligands around the sphere.

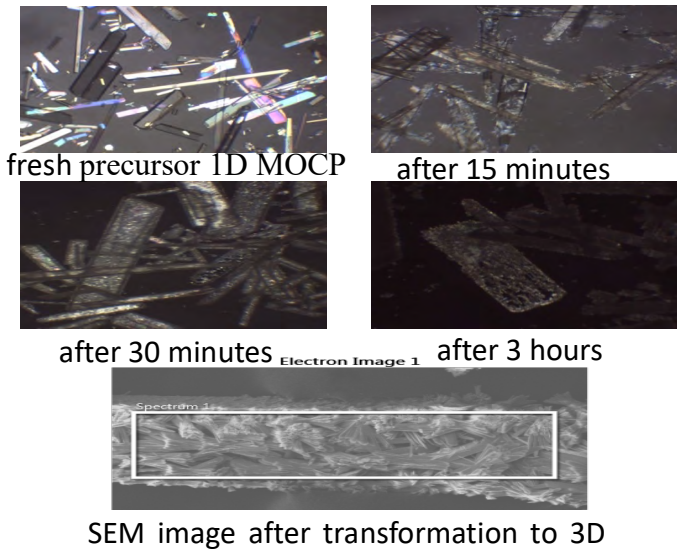

Figure 4.10: Microscopic images of the precursor 1D MOCP transformation to 3D MOCP after soaking in a typical solvent and the SEM morphology image after completion.

As such, pzdc adopt variety of coordination modes including monodentate, *O,O*-chelation, *N,O*-chelation, O-bridging, and presence of an uncoordinated N-atoms, Figure 4.11. The Pb(3) are edge-sharing polyhedrons with a dioxo-bridging, same bridging also exists between Pb(3) and Pb(2) polyhedrons. However, this dioxo-bridging does not exist between Pb(3) and Pb(1) polyhedrons, making it corner sharing, Figure 4.14 (B).

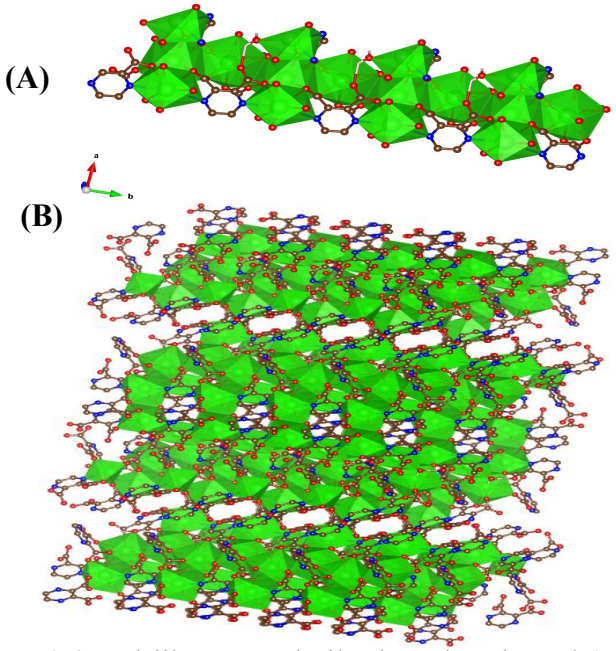

Figure 4.11: 3D MOCP (A) rod-like SBUs built along b-axis and (B) the extended 3D structure.

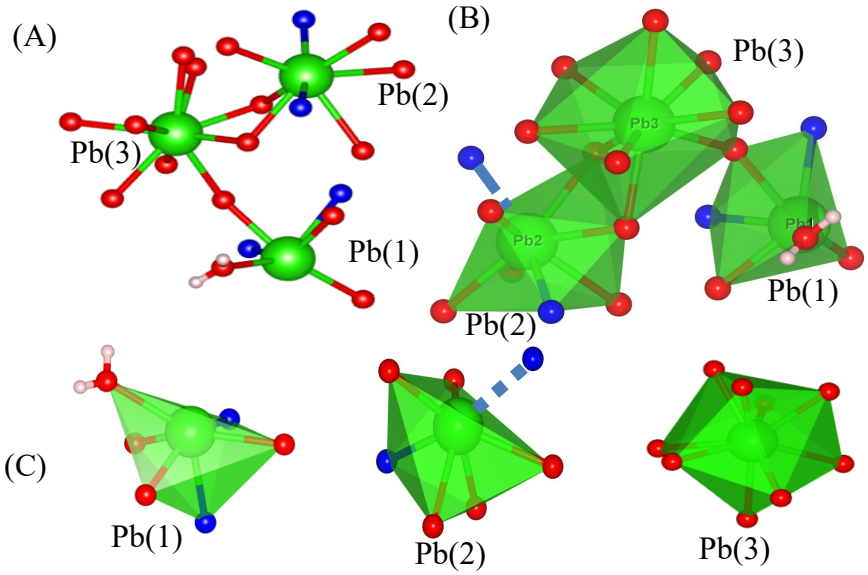

Figure 4.12: 3D MOCP showing CE and CN (A), edge and corner sharing between Pb(3) and Pb(2) and P(1) respectively (B) and geometrical polyhedra of Pb(1), Pb(2) and Pb(3). (Fendi Y. Wardana et al., 2015)

Topological analysis of the 3D MOCP, shows that the simplified structure has a 6-nodal network with 3,4,4,5,5,5-connected net with a stoichiometry of (3-c)(4-c)(4-c)(5-c) (5-c) (5-c), having a new topological structure. The Pb(1) sites are 4-connected node, while Pb(2) and Pb(3) are 5-connected nodes each in the simplified structure, Figure 4.15.

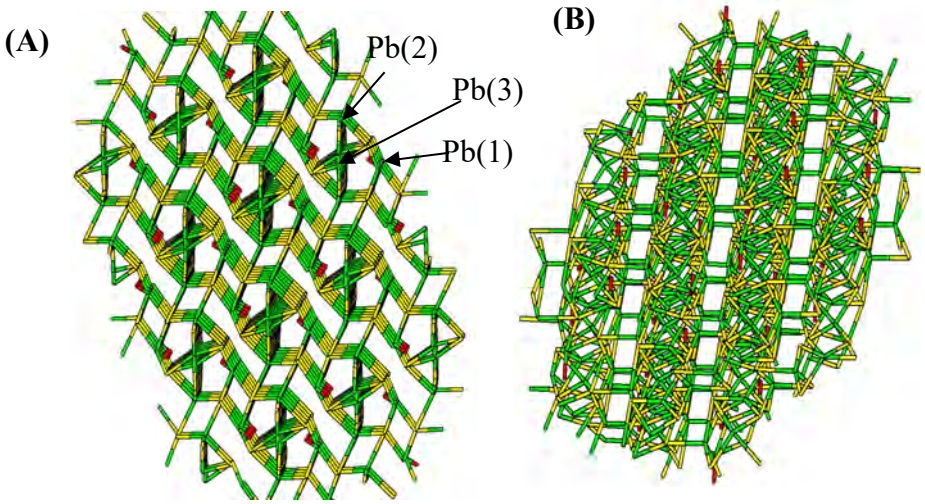

Figure 4.13: simplified 3D structure with 6-nodal network showing 4,5,5 connected nodes for Pb(1), Pb(2) and Pb(3) respectively (A) and the rod-like packing (B).

The PXRD pattern of the bulk 3D crystals matched exactly the simulated patterns from the single crystal diffractometry, without any additional polymorph, confirming the purity and the crystallinity of the bulk 3D MOCP crystals, Figure 4.16. (Fendi Y. Wardana et al., 2015)

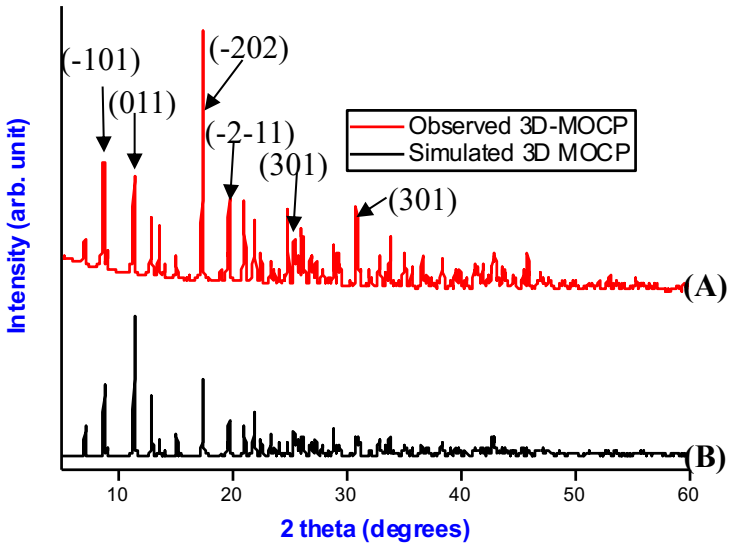

Figure 4.14: Powder X-ray diffraction patterns of 3D MOCP (A) observed and (B) the simulated patterns

4.5 Solid solution in 3D MOCP, *$Pb_3(pzdc)_3(H_2O)$* via dissolution-exchange-recrystallization accompanied by simultaneous structural transformation.

The distinct crystallographic sites, each with different CN and CE in 3D MOCP, inspire our interest to judiciously conduct solid solution with variety of cations. Since cations of different sizes and chemistry has dissimilar preference for CN and CE, and based on this notion, different cations can be directed to dope into different locations based on their preferences under suitable synthesis conditions. Remarkably, Pb^{2+} ions in the MOCP underwent substitutions with aliovalent cations including mono and tri-valent cations and also with other transition metals. Multiple doping including double and triple doping was also successfully conducted, guided by the principle of HSAB, different percentage dopants amounts were synthesized all via the solvent mediated structural transformation and cation exchange.

4.5.1 Doping Lanthanides into the 3D MOCP, *$Pb_3(pzdc)_3(H_2O)$*.

Doping Ln into a preformed MOCPs typically endows them with intense and tunable luminescence emissions, large stokes shift, and long-lived emissions (Y. Cui, Y. Yue, et al., 2012; Z. Hu et al., 2014). MOCPs doped with Ln are of particular importance owing to their potential applications for solid state lighting or optical sensing luminescence materials (Y. Lu & Yan, 2014; X.-Y. Xu & Yan, 2015; Y. Zhou et al., 2014). Single-phase but multi-coloured emitting materials are also of great importance due to their potentials for security and display applications. (R. An et al., 2016; Z.-F. Liu et al., 2013; Q.-Y. Yang et al., 2015) Usually, multi-coloured emitting materials are made by incorporating Ln into the framework to form heterometallic structures which may undergo single excitation to attain dual or multiple color emission. Lanthanides are *f*-block cations which has a relatively large ionic radii, reasonably flexible, in terms of CN and CE. (Marques et al., 2002) Due to the large size and predominant ionic bonding, the steric saturation is a critical factor in controlling the geometry, CN and the chemistry of

their complexes. Their large ionic radius endows them with flexibility to adopt several CE and CN.

Knowing the fact that Ln^{3+} are oxophilic (Kepp, 2016; Steed & Atwood, 2009) and Pb(3) site is surrounded by oxygen atoms, soaking the precursor 1D MOCP into Ln^{3+} (La, Eu, Gd, Tb, Sm, or Er) aqueous solution, using 1:2 mole ratio Ln:1D-MOCP for 3 days, resulted in the mixed valent substituted Ln^{3+}/Pb 3D MOCP. As usual, the precursor 1D MOCP starts to loss its transparency within the first 10 minutes of soaking with appearance of new crystals on the surface of the precursor 1D MOCP. Analysis of the single crystal data of the exchanged product (Ln^{3+}-*doped* MOCP) revealed that, the Ln^{3+} went into Pb(3) oxophilic sites as expected, in addition to Pb(1) sites. Remarkably, we found that Pb^{2+} in Pb(2) sites were exchanged more by Ln^{3+}. Although all the three Pb sites accommodate Ln, Figure 4.17, Pb(2) sites with CN 7, comprising O and N-donor atoms are more preferred by Ln. This preference can be attributed to the high CN preference for Ln^{3+}, although Pb(3) is surrounded by all O-donor atoms and CN 9, albeit high number of connectivity (CN) might be slightly more difficult to break and exchange, extra energy might be needed to overcome the M–L dissociation energy. On the other hand, Pb(1) sites are having relatively low CN, hence Pb(2) sites with CN 7 would be more preferred. The result of substitutions at all Pb^{2+} sites was however expected, due to the Ln^{3+} flexibilities in terms of CN and CE, examples of Ln-based compounds with 6, 7, and 9 CNs are available. (Bunzli, 2014; Einkauf et al., 2017; Karraker, 1967)

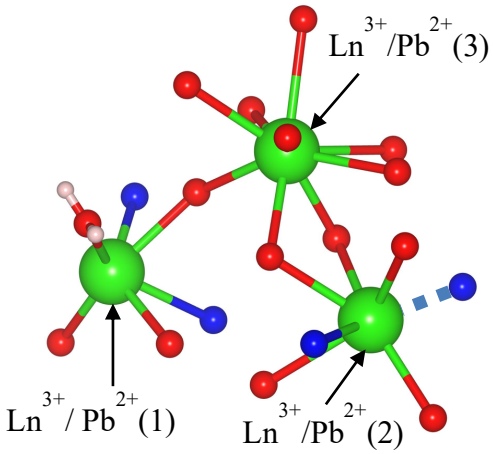

Figure 4.15: Ln^{3+} exchange site preference in 3D MOCP, more preference at Pb(2) sites

Since an aliovalent cations were used for the substitution of divalent Pb^{2+} cation vacancy was refined in these cases to obtain charge balances due to absence of any extra electron density to be considered as the counter ions during the refinement. Therefore, each Ln exchanged compound featured cation vacancy (Vac) giving a total formula of $Pb_{2.93}La_{0.05}Vac_{0.02}(pzdc)_3(H_2O)_{0.60}$, $Pb_{2.76}Eu_{0.16}Vac_{0.08}(pzdc)_3(H_2O)_{0.56}$, $Pb_{2.73}Gd_{0.18}Vac_{0.09}(pzdc)_3(H_2O)_{0.58}$, $Pb_{2.73}Tb_{0.18}Vac_{0.09}(pzdc)_3(H_2O)_{0.60}$, and $Pb_{2.76}Er_{0.16}Vac_{0.08}$ $(pzdc)_3(H_2O)_{0.59}$, respectively for La^{3+}, Eu^{3+}, Gd^{3+}, Tb^{3+}, and Er^{3+}. The structural integrity, purity and crystallinity was confirmed using PXRD measurement Figure 4.18, in which the observed patterns and the simulated patterns agrees well. Presence of Ln^{3+} is further confirmed by SEM-EDS and ICP-OES analysis, with Eu^{3+}, Gd^{3+}, Sm^{3+}, and Tb^{3+} exchanging 6 atomic (at.) % each, while Er^{3+} exchanged 5 at.% and La^{3+} exchanged only about 2 at.%, Table 4.1.

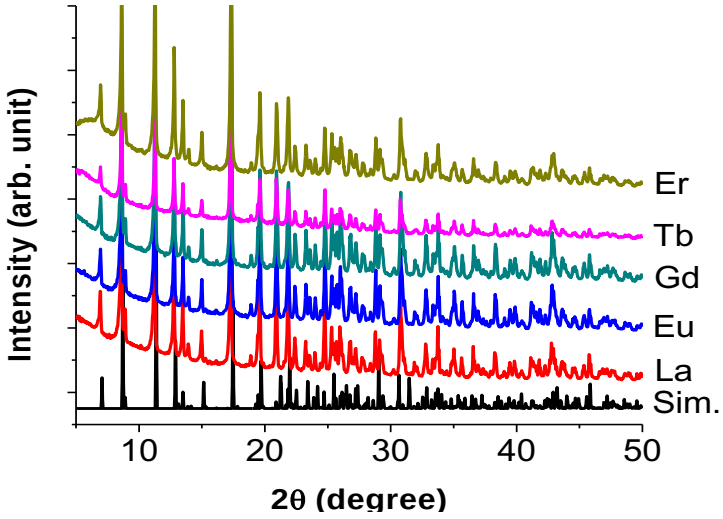

Figure 4.16: Powder X-ray diffraction patterns of La^{3+}, Eu^{3+}, Gd^{3+}, Tb^{3+}, and Er^{3+} doped MOCPs vs the simulated patterns.

The XPS spectra of the representative Ln^{3+} (Eu^{3+}) was used to investigate the oxidation state and the chemical environment of Eu^{3+}. The analysis indicates that, the splitting of the binding energy of 4*f* orbitals, 143.3 ($4f_{5/2}$) and 138.4 ($4f_{7/2}$) eV in Pb^{2+} is consistent with the oxidation state of +2 (A. Y. Lee et al., 2002). Whereas, the splitting of *3d* orbitals for Eu are attributed to the strong spin-orbit coupling and the binding energy of 1135.2 ($3d_{3/2}$) corresponds to Eu in Eu^{3+}/Pb^{2+}, which is also consistent with +3 oxidation state, Figure 4.19.

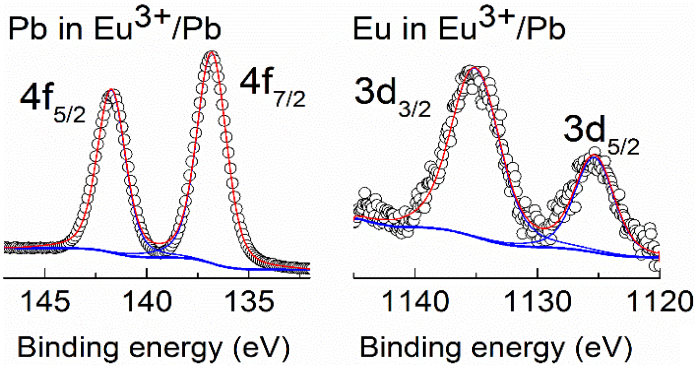

Figure 4.17: XPS spectra of Pb^{2+} and Eu^{3+} in Eu^{3+}-doped Pb-MOCP

Table 4.1: SEM-EDS dopant amounts in 3D MOCP

Dopant	Amount (atomic %)
La^{3+}	2.0
Eu^{3+}	6.0
Gd^{3+}	6.0
Tb^{3+}	6.0
Er^{3+}	5.0
Sm^{3+}	6.0

4.5.1.1 Tuning the Ln^{3+} doped amounts in 3D MOCP

The low amount of cation exchange in aqueous solution is however expected since hard Lewis acid (Ln^{3+}) salts were dissolved in hard Lewis base solvent (H_2O) and based on the HSAB principle, there is a strong preference for hard-hard or soft-soft to interact and bind well with each other. Hence, Ln^{3+} ions were strongly solvated by H_2O forming strong M–solvent bonds and preventing it from substituting Pb^{2+} in the framework. To vary the Ln^{3+} amounts in the 3D MOCP, series of experiments were conducted under the guidance of HSAB principle by systematically exploring the effect of different synthetic conditions such as mole ratio, pH, temperature or the reaction time.

(a) ***Effects of solvents***

In this regard, different solvents of different solvation effects (e.g. DMF, DMSO, THF, dioxane, ethanol, methanol, acetone, pyridine, etc.) were explored. For example when DMSO or pyridine was used, the precursor 1D MOCP slowly dissolved without growth of new crystal even after 1 month, which could be attributed to the high solvation power of DMSO or pyridine and also the solubility of pzdc ligand in these solvents. Whereas, when DMF was used, the transformation was extremely slow, with no visible sign of dissolution-recrystallization process. Similarly, when THF or dioxane is used the transformation is also slowed. In MeOH or EtOH the transformation was very fast, typically less than 2 hours, but impurities in form of other crystalline phases were identified in the PXRD pattern Figure 4.20. Generally, in this case, we can infer that,

transformation of the precursor 1D MOCP to 3D MOCP is favoured in protic solvents and the kinetics is either slowed down or favoured the formation of other crystal phases in aprotic solvents.

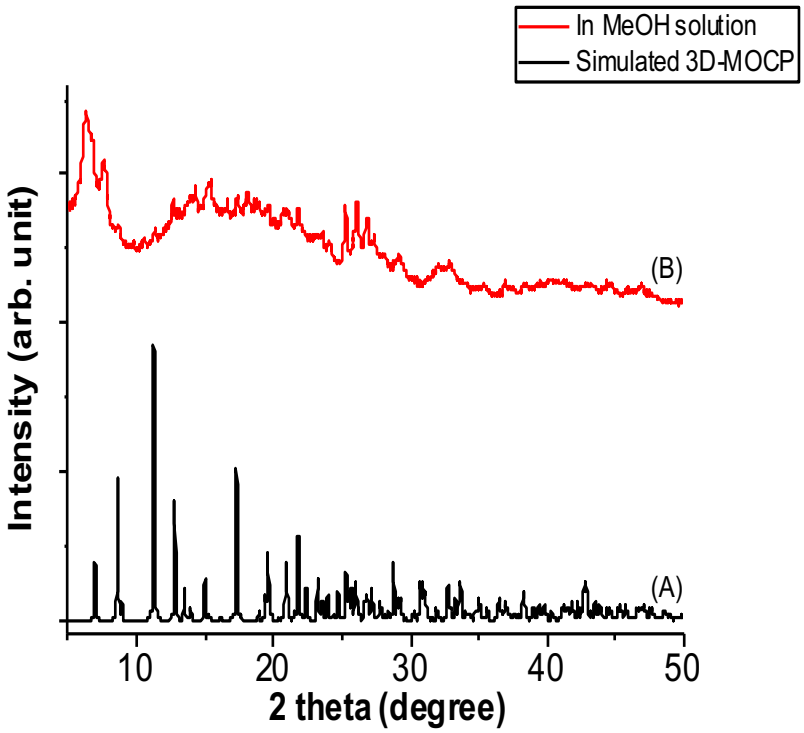

Figure 4.18: PXRD patterns of 3D MOCP soaked in MeOH solution of Tb^{3+} salt (A) and the simulated 3D MOCP (B).

(b) ***Effects of pH and concentration***

The effect of pH change was also explored, for instance when 1 drop of conc. HCl was added in to an aqueous solution containing Ln^{3+}, the pH of the solution drops to 1 from around 6. At this pH, there is no visible transformation or change in morphology of the precursor 1D MOCP even after a long duration. This is connected to the fact that, at lower pH the deprotonation free hydroxyl groups are suppressed and the presence of the chloride ions may also suppressed the breakage of the chloride bridging which are integral to the structural transformation of the precursor 1D MOCP. The PXRD confirmed the precursor 1D MOCP remains intact Figure 4.21. The lower pH may suppresses the deprotonation

of the monoprotonated pzdc and the breakage of the chloride bridging which are the basic features that makes the precursor 1D MOCP amenable to transformation. Remarkably, adding 1 drop of diluted (2M) HCl, the transformation proceeded albeit slow pace, allowing the growth of good quality 3D MOCP single crystals but without an increase in the dopant amount. The effect of the addition of diluted HCl (H_2SO_4, acetic acid, same effect) can be regarded as modulator approach in which an acid of only one coordination site is added to compete with the linker/ligands for coordination with metal cation which slows down the rate of nucleation and allow the growth of big crystals especially for high valent cations and carboxylate linkers (Diring et al., 2010; Tsuruoka et al., 2009; Shuai Yuan et al., 2018).

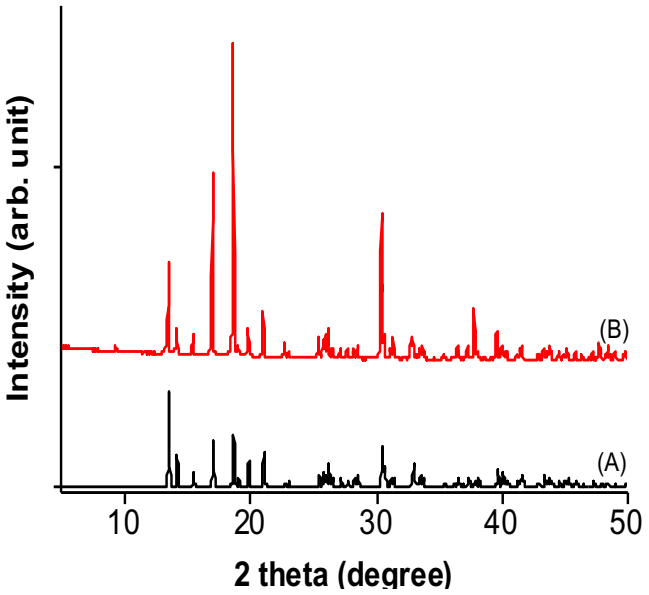

Figure 4.19: PXRD patterns of simulated precursor 1D MOCP (A), and the precursor 1D MOCP soaked in aqueous solution at pH = 1 (B).

On the other hand, when the pH was raised to above 7, the transformation proceeded at a very fast pace, in some cases completing the transformation in less than 30 minutes. Although the PXRD is pure, however the dopant amount has not improve. Increasing the mole ratio of exogenous cation to the precursor 1D MOCP from 1:1 up to 8:1 also does not show any significant increase in the dopant amount.

(c) ***Solvent mixture***

Since pH and concentration has no direct effect on increasing the dopants, mixture of solvent was then explored to manipulate the transformation as well as the exchange. The aim is to have a combination of solvents that can allow transformation of the precursor 1D MOCP to 3D MOCP and a weak interaction with the exogenous cations to allow simultaneous solvent mediated structural transformation and cation exchange. For example, mixture of 1:1 ratio H_2O/Dioxane or H_2O/DMF or DMF/dioxane or H_2O/MeOH or H_2O/EtOH does not improve the dopant amounts significantly, but the kinetics of the transformation is slowed especially for H_2O/DMF.

Since in protic solvents the transformation is fast and slowed in aprotic solvents, and mixing the protic and aprotic solvents does not improve significantly. Triple mixture of solvents was further explored. After several combinations of solvents of different solvation capabilities, a mixture of three solvents, H_2O/Dioxane/DMF at 3:2:2 v/v ratio was found to improve the dopant amounts. Using the mixture of H_2O/Dioxane/DMF at 3:2:2 increases the exchange from typical 6 at. % to about 15 at. % for Eu^{3+}, Er^{3+} or Tb^{3+}. The crystallinity and the phase purity remains intact based on the PXRD analysis of the observed against the simulated patterns, Figure 4.22. Although there is an improvement from 6 to about 15 at. %, other synthesis conditions must be explored to increase the % Ln^{3+} since they can exchange at all the 3 Pb^{2+} sites, 100 % exchange of Pb^{2+} is the target.

(d) ***Use of modulator ligand***

Since the cation exchange and the structural transformation process in this material is concurrent and simultaneous, addition of a modulator ligand that can interact strongly with Pb^{2+} ions in the framework during the transformation and weakly with the exogenous ions can enable the exogenous cations to exchange Pb^{2+} ions during the transformation. According to the principle of HSAB, Pb^{2+} is a borderline Lewis acid, addition of a borderline Lewis base with one coordination site can act as modulator ligand that can

preferentially interact with Pb^{2+} by deactivating and suppressing it from going back to the framework.

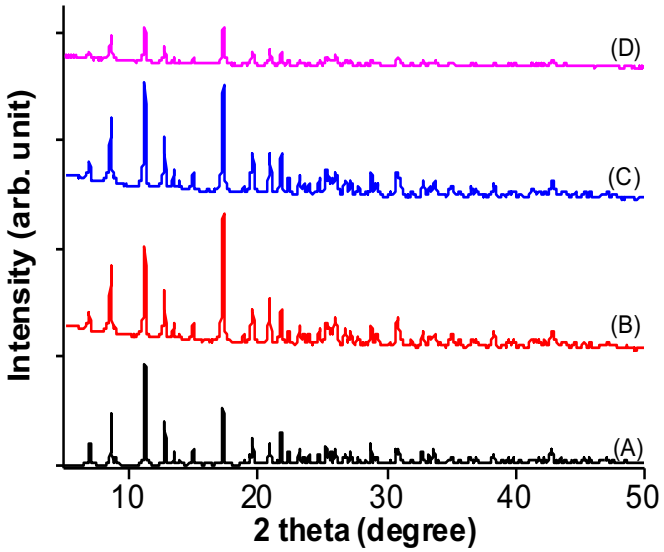

Figure 4.20: PXRD patterns of simulated 3D MOCP (A), and 15 wt. % Eu^{3+}-doped (B), Er^{3+}-doped (C) and Tb^{3+}-doped (D).

Several borderline and soft Lewis bases such as Piperazine, pyridine, pyradazine, imidazole, ethylenediamine, or diethylamine were explored. Pyridine was found to be the most suitable modulator ligand, addition of two drops of pyridine increases the dopant amount while maintaining the integrity of the 3D structures with no additional peaks in the PXRD after the transformation. However, addition of more than 2 drops rises the pH and increases the transformation kinetics, so fast that no Ln^{3+} was able to dope into the 3D MOCP structure. Addition of excess pyridine dissolves the precursor 1D MOCP and no 3D structure form, hence 2 drop is the optimum amount. Addition of 2 drops of pyridine, in a three solvent mixture H_2O/Dioxane/DMF, 3:2:2 v/v ratio solution of Er^{3+}, Eu^{3+} or Tb^{3+} for instance, remarkably increases the dopant amounts to approximately 35 at. %. Based on the principle of HSAB, Pb^{2+} and pyridine are borderline acid and base respectively. As such, there will be a preferential interaction between Pb^{2+} and pyridine and such interaction is very less between a hard Ln^{3+} ions and pyridine. Hence this will cause more borderline Pb^{2+} to be pulled into the solvents aided by the presence the

borderline pyridine and allowed more Ln^{3+} ions to be doped into the structure. PXRD patterns indicates the phase purity and the crystallinity of the exchanged products, Figure 4.23.

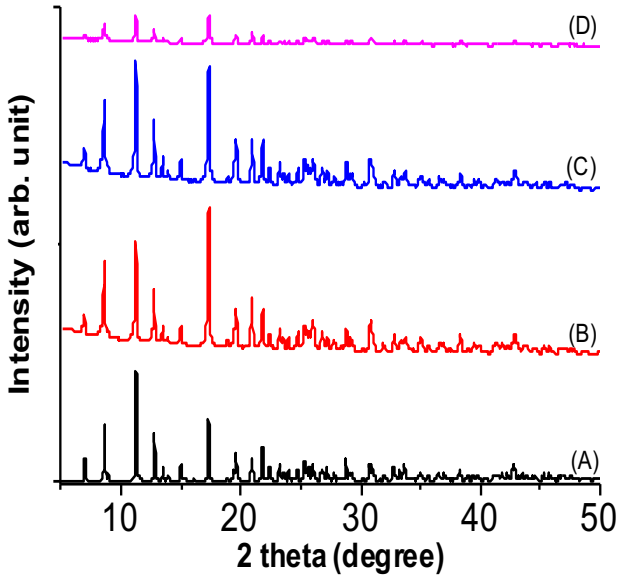

Figure 4.21: PXRD patterns of simulated 3D MOCP (A), and 35 wt. % Eu^{3+}-doped (B), 35 wt. % Er^{3+}-doped (C) and 35 wt. % Tb^{3+}-doped (D).

(e) ***The effect of temperature***

To push the limit further, as we envisage to have 100 % Pb^{2+} exchange and higher Ln^{3+} dopant to tune the photoluminescence emissions, effect of temperature was then explored. Enclosing a three solvent mixture H_2O/Dioxane/DMF, 3:2:2 v/v ratio solution of Eu^{3+}, Er^{3+} or Tb^{3+} in a preheated teflon liner and stainless steel autoclave at 60 or 90 °C for 1–5 days, increases the dopant amounts up to 80 wt. %, maintaining the crystallinity and phase purity, Table 2. However, in the case of Tb^{3+}, increasing the temperature above 60 °C or increasing the reaction time to more than 24 hours led to loss of crystallinity with weak and less sharp PXRD pattern, Figure 4.24 (II). While Er^{3+} and Eu^{3+} dopants can be increased up to 99 wt. % at 90 °C for 5 days Figure 4.24 (B) and (C).

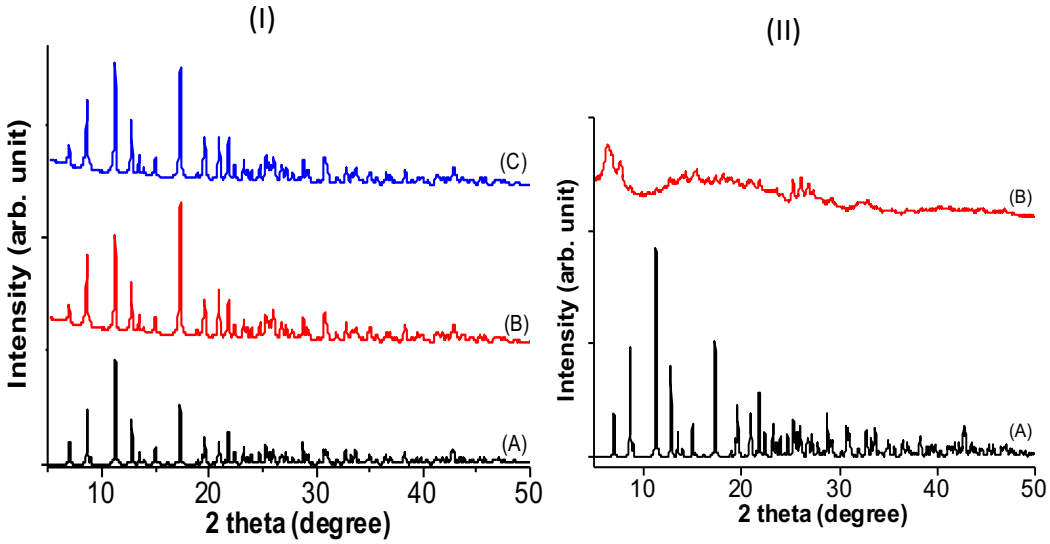

Figure 4.22: (I) PXRD patterns of simulated 3D MOCP (A), and 99 wt. % Eu^{3+}-doped (B), 99 wt. % Er^{3+}-doped (C) and (II) PXRD patterns of simulated 3D MOCP (A), collapse Tb^{3+}-doped (B).

Table 4.2: SEM-EDS (average at. %) or ICP-OES (wt.%)* results of dopant in Ln^{3+} doped Pb^{2+} MOCPs.

Synthesis condition	Dopants	Amount (at. or wt. %)
H_2O/Dioxane/DMF, 3 d.	Eu^{3+}, Tb^{3+} or Er^{3+}	15.0*
H_2O/Dioxane/DMF, 2 drops pyridine, 3 d.	Eu^{3+}, Tb^{3+} or Er^{3+}	35.0
H_2O/Dioxane/DMF, 2 drops pyridine @60 °C, 1 d.	Eu^{3+}, Tb^{3+} or Er^{3+}	80.0
H_2O/Dioxane/DMF, 2 drops pyridine @90 °C, 5 d.	Eu^{3+}, Tb^{3+} or Er^{3+}	99.0

Although only the single crystals of 3D MOCP containing about 6 wt. % of La^{3+}, Eu^{3+}, Gd^{3+}, Tb^{3+}, or Er^{3+} was solved using SCXRD, increasing the dopant amount in the 3D MOCP is expected to be distributed in all the 3 Pb-sites with more preference to Pb(2) sites for exchange amounts 35 at. % and below, however above that threshold, the preference may not be important. Such results give a general formula of $Pb_{3-3x}Ln_{2x}Vac_x(pzdc)_3(H_2O)$ in which x = 0.08, 0.52, and 1.2 for 6, 35, and 80 wt.% of Ln (Er^{3+}, Eu^{3+} or Tb^{3+}), respectively. Note that only 6 wt.% doped samples have been confirmed their cation vacancy (Vac) stoichiometry as refined crystallographically as crystalline powder are mostly obtained for other samples with higher at.%. Scheme 1

provides a summary of the transformations and tuning the dopant amounts under different synthesis conditions.

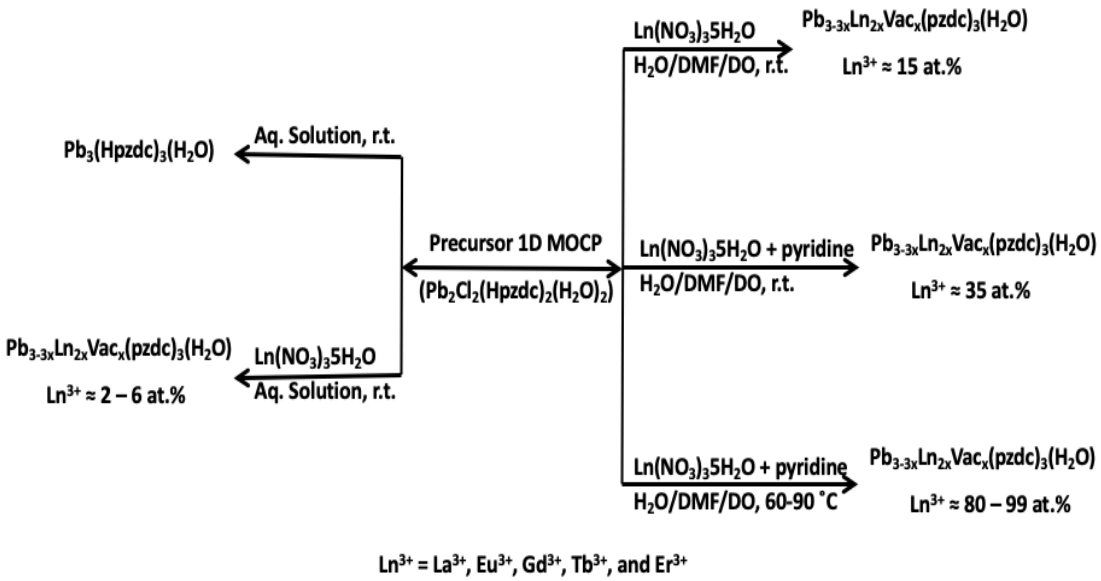

Scheme 1: Summary of Ln^{3+} incorporation in to 3D MOCP using the precursor 1D MOCP under various synthesis conditions.

(f) ***Peaks shifts and Vegard's law analysis***

Besides indicating phase purity and structural integrity, the 3 hour long scan PXRD patterns of the Ln^{3+} (Eu^{3+} and Tb^{3+}), showcases the expected peak shifts to the higher 2θ as dopant amount increases due to relatively smaller size of Eu^{3+} or Tb^{3+} to that of Pb^{2+}, Figure 4.25. Rietveld analysis of the PXRD data further shows a linear decrease in lattice parameter *a*, with an increase in Eu^{3+} or Tb^{3+} which obeys the Vegard's law Figure 4.26.

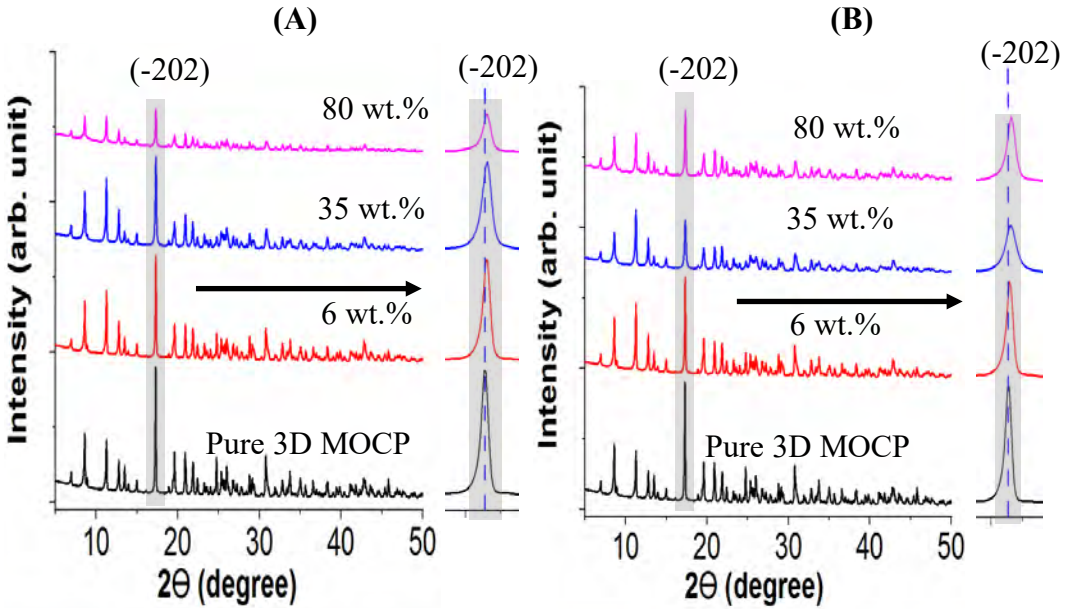

Figure 4.23: PXRD patterns of: (A) *Eu^{3+}-doped 3D MOCP* with 6, 35 and 80 wt. % of Eu^{3+}, and (B) *Tb^{3+}-doped 3D MOCP* with 6, 35 and 80 wt. % of Tb^{3+}. Insets show zoom-in patterns of small peak shifting at (-202).

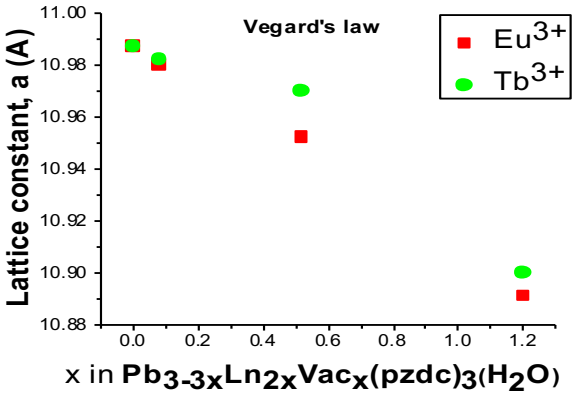

Figure 4.24: Rietveld refinements of powder X-ray diffraction data, showing decreasing lattice parameter, a (Å) with incorporation of smaller Eu^{3+} or Tb^{3+}.

(g) *Photoluminescence evaluation*

Based on the *Laporte* selection rule, the low absorption and the forbidden nature of the *f-f* transitions are inherent property of most Ln^{3+} ions which make them less efficient light energy absorbers. (Steemers et al., 1995) To overcome the poor light absorption, Ln^{3+} are typically introduced into a system with suitable organic chromophore that can efficiently absorb energy and transfer to the Ln^{3+} ions, the so-called *antennae effect*.

A photoluminescence evaluation was conducted on Ln^{3+} substituted 3D Pb MOCP, namely *Eu^{3+}-doped 3D MOCP*, *Tb^{3+}-doped 3D MOCP*, and *Eu^{3+}/Zn^{2+}-doped 3D MOCP*. The solid state photoluminescence analysis shows that only about ~6 wt.% of Eu^{3+} or Tb^{3+} doping, was enough to tune its photoluminescence emissions from weak greenish yellow emission of the pristine 3D MOCP with CIE coordinate of (0.38, 0.58), to bright yellowish red (*Eu^{3+}-doped 3D MOCP)* with corresponding CIE coordinate of (0.35, 0.37); while adding extra dopant, Zn^{2+}, to make *Eu^{3+}/Zn^{2+}-doped 3D MOCP* leads to yellowish orange luminescence color with CIE coordinate of (0.36, 0.42). Whereas, bright greenish yellow was observed for *Tb^{3+}/Pb* with CIE coordinate of (0.38, 0.48), Figure 4.27. Such results suggest a good antennae effect, especially in the case of *Eu^{3+}-doped 3D MOCP,* where typical Eu^{3+} *f-f* transitions were observed. (Y. J. Cui et al., 2012)

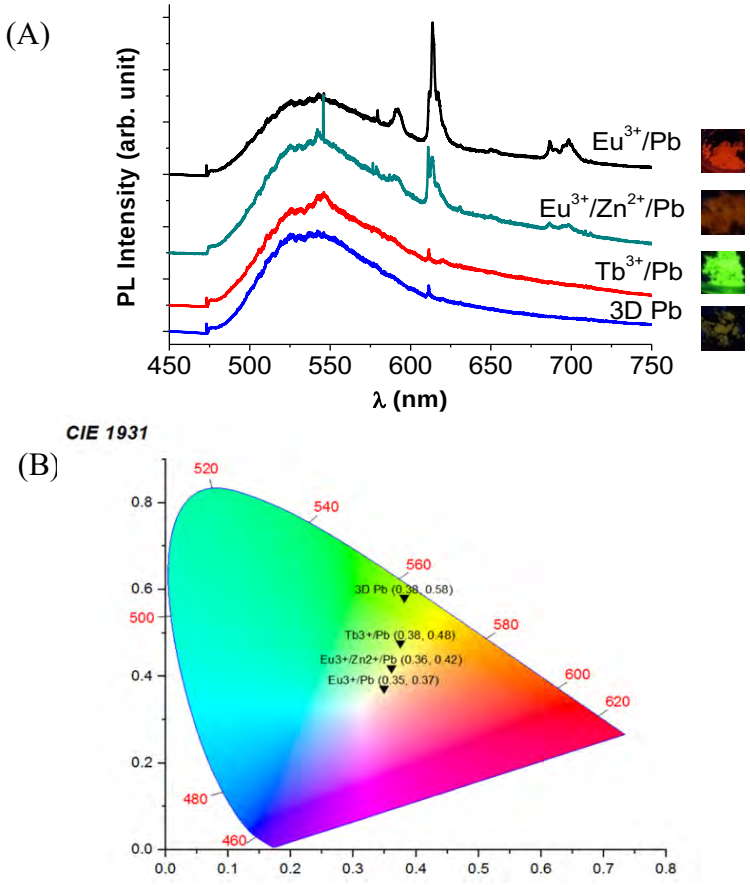

Figure 4.25: Photoluminescence (emission) spectra, (A), and CIE coordinates, (B), of pristine 3D MOCP, *Tb^{3+}-doped 3D MOCP*, *Eu^{3+}/Zn^{2+}-doped 3D MOCP*, and *Eu^{3+}-doped 3D MOCP*, excited at 473 nm. Insets are their corresponding digital images under 365 nm UV lamp.

Interestingly, the PL character of pristine 3D MOCP, a broad emission peaked at greenish yellow region, is sustained within the background, making this compound as a dual color luminescence under single-excitation wavelength (473 nm). However, this may indicate the absorbed energy by the organic ligands was only partly transferred to the Eu^{3+} or Tb^{3+}.

The efficiency of the energy transfer was improved, thus better antennae effect, when the excitation wavelength was increased to 350 nm, the broad peak of the pristine 3D MOCP disappeared indicating a more efficient energy transfer within the framework. In this case, only the characteristic peaks of Eu^{3+} *f-f* transitions ($^5D_0 \rightarrow {}^7F_j$, j = 0-4) and that of Tb^{3+} ($^5D_4 \rightarrow {}^7F_j$, j = 3-6) were observed, Figures 4.28, respectively. Observation of LMCT, as indicated by blue-shifting of the ligand's 260 nm band in Eu^{3+}-*doped 3D MOCP* and Tb^{3+}-*doped 3D MOCP* in solid state UV-Vis absorption Figures 4.29 support the observed antennae effect.

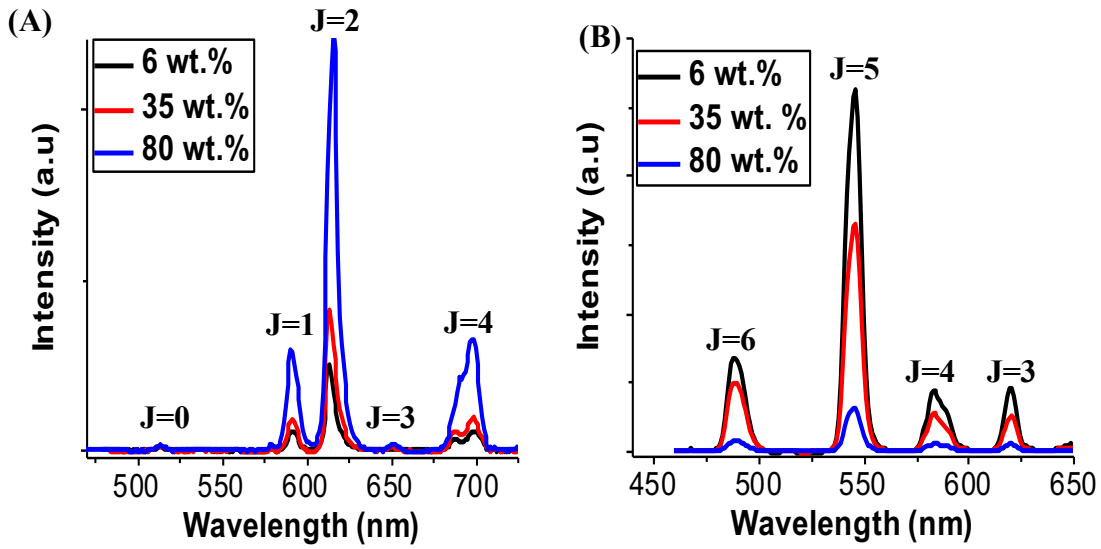

Figure 4.26: Solid-state photoluminescence (emission) spectra showing typical *f-f* transitions of *Eu^{3+}*-doped MOCP (A) and *Tb^{3+}*-doped MOCP (B)

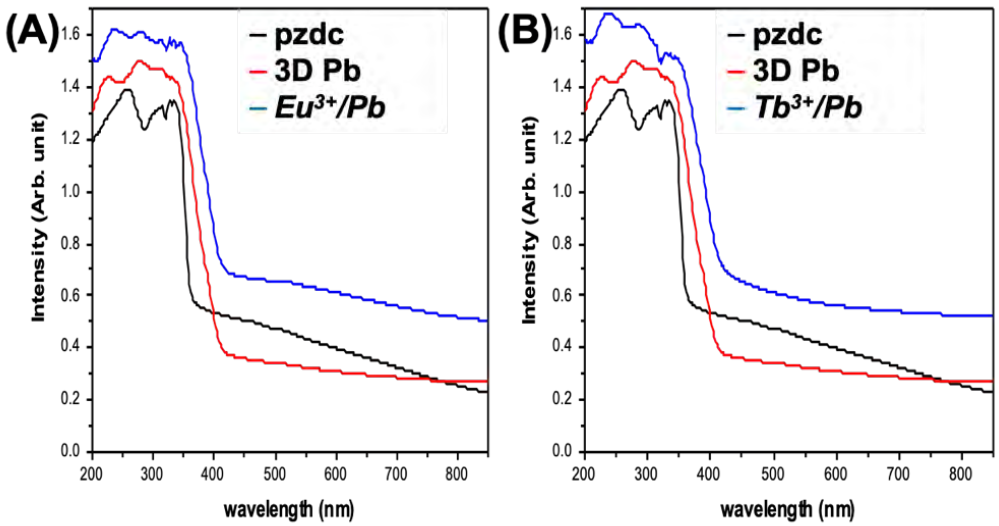

Figure 4.27: UV-Vis spectra of ligand (pzdc), Pristine 3D Pb and *Eu^{3+}-doped 3D MOCP* (A) and *Tb^{3+}-doped 3D MOCP* (B).

A decrease of PL intensity is typically observed in materials doped with 10-20 % Ln^{3+} dopants, hindering the solid state lighting efficiency. (Bünzli, 2014; Ritter et al., 2017) There are reports, however, that show an increase in PL intensity at higher dopant amount (>20%) which depends on synthesis pathway adopted that can leads to the absence of dopant cluster formation, i.e. homogeneous dopant distribution, which reduces PL quenching that occurs due to cross relaxation. (Bünzli, 2014; Ritter et al., 2017)

To enhance the PL efficiency, solid state PL emission was further investigated, the PL emission of as synthesized, 6, 35, and 80 wt. % of Eu^{3+} or Tb^{3+} doped MOCPs, were successfully engineered using the aforementioned synthetic conditions. When excited at 350 nm, both Eu^{3+} and Tb^{3+} doped compounds show only their expected characteristic *f-f* transition peaks. Eu^{3+} doped compounds show a remarkable increase in PL intensity when the dopant amount increases, Figure 4.30 (A), which may suggest the lack of Eu^{3+} clusters formation that can trigger cross relaxation resulting in PL quenching. (Bünzli, 2014; Ritter et al., 2017) Figure 4.30 (B) is the CIE chromaticity diagram and Figure 4.30 (C) is the corresponding digital image of the Eu^{3+} doped with 6, 35 and 80 wt. % under 365nm UV lamp.

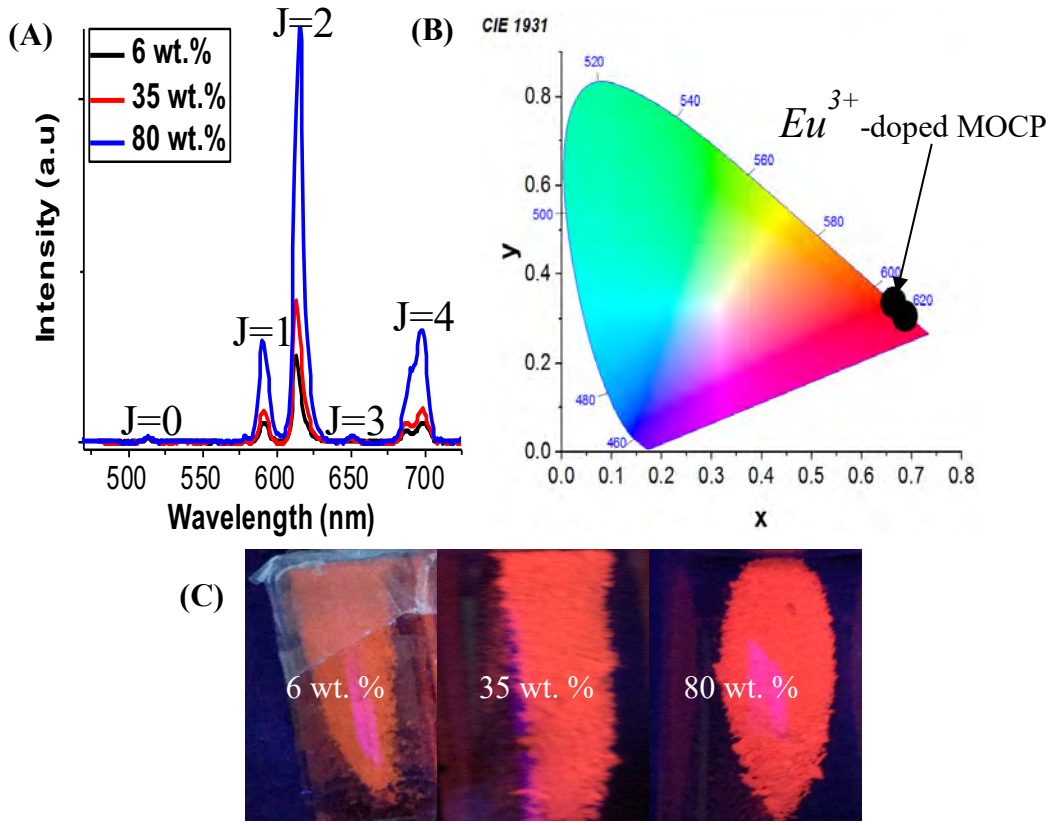

Figure 4.28: Solid-state photoluminescence (emission) spectra of Eu^{3+}-doped MOCP with 6, 35 and 80 wt.% of Eu^{3+} (A), the CIE chromaticity diagram (B) and the digital image of the Eu^{3+} doped with 6, 35 and 80 wt. % under 365nm UV lamp (C).

The fact that partial cation substitutions in this system occurred onto three crystallographically distinct Pb^{2+} sites, they are however well separated by the ligand, which may support the argument that such cluster formation of dopants may diminished or at least be minimized. However, in the case of Tb^{3+}, while displaying typical Tb^{3+} characteristic peaks, the peak intensity decreases as the dopant amount increases, Figure 4.31 (A), interestingly, without total PL quenching. Figure 4.31 (B and C) are the corresponding CIE chromaticity diagram and digital image of the Tb^{3+} doped with 6, 35 and 80 wt. % under 365nm UV lamp. This supports the argument above that the dopant cluster formation, in the case of Tb^{3+}, may well be minimized, hence total PL quenching is not observed.

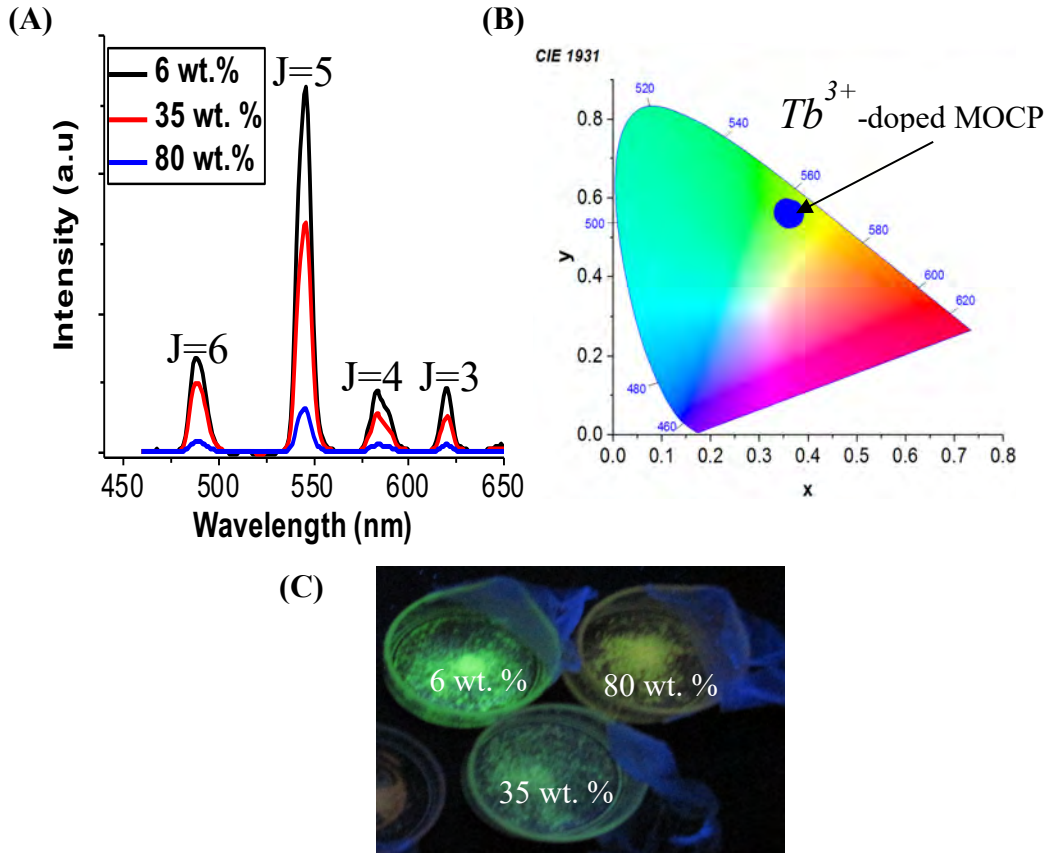

Figure 4.29: Solid-state photoluminescence (emission) spectra of *Tb* $^{3+}$-doped MOCP with 6, 35 and 80 wt.% of Tb^{3+} (A), the CIE chromaticity diagram (B) and digital image of the Tb^{3+} doped with 6, 35 and 80 wt. % under 365nm UV lamp (C).

(h) ***Conductivity measurement***

Preliminary electrochemical impedance spectroscopy was carried out on *Tb* $^{3+}$or *Eu* $^{3+}$-doped MOCPs at 25 ^{o}C to monitor the effect of Ln^{3+} substitutions. Two copper disc probe, room temperature AC impedance spectroscopy was used to analysed the electrical conductance using isostatically bulk powder pressed pellets (1.8 ton and 13 mm diameter) using 0 V DC and 250 mV AC bias with frequency range 1 Hz to 1 MHz. The conductivity values were obtained from the Nyquist plots of the corresponding doped 3D MOCP which present the impedance response and the fit. The pristine 3D MOCP was found to have a resistance (R) of 1.1689 x10^{9} Ω and the corresponding conductivity (σ) of 9.03x10^{-9} S/cm. For 35 wt. % *Eu* $^{3+}$-doped MOCP however, the impedance response at 25 ^{o}C, based

on the Nyquist plot using semicircle fit a resistance of 5.0615×10^5 Ω was obtained and the corresponding conductivity (σ) of 2.34×10^{-5} S/cm which is about 10000 fold improvement from the pristine material. This is despite the numerous grain boundaries, small particle size, and electrode contact resistance associated with measurement.

However, for higher dopant amounts (80 or 99 wt.%) reduction in the conductivity was observed, with 80 wt. % doped having a conductance of 4.267×10^{-7} S/cm, at 25 °C. Similar conductivities was also observed for Tb^{3+}-doped MOCP, but with lower conductivity values. For 35 wt. % Tb^{3+}-doped MOCP was found to have a conductivity (σ) of 1.08×10^{-7} S/cm, with conductance getting lower with increase in dopant amounts. In each case making the doped materials to behave as semiconductors. This improvement in conductivity can be connected to the presence of small cation vacancies that can allow the hoping charge transport typical for coordination polymers. High sensitive and variable temperature set up is however required to further analyze, evaluate and confirm the conductivity as a function of dopant amounts and temperature.

4.5.1.2 Multiple and mixed valence Ln^{3+} doped 3D MOCP

Multivariate materials especially those comprising more than one type of cation or ligand in the structure offered enhanced properties and exceptional applications. (Botas et al., 2011; Brozek & Dincă, 2013; H. Deng et al., 2010; Kong et al., 2013; Lisa J Wang et al., 2014) Devising methods for the design of multivariable MOCPs is very paramount to introducing heterogeneity in ordered materials leading to a higher degree of functionalities. It has been very challenging to introduce multiple building blocks without altering the integrity of the original structure. (Helal et al., 2017) It has also been a formidable task to design multi-cation MOCPs especially the 3*d*-4*f* multi-cation due to competitive reaction between 3*d* and 4*f* cations coordination or geometrical preferences and due to low stereochemical preference and variable or versatile CNs. However, an

MOCP featuring multiple cation centers with varying CN and CE can provide an opportunity to direct different cations into different sites. In this regard, multi-cation, multivariate 3D MOCP was envisaged and successfully engineered. Multiple doping with two or more different Ln^{3+} and also incorporating *3d-4f* mixed orbitals with TMs and Ln^{3+} were prepared.

(a) ***Double doping with Ln^{3+} in 3D MOCP***

Soaking the precursor 1D MOCP for 3 days in aqueous solution of Eu^{3+}/Tb^{3+} or Eu^{3+}/Gd^{3+} or Eu^{3+}/Er^{3+} 1:1:1 1D MOCP/Eu^{3+}/Ln^{3+} mole ratio, multiple and mixed valent MOCPs were obtained containing varying amounts. For instance, Tb^{3+} was found to exchange about 5 wt. % while Eu^{3+} exchange about 2 wt. % in aqueous solution, relatively similar exchange behavior was observed with other double dopants, Table 4.3, Figure 4.32. Changing the solvent to mixture of H_2O/Dioxane/DMF 3:2:2 ratio v/v with addition of 2 drops of pyridine and heated at 90 ^oC for 1 day, increases the dopants amounts, Tb^{3+} exchanging up to 45 wt. % and Eu^{3+} exchanging up to 18 wt. %, similar exchange behavior was also observed for other double dopants Ln^{3+}, Table 4.3. Such an increase is expected because hard Ln^{3+} ions is expected to interact less with the selected solvent mixture than with hard aqueous solution, on the other hand the framework's borderline Pb^{2+} is expected to interact more favorably with the solvent mixture than with hard O-donor environment of the framework paving way for the Ln^{3+} to exchange more Pb^{2+}. The increase in temperature helps to overcome the bond dissociation energy between the Pb^{2+} and the O or N-donor atoms of the pzdc ligands. The PXRD indicates that all the exchanged products are crystalline and pure without any phase separation, Figure 4.33, Scheme 2.

Table 4.3: SEM-EDS (average at. %) or ICP-OES (wt.%)* results of double doped Ln^{3+} 3D MOCPs.

Synthesis condition	Dopants	Amount (at. or wt. %)
H_2O, 3 days, room temp. (r.t)	Eu^{3+}/Tb^{3+}	2.0/5.0
	Eu^{3+}/Gd^{3+}	3.0/6.0
	Eu^{3+}/Er^{3+}	2.0/7.0
H_2O/Dioxane/DMF, pyridine, @90 °C.	Eu^{3+}/Tb^{3+}	18.0/45.0
	Eu^{3+}/Gd^{3+}	22.0/30.0
	Eu^{3+}/Er^{3+}	18.0/47.0

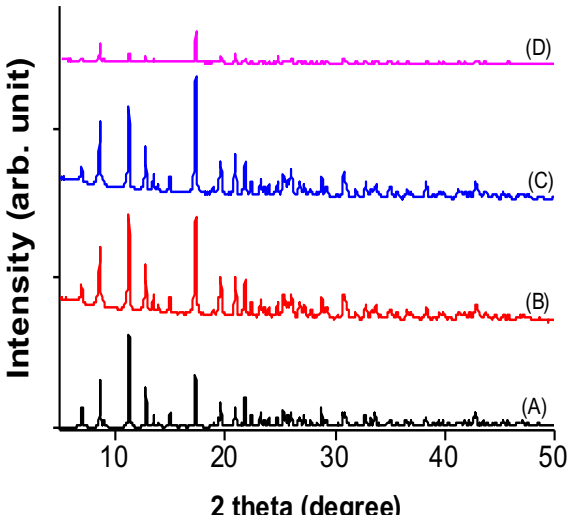

Figure 4.30: PXRD patterns of (A) simulated 3D MOCP, (B) Eu^{3+}/Tb^{3+} doped, (C) Eu^{3+}/Gd^{3+} doped, (D) Eu^{3+}/Er^{3+} doped 3D MOCPs in aqueous solution.

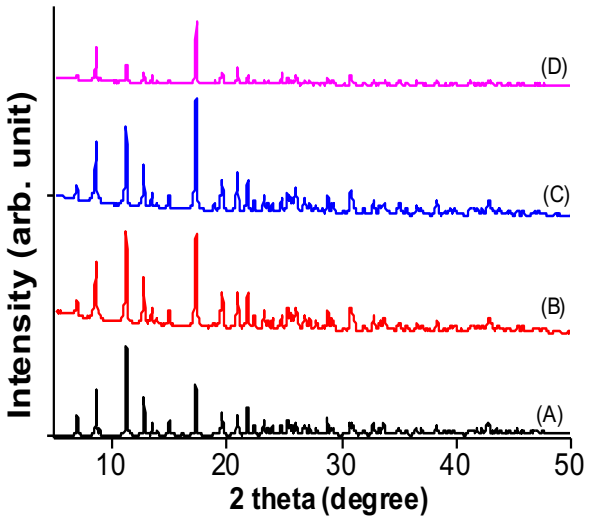

Figure 4.31: PXRD patterns of (A) simulated 3D MOCP, (B) Eu^{3+}/Tb^{3+} doped, (C) Eu^{3+}/Gd^{3+} doped, (D) Eu^{3+}/Er^{3+} doped 3D MOCPs in H_2O/DMF/dioxane solution with 2 drops of pyridine heated at 90 °C for 1 day.

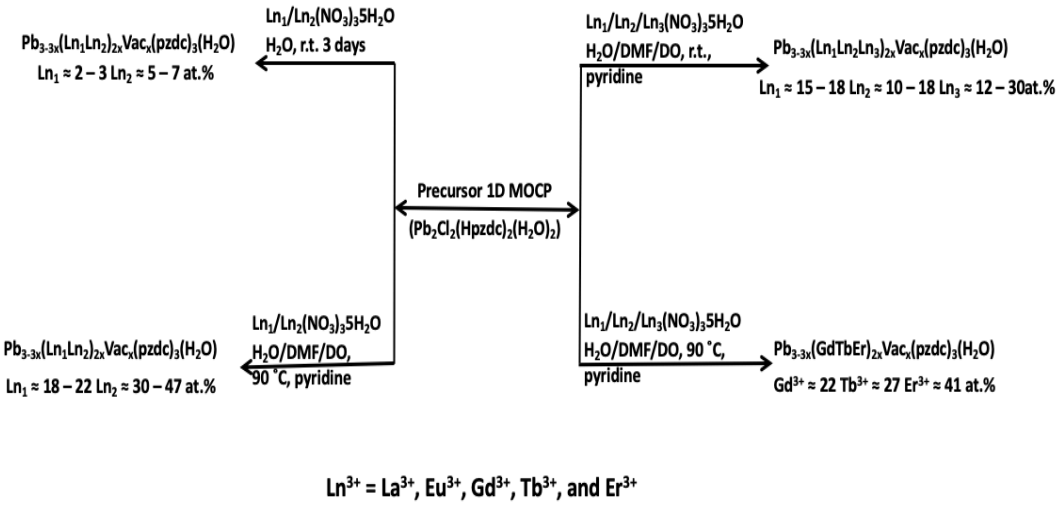

Scheme 2: Summary of multiple and mixed valent Ln^{3+} incorporated in to the 3D MOCPs under different optimized conditions, using the precursor 1D MOCP.

(b) ***Double doping with Zn^{2+}/Ln^{3+} in 3D MOCP***

Doping with *3d*-TMs and *4f*-Ln^{3+} ions such as Zn^{2+} with Eu^{3+} or Tb^{3+} or Gd^{3+} was also carried out by exploring different synthesis conditions. However, based on the SEM-EDX results, Zn^{2+} was found to substitutes more Pb^{2+} than Ln^{3+} in all cases. For instance in aqueous solution as anticipated, while hard Eu^{3+} was only able to exchange about 1 at. % of borderline Pb^{2+}, Zn^{2+} which is a borderline acid was able to exchange up to 4 at. %, giving a general formula of $Pb_{2.84}Zn_{0.12}Eu_{0.02}Vac_{0.02}(pzdc)_3(H_2O)_{0.47}$. SEM-EDX mapping shows a very uniform distribution of both Eu^{3+} and Zn^{2+} in Eu^{3+}/Zn^{2+}-doped 3D MOCP, Figure 4.34. Similar exchange pattern was observed doping the 3D MOCP with other Zn^{2+}/Ln^{3+}, Table 4.4. The phase purity and crystallinity was confirmed by PXRD analysis, Figure 4.35, Scheme 2.

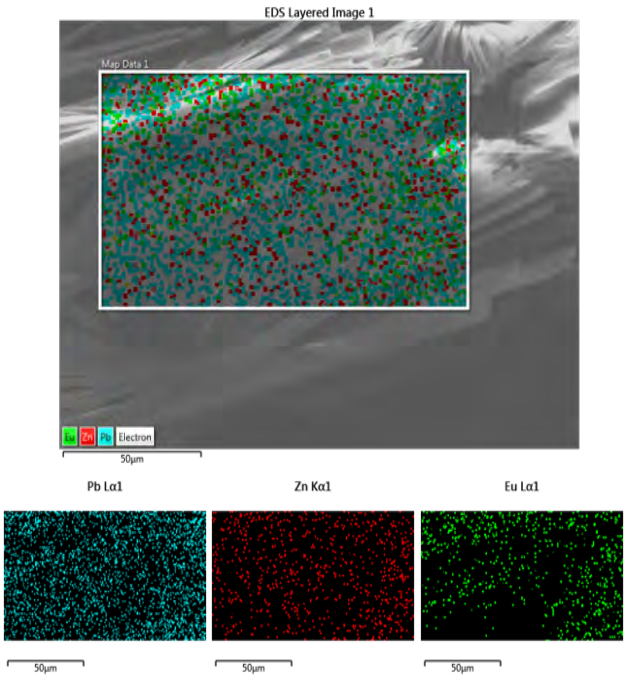

Figure 4.32: SEM-EDS mapping of Eu^{3+}/Zn^{2+}-doped 3D MOCP.

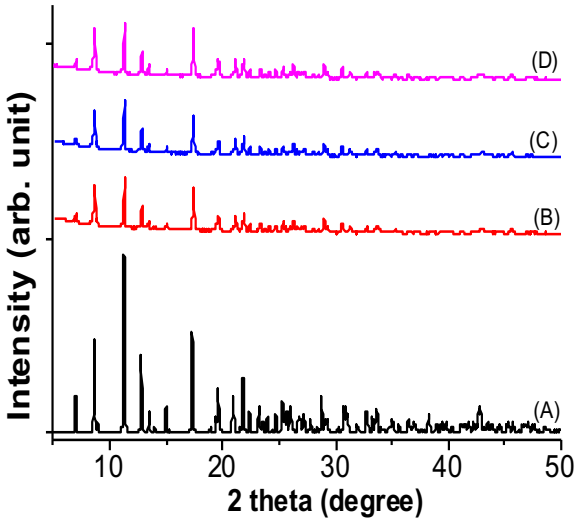

Figure 4.33: PXRD patterns of (A) simulated 3D MOCP, (B) Tb^{3+}/Zn^{2+} doped, (C) Eu^{3+}/Zn^{2+} doped, (D) Gd^{3+}/Zn^{2+} doped 3D MOCPs in aqueous solution.

Further, changing the solvent from H_2O to mixture of H_2O/Dioxane/DMF 3:2:2 ratio v/v for 3 days, as expected increases the amounts of Eu^{3+} doped into 3D MOCP to 12 wt. % while Zn^{2+} amount increases to 20 at. %. On heating at 90 °C for 1 day, the amount of Zn^{2+} increases further to about 35 at. % while that of Eu^{3+} remains about 12 wt. %. Similar exchange behaviour was observed for other Ln^{3+} mixed valent with Zn^{2+}, Table 4.4, scheme 3.

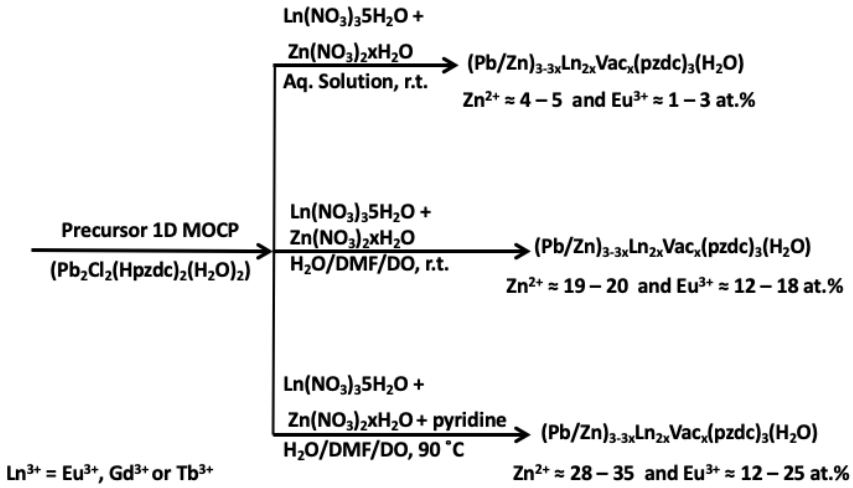

Scheme 3: Summary of mixed valent doping with Ln^{3+} and Zn^{2+} in the 3D MOCP using the 1D precursor MOCP under different conditions.

Table 4.4: SEM-EDS (average at. %) or ICP-OES (wt.%)* results of double and mixed valent Zn^{2+}/Ln^{3+} doped 3D MOCPs.

Synthesis condition	Dopants	Amount (at. or wt. %)
H_2O, 3 days, room temp. (r.t)	Zn^{2+}/Eu^{3+}	4.0/1.0
	Zn^{2+}/Tb^{3+}	5.0/3.0
	Zn^{2+}/Gd^{3+}	4.0/1.0
H_2O/Dioxane/DMF, 3 days, r.t	Zn^{2+}/Eu^{3+}	20.0/12.0
	Zn^{2+}/Tb^{3+}	19.0/18.0
	Zn^{2+}/Gd^{3+}	20.0/16.0
H_2O/Dioxane/DMF, pyridine, @90 ^oC, 1 day	Zn^{2+}/Eu^{3+}	35.0/12.0
	Zn^{2+}/Tb^{3+}	28.0/25.0
	Zn^{2+}/Gd^{3+}	34.0/17.0

(c) ***Multiple doping with Ln^{3+}***

Multiple Ln^{3+} were successfully incorporated into the 3D MOCP in a mixture of solvents with addition of 2 drops of pyridine. Soaking the precursor 1D MOCP in a mixture of H_2O/dioxane/DMF containing 1:1:1 mole ratio of $Tb^{3+}/Eu^{3+}/Gd^{3+}$ or $Sm^{3+}/Gd^{3+}/Tb^{3+}$ or $Gd^{3+}/Tb^{3+}/Er^{3+}$ and 2 drops of pyridine, for 3 days afforded multiple Ln^{3+}-doped 3D MOCP. FESEM-EDS analysis of $Tb^{3+}/Eu^{3+}/Gd^{3+}$-doped MOCP was found to contain 15, 18 and 12 wt. % of Tb^{3+}, Eu^{3+} and Gd^{3+} respectively. Whereas,

$Sm^{3+}/Gd^{3+}/Tb^{3+}$-doped MOCP contains 18, 10 and 20 wt. % for Sm^{3+}, Gd^{3+} and Tb^{3+} respectively. For $Gd^{3+}/Tb^{3+}/Er^{3+}$-doped MOCP the dopant amounts are 18, 18 and 30 wt. % for Gd^{3+}, Tb^{3+} and Er^{3+} respectively, Table 4.5. More than 45 wt. % of Pb^{2+} combined was exchange in each case by 3 Ln^{3+} dopants in each case, this can be attributed to the solvent and modulator effects. The solvent combination used may not favorably solvate hard Ln^{3+} and the addition of borderline modulator ligand (pyridine) is expected to further interacts favorably with borderline Pb^{2+} and deactivate it, paving a way for more Ln^{3+} to be incorporated. Since combination of Gd^{3+}, Tb^{3+} and Er^{3+} was found to exchange more Pb^{2+}, same synthesis conditions but heated solvothermally at 90 °C for 1 day afforded, $Gd^{3+}/Tb^{3+}/Er^{3+}$-doped 3D MOCP containing 22, 27 and 41 wt. % of Gd^{3+}, Tb^{3+} and Er^{3+} respectively, Table 4.5. The increase in temperature to 90 °C aids to overcomes the bond dissociation energies and increases the dopants with combined doped amounts of 90 wt. %. The PXRD indicates that all the exchanged products are pure without any phase separation, Figure 4.36, Scheme 2.

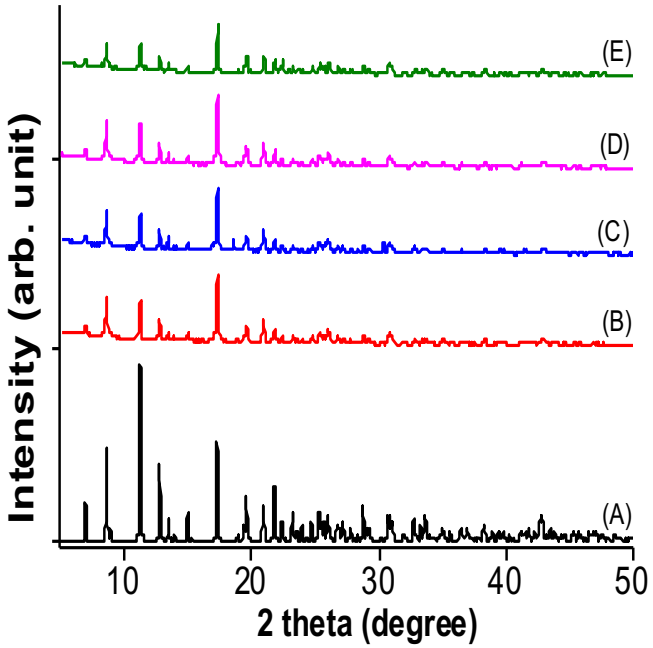

Figure 4.34: PXRD patterns of (A) simulated 3D MOCP, (B) $Tb^{3+}/Eu^{3+}/Gd^{3+}$ doped, (C) $Sm^{3+}/Gd^{3+}/Tb^{3+}$ doped, (D) $Gd^{3+}/Tb^{3+}/Er^{3+}$ doped 3D MOCPs in H_2O/DMF/dioxane, (E) $Gd^{3+}/Tb^{3+}/Er^{3+}$ doped 3D MOCPs in H_2O/DMF/dioxane at 90 °C for 1 day.

Table 4.5: SEM-EDS (average at. %) or ICP-OES (wt.%)* results of multiple Ln^{3+} doped 3D MOCPs.

Synthesis condition	Dopants	Amount (at. or wt. %)
H_2O/Dioxane/DMF, pyridine, 3 days, r.t	$Tb^{3+}/Eu^{3+}/Gd^{3+}$	15.0/18.0/12.0
	$Sm^{3+}/Gd^{3+}/Tb^{3+}$	18.0/10.0/20.0
	$Gd^{3+}/ Tb^{3+}/Er^{3+}$	18.0/18.0/30.0
H_2O/Dioxane/DMF, pyridine, @90 °C, 1 day	$Gd^{3+}/ Tb^{3+}/Er^{3+}$	22.0/27.0/41.0

4.5.2 Doping transition and post transition metals into the 3D MOCP, *$Pb_3(pzdc)_3(H_2O)$*.

Based on the concept of HSAB principle, the first row transition metals (except Sc, Ti, V and Cr which are hard Lewis acids) are borderline Lewis acids that can adopt different chemical environments. Large number of MOCPs reported to date are TMs and carboxylate-based MOCPs that exhibited very fascinating dynamics owing to the lability of their M–L. However, TMs with coordination sphere surrounded by both O and some N-atom donors are more stable than those with all O-donors. N-donor containing ligands tend to increase the stabilities of divalent TMs, due to the decreased bond lability between the TMs and N-donor ligands. Also, many N-based or N and O mixed ligand-based stable MOCPs with divalent TMs was reported. (Burd et al., 2012; Cadiau et al., 2016; Cadiau et al., 2017; Gao et al., 2016; Heering et al., 2013; Y. Hu et al., 2016; Masciocchi et al., 2010; Montoro et al., 2011; Nugent et al., 2013; Shekhah et al., 2014; Tan et al., 2012; Tonigold et al., 2009; X. Wang et al., 2016) The effect of N-donor atoms containing ligand presence in TM's coordination sphere can be observed in large number of relatively stable TM-based MOCPs, featuring slow cation exchange kinetics or in some cases not proceeding to completion (Yao et al., 2012; Z. Zhang et al., 2013).

Both first row TMs and Pb^{2+} ions are borderline Lewis acids, it is therefore expected for the TMs to exchange Pb^{2+} using suitable conditions since they are in the same

category, though to a varying degrees as their hardness or softness varies. Based on the HSAB, the stability of the TMs complexes may increases as a function of increasing hardness of the TM from Mn^{2+}< Co^{2+} < Ni^{2+} < Zn^{2+} < Cu^{2+}, especially in a typical all O-donor environment, that is also in line with the Irving-Williams series (Irving & Williams, 1953). With the exception of Cu due to its anomalous electronic configuration and coordination preference, TMs are reported to have more preference for either square planner, trigonal prism, tetrahedral and octahedral geometries. Since the 3D MOCP has three unique crystallographic sites Figure 4.14 (A), TMs are expected to exchange more preferentially at Pb(1) site having an octahedral geometry with CN of 6 and also surrounded by both hard O-donors and soft N-donors in addition to the presence of coordinated H_2O. Other TMs such as Cu^{2+}, Fe^{2+} or Mn^{2+} are expected to exchange at all the Pb-sites owing to their ability to adopt different CN and CE. Since the exchange is solvent mediated and taking place simultaneously with structural transformation, a careful and judicious control of the phase formation, stability and integrity of the final structure must be ensured through the use of suitable solvent or solvent mixture.

4.5.2.1 Aqueous solution mediated divalent TMs doping into 3D MOCP $Pb_3(pzdc)_3(H_2O)$

When 0.035 mmol of the precursor 1D MOCP (*$Pb_2Cl_2(Hpzdc)_2(H_2O)_2$*, was immersed in 7 mL, aqueous solution of 0.07 mmol of various nitrate salts of TM cations (Mn^{2+}, Co^{2+}, Ni^{2+}, Fe^{2+}, Cu^{2+}, Cd^{2+}, Zn^{2+} or Hg^{2+}) for 3 days TM-doped 3D MOCPs were successfully synthesized. However, Fe^{2+} and Cu^{2+} does not proceeds to the preferred 3D structure. Cu^{2+} transformed to another 1D MOCP, Figure 4.9 and Fe^{2+} exchanged all Pb^{2+} in the precursor 1D MOCP without structural transformation, all exchanges proceeded very fast in each case. To render Fe^{2+} or Cu^{2+} cation exchange in to doped 3D MOCPs, a mixture of solvent were used. For instance, soaking chloride salts of Fe^{2+} in 1:1 ratio, DMF/H_2O or acetate salt of Cu^{2+} in 1:1:1 ratio, DMF/H_2O/dioxane favors the formation

of doped 3D MOCP. Scheme 4, provides a summary of TM^{2+} exchanged in aqueous solution.

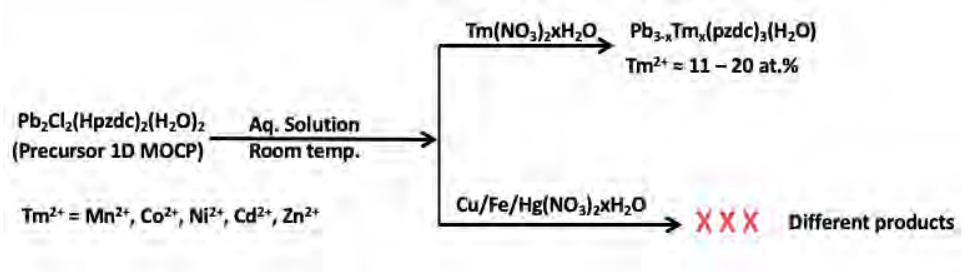

Scheme 4: Summary of Tm^{2+} doped into the 3D MOCP using the precursor 1D MOCP under different conditions.

Quantitative analysis of these compounds using SEM-EDS shows the presence of respective substituents in the range of 8 – 20 atomic %, Table 4.6. Due to the fact that these compounds were of similar structure to that of *Co^{2+}-doped* 3D MOCP, and the presence of respective divalent dopant was detected quantitatively, and their similar geometrical preference to that of Co^{2+}, (Howell & Burkinshaw, 1983) it is then assumed that each aqueous solvent mediated divalent dopant substitutes at the Pb(1) sites with a similar small shift from the actual Pb(1) sites, Figure 4.37, analogous to that of *Co^{2+}-doped* 3D MOCP. Such a shift can be attributed to the absence of lone pair in these transition metal (TM) dopants, as such, a less distorted octahedral was observed compared to that of Pb^{2+} with its pronounced lone pair effect. The preference for Pb(1) sites by exogenous borderline TM dopants is likely due to favourable CN (i.e., six) and CE (having both N and O donors including coordinated water), Figures 4.37. The purity and crystallinity was confirmed using PXRD, Figure 4.38.

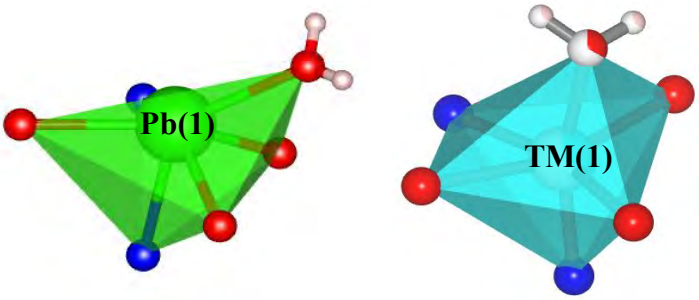

Figure 4.35: Pb(1) coordination geometry before and after exchange with TMs

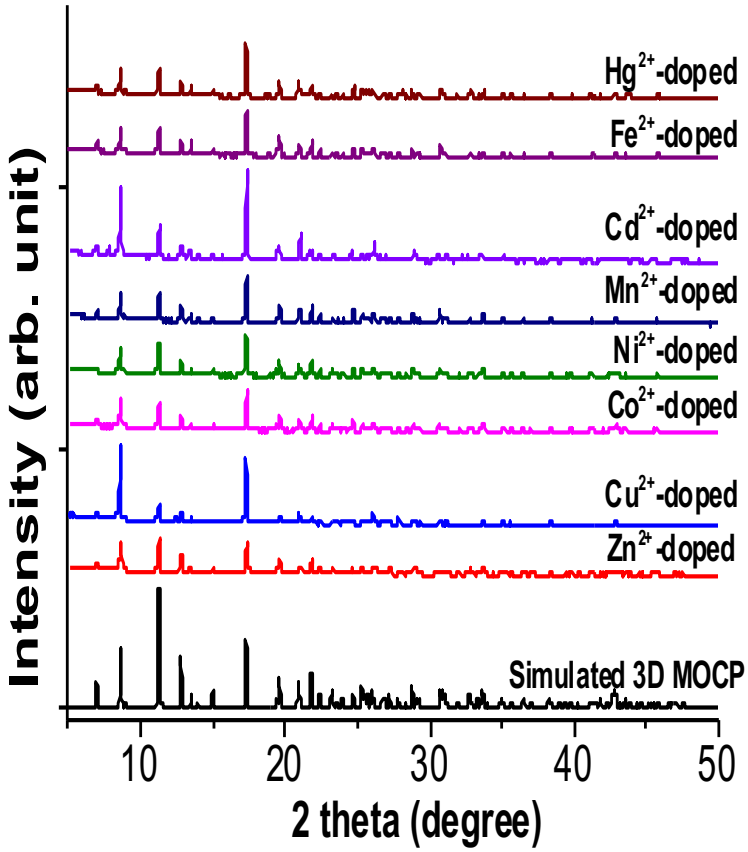

Figure 4.36: PXRD patterns of simulated and observed patterns of M^{2+}-*doped* 3D MOCP in aqueous solution (M = Co, Ni, Zn, Cu, Cd, Fe, Mn or Hg).

Fe^{2+} and *Zn^{2+}-doped 3D MOCPs,* as representatives were characterized by XPS to investigate their oxidation state and CE. The binding energy of Pb 4*f* orbital is assigned as 143.3 ($4f_{5/2}$) and 138.4 ($4f_{7/2}$) eV which is consistent with +2 oxidation states of Pb. (A. Y. Lee et al., 2012) The binding energies at 1022.5eV and 710.2eV correspond to the Zn

($2p_{3/2}$) and Fe ($2p_{3/2}$) orbitals in *Eu^{3+}/Zn^{2+}-doped MOCP* and *Fe^{2+}-doped MOCP*, respectively, Figure 4.39.

Table 4.6: SEM-EDS (average at. %) or ICP-OES (wt.%)* results of dopant in Ln^{3+} doped Pb^{2+} MOCPs.

Dopant	Amount (atomic or wt.%)
Co^{2+}	11
Ni^{2+}	20
Zn^{2+}	17
Cu^{2+}	11
Cd^{2+}	12
$Fe^{2+,}$ *	11
Mn^{2+}	17
Hg^{2+}	8

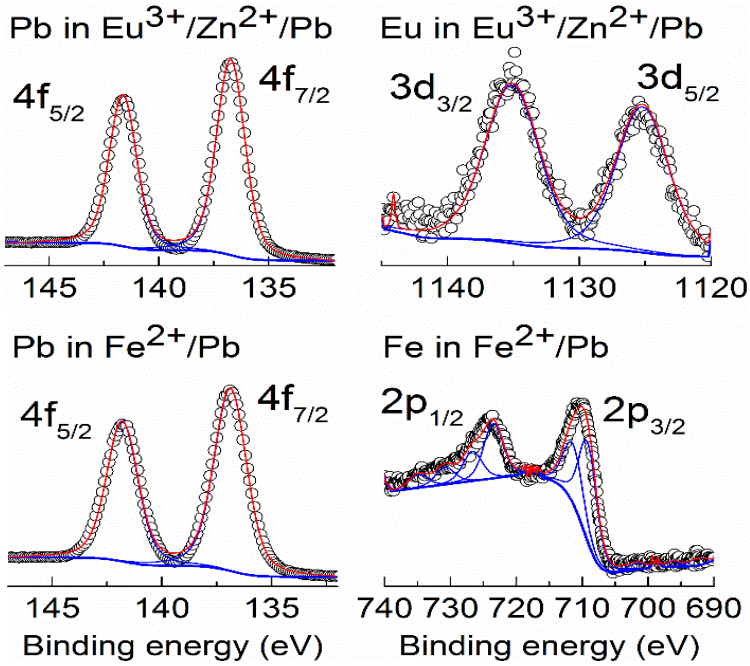

Figure 4.37: XPS spectra of Fe^{2+}-doped and Eu^{3+}/Zn^{2+}-doped 3D MOCP

(a) ***Cu^{2+}-doped 3D MOCP $Pb_3(pzdc)_3(H_2O)$***

Cu^{2+} is the most electronegative first row TM, with an anomalous electronic configuration. It is found in the literature to virtually and aggressively exchange all other TMs and in most cases irreversibly irrespective of the CE or coordination geometry (Brozek & Dinca, 2014). For example, Cu^{2+} readily substitutes Fe^{2+}, Zn^{2+}, Co^{2+}, Mn^{2+} or

Ni^{2+} in many labile MOFs to thermodynamically more stable Cu^{2+} MOCPs, which makes the reverse exchange to be difficult in many cases. Based on the HSAB, the stability of these TM product increases as a function of increasing hardness of the TM from Mn^{2+}< Co^{2+} < Ni^{2+} < Zn^{2+} < Cu^{2+}, especially in a typical all O-donor environment, also in line with the Irving-Williams series. So, it is expected for Cu^{2+} to substitutes at all the 3 Pb(sites) having 6, 7 and 9 CNs.

Owing to its fast kinetics and aggressiveness, Cu^{2+} totally exchanged the precursor 1D MOCP into another 1 D structure without allowing structural transformation to 3D MOCP upon soaking in aqueous solution, Figure 4.10. However, when a mixture of H_2O/DMF/dioxane as the solvent, the kinetics was slowed down and the precursor 1D MOCP transformed to 3D with 11 at. % substituted, using 1:1 mole ratio of the precursor 1D MOCP to Cu^{2+} salt. But since Cu^{2+} has the potential to substitutes at all the 3 Pb-sites, further techniques was explored. For example, slowing down the kinetics was the first consideration and as such, lowering the pH by addition of 2 drops of 2M HCl the doping amount increases to 43 at. %. The addition of HCl was intended to suppress the kinetics aggressiveness of Cu^{2+} in breaking the chloride bridging of the precursor 1D MOCP. Presence of excess H^+/H_3O^+ and Cl^+ in the solution may slows the transformation by suppressing the deprotonation of free protonated OH group and chloride bridging breakage during the transformation of the precursor 1D MOCP to 3D MOCP. To further increases the dopant amount, 1 drop of pyridine or 0.002 mmol of piperazine was also further added and in this case the Cu^{2+} ions exchanged more than 99 at. % with clean PXRD in all cases, Figure 4.40. FESEM-EDX was used to confirm the at. %, Table 4.7. Addition of piperazine alone without HCl also allowed the transformation with 98 at. % of Cu^{2+} doped in to the 3D MOCP structure. Remarkably, all the transformations and exchanges are only done in 1:2 ratio of the precursor 1D MOCP to Cu^{2+} salt, increasing the mole ratio to 1:4 as in the case of most Ln^{3+}, does not produce pure 3D MOCP, as

more concentration led to the collapse of the framework. Though, using 1:1 mole ratio also allows the transformation to 3D MOCP with Cu^{2+} exchanging between 35 to 50 at. %, Table 4.7, Scheme 5.

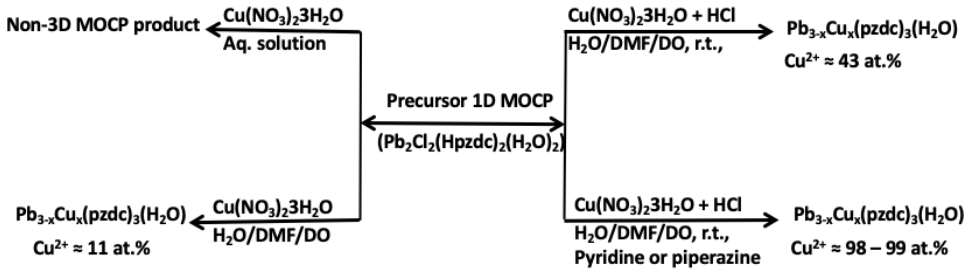

Scheme 5: Summary of Cu^{2+} doped 3D MOCP using the precursor 1D MOCP under different conditions.

Table 4.7: SEM-EDS (average at. %) or ICP-OES (wt.%)* results of Cu^{2+} doped 3D MOCPs.

Synthesis condition	Dopant at. %
H_2O/Dioxane/DMF, HCl, 3 days, r.t	43
H_2O/Dioxane/DMF, HCl, pyridine, 3 days, r.t	99
H_2O/Dioxane/DMF, HCl, piperazine, 3 days, r.t	98
H_2O/Dioxane/DMF, piperazine, 3 days, r.t	98
H_2O/Dioxane/DMF, pyridine, 1:1 mole ratio 1D MOCP to Cu^{2+} 3 days, r.t	50

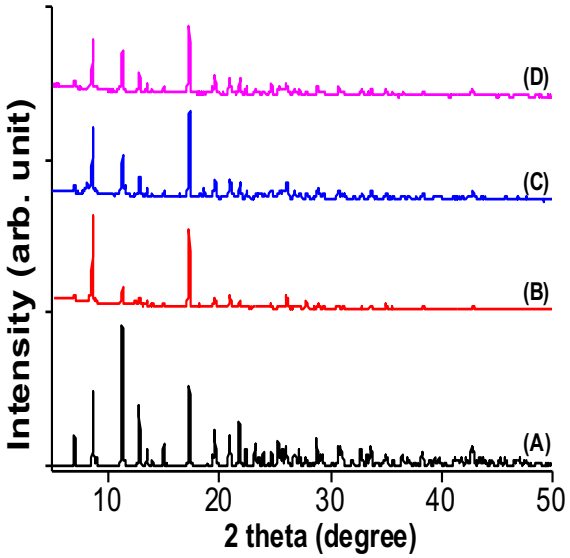

Figure 4.38: PXRD patterns of simulated 3D MOCP (A) and observed Cu^{2+}-doped 3D MOCP in H_2O/DMF/dioxane with (B) 2 drops HCl (C) HCl and pyridine (D) HCl and piperazine.

(b) ***Zn^{2+}-doped 3D MOCP $Pb_3(pzdc)_3(H_2O)$***

Since Pb(1) and Pb(2) sites are six and seven coordinated respectively and Zn^{2+} can adopt also octahedral geometry and in some special cases adopts CN 7, although its most preferred CN in structure formation is four (tetrahedral). (Abdelhameed et al., 2016; Ataie et al., 2008; Dudev et al., 2006) Strategies needs to be devised to increases the amount of Zn^{2+} doping in to the 3D MOCP. In this regard, several synthetic procedures were explored, including the use of solvent mixture, varying mole ratio, temperature or addition of modulator ligand.

For instance soaking the precursor 1D MOCP in a mixture of H_2O/dioxane 5:2 ratio for 3 days, the structural transformation proceeded with exogenous Zn^{2+} ions exchanging up to 25 at. %. While in a mixture of H_2O/DMF/ACN 1:3:3 ratio for 3 days, the amount of Zn^{2+} increases to about 28 at. %, however soaking in H_2O/DMF/dioxane 2:2.5:2.5 ratio for 3 days afforded Zn^{2+}-doped 3D MOCP containing about 20 at. %. The PXRD patterns indicates the phase purity and absence of any impurity in the doped materials, Figure 4.41, and the dopant amounts are confirmed by FESEM-EDX analysis Table 4.8, Scheme 6.

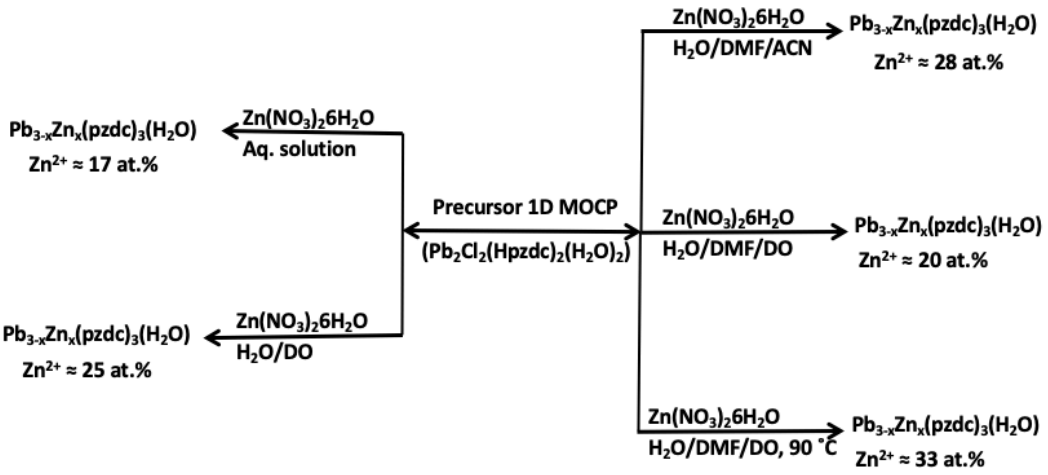

Scheme 6: Summary of Zn^{2+} incorporated into the 3D MOCP using the precursor 1D MOCP under different conditions.

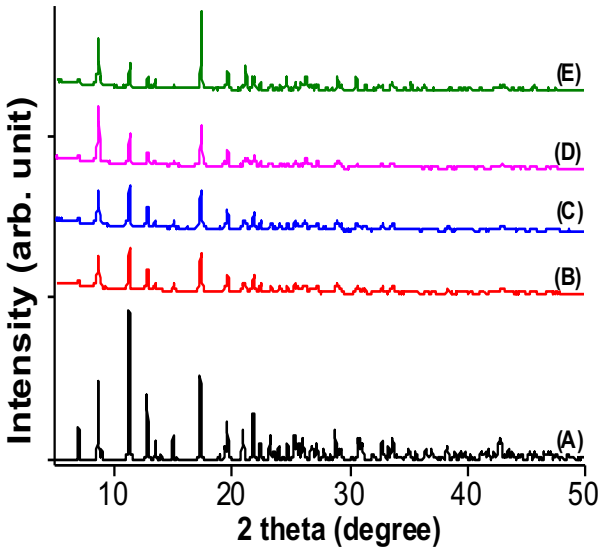

Figure 4.39: PXRD patterns of simulated 3D MOCP (A) and observed Zn^{2+}-doped 3D MOCP in H_2O/DMF/ACN (B) H_2O/DMF/dioxane (C) H_2O/DMF/dioxane and pyridine (D) H_2O/DMF/dioxane, pyridine at 90 ^oC (E).

Table 4.8: SEM-EDS (average at. %) or ICP-OES (wt.%)* results of Zn^{2+} doped 3D MOCPs.

Synthesis condition	Dopant at. %
H_2O, 3 days, r.t	17
H_2O, pyridine, 3 days, r.t	25
H_2O/Dioxane, 3 days, r.t	25
H_2O/DMF/ACN, 3 days, r.t	28
H_2O/DMF/dioxane, 3 days, r.t	20
H_2O/Dioxane/DMF, at 90 ^oC for 3 hours.	33

The effect of modulator ligand can be observed when 2 drops of pyridine was added into an aqueous solution of nitrate salt of Zn^{2+} for 1 day, the exogenous Zn^{2+} further increases from 17 to 25 at. %. When 2 drops of pyridine is added into the solvent mixture H_2O/DMF/dioxane solution of nitrate salt of Zn^{2+} with heating at 90 ^oC for only 3 hours, the dopant amount increases from 20 to 33 at. % after addition of pyridine. Although based on the HSAB principle both Pb^{2+} and Zn^{2+} are borderline acid, Zn^{2+} is relatively harder than Pb^{2+} as such the modulator ligand is expected to relatively interact more with Pb^{2+} than with Zn^{2+}, paving a way for the slight increase due to the addition of pyridine. The purity is also ascertained using PXRD, Figure 4.41 and the dopant amount confirmed

by FESEM-EDS analysis Table 4.8. Changing the mole ratio of exogenous Zn^{2+} to the precursor 1D MOCP does not show any improvement in the dopant amount. For example, changing the ratio from 1:2 to 1:4 the precursor 1D MOCP to exogeneous Zn^{2+} in aqueous solution does not increases the dopant amount.

(c) ***Ni^{2+}-doped 3D MOCP $Pb_3(pzdc)_3(H_2O)$***

Complexes of Ni^{2+} are more stable than that of Co^{2+}, Fe^{2+}, or Mn^{2+} based on the Irvin-Williams series and also based on the concept of HSAB principle, Ni^{2+} is also harder than both Co^{2+}, Fe^{2+}, or Mn^{2+}. In addition to this, since Ni^{2+} can preferentially adopts CN up to 7, it is expected to exchange both Pb(1) and Pb(2) sites with 6 and 7 coordination numbers.

Soaking the precursor 1D MOCP in aqueous nitrate solution of Ni^{2+} for 3 days, 20 at. % exchanged in to the 3D structure. Addition of 2 drops of pyridine into the aqueous solution reduces the exchanged amounts to only 8 at. % which could be attributed to the interactions of Ni^{2+} ions with pyridine in solution preventing it from exchanging Pb^{2+}. Changing the precursor salt from nitrate to chloride, in aqueous solution increases the dopant amounts to 29 at. %. This may be attributed to the presence of chloride ions which may suppresses the breakage of chloride bridging in the precursor 1D MOCP which slow down the transformation kinetics of he precursor 1D MOCP to 3D MOCP. Soaking in a mixture of H_2O/DMF/dioxane and addition of 2 drops of pyridine using 1:4 mole ratio of the precursor 1D MOCP to Ni^{2+} salt, 30 at. % of Pb^{2+} was exchanged by Ni^{2+}, using 1:2 mole ratio of the precursor 1D MOCP to Ni^{2+} salt however, it exchanged about 20 at. %. To increase the dopant, dioxane was substituted with acetonitrile in the solvent mixture H_2O/DMF/ACN, the dopant amount increases to 40 at. %, heating or adding pyridine does not improved the dopant amount. The phase purity of all the exchanged products

were indicated by PXRD, Figure 4.42 and the dopant amounts are were confirmed using FESEM-EDS, Table 4.9, Scheme 7.

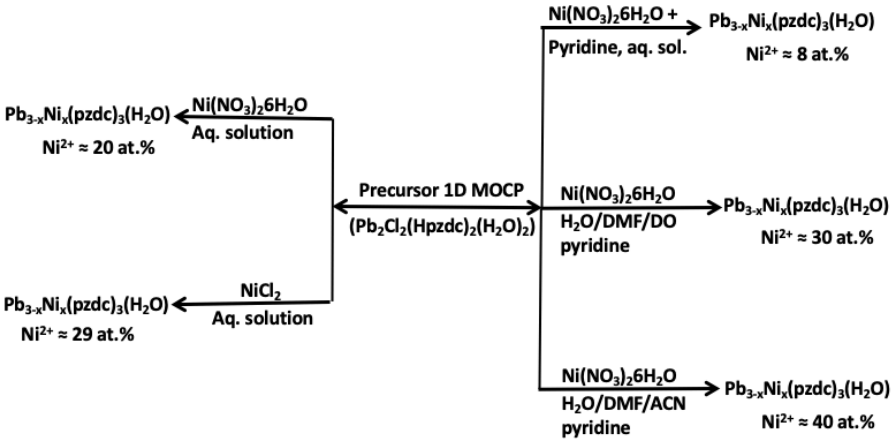

Scheme 7: Summary of Ni^{2+} incorporated into the 3D MOCP using the precursor 1D MOCP under different conditions.

Table 4.9: SEM-EDS (average at. %) or ICP-OES (wt.%)* results of Ni^{2+} doped 3D MOCPs.

Synthesis condition	Dopant at. %
H_2O, 3 days, r.t	20
H_2O, pyridine, 3 days, r.t	8
H_2O, using chloride salt, 3 days, r.t	29
H_2O/DMF/dioxane, pyridine, 1 day, r.t	30
H_2O/DMF/ACN, 1 day, r.t	40

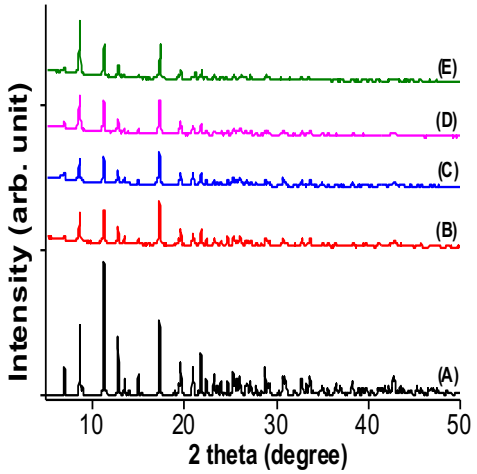

Figure 4.40: PXRD patterns of simulated 3D MOCP (A) and observed Ni^{2+}-doped 3D MOCP in H_2O and pyridine (B) H_2O/DMF/dioxane (C) H_2O/DMF/dioxane and pyridine (D) H_2O/DMF/ACN (E).

(d) ***Co^{2+}-doped 3D MOCP $Pb_3(pzdc)_3(H_2O)$***

Based on the Irvin-Williams series, Co^{2+} complexes may be less stable than Cu^{2+} or Zn^{2+} complexes which can be attributed to the fact that, based on the HSAB principle, Co^{2+} is softer than both Cu^{2+}, Ni^{2+} and Zn^{2+}. Soaking the precursor 1D MOCP in aqueous solution of nitrate salt of Co^{2+} for 3 days, afforded only 11 at. %, whereas when 2 drops of pyridine was added to the aqueous solution, the dopant amount drops to only about 2 at. %, this can attributed to the softness of Co^{2+} in which on addition of pyridine, prevents Co^{2+} from doping in to the 3D structure. To increase the dopant amount, solvent mixture was used, in H_2O/DMF/dioxane, increases the dopant amount to 19 at. %. Using the solvent mixture with addition of 2 drops pyridine and heating at 90 ^oC also decreases the dopant amount to 8 at. %. However, when soaked using H_2O/DMF/ACN with 2 drops of pyridine, the dopant amount increases to 43 at. %, Figure 4.43, Table 4.10, Scheme 8.

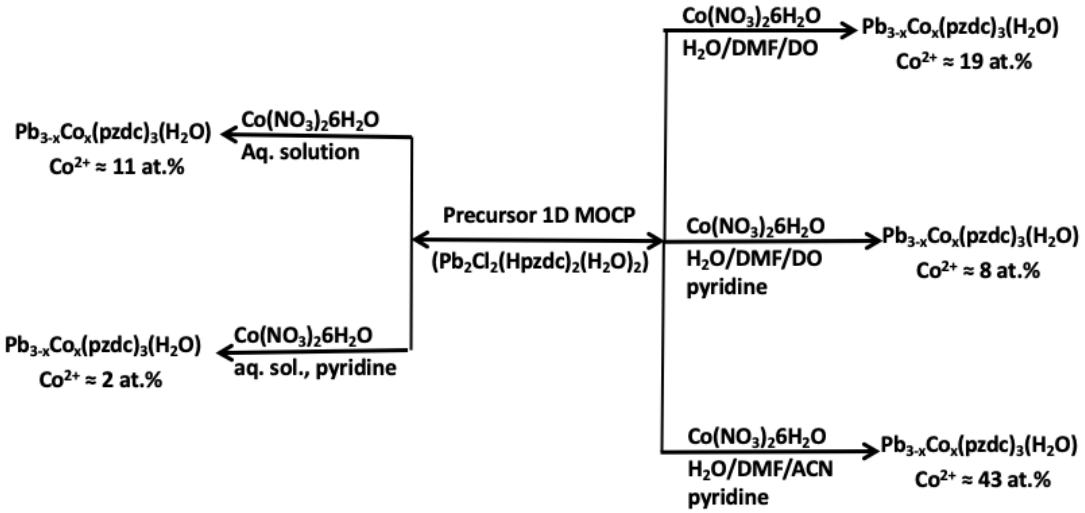

Scheme 8: Summary of Co^{2+} incorporated into the 3D MOCP using the precursor 1D MOCP under different conditions.

Table 4.10: SEM-EDS (average at. %) or ICP-OES (wt.%)* results of Co^{2+} doped 3D MOCPs.

Synthesis condition	Dopant at. %
H_2O, 3 days, r.t	11
H_2O, pyridine, 3 days, r.t	2
H_2O/DMF/dioxane, 3 days, r.t	19
H_2O/DMF/dioxane, pyridine, 1 days, at 90 °C.	8
H_2O/DMF/ACN, pyridine, 3days, r.t	43

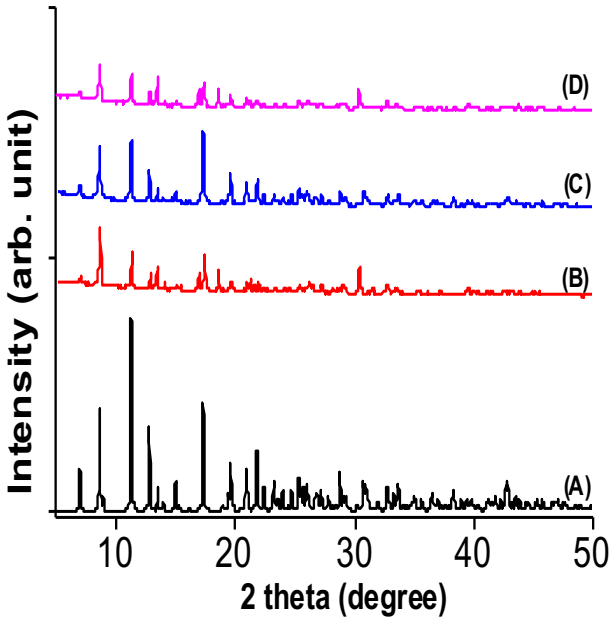

Figure 4.41: PXRD patterns of simulated 3D MOCP (A) and observed Co^{2+}-doped 3D MOCP in H_2O/DMF/dioxane (B) H_2O/DMF/dioxane and pyridine (C) H_2O/DMF/ACN and pyridine(D).

(e) ***Mn^{2+}-doped 3D MOCP $Pb_3(pzdc)_3(H_2O)$***

Mn^{2+} is large and flexible borderline Lewis acid that can adopt variety of CN and CE, although it is expected to exchange at all the 3 crystallographic Pb-sites, however the thermodynamic stability for Mn^{2+} complexes based on the Irvin-Williams series are less stable than other first row TMs.

Soaking the precursor 1D MOCP in aqueous solution of Mn^{2+} for 3 days at room temperature, afforded a 3D MOCP containing 17 at. % Mn^{2+}. Addition of 2 drops of pyridine in the aqueous solution of Mn^{2+} as expected prevented the relatively soft Mn^{2+}

from substituting Pb^{2+}, with only about 5 at. % substituted. The use of solvent mixture H_2O/DMF/dioxane, does not improve the exchange either with only about 4 at. % exchanged in to the 3D MOCP, addition of 2 drops of pyridine in the solvent mixture also no improvement was recorded, exchanging only about 5 at. % of Pb^{2+} into the 3D MOCP. Since Mn^{2+} is relatively soft it may stay and interact more favorably with the relatively soft solvent mixture and the addition of pyridine further prevents its substitution into the 3D structure. However, using a mixture of H_2O/DMF/ACN more than 98 at. % of Mn^{2+} was exchanged in to the 3D MOCP in a relatively fast structural transformation. ACN is stronger base than dioxane and as such, Mn^{2+} may not interact strongly and this allows it to exchange more Pb^{2+}. To slow down the kinetics of transformation, dilute acid was added, although the transformation slowed down, slightly less amount of Mn^{2+} exchanged in to the 3D MOCP exchanging 87 at. %. See summary, Scheme 9. The phase purity and the crystallinity of the doped products was confirmed using PXRD, Figure 4.44 and the presence of these dopants and their at. %, Table 4.11 was determined using FESEM-EDX.

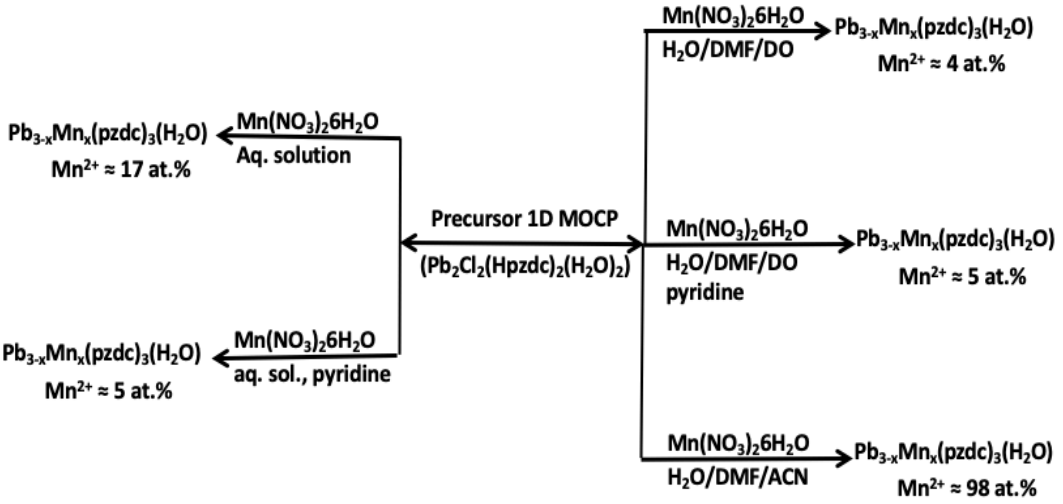

Scheme 9: Summary of Co^{2+} incorporated into the 3D MOCP using the precursor 1D MOCP under different conditions.

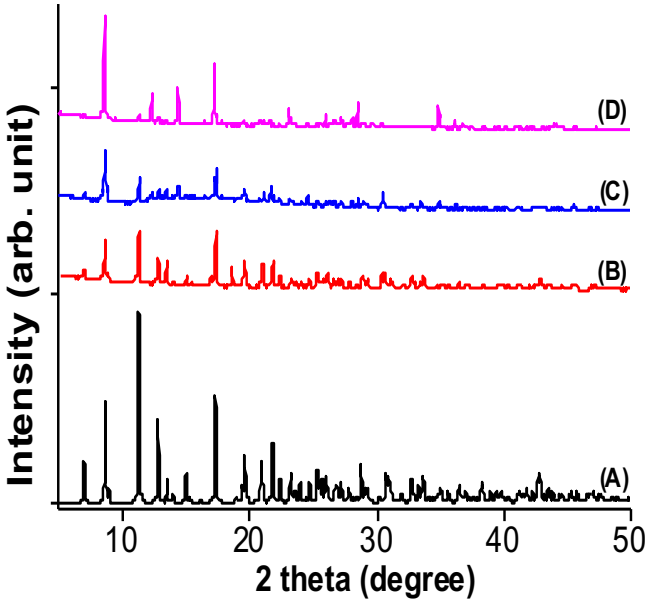

Figure 4.42: PXRD patterns of simulated 3D MOCP (A) and observed Mn^{2+}-doped 3D MOCP in H_2O/DMF/dioxane (B) H_2O/DMF/ACN (C) H_2O/DMF/ACN and H_2SO_4 (D).

Table 4.11: SEM-EDS (average at. %) or ICP-OES (wt.%)* results of Mn^{2+} doped 3D MOCPs.

Synthesis condition	Dopant at. %
H_2O, 3 days, r.t	17
H_2O, pyridine, 3 days, r.t	5
H_2O/DMF/dioxane, 3 days, r.t	4
H_2O/DMF/dioxane, pyridine, 3 days.	5
H_2O/DMF/ACN, 3days, r.t	98
H_2O/DMF/ACN, H_2SO_4, 3days, r.t	87

(f) ***Fe^{2+}-doped 3D MOCP $Pb_3(pzdc)_3(H_2O)$***

Fe^{2+} is a borderline Lewis acid that can adopt different CE and CN, it is therefore expected to exchange at all the 3 unique Pb-sites. However, owing to its high ligand exchange kinetics and lower hydrolysis equilibrium constant compared to its higher oxidation state, Fe^{3+}. (T.-F. Liu et al., 2014) As such, the Fe^{2+} may not be able to easily form stable exchanged products especially with high dopant amounts.

Soaking the precursor 1D MOCP in H_2O/DMF solution of nitrate salt of Fe^{2+} for 3 days at room temperature afforded the 3D MOCP with 11 wt. % Fe^{2+} exchanged in to the structure. Changing the precursor salt to chloride salt of Fe^{2+} in H_2O/DMF solution afforded an increase in the dopant to 36 at. % after 2 weeks. Further, using a triple solvent mixture H_2O/DMF/dioxane afforded only about 15 at. %. And addition of pyridine does not increases the dopant amount as expected, because relatively soft Fe^{2+} may interacts more with the solvent mixture and this may prevents it from exchanging the Pb^{2+}. Increasing the synthesis temperature also does not yield any improvement on the amount doped. Other Fe^{2+} precursors were then explored using a 3 solvent mixture system, for instance, using an acetate salt of Fe^{2+} solution in H_2O/DMF/dioxane for 2 weeks, the dopant amount increases to 21 at. %. However, when chloride salt of Fe^{2+} is used 63 at. % of Fe^{2+} was substituted in to the 3D MOCP. Since Fe^{2+} has the potential to exchange at all the 3 Pb-sites, to further increase the dopant amount, the chloride salt of Fe^{2+} in H_2O/DMF/dioxane solution was heated at 90 ^oC for 1 and 5 days, nonetheless, the amount of Fe^{2+} doped reduces as the heating time increases with 40 and 13 at. % for 1 and 5 days heating periods respectively. This reduction can be connected to the high ligand exchange rate associated with Fe^{2+}. The phase purity and the crystallinity of the doped products was confirmed using PXRD, Figure 4.45 and the presence of these dopants and their at. %, Table 4.12 was determined using FESEM-EDX. Scheme 10 summarized the processes and the products obtained.

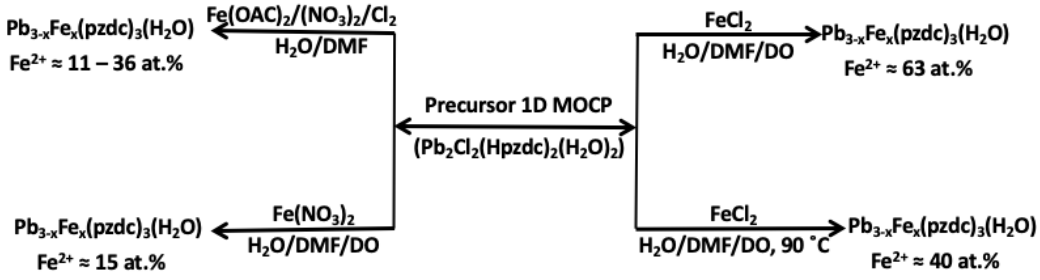

Scheme 10: Summary of Fe^{2+} incorporated into the 3D MOCP using the precursor 1D MOCP under different conditions.

Table 4.12: SEM-EDS (average at. %) or ICP-OES (wt.%)* results of Fe^{2+} doped 3D MOCPs.

Synthesis condition	Dopant at. %
H_2O/DMF, Iron(II)nitrate, 3 days, r.t.	11*
H_2O/DMF/dioxane, Iron(II)nitrate, 3 days, r.t.	15
H_2O/DMF, Iron(II)acetate, 2 weeks, r.t.	21
H_2O/DMF, Iron(II)chloride, 3 days, r.t.	36
H_2O/DMF/dioxane, Iron(II)chloride, 2 weeks, r.t.	63
H_2O/DMF/dioxane, Iron(II)chloride, 1 day, at 90 °C.	40
H_2O/DMF/dioxane, Iron(II)chloride, 5 days, at 90 °C.	13

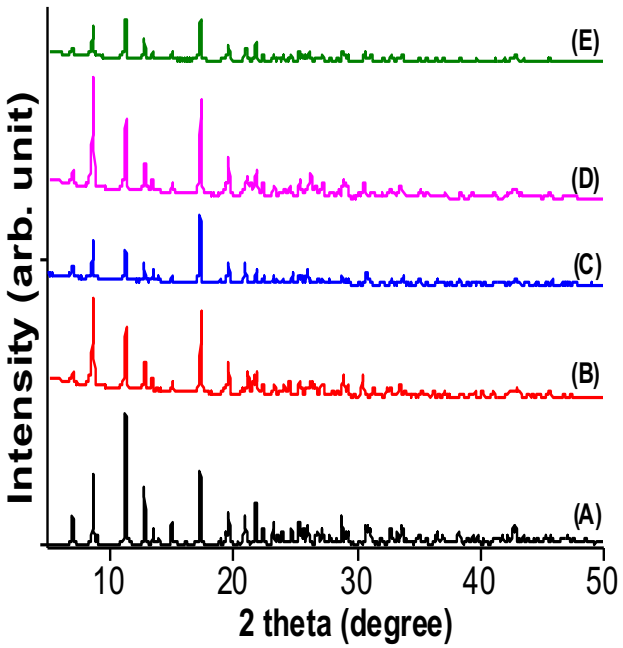

Figure 4.43: PXRD patterns of simulated 3D MOCP (A) and observed Fe^{2+}-doped 3D MOCP in H_2O/DMF (B) H_2O/DMF/dioxane (C) H_2O/DMF/ACN at 90 °C (D) H_2O/DMF/dioxane using Fe(II)acetate precursor(E).

X-ray Photoelectron Spectroscopy (XPS) was used to confirm the oxidation state and the chemical environment of both the Fe^{2+} and Pb^{2+} in Fe^{2+}-doped 3D MOCP. The splitting of the binding energy of 4*f* orbitals as 143.3 ($4f_{5/2}$) and 138.4 ($4f_{7/2}$) eV in the Pb is consistent with the oxidation state of +2 (A. Y. Lee et al., 2002). The binding energy of 710.2 eV ($2p_{3/2}$) corresponds to the oxidation state of +2 for Fe in the Fe^{2+}- doped Pb-MOCP Figure 4.46.

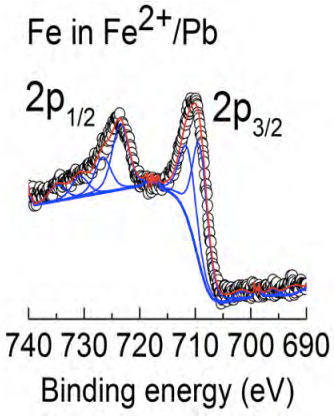

Figure 4.44: XPS spectra of Fe^{2+} in Fe-doped Pb-MOCP

(g) ***Fe^{3+}-doped 3D MOCP $Pb_3(pzdc)_3(H_2O)$***

Fe^{3+} is a hard Lewis acid with a high preference for hard Lewis base, it is flexible with CN and is expected to into all the 3 Pb-sites. Since all the 3 Pb-sites are surrounded mainly by hard carboxylate O-donor, Fe^{3+} is expected to easily exchange all the borderline Pb^{2+}.

Soaking the precursor 1D MOCP in nitrate salt of Fe^{3+} led to a cation exchange of the precursor 1D MOCP without transforming to the 3D MOCP. However, when soaked in a mixture of H_2O/DMF, 1:1 ratio, the precursor 1D MOCP transformed to the 3D MOCP within 2 days and 34 at. % of Fe^{3+} was substituted into the 3D MOCP. Warming the solution at 40 ^oC or adding 2 drops of pyridine in H_2O/DMF afforded 3D MOCP with 51 and 49 at. % of substituted Fe^{3+} respectively. To further increase the dopant amount, the precursor salt was changed from nitrate to chloride, hence using chloride salt of Fe^{3+} in aqueous solution within 1 day it afforded the 3D MOCP with 98 at. % of substituted Fe^{3+} albeit low crystallinity indicated by weak PXRD pattern, Figure 4.47, Table 4.13, Scheme 11.

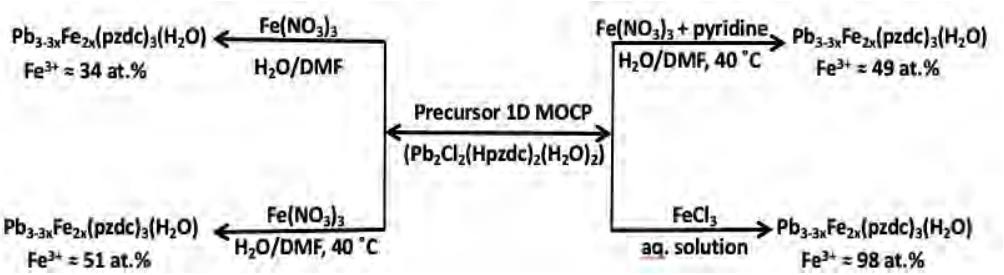

Scheme 11: Summary of Fe^{3+} incorporated into the 3D MOCP using the precursor 1D MOCP under different conditions.

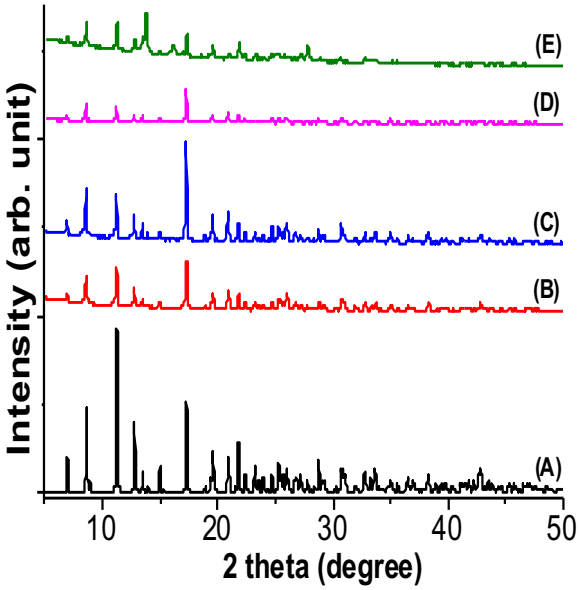

Figure 4.45: PXRD patterns of simulated 3D MOCP (A) and observed Fe^{3+}-doped 3D MOCP in H_2O/DMF (B) H_2O/DMF and pyridine (C) H_2O/DMF at 40 °C (D) H_2O Fe(III)chloride precursor (E).

Table 4.13: SEM-EDS (average at. %) or ICP-OES (wt.%)* results of Fe^{2+} doped 3D MOCPs.

Synthesis condition	Dopant at. %
H_2O/DMF, Iron(III)nitrate, 2 days, r.t.	34
H_2O/DMF, Iron(III)nitrate, @40 °C, 1 day.	51
H_2O/DMF, Iron(III)nitrate, 2 days, pyridine, r.t.	49
H_2O, Iron(III)chloride, 1 days, r.t.	98

(h) ***Cd^{2+} or Hg^{2+}-doped 3D MOCP $Pb_3(pzdc)_3(H_2O)$***

Both Cd^{2+} and Hg^{2+} are soft Lewis acids with preference for soft CE, they both have very similar coordination behavior. (Borsari, 2011; Morsali & Masoomi, 2009) They can

adopt variety of CN and CE and are therefore expected to exchange at least at Pb(1) and (2) sites. Soaking the precursor 1D MOCP in nitrate salt of Cd^{2+} or Hg^{2+} in aqueous solution for 3 days, the precursor 1D MOCP proceeded to structural transformation to 3D MOCP in Cd^{2+} solution with 12 at. % of Cd^{2+} exchanged into the 3D MOCP, while in Hg^{2+} solution, the precursor 1D MOCP proceeded to another 2D structure, Figure 4.10. Immersing the precursor 1D MOCP in nitrate salt of Cd^{2+} or Hg^{2+} in a mixture of H_2O/DMF/DO for 3 days at room temperature, in both Cd^{2+} and Hg^{2+} solution the precursor 1D MOCP transformed to the 3D structure with 41 and 60 at. % substituted by Cd^{2+} and Hg^{2+} respectively. Addition of soft pyridine or heating at 90 ^oC does not increases the dopant amounts in all cases as expected owing to their soft nature. The presence of Cd^{2+} or Hg^{2+} are confirmed using FESEM-EDS, Table 4.14 and the phase purity and crystallinity of the products are confirmed by PXRD analysis, Figure 4.48, Scheme 12.

Table 4.14: SEM-EDS (average at. %) results for Cd^{2+} or Hg^{2+}-doped 3D MOCPs.

Synthesis condition	Dopants	at. %
H_2O/DMF/dioxane, r.t, 3 d.	Cd^{2+}	41
H_2O/DMF/dioxane, r.t, 3 d.	Hg^{2+}	60

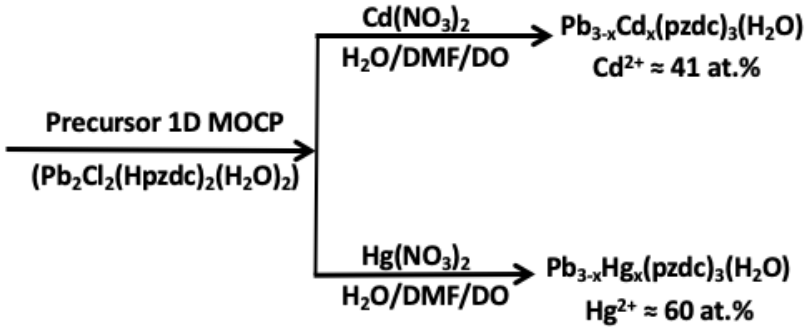

Scheme 12: Incorporation of Cd^{2+} or Hg^{2+} into the 3D MOCP using the precursor 1D MOCP in H_2O/DMF/DO

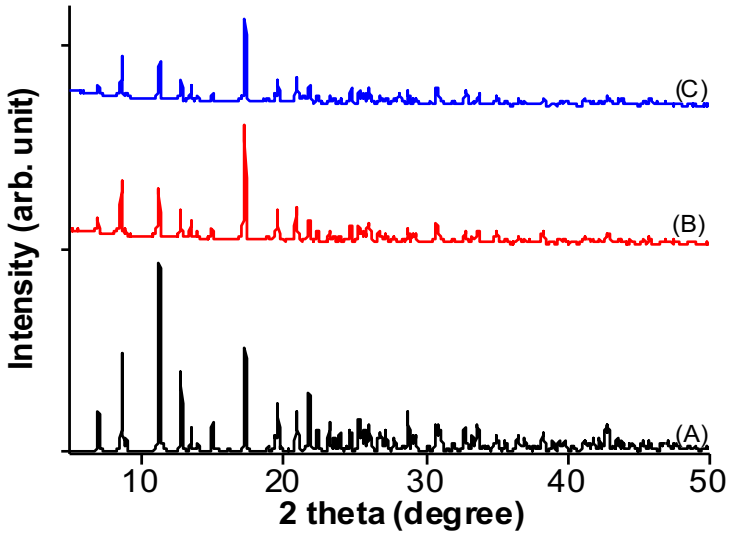

Figure 4.46: PXRD patterns of simulated 3D MOCP (A) and observed Cd^{2+}-doped 3D MOCP (B) Hg^{2+}-doped 3D MOCP (C) in H_2O/DMF/dioxane

(i) ***Li^+-doped 3D MOCP $Pb_3(pzdc)_3(H_2O)$***

Li^+ substituted Pb 3D MOCP, was successfully synthesized using a variety of Li^+ precursors, with the largest resulting substituted crystals obtained from $LiNO_3$ precursors with the resulting formula of $Pb_{2.89}Li_{0.11}(pzdc)_3(H_2O)_{0.60}$, as refined by the single crystal X-ray diffraction, and the presence of Li, ~3.6 wt.%, was confirmed by ICP-OES, corresponding nicely to crystallographic refinement. Theoretically, monovalent substitution into divalent host, should create anion vacancy, (West, 2014) however, our crystallographic refinement did not detect the presence of anion deficiency. The PXRD pattern indicates its phase purity, Figure 4.49. In this case, Li^+ cations were found to partially substitute all the three Pb^{2+} sites with CN of 6, 7, and 9, for Pb(1), (2), and (3), respectively, Figure 4.10. The latter displays two longer, hence weaker Li-O coordination bonds for O(2) and O(6), expected for smaller Li^+. Examples of Li-based compounds with such CNs have been reported before. (Holleman et al., 2001; Redhammer & Roth, 2003)

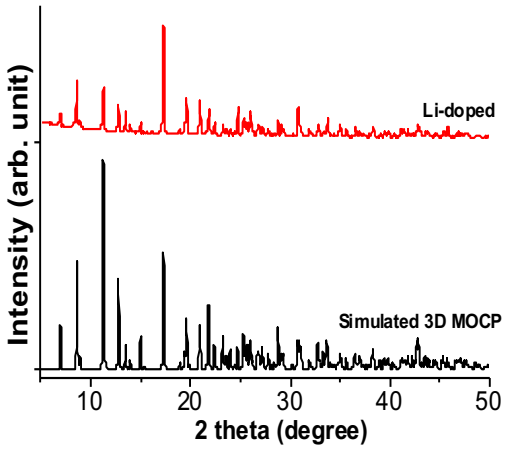

Figure 4.47: PXRD patterns of simulated 3D MOCP and observed Li^{+}-doped 3D MOCP.

XPS was used to determine the oxidation state and chemical environment of both Pb and Li ions in Li-doped MOCP. The splitting of the binding energy of 4*f* orbitals as 143.3 ($4f_{5/2}$) and 138.4 ($4f_{7/2}$) eV in the Pb is consistent with its oxidation state of +2, however, Li^{+} was not detected due to its low concentration and smaller electronic density.

4.5.3 Evaluation of magnetic susceptibility in doped 3D MOCPs

Evaluation of the magnetic susceptibility behavior of Fe^{2+}, Co^{2+}, Eu^{3+}, Tb^{3+}, and Fe^{3+}-doped 3D MOCPs were carried out using a VSM at room temperature with a field sweeping from -8000 to 8000 Oe. The 3D structure is made up of trinuclear units bridged by carboxylate groups. Although Pb^{2+} is purely diamagnetic, substitution into these multinuclear units with a ferromagnetic Fe^{2+} or Fe^{3+} and other cations with unpaired electrons such as Co^{2+}, Eu^{3+}, or Tb^{3+}, may endows the material with some magnetic properties. (Hao et al., 2017; Y.-W. Li et al., 2014; Lü et al., 2016; Qu et al., 2018) However, the lack planarity of the ligands in the structure will make it less efficient by affecting the super exchange through the delocalized π-orbitals of the carboxylate group. Figure 4.50, shows the trinuclear SBUs linked by *meta*-substituted pyrazinyl groups, with a 4.332 Å distance between the metal centers (the spin carriers), Figure 4.51. Meta-substituted phenyl or pyrazinyl ring is reported to leads to weak ferromagnetic coupling. (Agarwal et al., 2013; Laye & Sañudo, 2009; Paital et al., 2005)

Although temperature dependent magnetic susceptibility measurement is required to confirm our observation, interestingly, the Fe^{2+}-doped 3D MOCP was found to show typical antiferromagnetic behavior displaying some hysteresis loop at room temperature with a small magnetization of 0.5 emu/g, Figure 4.51. Such narrow hysteresis suggests a very small amount of dissipated energy in recurrently reversing the magnetization. It is very rare for a mononuclear Fe(II) or Fe(II) cluster to show hysteresis at room temperature. (Gómez et al., 2014; L. Li, 2011) Other dopants, Fe^{3+}, Co^{2+}, Eu^{3+}, and Tb^{3+}, also shows some small magnetizations of 16.12 x 10^{-3}, 47.42 x 10^{-3}, 24.56 x 10^{-3}, and 73.66 x 10^{-3} emu/g respectively.

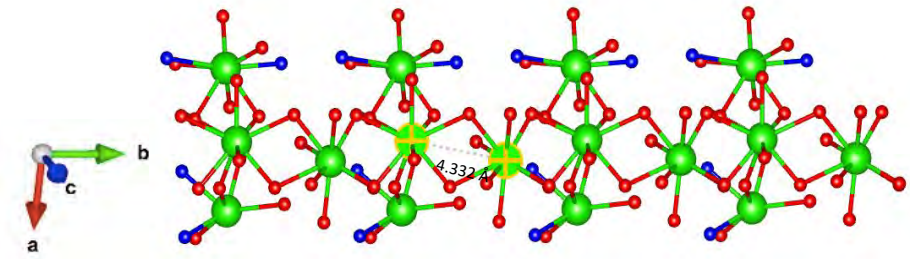

Figure 4.48: Distance between proximal cation centers in3D MOCP view showing metal chain along *b* axis.

(A) (B)

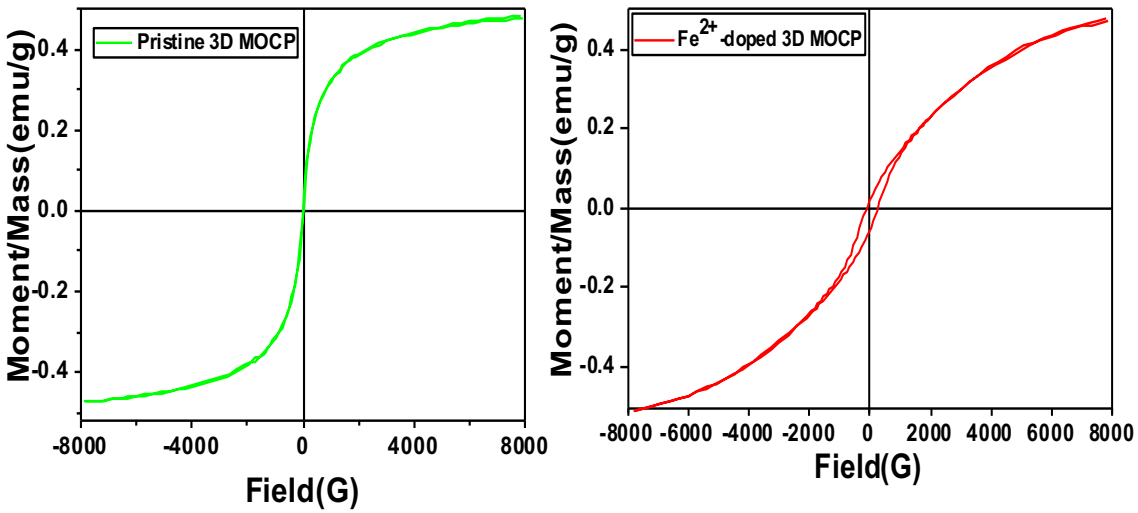

Figure 4.49: Magnetic hysteresis loop of the pristine 3D MOCP (A) and Fe^{2+}-doped 3D MOCP (B) measured at room temperature.

CHAPTER 5: CONCLUSION

In this study, labile and dynamic 1D MOCP built from 2,3-H_2pzdc, and Pb^{2+} through simple solution chemistry was explored. Upon judicious soaking in various solvent(s), the 1D MOCP was made to undergo a solvent-mediated, simultaneous structural transformation and dissolution-exchange-recrystallization to a robust 3D MOCP. We carefully selected a ladder-like, 1D MOCP (*$Pb_2Cl_2(Hpzdc)_2(H_2O)_2$)* containing a centro-symmetric Pb_2Cl_2 dimers which are connected into a chain by mono-protonated carboxylic ($Hpzdc^-$) owing to its amenable features. The 1D MOCP was transformed into a 3D, *$Pb_3(pzdc)_3(H_2O)$* MOCP featuring 1D moiety having three distinctive Pb^{2+} sites each with different CN and CE that underwent numerous solid solution/cation exchange with exogenous divalent and aliovalent including mono- or trivalent cations. The purity of all the doped 3D MOCP products, was confirmed by PXRD, while the dopant amounts was determined using FESEM-EDS/ICP-OES, the valency and chemical environments of some representative doped 3D MOPCs were confirmed using XPS.

Trivalent Ln^{3+} ions were successfully incorporated into the 3D structure, featuring cation vacancies due to the partial cation exchange with aliovalent Ln^{3+} cations, under optimized conditions. For example, in aqueous solution, La^{3+}, Eu^{3+}, Gd^{3+}, Tb^{3+}, or Er^{3+} was successfully incorporated, however no more than 6 wt. % was incorporated, which was attributed to their favorable interaction and subsequent solvation in hard aqueous solvent. Remarkably, the amount is enough to tune the emission properties of both Eu^{3+}, or Tb^{3+}-doped 3D MOCP from the weak greenish yellow luminescence emission of the pristine 3D MOCP to bright yellowish red for Eu^{3+}-doped or to bright greenish yellow for Tb^{3+}-doped MOCP, while sustaining the broad emission peak of the pristine 3D MOCP at the background, making the compounds a dual luminescence emitters under single excitation wavelength. Solvent mixtures, temperature, modulator ligands, or reaction time

was used to increase the amounts of Ln^{3+}. When mixture of H_2O, DMF and dioxane was used as the solvent, the amount of Ln^{3+} incorporated into the 3D MOCP was increased significantly. This is attributed largely to the less favourable interactions of Ln^{3+} with softer solvents and favourable interaction of Pb^{2+} ions with the solvents, paving a way for the increased incorporation. Addition of modulator ligand (pyridine or piperazine) and increasing the temperature (90 ^oC) further increases the exchange amounts up to 99 wt. %. Interestingly, the photoluminescence emission intensity of Eu^{3+}-doped MOCPs increases simultaneously with increase in Eu^{3+} amounts, up to 80 wt. %. However, a decrease in emission intensity was observed in Tb^{3+}-doped MOCPs, with the highest intensity observed for 6 wt. % and lowest for 80 wt. % doped Tb^{3+} MOCPs. Double and triple Ln^{3+}-doped 3D MOCPs were also successfully synthesized in aqueous and solvent mixture. Similarly, more dopants were obtained in solvent mixture and further increases as modulator ligand was added, which also increases significantly at higher temperatures.

In addition to this, doping with divalent transition and post-transition metals were also successfully achieved. For example, in aqueous solution all transition and post-transition metals exchanged between 11 to 20 atomic % of Pb^{2+}. Remarkably, Cu^{2+}, Mn^{2+}, and Fe^{3+} underwent almost complete exchange of Pb^{2+} (more than 98 at. %) in an optimized solvent mixtures and variable exchange amounts was achieved by controlling and modulating the exchange conditions. Other metal cations was tuned to a variable amounts under appropriate conditions, however, complete substitution was not attained. For instance, Ni^{2+} was tuned from 20 at. % in aqueous solution to 40 at. % in H_2O/DMF/ACN, while Zn^{2+} was increased from 17 to 33 at. % in H_2O/DMF/dioxane, Co^{2+}, Fe^{2+}, Cd^{2+}, and Hg^{2+} was tuned from 11, 11, 12, and 8 at. % to 43, 63, 41, and 60 at. % respectively, in solvent mixtures.

After successfully incorporating di- and tri-valent cations under optimized conditions, as a proof of concept, monovalent Li^{+}, and mixed valent 3*d*-4*f*, Zn^{2+}/Ln^{3+} were also successfully incorporated into the structure demonstrating the amenability of the MOCP to be used as a template for facile solid solution, irrespective of the metal cation type and chemistry.

Doping with metal cations having unpaired electrons such as Co^{2+}, Fe^{3+}, Fe^{2+}, Tb^{3+}, or Eu^{3+} in to a typical diamagnetic and insulating Pb^{2+}-based MOCP framework may endow the MOCP with some charge transport capabilities which came not only from the exogenous cation but on the proximal interactions and interplay amongst the interacting partners. For instance, when the electrical conductivities of Eu^{3+}, Tb^{3+}, and Fe^{3+}-doped and the pristine 3D MOCPs were evaluated, a significant improvement in electrical conductance was recorded, especially for Eu^{3+}-doped, compared to the typically insulating pristine 3D MOCP at 25 ^{o}C. Remarkably, the Fe^{2+}-doped 3D MOCP was also found to show some antiferromagnetic behaviour with a hysteresis loop at room temperature and a magnetization of 0.5 emu/g. Fe^{3+}, Co^{2+}, Eu^{3+}, and Tb^{3+}-doped 3D MOCPs also shows some small magnetizations of 16.12×10^{-3}, 47.42×10^{-3}, 24.56×10^{-3}, and 73.66×10^{-3} emu/g respectively.

In a nutshell, this research provides useful strategies for conducting solid solution using dynamic and robust MOCPs. Useful functionalities such as tunable photoluminescence, conductivity and magnetism were obtained from typically weak luminescing, non-conducting or insulating and diamagnetic 3D MOCP. Combination of functionalities was actualized, for instance Ln^{3+} doped possessed both optical and electrical properties.

5.1 Limitations

Funding have been our greatest limitation, several measurements could not be made owing to the unavailability of funds, resources and facilities. For example, high sensitive and variable temperature measurements are required to further analyze both the electrical conductivities and the magnetic susceptibilities of all the substituted MOCPs. Further solid state UV-Vis and photoluminescence measurements for the triple and double Ln^{3+}-doped MOCPs, spanning from UV- to-Visible-to-NIR could not be achieved due to lack of funding, resources and facilities.

5.2 Recommendations

This work has established a simple strategy to modify the chemical compositions of $Pb_3(pzdc)_3(H_2O)$ with variety of cations of different chemistry, including aliovalent cations creating cation vacancies. Numerous multivariate 3D MOCPs have been isolated that may be of importance especially for catalysis or solid state lighting. As a recommendation for further work, theoretical investigation on the details cation exchange and photoluminescence mechanisms would be very paramount to gaining further understanding that can allow the strategy to be applied to other dynamic MOCP systems that may paves a way for the realization of other complex functional materials.

In addition to this, calcination of the Ln^{3+} and transition metal doped 3D MOCPs may realize very important catalysts for small molecule reactivities, such as CO_2 reformation. For instance, Ni-based catalyst are well known for their potent in CO_2 reforming and decomposition of methane. (Amin, 2020; J. Zhang et al., 2020) The Ni-doped and other transition metal doped MOCPs synthesized in this work, may provide a very good opportunity when calcinated and used as a catalyst. Exploring lanthanide doped MOCPs may also provide some more important solid state photoluminescence emitting materials or as a catalyst especially owing to the presence cation vacancies.

Doping and cation vacancies has a strong influence on solid-state electronic materials For instance, thermal induced cation vacancy disorder in tetragonal tungsten bronze $Sr_xBa_{1-x}Nb_2O_6$ ceramic, strongly influences the electrical and structural property of the ceramic. (Aamlid et al., 2019) Also, sintering defective Eu^{3+} or Eu^{2+} doped Mg–Al and Ca–Al layered double hydroxides results in to a three primary color emitting phosphors that can be control by changing the consistent layered double hydroxides ions. The luminescence phenomenon in sintered Eu^{3+} doped Mg–Al layered double hydroxide is triggered by the reduction of the symmetry around Eu^{3+} ion owing to the incorporation of the Al^{3+} ion and the cation vacancies in the host, MgO rock salt. (Sonoyama et al., 2020) Presence of cation vacancies can influences the electronic properties of materials. For example, $La_{0.9}Ba_{0.1}Mn_{0.96}O_{2.43}$ prepared through topochemical reduction of $La_{0.9}Ba_{0.1}MnO_3$ via deintercalation of manganese cations and oxide anions. The existence of manganese cation vacancies altered a simple G-type antiferromagnetic arrangement into a ferrimagnetic structure. (Parsons et al., 2020)

REFERENCES

Aamlid, S. S., Selbach, S. M., & Grande, T. (2019). The effect of cation disorder on ferroelectric properties of SrxBa1− xNb2O6 Tungsten Bronzes. *Materials, 12*(7), Article#1156.

Abdelhameed, R. M., Abdel-Gawad, H., Elshahat, M., & Emam, H. E. (2016). Cu–BTC@ cotton composite: design and removal of ethion insecticide from water. *Rsc Advances, 6*(48), 42324-42333.

Abdelhameed, R. M., el-deib, H. R., El-Dars, F. M., Ahmed, H. B., & Emam, H. E. (2018). Applicable strategy for removing liquid fuel nitrogenated contaminants using MIL-53-NH2@ natural fabric composites. *Industrial & Engineering Chemistry Research, 57*(44), 15054-15065.

Abdelhameed, R. M., & Emam, H. E. (2019). Design of ZIF (Co & Zn)@ wool composite for efficient removal of pharmaceutical intermediate from wastewater. *Journal of Colloid and Interface Science, 552*, 494-505.

Abdelhameed, R. M., Emam, H. E., Rocha, J., & Silva, A. M. (2017). Cu-BTC metal-organic framework natural fabric composites for fuel purification. *Fuel Processing Technology, 159*, 306-312.

Abdelhameed, R. M., Rehan, M., & Emam, H. E. (2018). Figuration of Zr-based MOF@ cotton fabric composite for potential kidney application. *Carbohydrate Polymers, 195*, 460-467.

Aboutorabi, L., & Morsali, A. (2016). Structural transformations and solid-state reactivity involving nano lead (II) coordination polymers via thermal, mechanochemical and photochemical approaches. *Coordination Chemistry Reviews, 310*, 116-130.

Agarwal, R. A., Aijaz, A., Sañudo, C., Xu, Q., & Bharadwaj, P. K. (2013). Gas adsorption and magnetic properties in isostructural Ni (II), Mn (II), and Co (II) coordination polymers. *Crystal Growth & Design, 13*(3), 1238-1245.

Aguirre-Diaz, L. M., Gandara, F., Iglesias, M., Snejko, N., Gutierrez-Puebla, E., & Monge, M. A. (2015). Tunable catalytic activity of solid solution metal-organic frameworks in one-pot multicomponent reactions. *Journal of the American Chemical Society, 137*(19), 6132-6135.

Ahrland, S., Chatt, J., & Davies, N. R. (1958). The relative affinities of ligand atoms for acceptor molecules and ions. *Quarterly Reviews, Chemical Society, 12*(3), 265-276.

Akhbari, K., & Morsali, A. (2013). Solid-and solution-state structural transformations in flexible lead (II) supramolecular polymers. *Crystengcomm, 15*(44), 8915-8918.

Akhbari, K., & Morsali, A. (2015). Direct synthesis of lead and lead chloride nanoparticles via simple one-pot calcination of one-dimensional lead (II) coordination polymer. *Journal of Inorganic and Organometallic Polymers and Materials, 25*(4), 930-935.

Akiba, K., & Inamoto, N. (1975). Application of hard and soft acids and bases principle to Organic-Chemistry. *Journal of Synthetic Organic Chemistry Japan, 33*(11), 834-841.

Al-Janabi, N., Hill, P., Torrente-Murciano, L., Garforth, A., Gorgojo, P., Siperstein, F., & Fan, X. (2015). Mapping the Cu-BTC metal–organic framework (HKUST-1) stability envelope in the presence of water vapour for CO2 adsorption from flue gases. *Chemical Engineering Journal, 281*, 669-677.

Al-Nubi, M. A., Hamisu, A. M., Wardana, F. Y., Ariffin, A., Jo, H., Ok, K. M., & Wibowo, A. C. (2019). Lead–organic frameworks containing trimesic acid: Facile dissolution–crystallization and near-white light emission. *Crystal Growth & Design, 19*(11), 6274-6282.

Alfarra, A., Frackowiak, E., & Beguin, F. (2004). The HSAB concept as a means to interpret the adsorption of metal ions onto activated carbons. *Applied Surface Science, 228*(1-4), 84-92.

Allendorf, M., Bauer, C., Bhakta, R., & Houk, R. (2009). Luminescent metal–organic frameworks. *Chemical Society Reviews, 38*(5), 1330-1352.

Amin, M. H. (2020). Relationship between the pore structure of mesoporous silica supports and the activity of nickel nanocatalysts in the CO2 reforming of methane. *Catalysts, 10*(1), Article#51.

An, J., Shade, C. M., Chengelis-Czegan, D. A., Petoud, S., & Rosi, N. L. (2011). Zinc-adeninate metal− organic framework for aqueous encapsulation and sensitization of near-infrared and visible emitting lanthanide cations. *Journal of the American Chemical Society, 133*(5), 1220-1223.

An, R., Zhao, H., Hu, H.-M., Wang, X., Yang, M.-L., & Xue, G. (2016). Synthesis, structure, white-light emission, and temperature recognition properties of Eu/Tb mixed coordination polymers. *Inorganic Chemistry, 55*(2), 871-876.

Askarinejad, A., & Morsali, A. (2009). Synthesis of cadmium (II) hydroxide, cadmium (II) carbonate and cadmium (II) oxide nanoparticles; investigation of intermediate products. *Chemical Engineering Journal, 150*(2-3), 569-571.

Ataie, N. J., Hoang, Q. Q., Zahniser, M. P. D., Tu, Y., Milne, A., Petsko, G. A., & Ringe, D. (2008). Zinc coordination geometry and ligand binding affinity: the structural and kinetic analysis of the second-shell serine 228 residue and the methionine 180 residue of the aminopeptidase from Vibrio proteolyticus. *Biochemistry, 47*(29), 7673-7683.

Ayers, P. W., & Cárdenas, C. (2013). Communication: A case where the hard/soft acid/base principle holds regardless of acid/base strength: AIP Conference Proceedinds.

Ayers, P. W., Parr, R. G., & Pearson, R. G. (2006). Elucidating the hard/soft acid/base principle: A perspective based on half-reactions. *Journal of Chemical Physics, 124*(19).

Balestri, D., Bassanetti, I., Canossa, S., Gazzurelli, C., Bacchi, A., Bracco, S., Comotti, A., & Pelagatti, P. (2018). Changing the dress to a MOF through fluorination and transmetalation. Structural and Gas-Sorption effects. *Crystal Growth & Design, 18*(11), 6824-6832.

Barth, J. V., Costantini, G., & Kern, K. (2010). Engineering atomic and molecular nanostructures at surfaces *Nanoscience and technology: a collection of reviews from Nature journals* (pp. 67-75): World Scientific.

Batten, S. R., Champness, N. R., Chen, X.-M., Garcia-Martinez, J., Kitagawa, S., Öhrström, L., O'Keeffe, M., Suh, M. P., & Reedijk, J. (2013). Terminology of metal–organic frameworks and coordination polymers (IUPAC Recommendations 2013). *Pure and Applied Chemistry, 85*(8), 1715-1724.

Binnemans, K. (2009). Lanthanide-based luminescent hybrid materials. *Chemical reviews, 109*(9), 4283-4374.

Biradha, K., Ramana, A., & Vittal, J. J. (2009). Coordination polymers versus metal-organic frameworks. *Crystal Growth & Design, 9*(7), 2969-2970.

Bo, Q.-B., Sun, G.-X., & Geng, D.-L. (2010). Novel three-dimensional pillared-layer Ln (III)− Cu (I) coordination polymers featuring spindle-shaped heterometallic building units. *Inorganic Chemistry, 49*(2), 561-571.

Bommakanti, S., Venkataramudu, U., & Das, S. K. (2018). Functional coordination polymers from a bifunctional ligand: A quantitative transmetalation via single crystal to single crystal transformation. *Crystal Growth & Design, 19*(2), 1155-1166.

Borsari, M. (2011). Cadmium: coordination chemistry. *Encyclopedia of Inorganic and Bioinorganic Chemistry*, J. Wiley & Sons: Chichester, U.K. Volume 1, pp 1-16.

Botas, J. A., Calleja, G., Sánchez-Sánchez, M., & Orcajo, M. G. (2011). Effect of Zn/Co ratio in MOF-74 type materials containing exposed metal sites on their hydrogen adsorption behaviour and on their band gap energy. *International Journal of Hydrogen Energy, 36*(17), 10834-10844.

Brandt, R. E., Poindexter, J. R., Gorai, P., Kurchin, R. C., Hoye, R. L., Nienhaus, L., Wilson, M. W., Polizzotti, J. A., Sereika, R., & Žaltauskas, R. (2017). Searching for "defect-tolerant" photovoltaic materials: combined theoretical and experimental screening. *Chemistry of Materials, 29*(11), 4667-4674.

Breugst, M., & Mayr, H. (2010). Ambident reactivities of pyridone anions. *Journal of the American Chemical Society, 132*(43), 15380-15389.

Briand, G. G., & Burford, N. (2000). Coordination complexes of bismuth(III) involving organic ligands with pnictogen or chalcogen donors. *Advances in Inorganic Chemistry, 50*, 285-357.

Brown, J. (2011). Controllable metalation of multivariate metal organic frameworks with retention of porosity and crystallinity. *Abstracts of Papers of the American Chemical Society, Article#241*.

Brown, J. W., Jarenwattananon, N. N., Otto, T., Wang, J. L., Gloggler, S., & Bouchard, L. S. (2015). Heterogeneous heck coupling in multivariate metal-organic frameworks for enhanced selectivity. *Catalysis Communications, 65*, 105-107.

Brozek, C. K., Bellarosa, L., Soejima, T., Clark, T. V., Lopez, N., & Dinca, M. (2014a). Solvent-Dependent cation exchange in Metal-Organic frameworks. *Chemistry-a European Journal, 20*(23), 6871-6874.

Brozek, C. K., Bellarosa, L., Soejima, T., Clark, T. V., Lopez, N., & Dinca, M. (2014b). Solvent-dependent cation exchange in metal-organic frameworks. *Chemistry-a European Journal, 20*(29), 8825-8825.

Brozek, C. K., Cozzolino, A. F., Teat, S. J., Chen, Y.-S., & Dincă, M. (2013). Quantification of site-specific cation exchange in metal–organic frameworks using multi-wavelength anomalous X-ray dispersion. *Chemistry of Materials, 25*(15), 2998-3002.

Brozek, C. K., & Dinca, M. (2014). Cation exchange at the secondary building units of metal-organic frameworks. *Chemical Society Reviews, 43*(16), 5456-5467.

Brozek, C. K., & Dinca, M. (2015). Thermodynamic parameters of cation exchange in MOF-5 and MFU-4l. *Chemical Communications, 51*(59), 11780-11782.

Brozek, C. K., & Dincă, M. (2013). Ti3+-, V2+/3+-, Cr2+/3+-, Mn2+-, and Fe2+-substituted MOF-5 and redox reactivity in Cr-and Fe-MOF-5. *Journal of the American Chemical Society, 135*(34), 12886-12891.

Bruker, S. (2002). Saint. *Bruker AXS Inc., Madison, Wisconsin, USA*.

Bunzli, J.-C. G. (2014). Review: Lanthanide coordination chemistry: from old concept to coordination polymers. *Journal of Coordination Chemistry, 67*, 3706-3733.

Bünzli, J.-C. G. (2014). Lanthanide coordination chemistry: from old concepts to coordination polymers. *Journal of Coordination Chemistry, 67*(23-24), 3706-3733.

Burd, S. D., Ma, S., Perman, J. A., Sikora, B. J., Snurr, R. Q., Thallapally, P. K., Tian, J., Wojtas, L., & Zaworotko, M. J. (2012). Highly selective carbon dioxide uptake by [Cu (bpy-n) 2 (SiF6)](bpy-1= 4, 4′-bipyridine; bpy-2= 1, 2-bis (4-pyridyl) ethene). *Journal of the American Chemical Society, 134*(8), 3663-3666.

Burtch, N. C., Jasuja, H., & Walton, K. S. (2014). Water stability and adsorption in metal–organic frameworks. *Chemical reviews, 114*(20), 10575-10612.

Buschow, K. H. J., & Boer, F. R. (2003). *Physics of magnetism and magnetic materials* (Vol. 7): Springer.

Cadiau, A., Adil, K., Bhatt, P., Belmabkhout, Y., & Eddaoudi, M. (2016). A metal-organic framework–based splitter for separating propylene from propane. *Science, 353*(6295), 137-140.

Cadiau, A., Belmabkhout, Y., Adil, K., Bhatt, P. M., Pillai, R. S., Shkurenko, A., Martineau-Corcos, C., Maurin, G., & Eddaoudi, M. (2017). Hydrolytically stable fluorinated metal-organic frameworks for energy-efficient dehydration. *Science, 356*(6339), 731-735.

Cadman, L. K., Bristow, J. K., Stubbs, N. E., Tiana, D., Mahon, M. F., Walsh, A., & Burrows, A. D. (2016). Compositional control of pore geometry in multivariate metal-organic frameworks: an experimental and computational study. *Dalton Transactions, 45*(10), 4316-4326.

Cametti, M., Bargigia, I., & Marti-Rujas, J. (2016). Dynamic single crystal to polycrystal transformation of a 1D-coordination polymer and its second harmonic generation. *Dalton Transactions, 45*(4), 1674-1678.

Canivet, J., Fateeva, A., Guo, Y., Coasne, B., & Farrusseng, D. (2014). Water adsorption in MOFs: fundamentals and applications. *Chemical Society Reviews, 43*(16), 5594-5617.

Capper, P. (Ed.) (2005). *Bulk Crystal Growth in Electronic, Optical, and Optoelectronic Materials*. New York: Wiley.

Carlos, L. D., Ferreira, R. A., de Zea Bermudez, V., Julian-Lopez, B., & Escribano, P. (2011). Progress on lanthanide-based organic–inorganic hybrid phosphors. *Chemical Society Reviews, 40*(2), 536-549.

Cavka, J. H., Jakobsen, S., Olsbye, U., Guillou, N., Lamberti, C., Bordiga, S., & Lillerud, K. P. (2008). A new zirconium inorganic building brick forming metal organic frameworks with exceptional stability. *Journal of the American Chemical Society, 130*(42), 13850-13851.

Chaemchuem, S., Kui, Z., & Verpoort, F. (2016). Control of interpenetration via in situ lithium incorporation in MOFs and their gas adsorption properties and selectivity. *Crystengcomm, 18*(39), 7614-7619.

Chaemchuen, S., Zhou, K., & Verpoort, F. (2016). From biogas to biofuel: Materials used for biogas cleaning to biomethane. *ChemBioEng Reviews, 3*(6), 250-265.

Chaudhary, A., Mohammad, A., & Mobin, S. M. (2017). Recent advances in Single-Crystal-to-Single-Crystal transformation at the discrete molecular level. *Crystal Growth & Design, 17*(5), 2893-2910.

Cheetham, A. K., Bennett, T. D., Coudert, F. X., & Goodwin, A. L. (2016). Defects and disorder in metal organic frameworks. *Dalton Transactions, 45*(10), 4113-4126.

Chemaly, S. M., Florczak, M., Dirr, H., & Marques, H. M. (2011). Probing the nature of the CoIII ion in corrins: A comparison of the thermodynamics and kinetics of the ligand substitution reactions of aquacyanocobyrinic acid heptamethyl ester and stable yellow aquacyanocobyrinic acid heptamethyl ester. *Inorganic Chemistry, 50*(18), 8719-8727.

Chen, B., Yang, Z., Zhu, Y., & Xia, Y. (2014). Zeolitic imidazolate framework materials: recent progress in synthesis and applications. *Journal of Materials Chemistry A, 2*(40), 16811-16831.

Chen, B. L., Yang, Z. X., Zhu, Y. Q., & Xia, Y. D. (2014). Zeolitic imidazolate framework materials: recent progress in synthesis and applications. *Journal of Materials Chemistry A, 2*(40), 16811-16831.

Chuan Tan, Y., & Chun Zeng, H. (2016). Self-templating synthesis of hollow spheres of MOFs and their derived nanostructures. *Chemical Communications, 52*(77), 11591-11594.

Chui, S. S. Y., Lo, S. M. F., Charmant, J. P. H., Orpen, A. G., & Williams, I. D. (1999). A chemically functionalizable nanoporous material [Cu-3(TMA)(2)(H2O)(3)](n). *Science, 283*(5405), 1148-1150.

Ci, L., Song, L., Jin, C., Jariwala, D., Wu, D., Li, Y., Srivastava, A., Wang, Z., Storr, K., & Balicas, L. (2010). Atomic layers of hybridized boron nitride and graphene domains. *Nature Materials, 9*(5), 430-435.

Cimen, E., Gumus, I., & Arslan, H. (2018). The role of intermolecular interactions in the assembly of Zinc (II) and Lead (II) complexes containing carboxylate ligand and their conversion to metal oxides. *Journal of Molecular Structure, 1166*, 397-406.

Cohen, S. M. (2010). Modifying MOFs: new chemistry, new materials. *Chemical Science, 1*(1), 32-36.

Cui, K. J., Wang, D., Zhang, H., Guo, J., Cai, C., Zhu, C. Z., Zhao, N., & Xu, J. (2017). Preparation of recyclable polybutadiene rubber based on acid-base complexation. *Journal of Applied Polymer Science, 134*(36).

Cui, P.-P., Zhang, X.-D., Wang, P., Zhao, Y., Azam, M., Al-Resayes, S. I., & Sun, W.-Y. (2017). Zinc (II) and Copper (II) Hybrid frameworks via Metal-Ion metathesis with enhanced gas uptake and photoluminescence properties. *Inorganic Chemistry, 56*(22), 14157-14163.

Cui, X. J., Khlobystov, A. N., Chen, X. Y., Marsh, D. H., Blake, A. J., Lewis, W., Champness, N. R., Roberts, C. J., & Schroder, M. (2009). Dynamic equilibria in solvent-mediated anion, cation and ligand exchange in transition-metal coordination polymers: Solid-state transfer or recrystallisation? *Chemistry-a European Journal, 15*(35), 8861-8873.

Cui, Y., Xu, H., Yue, Y., Guo, Z., Yu, J., Chen, Z., Gao, J., Yang, Y., Qian, G., & Chen, B. (2012). A luminescent mixed-lanthanide metal–organic framework thermometer. *Journal of the American Chemical Society, 134*(9), 3979-3982.

Cui, Y., Yue, Y., Qian, G., & Chen, B. (2012). Luminescent functional Metal–Organic frameworks. *Chemical Reviews, 112*(2), 1126-1162.

Czaja, A. U., Trukhan, N., & Muller, U. (2009). Industrial applications of metal-organic frameworks. *Chemical Society Reviews, 38*(5), 1284-1293.

Dang, S., Zhu, Q.-L., & Xu, Q. (2017). Nanomaterials derived from metal–organic frameworks. *Nature Reviews Materials, 3*, Article#17075.

Das, M. C., Guo, Q., He, Y., Kim, J., Zhao, C.-G., Hong, K., Xiang, S., Zhang, Z., Thomas, K. M., & Krishna, R. (2012). Interplay of metalloligand and organic ligand to tune micropores within isostructural mixed-metal organic frameworks (M′ MOFs) for their highly selective separation of chiral and achiral small molecules. *Journal of the American Chemical Society, 134*(20), 8703-8710.

Das, S., Kim, H., & Kim, K. (2009). Metathesis in single crystal: Complete and reversible exchange of metal ions constituting the frameworks of metal-organic frameworks. *Journal of the American Chemical Society, 131*(11), 3814-3815.

de la Cruz, C., Huang, Q., Lynn, J. W., Li, J. Y., Ratcliff, W., Zarestky, J. L., Mook, H. A., Chen, G. F., Luo, J. L., Wang, N. L., & Dai, P. C. (2008). Magnetic order close to superconductivity in the iron-based layered LaO(1-x)F(x)FeAs systems. *Nature, 453*(7197), 899-902.

Demas, J. (1983). Photophysical pathways in metal complexes: ACS Publications.

Demuynck, R., Wieme, J., Rogge, S. M. J., Dedecker, K. D., Vanduyfhuys, L., Waroquier, M., & Van Speybroeck, V. (2018). Protocol for identifying accurate collective variables in enhanced molecular dynamics simulations for the description of structural transformations in flexible Metal-Organic frameworks. *Journal of Chemical Theory and Computation, 14*(11), 5511-5526.

Deng, H., Doonan, C. J., Furukawa, H., Ferreira, R. B., Towne, J., Knobler, C. B., Wang, B., & Yaghi, O. M. (2010). Multiple functional groups of varying ratios in metal-organic frameworks. *Science, 327*(5967), 846-850.

Deng, H. X., & Yaghi, O. M. (2011). Multivariate metal-organic frameworks with significant enhancement in carbon dioxide capture. *Abstracts of Papers of the American Chemical Society (Vol. 242)*. 1155 16th St, NW, Washington, DC 20036 USA: American Chemical Society.

Denysenko, D., Werner, T., Grzywa, M., Puls, A., Hagen, V., Eickerling, G., Jelic, J., Reuter, K., & Volkmer, D. (2012). Reversible gas-phase redox processes catalyzed by Co-exchanged MFU-4 l (arge). *Chemical Communications, 48*(9), 1236-1238.

Dinca, M., & Long, J. R. (2007). High-enthalpy hydrogen adsorption in cation-exchanged variants of the microporous metal-organic framework Mn-3[(Mn4Cl)(3)(BTT)(8)(CH3OH)(10)](2). *Journal of the American Chemical Society, 129*(36), 11172-11176.

Ding, B., Yang, E. C., Guo, J. H., Zhao, X. J., & Wang, X. G. (2008). A novel lead(II) framework containing Pb-O-Pb and Pb-Cl-Pb helical chains. *Inorganic Chemistry Communications, 11*(5), 509-512.

Diring, S., Furukawa, S., Takashima, Y., Tsuruoka, T., & Kitagawa, S. (2010). Controlled multiscale synthesis of porous coordination polymer in nano/micro regimes. *Chemistry of Materials, 22*(16), 4531-4538.

Dolgopolova, E. A., Ejegbavwo, O. A., Martin, C. R., Smith, M. D., Setyawan, W., Karakalos, S. G., Henager, C. H., zur Loye, H.-C., & Shustova, N. B. (2017). Multifaceted modularity: A key for stepwise building of hierarchical complexity in actinide Metal–Organic frameworks. *Journal of the American Chemical Society, 139*(46), 16852-16861.

Dolomanov, O. V., Bourhis, L. J., Gildea, R. J., Howard, J. A. K., & Puschmann, H. (2009). OLEX2: a complete structure solution, refinement and analysis program. *Journal of Applied Crystallography, 42*(2), 339-341.

Dong, Z. Y., Sun, Y. Z. S., Chu, J., Zhang, X. Z., & Deng, H. X. (2017). Multivariate metal-organic frameworks for dialing-in the binding and programming the release of drug molecules. *Journal of the American Chemical Society, 139*(40), 14209-14216.

Donkova, B., Dimitrov, D., Kostadinov, M., Mitkova, E., & Mehandjiev, D. (2010). Catalytic and photocatalytic activity of lightly doped catalysts M:ZnO (M = Cu, Mn). *Materials Chemistry and Physics, 123*(2-3), 563-568.

Duan, Z., Zhang, Y., Zhang, B., & Zhu, D. (2009). Crystal-to-crystal transformation from antiferromagnetic chains into a ferromagnetic diamondoid framework. *Journal of the American Chemical Society, 131*(20), 6934-6935.

Dudev, M., Wang, J., Dudev, T., & Lim, C. (2006). Factors governing the metal coordination number in metal complexes from Cambridge Structural Database analyses. *The Journal of Physical Chemistry B, 110*(4), 1889-1895.

Eddaoudi, M., Kim, J., Rosi, N., Vodak, D., Wachter, J., O'Keeffe, M., & Yaghi, O. M. (2002). Systematic design of pore size and functionality in isoreticular MOFs and their application in methane storage. *Science, 295*(5554), 469-472.

Eigen, M. (1963). Fast elementary steps in chemical reaction mechanisms. *Pure and Applied Chemistry, 6*(1), 97-116.

Einkauf, J. D., Clark, J. M., Paulive, A., Tanner, G. P., & de Lill, D. T. (2017). A general model of sensitized luminescence in lanthanide-based coordination polymers and metal-organic framework materials. *Inorganic Chemistry, 56*, 5544-5552.

Eliseeva, S. V., & Bünzli, J.-C. G. (2010). Lanthanide luminescence for functional materials and bio-sciences. *Chemical Society Reviews, 39*(1), 189-227.

Emam, H. E., Abdelhamid, A. E., & Abdelhameed, R. M. (2019). Refining of liquid fuel from N-Containing compounds via using designed Polysulfone@ Metal organic framework composite film. *Journal of Cleaner Production, 218*, 347-356.

Emam, H. E., Abdelhamid, H. N., & Abdelhameed, R. M. (2018). Self-cleaned photoluminescent viscose fabric incorporated lanthanide-organic framework (Ln-MOF). *Dyes and Pigments, 159*, 491-498.

Fabini, D. H., Labram, J. G., Lehner, A. J., Bechtel, J. S., Evans, H. A., Van der Ven, A., Wudl, F., Chabinyc, M. L., & Seshadri, R. (2016). Main-group halide semiconductors derived from perovskite: distinguishing chemical, structural, and electronic aspects. *Inorganic Chemistry, 56*(1), 11-25.

Fan, S. R., & Zhu, L. G. (2007). Syntheses, structures, and characterizations of four new lead(II) 5-sulfosalicylate complexes with both chelating and bridging neutral ligands. *Inorganic Chemistry, 46*(16), 6785-6793.

Fang, Q., Zhu, G., Xue, M., Sun, J., Sun, F., & Qiu, S. (2006). Structure, luminescence, and adsorption properties of two chiral microporous metal−organic frameworks. *Inorganic Chemistry, 45*(9), 3582-3587.

Fang, Q. R., Zhu, G. S., Jin, Z., Ji, Y. Y., Ye, J. W., Xue, M., Yang, H., Wang, Y., & Qiu, S. L. (2007). Mesoporous metal–organic framework with rare etb topology for hydrogen storage and dye assembly. *Angewandte Chemie International Edition, 46*(35), 6638-6642.

Fang, Z., Bueken, B., De Vos, D. E., & Fischer, R. A. (2015). Defect-engineered metal-organic frameworks. *Angewandte Chemie International Edition, 54*(25), 7234-7254.

Fang, Z., Durholt, J. P., Kauer, M., Zhang, W., Lochenie, C., Jee, B., Albada, B., Metzler-Nolte, N., Poppl, A., Weber, B., Muhler, M., Wang, Y., Schmid, R., & Fischer, R. A. (2014). Structural complexity in metal-organic frameworks: simultaneous modification of open metal sites and hierarchical porosity by systematic doping with defective linkers. *Angewandte Chemie International Edition, 136*(27), 9627-9636.

Farrell, D. E., Chandrasekhar, B. S., Deguire, M. R., Fang, M. M., Kogan, V. G., Clem, J. R., & Finnemore, D. K. (1987). Superconducting properties of aligned crystalline grains of Y1ba2cu3o7-Delta. *Physical Review B, 36*(7), 4025-4027.

Fei, H., Cahill, J. F., Prather, K. A., & Cohen, S. M. (2013). Tandem postsynthetic metal ion and ligand exchange in zeolitic imidazolate frameworks. *Inorganic Chemistry, 52*(7), 4011-4016.

Feng, R., Jiang, F.-L., Chen, L., Yan, C.-F., Wu, M.-Y., & Hong, M.-C. (2009). A luminescent homochiral 3D Cd (ii) framework with a threefold interpenetrating uniform net 8 6. *Chemical Communications*(35), 5296-5298.

Férey, G. (2008). Hybrid porous solids: past, present, future. *Chemical Society Reviews, 37*(1), 191-214.

Férey, G., Mellot-Draznieks, C., Serre, C., Millange, F., Dutour, J., Surblé, S., & Margiolaki, I. (2005). A chromium terephthalate-based solid with unusually large pore volumes and surface area. *Science, 309*(5743), 2040-2042.

Férey, G., Serre, C., Mellot-Draznieks, C., Millange, F., Surblé, S., Dutour, J., & Margiolaki, I. (2004). A hybrid solid with giant pores prepared by a combination of targeted chemistry, simulation, and powder diffraction. *Angewandte Chemie International Edition, 43*(46), 6296-6301.

Feynman, R. P. (1960). There's plenty of room at the bottom. *California Institute of Technology, Engineering and Science magazine*.

Fischer, R. A. (2013). Multivariate surface mounted metal-organic frameworks. *Abstracts of Papers of the American Chemical Society (Vol. 245)*. 1155 16th St, NW, Washington, DC 20036 USA: American Chemical Society.

Frackowiak, D. (1988). The jablonski diagram. *Journal of Photochemistry and Photobiology B: Biology, 2*(3), Article#399.

Fu, J. H., Fu, J. X., Mu, Y. J., Liu, Y. H., Hou, H. W., & Fan, Y. T. (2011). The structural transformation from 2D layers to 3D nets by solvent-mediated cation-exchange reaction. *Inorganic Chemistry Communications, 14*(11), 1823-1826.

Fukui, K. (1970). Theory of orientation and stereoselection *Orientation and Stereoselection* (pp. 1-85): Springer.

Fukushima, T., Horike, S., Inubushi, Y., Nakagawa, K., Kubota, Y., Takata, M., & Kitagawa, S. (2010). Solid solutions of soft porous coordination polymers: Fine-tuning of gas adsorption properties. *Angewandte Chemie-International Edition, 49*(28), 4820-4824.

Furukawa, H., Cordova, K. E., O'Keeffe, M., & Yaghi, O. M. (2013). The chemistry and applications of metal-organic frameworks. *Science, 341*(6149), Article#1230444.

Furukawa, H., Muller, U., & Yaghi, O. M. (2015). "Heterogeneity within order" in metal-organic frameworks. *Angewandte Chemie International Edition, 54*(11), 3417-3430.

Furukawa, S., Hirai, K., Nakagawa, K., Takashima, Y., Matsuda, R., Tsuruoka, T., Kondo, M., Haruki, R., Tanaka, D., Sakamoto, H., Shimomura, S., Sakata, O., & Kitagawa, S. (2009). Heterogeneously hybridized porous coordination polymer crystals: Fabrication of heterometallic core-shell single crystals with an in-plane rotational epitaxial relationship. *Angewandte Chemie-International Edition, 48*(10), 1766-1770.

Gao, Q., Zhao, X.-L., Chang, Z., Xu, J., & Bu, X.-H. (2016). Structural stabilization of a metal–organic framework for gas sorption investigation. *Dalton Transactions, 45*(16), 6830-6833.

Ge, X., Gu, C. D., Wang, X. L., & Tu, J. P. (2017). Deep eutectic solvents (DESs)-derived advanced functional materials for energy and environmental applications: challenges, opportunities, and future vision. *Journal of Materials Chemistry A, 5*(18), 8209-8229.

Gómez, V., Benet-Buchholz, J., Martin, E., & Galán-Mascarós, J. (2014). Hysteretic spin crossover above room temperature and magnetic coupling in trinuclear transition-metal complexes with anionic 1, 2, 4-Triazole Ligands. *Chemistry–A European Journal, 20*(18), 5369-5379.

Goodenough, J. B., & Park, K. S. (2013). The Li-Ion Rechargeable Battery: A Perspective. *Journal of the American Chemical Society, 135*(4), 1167-1176.

Grall, R., Hidalgo, T., Delic, J., Garcia-Marquez, A., Chevillard, S., & Horcajada, P. (2015). In vitro biocompatibility of mesoporous metal (III; Fe, Al, Cr) trimesate MOF nanocarriers. *Journal of Materials Chemistry B, 3*(42), 8279-8292.

Grancha, T., Ferrando-Soria, J., Zhou, H. C., Gascon, J., Seoane, B., Pasán, J., Fabelo, O., Julve, M., & Pardo, E. (2015). Postsynthetic improvement of the physical properties in a metal–organic framework through a single crystal to single crystal transmetallation. *Angewandte Chemie International Edition, 54*(22), 6521-6525.

Guillerm, V., Kim, D., Eubank, J. F., Luebke, R., Liu, X., Adil, K., Lah, M. S., & Eddaoudi, M. (2014). A supermolecular building approach for the design and construction of metal-organic frameworks. *Chemical Society Reviews, 43*(16), 6141-6172.

Gul-E-Noor, F., Jee, B., Mendt, M., Himsl, D., Poppl, A., Hartmann, M., Haase, J., Krautscheid, H., & Bertmer, M. (2012). Formation of mixed metal Cu3-xZnx(btc)(2) frameworks with different Zinc contents: Incorporation of Zn2+ into the Metal-Organic framework structure as studied by Solid-State NMR. *Journal of Physical Chemistry C, 116*(39), 20866-20873.

Guo, H., Zhu, Y., Qiu, S., Lercher, J. A., & Zhang, H. (2010). Coordination modulation induced synthesis of nanoscale Eu1-xTbx-Metal-organic frameworks for luminescent thin films. *Advanced Materials, 22*(37), 4190-4192.

Han, Y., Chilton, N. F., Li, M., Huang, C., Xu, H., Hou, H., Moubaraki, B., Langley, S. K., Batten, S. R., & Fan, Y. (2013). Post-Synthetic monovalent Central-Metal exchange, specific I2 sensing, and polymerization of a catalytic [3× 3] grid of [CuII5CuI4L6]·(I)2·13H2O. *Chemistry–A European Journal, 19*(20), 6321-6328.

Hao, L., Wei, J., Zheng, R., Wang, C., Wu, Q., & Wang, Z. (2017). Magnetic porous carbon derived from Co-doped metal–organic frameworks for the magnetic solid-phase extraction of endocrine disrupting chemicals. *Journal of Separation Science, 40*(20), 3969-3975.

Heering, C., Boldog, I., Vasylyeva, V., Sanchiz, J., & Janiak, C. (2013). Bifunctional pyrazolate–carboxylate ligands for isoreticular cobalt and zinc MOF-5 analogs with magnetic analysis of the {Co 4 (μ 4-O)} node. *Crystengcomm, 15*(45), 9757-9768.

Heine, J., & Müller-Buschbaum, K. (2013). Engineering metal-based luminescence in coordination polymers and metal–organic frameworks. *Chemical Society Reviews, 42*(24), 9232-9242.

Helal, A., Yamani, Z. H., Cordova, K. E., & Yaghi, O. M. (2017). Multivariate metal-organic frameworks. *National Science Review, 4*(3), 296-298.

Hendon, C. H., Tiana, D., & Walsh, A. (2012). Conductive metal-organic frameworks and networks: fact or fantasy? *Physical Chemistry Chemical Physics, 14*(38), 13120-13132.

Ho, T. L. (1975). Hard Soft Acids Bases (Hsab) Principle and Organic-Chemistry. *Chemical Reviews, 75*(1), 1-20.

Holleman, A. F., Wiberg, E., & Wiberg, N. (2001). *Inorganic Chemistry*: Academic Press.

Horcajada, P., Gref, R., Baati, T., Allan, P. K., Maurin, G., Couvreur, P., Férey, G., Morris, R. E., & Serre, C. (2012). Metal–Organic frameworks in biomedicine. *Chemical Reviews, 112*(2), 1232-1268.

Horike, S., Umeyama, D., & Kitagawa, S. (2013). Ion conductivity and transport by porous coordination polymers and metal-organic frameworks. *Accounts of Chemical Research, 46*(11), 2376-2384.

Hoskins, B. F., & Robson, R. (1990). Design and construction of a new class of Scaffolding-Like materials comprising infinite polymeric frameworks of 3-D-linked molecular rods - a reappraisal of the Zn(Cn)2 and Cd(Cn)2 structures and the synthesis and structure of the diamond-related frameworks [N(Ch3)4] [Cuiznii(Cn)4] and Cui[4,4',4",4'"-Tetracyanotetraphenylmethane] Bf4.Xc6h5no2. *Journal of the American Chemical Society, 112*(4), 1546-1554.

Howarth, A. J., Liu, Y., Li, P., Li, Z., Wang, T. C., Hupp, J. T., & Farha, O. K. (2016). Chemical, thermal and mechanical stabilities of metal–organic frameworks. *Nature Reviews Materials, 1*(3), Article#15018.

Howell, J. A. S., & Burkinshaw, P. M. (1983). Ligand substitution reactions at low-valent four-, five-, and six-coordinate transition metal centers. *Chemical Reviews, 83*(5), 557-599.

Hu, M. L., Morsali, A., & Aboutorabi, L. (2011). Lead(II) carboxylate supramolecular compounds: Coordination modes, structures and nano-structures aspects. *Coordination Chemistry Reviews, 255*(23-24), 2821-2859.

Hu, Y., Ding, M., Liu, X.-Q., Sun, L.-B., & Jiang, H.-L. (2016). Rational synthesis of an exceptionally stable Zn (II) metal–organic framework for the highly selective and sensitive detection of picric acid. *Chemical Communications, 52*(33), 5734-5737.

Hu, Z., Deibert, B. J., & Li, J. (2014). Luminescent metal–organic frameworks for chemical sensing and explosive detection. *Chemical Society Reviews, 43*(16), 5815-5840.

Huang, C., Wang, Y., Wei, C. S., Li, N., Ji, F. X., Wu, J., & Hou, H. W. (2013). Cation-exchange-induced single-crystal-to-single-crystal transformations of a nanoporous coordination complex. *Inorganic Chemistry Communications, 32*, 68-73.

Huang, S., Li, X., Shi, X., Hou, H., & Fan, Y. (2010). Structure extending and cation exchange of Cd (II) and Co (II) materials compounds inducing fluorescence signal mutation. *Journal of Materials Chemistry, 20*(27), 5695-5699.

Hwang, S.-H., Moorefield, C. N., & Newkome, G. R. (2008). Dendritic macromolecules for organic light-emitting diodes. *Chemical Society Reviews, 37*(11), 2543-2557.

Irving, H., & Williams, R. (1953). 637. The stability of transition-metal complexes. *Journal of the Chemical Society (Resumed)*, 3192-3210.

Isaeva, V. I., & Kustov, L. M. (2010). The application of metal-organic frameworks in catalysis (Review). *Petroleum Chemistry, 50*(3), 167-180.

IUPAC, I. (1997). Compendium of chemical terminology: Blackwell Scientific Publications Oxford.

Janiak, C. (2003). Engineering coordination polymers towards applications. *Dalton Transactions*(14), 2781-2804.

Jensen, K. M. O., Tyrsted, C., Bremholm, M., & Iversen, B. B. (2014). In situ studies of solvothermal synthesis of energy materials. *ChemSusChem, 7*(6), 1594-1611.

Jiang, Y.-Y., Ren, S.-K., Ma, J.-P., Liu, Q.-K., & Dong, Y.-B. (2009). Crown-Ether-Like PbII-Metal framework with dual and bimodal emissive properties based on its photochromic precursor by leaching. *Chemistry – A European Journal, 15*(41), 10742-10746.

Jiao, Y., Morelock, C. R., Burtch, N. C., Mounfield, W. P., Hungerford, J. T., & Walton, K. S. (2015). Tuning the kinetic water stability and adsorption interactions of Mg-MOF-74 by partial substitution with Co or Ni. *Industrial & Engineering Chemistry Research, 54*(49), 12408-12414.

Jiles, D. (2015). *Introduction to magnetism and magnetic materials*: CRC press.

Jin, J., Niu, S., Han, Q., & Chi, Y. (2010). Synthesis and structure of a series of new luminescent Ag–Ln coordination polymers and the influence of the introduction of an Ag (I) ion on nir luminescence from the Ln (III) centre. *New Journal of Chemistry, 34*(6), 1176-1183.

Jin, Z. W., Fukumura, T., Kawasaki, M., Ando, K., Saito, H., Sekiguchi, T., Yoo, Y. Z., Murakami, M., Matsumoto, Y., Hasegawa, T., & Koinuma, H. (2001). High throughput fabrication of transition-metal-doped epitaxial ZnO thin films: A series of oxide-diluted magnetic semiconductors and their properties. *Applied Physics Letters, 78*(24), 3824-3826.

Kalmutzki, M. J., Hanikel, N., & Yaghi, O. M. (2018). Secondary building units as the turning point in the development of the reticular chemistry of MOFs. *Science Advances, 4*(10), Article#eaat9180.

Kang, M., Yang, G.-P., Hou, L., Wu, W.-P., Wu, Y.-L., & Wang, Y.-Y. (2015). Peculiar phenomena of structural transformations triggered from a nickel coordination polymer. *Crystengcomm, 17*(8), 1839-1847.

Karagiaridi, O., Bury, W., Mondloch, J. E., Hupp, J. T., & Farha, O. K. (2014). Solvent-Assisted linker exchange: An alternative to the de novo synthesis of unattainable Metal–Organic frameworks. *Angewandte Chemie International Edition, 53*(18), 4530-4540.

Karraker, D. G. (1967). Hypersensitive transitions of six-, seven-, and eight-coordinate neodymium, holmium, and erbium chelates. *Inorganic Chemistry, 6*, 1863-1868.

Kato, M., & Muto, Y. (1988). Factors affecting the magnetic properties of dimeric copper (II) complexes. *Coordination Chemistry Reviews, 92*, 45-83.

Kawano, M., & Fujita, M. (2007). Direct observation of crystalline-state guest exchange in coordination networks. *Coordination Chemistry Reviews, 251*(21-24), 2592-2605.

Kempahanumakkagari, S., Vellingiri, K., Deep, A., Kwon, E. E., Bolan, N., & Kim, K. H. (2018). Metal-organic framework composites as electrocatalysts for electrochemical sensing applications. *Coordination Chemistry Reviews, 357*, 105-129.

Kepp, K. P. (2016). A Quantitative Scale of Oxophilicity and Thiophilicity. *Inorganic Chemistry, 55*(18), 9461-9470.

Khlobystov, A. N., Champness, N. R., Roberts, C. J., Tendler, S. J. B., Thompson, C., & Schroder, M. (2002). Anion exchange in co-ordination polymers: A solid-state or a solvent-mediated process? *Crystengcomm, 4*, 426-431.

Kim, J. (2014). Computational generation of user-desired multivariate metal-organic framework structures. *ChemPhysChem, 15*(1), 61-63.

Kim, M., Cahill, J. F., Fei, H., Prather, K. A., & Cohen, S. M. (2012). Postsynthetic ligand and cation exchange in robust metal–organic frameworks. *Journal of the American Chemical Society, 134*(43), 18082-18088.

Kim, Y., Das, S., Bhattacharya, S., Hong, S., Kim, M. G., Yoon, M., Natarajan, S., & Kim, K. (2012). Metal-ion metathesis in metal-organic frameworks: A synthetic route to new metal-organic frameworks. *Chemistry-a European Journal, 18*(52), 16642-16648.

King, P., Clerac, R., Anson, C. E., Coulon, C., & Powell, A. K. (2003). Antiferromagnetic three-dimensional order induced by carboxylate bridges in a two-dimensional network of [Cu3 (dcp) 2 (H2O) 4] trimers. *Inorganic Chemistry, 42*(11), 3492-3500.

King, S. C., Lin, R. B., Wang, H. L., Arman, H. D., & Chen, B. L. (2017). Two-dimensional metal-organic frameworks for selective separation of CO2/CH4 and CO2/N-2. *Materials Chemistry Frontiers, 1*(8), 1514-1519.

Kirchon, A., Feng, L., Drake, H. F., Joseph, E. A., & Zhou, H. C. (2018). From fundamentals to applications: a toolbox for robust and multifunctional MOF materials. *Chemical Society Reviews, 47*(23), 8611-8638.

Kitagawa, S. (2014). Metal–organic frameworks (MOFs). *Chemical Society Reviews, 43*(16), 5415-5418.

Kitagawa, S., Kitaura, R., & Noro, S. (2004). Functional porous coordination polymers. *Angewandte Chemie International Edition, 43*(18), 2334-2375.

Kitagawa, S., Munakata, M., & Tanimura, T. (1992). Synthesis of the novel infinite-sheet and infinite-chain Copper(I) complex polymers ([Cu(C4h4n2)3/2 (Ch3cn)](Pf6).0.5c3h6o) infinity ([Cu2(C8h12n2)3](Clo4)2) infinity and their X-ray crystal-structures. *Inorganic Chemistry, 31*(9), 1714-1717.

Klopman, G. (1974). *Chemical reactivity and reaction paths*: WILEY-INTERSCIENCE.

Kole, G. K., & Vittal, J. J. (2013). Solid-state reactivity and structural transformations involving coordination polymers. *Chemical Society Reviews, 42*(4), 1755-1775.

Kong, X., Deng, H., Yan, F., Kim, J., Swisher, J. A., Smit, B., Yaghi, O. M., & Reimer, J. A. (2013). Mapping of functional groups in metal-organic frameworks. *Science, 341*(6148), 882-885.

Kostyk, R., & Whitehead, M. (1991). Electronegativity and hardness of molecular groups from the localized electronegativity group orbital (LEGO) and generalized exchange local spin density functional (LSD-GX) theories. *Journal of Molecular Structure: THEOCHEM, 230*, 83-125.

Kozachuk, O., Khaletskaya, K., Halbherr, M., Betard, A., Meilikhov, M., Seidel, R. W., Jee, B., Poppl, A., & Fischer, R. A. (2012). Microporous mixed-metal layer-pillared [Zn1-xCux(bdc)(dabco)0.5] MOFs: Preparation and characterization. *European Journal of Inorganic Chemistry, 2012*(10), 1688-1695.

Kozachuk, O., Luz, I., Llabres i Xamena, F. X., Noei, H., Kauer, M., Albada, H. B., Bloch, E. D., Marler, B., Wang, Y., Muhler, M., & Fischer, R. A. (2014). Multifunctional, defect-engineered metal-organic frameworks with ruthenium centers: sorption and catalytic properties. *Angewandte Chemie International Edition, 53*(27), 7058-7062.

Kozachuk, O., Meilikhov, M., Yusenko, K., Schneemann, A., Jee, B., Kuttatheyil, A. V., Bertmer, M., Sternemann, C., Pöppl, A., & Fischer, R. A. (2013). A solid-solution approach to mixed-metal metal-organic frameworks - detailed characterization of local structures, defects and breathing behaviour of Al/V frameworks. *European Journal of Inorganic Chemistry, 2013*(26), 4546-4557.

Kreno, L. E., Leong, K., Farha, O. K., Allendorf, M., Van Duyne, R. P., & Hupp, J. T. (2012). Metal–organic framework materials as chemical sensors. *Chemical Reviews, 112*(2), 1105-1125.

Kumar, P., Deep, A., Kim, K.-H., & Brown, R. J. C. (2015). Coordination polymers: Opportunities and challenges formonitoring volatile organic compounds. *Progress in Polymer Science, 45*, 102-118.

L. Soderholm, & J. F. Mitchell. (2016). Perspective: Toward "synthesis by design": Exploring atomic correlations during inorganic materials synthesis. *APL Materials, 4(5)* 053212.

Lau, C. H., Babarao, R., & Hill, M. R. (2013). A route to drastic increase of CO 2 uptake in Zr metal organic framework UiO-66. *Chemical Communications, 49*(35), 3634-3636.

Laurita, G., Fabini, D. H., Stoumpos, C. C., Kanatzidis, M. G., & Seshadri, R. (2017). Chemical tuning of dynamic cation off-centering in the cubic phases of hybrid tin and lead halide perovskites. *Chemical Science, 8*(8), 5628-5635.

Laye, R. H., & Sañudo, E. C. (2009). Synthesis of Fe (II) and Cu (II) building blocks for metal–organic frameworks. *Inorganica Chimica Acta, 362*(7), 2205-2212.

Le Chatelier, H., & Boudouard, O. (1898). Limits of flammability of gaseous mixtures. *Bulletin de la Societe Chimique de France, 19*, Article#483.

Lee, A. Y., Blakeslee, D. M., Powell, C. J., & Rumble, J. R. (2002). The NIST X-ray photoelectron spectroscopy (XPS) database. *Data Science Journal, 1*(1) 1-12.

Lee, A. Y., Blakeslee, D. M., Powell, C. J., & Rumble, J. R. (2012). The NIST X-ray photoelectron spectroscopy (XPS) database. http://srdata.nist.gov/xps/intro.aspx

Lee, J. Y., Roberts, J. M., Farha, O. K., Sarjeant, A. A., Scheidt, K. A., & Hupp, J. T. (2009). Synthesis and gas sorption properties of a metal-azolium framework (MAF) material. *Inorganic Chemistry, 48*(21), 9971-9973.

Lee, L.-W., Kao, Y.-C., Chung, M.-Y., Chang, B.-C., Lee, G.-H., Peng, S.-M., Wang, C.-M., Liu, Y.-H., Lee, S.-L., & Lu, K.-L. (2019). Rare metal-ion metathesis of a tetrahedral Zn (ii) core of a noncentrosymmetric (3, 4)-connected 3D MOF. *Dalton Transactions, 48*(6), 1950-1954.

Li, B., Wen, H.-M., Wang, H., Wu, H., Tyagi, M., Yildirim, T., Zhou, W., & Chen, B. (2014). A porous metal–organic framework with dynamic pyrimidine groups exhibiting record high methane storage working capacity. *Journal of the American Chemical Society, 136*(17), 6207-6210.

Li, H., Eddaoudi, M., O'Keeffe, M., & Yaghi, O. M. (1999). Design and synthesis of an exceptionally stable and highly porous metal-organic framework. *Nature, 402*(6759), 276-279.

Li, J., Fan, Y., Ren, Y., Liao, J., Qi, C., & Jiang, H. (2018). Development of isostructural porphyrin–salen chiral metal–organic frameworks through postsynthetic metalation based on single-crystal to single-crystal transformation. *Inorganic Chemistry, 57*(3), 1203-1212.

Li, J., Li, L., Hou, H., & Fan, Y. (2009). Study on the reaction of polymeric zinc ferrocenyl carboxylate with Pb (II) or Cd (II). *Crystal Growth & Design, 9*(10), 4504-4513.

Li, J.-R., Kuppler, R. J., & Zhou, H.-C. (2009). Selective gas adsorption and separation in metal–organic frameworks. *Chemical Society Reviews, 38*(5), 1477-1504.

Li, J.-R., Sculley, J., & Zhou, H.-C. (2012). Metal–organic frameworks for separations. *Chemical Reviews, 112*(2), 869-932.

Li, L. (2011). *The design and synthesis of new molecule-based magnetic materials.* University of Warwick.

Li, M., Li, D., O'Keeffe, M., & Yaghi, O. M. (2014). Topological analysis of metal-organic frameworks with polytopic linkers and/or multiple building units and the minimal transitivity principle. *Chemical Reviews, 114*(2), 1343-1370.

Li, M.-X., Wang, H., Liang, S.-W., Shao, M., He, X., Wang, Z.-X., & Zhu, S.-R. (2009). Solvothermal synthesis and diverse coordinate structures of a series of luminescent copper (I) thiocyanate coordination polymers based on N-heterocyclic ligands. *Crystal Growth & Design, 9*(11), 4626-4633.

Li, S., Chung, Y. G., Simon, C. M., & Snurr, R. Q. (2017). High-throughput computational screening of multivariate metal-organic frameworks (MTV-MOFs) for CO2 capture. *Journal of Physical Chemistry Letters, 8*(24), 6135-6141.

Li, S., & Huo, F. (2015). Metal–organic framework composites: from fundamentals to applications. *Nanoscale, 7*(17), 7482-7501.

Li, X., Wang, X.-W., & Zhang, Y.-H. (2008). Blue photoluminescent 3D Zn (II) metal-organic framework constructing from pyridine-2, 4, 6-tricarboxylate. *Inorganic Chemistry Communications, 11*(8), 832-834.

Li, X., Yu, Z., Li, X., & Guo, X. (2015). Solvent-mediated transformation from achiral to chiral Nickel(II) metal–organic frameworks and reassembly in solution. *Chemistry – A European Journal, 21*(46), 16593-16600.

Li, Y.-W., Liu, S.-J., Hu, T.-L., & Bu, X.-H. (2014). Doping cobalt into a [Zn 7] cluster-based MOF to tune magnetic behaviour and induce fluorescence signal mutation. *Dalton Transactions, 43*(30), 11470-11473.

Li, Z.-X., Zeng, Y.-F., Ma, H., & Bu, X.-H. (2010). Homospin single-chain magnet with 1D ferromagnetic azido-cobalt Ising-type chain. *Chemical Communications, 46*(45), 8540-8542.

Li, Z.-X., Zhao, J.-P., Sañudo, E., Ma, H., Pan, Z.-D., Zeng, Y.-F., & Bu, X.-H. (2009). New 3D coordination polymers constructed from pillared metal− formate kagomé layers exhibiting spin canting only in the nickel (II) complex. *Inorganic Chemistry, 48*(24), 11601-11607.

Liang, W., Coghlan, C. J., Ragon, F., Rubio-Martinez, M., D'Alessandro, D. M., & Babarao, R. (2016). Defect engineering of UiO-66 for CO2 and H2O uptake - a combined experimental and simulation study. *Dalton Transactions, 45*(11), 4496-4500.

Liang, Y. C., Hong, M. C., Cao, R., Su, W. P., Zhao, Y. J., Weng, J. B., & Xiong, R. G. (2002). Hydrothermal syntheses, structures and luminescent properties of lanthanide-zinc coordination polymers, [Ln(2)Zn(pzdc)(4)(H2O)(6)center dot 2H(2)O](n) (pzdc=pyrazine-2,3-dicarboxylate, Ln=Gd, Nd, Sm). *Bulletin of the Chemical Society of Japan, 75*(7), 1521-1526.

Liao, J.-H., Chen, W.-T., Tsai, C.-S., & Wang, C.-C. (2013). Characterization, adsorption properties, metal ion-exchange and crystal-to-crystal transformation of Cd 3 [(Cd 4 Cl) 3 (BTT) 8 (H 2 O) 12] 2 framework, where BTT 3−= 1, 3, 5-benzenetristetrazolate. *Crystengcomm, 15*(17), 3377-3384.

Lin, L., Yang, Y. C., Men, L., Wang, X., He, D. N., Chai, Y. C., Zhao, B., Ghoshroy, S., & Tang, Q. W. (2013). A highly efficient TiO2@ZnO n-p-n heterojunction nanorod photocatalyst. *Nanoscale, 5*(2), 588-593.

Liu, A. Y., & Cohen, M. L. (1990). Structural properties and electronic structure of low-compressibility materials: β-Si3N4 and hypothetical β-C3N4. *Physical Review B, 41*(15).

Liu, J., Zhang, X., Wu, T., Ma, B., Wang, T., Li, C., Li, Y., & You, X. Z. (2012). Solvent-induced single-crystal-to-single-crystal transformation in multifunctional chiral dysprosium(III) compounds. *Inorganic Chemistry, 51*, 8649-8651.

Liu, M., Bi, Y., Danga, Q., & Zhang, X. (2015). Reversible single-crystal-to-single-crystal transformation from a mononuclear complex to a fourfold interpenetrated MOF with selective adsorption of CO2. *Dalton Transactions, 44*(46), 19796-19799.

Liu, Q., Cong, H. J., & Deng, H. X. (2016). Deciphering the spatial arrangement of metals and correlation to reactivity in multivariate metal-organic frameworks. *Journal of the American Chemical Society, 138*(42), 13822-13825.

Liu, T.-F., Zou, L., Feng, D., Chen, Y.-P., Fordham, S., Wang, X., Liu, Y., & Zhou, H.-C. (2014). Stepwise synthesis of robust metal–organic frameworks via postsynthetic metathesis and oxidation of metal nodes in a single-crystal to single-crystal transformation. *Journal of the American Chemical Society, 136*(22), 7813-7816.

Liu, X., Demir, N. K., Wu, Z., & Li, K. (2015). Highly water-stable zirconium metal–organic framework UiO-66 membranes supported on alumina hollow fibers for desalination. *Journal of the American Chemical Society, 137*(22), 6999-7002.

Liu, Y., Klet, R. C., Hupp, J. T., & Farha, O. (2016). Probing the correlations between the defects in metal-organic frameworks and their catalytic activity by an epoxide ring-opening reaction. *Chemical Communications, 52*(50), 7806-7809.

Liu, Z.-F., Wu, M.-F., Wang, S.-H., Zheng, F.-K., Wang, G.-E., Chen, J., Xiao, Y., Wu, A.-Q., Guo, G.-C., & Huang, J.-S. (2013). Eu 3+-doped Tb 3+ metal–organic frameworks emitting tunable three primary colors towards white light. *Journal of Materials Chemistry C, 1*(31), 4634-4639.

Low, J. J., Benin, A. I., Jakubczak, P., Abrahamian, J. F., Faheem, S. A., & Willis, R. R. (2009). Virtual high throughput screening confirmed experimentally: porous coordination polymer hydration. *Journal of the American Chemical Society, 131*(43), 15834-15842.

Lu, W., Wei, Z., Gu, Z.-Y., Liu, T.-F., Park, J., Park, J., Tian, J., Zhang, M., Zhang, Q., Gentle Iii, T., Bosch, M., & Zhou, H.-C. (2014). Tuning the structure and function of metal–organic frameworks via linker design. *Chemical Society Reviews, 43*(16), 5561-5593.

Lu, Y., & Yan, B. (2014). Lanthanide organic–inorganic hybrids based on functionalized metal–organic frameworks (MOFs) for a near-UV white LED. *Chemical Communications, 50*(97), 15443-15446.

Lü, Y., Zhou, Q., Chen, L., Zhan, W., Xie, Z., Kuang, Q., & Zheng, L. (2016). Templated synthesis of diluted magnetic semiconductors using transition metal ion-doped metal–organic frameworks: the case of Co-doped ZnO. *Crystengcomm, 18*(22), 4121-4126.

Luo, F., & Batten, S. R. (2010). Metal–organic framework (MOF): lanthanide (III)-doped approach for luminescence modulation and luminescent sensing. *Dalton Transactions, 39*(19), 4485-4488.

Mahata, P., Mondal, S. K., Singha, D. K., & Majee, P. (2017). Luminescent rare-earth-based MOFs as optical sensors. *Dalton Transactions, 46*(2), 301-328.

Mahmoudi, G., & Morsali, A. (2008). Crystal-to-crystal transformation from a weak hydrogen-bonded two-dimensional network structure to a two-dimensional coordination polymer on heating. *Crystal Growth & Design, 8*(2), 391-394.

Manriquez, J. M., Yee, G. T., McLean, R. S., Epstein, A. J., & Miller, J. S. (1991). A room-temperature molecular/organic-based magnet. *Science, 252*(5011), 1415-1417.

Marques, N., Sella, A., & Takats, J. (2002). Chemistry of the lanthanides using pyrazolylborate ligands. *Chemical Reviews, 102*(6), 2137-2160.

Masciocchi, N., Galli, S., Colombo, V., Maspero, A., Palmisano, G., Seyyedi, B., Lamberti, C., & Bordiga, S. (2010). Cubic Octanuclear Ni (II) clusters in highly porous polypyrazolyl-based materials. *Journal of the American Chemical Society, 132*(23), 7902-7904.

Masoomi, M. Y., Beheshti, S., & Morsali, A. (2014). Mechanosynthesis of new azine-functionalized Zn (II) metal–organic frameworks for improved catalytic performance. *Journal of Materials Chemistry A, 2*(40), 16863-16866.

Masoomi, M. Y., Morsali, A., & Junk, P. C. (2015). Rapid mechanochemical synthesis of two new Cd (II)-based metal–organic frameworks with high removal efficiency of Congo red. *Crystengcomm, 17*(3), 686-692.

McKinstry, C., Cathcart, R. J., Cussen, E. J., Fletcher, A. J., Patwardhan, S. V., & Sefcik, J. (2016). Scalable continuous solvothermal synthesis of metal organic framework (MOF-5) crystals. *Chemical Engineering Journal, 285*, 718-725.

Meng, W., Li, H. J., Xu, Z. Q., Du, S. S., Li, Y. X., Zhu, Y. Y., Han, Y., Hou, H. W., Fan, Y. T., & Tang, M. S. (2014). New mechanistic insight into stepwise metal-center exchange in a metal-organic framework based on asymmetric Zn-4 clusters. *Chemistry-a European Journal, 20*(10), 2945-2952.

Meyer, L., Schönfeld, F., & Müller-Buschbaum, K. (2014). Lanthanide based tuning of luminescence in MOFs and dense frameworks–from mono-and multimetal systems to sensors and films. *Chemical Communications, 50*(60), 8093-8108.

Mi, L. W., Hou, H. W., Song, Z. Y., Han, H. Y., & Fan, Y. T. (2008). Polymeric zinc ferrocenyl sulfonate as a molecular aspirator for the removal of toxic metal ions. *Chemistry-a European Journal, 14*(6), 1814-1821.

Mi, X., Sheng, D., Yu, Y. e., Wang, Y., Zhao, L., Lu, J., Li, Y., Li, D., Dou, J., & Duan, J. (2019). Tunable light emission and multiresponsive luminescent sensitivities in aqueous solutions of two series of lanthanide metal–organic frameworks based on structurally related ligands. *Acs Applied Materials & Interfaces, 11*(8), 7914-7926.

Min, K. S., & Suh, M. P. (2000). Silver(I)-polynitrile network solids for anion exchange: Anion-induced transformation of supramolecular structure in the crystalline state. *Journal of the American Chemical Society, 122*(29), 6834-6840.

Mon, M., Bruno, R., Elliani, R., Tagarelli, A., Qu, X. N., Chen, S. P., Ferrando-Soria, J., Armentano, D., & Pardo, E. (2018). Lanthanide discrimination with hydroxyl-decorated flexible metal-organic frameworks. *Inorganic Chemistry, 57*(21), 13895-13900.

Montoro, C., Linares, F., Quartapelle Procopio, E., Senkovska, I., Kaskel, S., Galli, S., Masciocchi, N., Barea, E., & Navarro, J. A. (2011). Capture of nerve agents and mustard gas analogues by hydrophobic robust MOF-5 type metal–organic frameworks. *Journal of the American Chemical Society, 133*(31), 11888-11891.

Moore, E. G., Samuel, A. P., & Raymond, K. N. (2009). From antenna to assay: lessons learned in lanthanide luminescence. *Accounts of Chemical Research, 42*(4), 542-552.

Morris, R. E., & Brammer, L. (2017). Coordination change, lability and hemilability in metal-organic frameworks. *Chemical Society Reviews, 46*(17), 5444-5462.

Morsali, A., & Masoomi, M. Y. (2009). Structures and properties of mercury(II) coordination polymers. *Coordination Chemistry Reviews, 253*(13), 1882-1905.

Mukherjee, G., & Biradha, K. (2012). Post-synthetic modification of isomorphic coordination layers: exchange dynamics of metal ions in a single crystal to single crystal fashion. *Chemical Communications, 48*(36), 4293-4295.

Muller, P. (2009). Practical suggestions for better crystal structures. *Crystallography Reviews, 15*(1), 57-83.

Nikas, V., Tabassum, N., Ford, B., Smith, L., Kaloyeros, A. E., & Gallis, S. (2015). Strong visible light emission from silicon-oxycarbide nanowire arrays prepared by electron beam lithography and reactive ion etching. *Journal of Materials Research, 30*(23), 3692-3699.

Noro, S., Kitaura, R., Kondo, M., Kitagawa, S., Ishii, T., Matsuzaka, H., & Yamashita, M. (2002). Framework engineering by anions and porous functionalities of Cu(II)/4,4 '-bpy coordination polymers. *Journal of the American Chemical Society, 124*(11), 2568-2583.

Noshiranzadeh, N., Ramazani, A., Morsali, A., Hunter, A. D., & Zeller, M. (2007). Novel coordination mode of chloride ion in holo- and hemidirected one-dimensional PbII coordination polymer. *Inorganic Chemistry Communications, 10*(7), 738-742.

Nugent, P., Belmabkhout, Y., Burd, S. D., Cairns, A. J., Luebke, R., Forrest, K., Pham, T., Ma, S., Space, B., & Wojtas, L. (2013). Porous materials with optimal adsorption thermodynamics and kinetics for CO 2 separation. *Nature, 495*(7439), 80.

O'Keeffe, M., Peskov, M. A., Ramsden, S. J., & Yaghi, O. M. (2008). The Reticular Chemistry Structure Resource (RCSR) database of, and symbols for, crystal nets. *Accounts of Chemical Research, 41*(12), 1782-1789.

Ogiwara, N., Kobayashi, H., Kobayashi, K., Yamamoto, T., Toriyama, T., Matsumura, S., & Kitagawa, H. (2019). Coating of 2D flexible metal-organic frameworks on metal nanocrystals. *Chemistry Letters, 48*(2), 173-176.

Paital, A. R., Mitra, T., Ray, D., Wong, W. T., Ribas-Ariño, J., Novoa, J. J., Ribas, J., & Aromí, G. (2005). Substituted m-phenylene bridges as strong ferromagnetic couplers for Cu ii–bridge–Cu ii magnetic interactions: New perspectives. *Chemical Communications*(41), 5172-5174.

Pan, L., Zheng, N., Wu, Y., Han, S., Yang, R., Huang, X., & Li, J. (2001). Synthesis, characterization and structural transformation of a condensed rare earth metal coordination polymer. *Inorganic Chemistry, 40*, 828-830.

Park, J., Chen, Y. P., Perry, Z., Li, J. R., & Zhou, H. C. (2014). Preparation of core-shell coordination molecular assemblies via the enrichment of structure-directing "codes" of bridging ligands and metathesis of metal units. *Journal of the American Chemical Society, 136*(48), 16895-16901.

Park, J., Feng, D., & Zhou, H.-C. (2015). Dual exchange in PCN-333: a facile strategy to chemically robust mesoporous chromium metal–organic framework with functional groups. *Journal of the American Chemical Society, 137*(36), 11801-11809.

Park, K. S., Ni, Z., Côté, A. P., Choi, J. Y., Huang, R., Uribe-Romo, F. J., Chae, H. K., O'Keeffe, M., & Yaghi, O. M. (2006). Exceptional chemical and thermal stability of zeolitic imidazolate frameworks. *Proceedings of the National Academy of Sciences, 103*(27), 10186-10191.

Parkes, M. V., Sava Gallis, D. F., Greathouse, J. A., & Nenoff, T. M. (2015). Effect of metal in M3(btc)2 and M2(dobdc) MOFs for O2/N2Separations: A combined density functional theory and experimental study. *Journal of Physical Chemistry C, 119*(12), 6556-6567.

Parsons, T. G., Hadermann, J., Halasyamani, P. S., & Hayward, M. A. (2020). Preparation of the noncentrosymmetric ferrimagnetic phase La0.9Ba0.1Mn0.96O2.43 by topochemical reduction. *Journal of Solid State Chemistry*, 121356.

Pearson, R. G. (1963a). Hard and soft acids and bases. *Journal of the American Chemical Society, 85*(22), 3533-3539.

Pearson, R. G. (1963b). Hard and soft acids and bases. *Journal of the American Chemical Society, 85*(22), 3533-3539.

Pearson, R. G. (1980). Citation classic - Hard and soft acids and bases. *Current Contents/Physical Chemical & Earth Sciences* 1(23), 12-12.

Pearson, R. G. (1986a). Citation-classic - Hard and soft acids and bases, HSAB .1. Fundamental principles. *Current Contents/Engineering Technology & Applied Sciences* 1(8), 18-18.

Pearson, R. G. (1986b). Citation-classic - Hard and soft acids and bases, HSAB .1. Fundamental Principles. *Current Contents/Physical Chemical & Earth Sciences*(8), 18-18.

Pearson, R. G. (1987). Recent advances in the concept of hard and soft acids and bases. *Journal of Chemical Education, 64*(7), 561-567.

Pearson, R. G. (1988). Absolute electronegativity and hardness: Application to inorganic chemistry. *Inorganic Chemistry, 27*(4), 734-740.

Pearson, R. G. (1990). Hard and soft acids and bases - The evolution of a chemical concept. *Coordination Chemistry Reviews, 100*, 403-425.

Pearson, R. G. (1995). The HSAB principle — More quantitative aspects. *Inorganica Chimica Acta, 240*(1), 93-98.

Peedikakkal, A. M. P., & Vittal, J. J. (2011). Structural transformations of Pb (II)-trans-1, 2-bis (4′-pyridyl) ethene coordination polymers in solution. *Crystal Growth & Design, 11*(10), 4697-4703.

Peng, Z., & Yang, H. (2009). Designer platinum nanoparticles: Control of shape, composition in alloy, nanostructure and electrocatalytic property. *Nano Today, 4*(2), 143-164.

Perry, J. J., Perman, J. A., & Zaworotko, M. J. (2009). Design and synthesis of metal-organic frameworks using metal-organic polyhedra as supermolecular building blocks. *Chemical Society Reviews, 38*(5), 1400-1417.

Pieterson, L. v., Wegh, R. T., Meijerink, A., & Reid, M. F. (2001). Emission spectra and trends for 4fn−15d↔4fn transitions of lanthanide ions: Experiment and theory. *The Journal of Chemical Physics, 115*(20), 9382-9392.

Prasad, T. K., Hong, D. H., & Suh, M. P. (2010). High gas sorption and metal-ion exchange of microporous metal–organic frameworks with incorporated imide groups. *Chemistry–a European Journal, 16*(47), 14043-14050.

Qu, T., Wei, Q., Ordonez, C., Lindline, J., Petronis, M., Fonari, M. S., & Timofeeva, T. (2018). Tuning of luminescent and magnetic properties via metal doping of Zn-BTC systems. *Crystals, 8*(4), Article#162.

Ramaswamy, P., Wong, N. E., & Shimizu, G. K. (2014). MOFs as proton conductors--challenges and opportunities. *Chemical Society Reviews, 43*(16), 5913-5932.

Rao, K. P., Thirumurugan, A., & Rao, C. N. (2007). Lamellar and three-dimensional hybrid compounds formed by cyclohexene- and cyclohexanedicarboxylates of Pb, La, and Cd. *Chemistry-a European Journal, 13*(11), 3193-3201.

Rao, X., Huang, Q., Yang, X., Cui, Y., Yang, Y., Wu, C., Chen, B., & Qian, G. (2012). Color tunable and white light emitting Tb 3+ and Eu 3+ doped lanthanide metal–organic framework materials. *Journal of Materials Chemistry, 22*(7), 3210-3214.

Rao, X., Song, T., Gao, J., Cui, Y., Yang, Y., Wu, C., Chen, B., & Qian, G. (2013). A highly sensitive mixed lanthanide metal–organic framework self-calibrated luminescent thermometer. *Journal of the American Chemical Society, 135*(41), 15559-15564.

Redhammer, G. R., & Roth, G. (2003). Lithium and sodium yttrium orthosilicate oxyapatite, LiY9(SiO4)6O2, at both 100 K and near room temperature. *Acta Crystallographica a-Foundation and Advances, 59*, 120-124.

Reed, J. L. (2012). Hard and Soft Acids and Bases: Structure and Process. *Journal of Physical Chemistry A, 116*(26), 7147-7153.

Ritter, B., Haida, P., Fink, F., Krahl, T., Gawlitza, K., Rurack, K., Scholz, G., & Kemnitz, E. (2017). Novel and easy access to highly luminescent Eu and Tb doped ultra-small CaF2, SrF2 and BaF2 nanoparticles – structure and luminescence. *Dalton Transactions, 46*(9), 2925-2936.

Robin, A. Y., & Fromm, K. M. (2006). Coordination polymer networks with O- and N-donors: What they are, why and how they are made. *Coordination Chemistry Reviews, 250*(15-16), 2127-2157.

Rogacka, J., Formalik, F., Triguero, A. L., Firlej, L., Kuchta, B., & Calero, S. (2019). Intermediate states approach for adsorption studies in flexible metal- organic frameworks. *Physical Chemistry Chemical Physics, 21*(6), 3294-3303.

Safarifard, V., & Morsali, A. (2012). Sonochemical syntheses of a nano-sized copper (II) supramolecule as a precursor for the synthesis of copper (II) oxide nanoparticles. *Ultrasonics Sonochemistry, 19*(4), 823-829.

Sava Gallis, D. F., Parkes, M. V., Greathouse, J. A., Zhang, X., & Nenoff, T. M. (2015). Enhanced O2 selectivity versus N2 by partial metal substitution in Cu-BTC. *Chemistry of Materials, 27*(6), 2018-2025.

Schneemann, A., Bon, V., Schwedler, I., Senkovska, I., Kaskel, S., & Fischer, R. A. (2014). Flexible metal–organic frameworks. *Chemical Society Reviews, 43*(16), 6062-6096.

Schoenecker, P. M., Carson, C. G., Jasuja, H., Flemming, C. J., & Walton, K. S. (2012). Effect of water adsorption on retention of structure and surface area of metal–organic frameworks. *Industrial & Engineering Chemistry Research, 51*(18), 6513-6519.

Schubert, D. M., Visi, M. Z., & Knobler, C. B. (2008). Acid-catalyzed synthesis of zinc imidazolates and related bimetallic metal-organic framework compounds. *Main Group Chemistry, 7*(4), 311-322.

Scott, D., Manos, S., Coveney, P. V., Rossiny, J., Fearn, S., Kilner, J., Pullar, R., Alford, N. M. N., Axelsson, A.-K., & Zhang, Y. (2008). Functional ceramic materials database: An online resource for materials research. *Journal of Chemical Information and Modeling, 48*(2), 449-455.

Sejeant, E., & Dempsey, B. (1979). Ionisation Constant of Organic Acids in Aqueous Solution, IUPAC Chemical Data Series, No. 23: Pergamon, Oxford.

Serre, C., Millange, F., & Thouvenot, C. (2002). M. Nogu s, G. Marsolier, D. Lou r, G. FØrey. *Journal of the American Chemical Society, 124*(13), 519-513.

Shearer, G. C., Chavan, S., Bordiga, S., Svelle, S., Olsbye, U., & Lillerud, K. P. (2016). Defect engineering: Tuning the porosity and composition of the metal–organic framework UiO-66 via modulated synthesis. *Chemistry of Materials, 28*(11), 3749-3761.

Shekhah, O., Belmabkhout, Y., Chen, Z., Guillerm, V., Cairns, A., Adil, K., & Eddaoudi, M. (2014). Made-to-order metal-organic frameworks for trace carbon dioxide removal and air capture. *Nature Communications, 5*, Article#4228.

Sheldrick, G. (2008). A short history of SHELX. *Acta Crystallographica a-Foundation and Advances, 64*(1), 112-122.

Siegel, R. W. (1994). What do we really know about the atomic-scale structures of nanophase materials. *Journal of Physics and Chemistry of Solids, 55*(10), 1097-1106.

Silva, C. G., Corma, A., & García, H. (2010). Metal–organic frameworks as semiconductors. *Journal of Materials Chemistry, 20*(16), 3141-3156.

Singh, J. (Ed.) (2003). *Electronic and Optoelectronic Properties of Semiconductor Structures*. Cambridge: Cambridge University Press.

Slabbert, C., & Rademeyer, M. (2015). One-dimensional halide-bridged polymers of metal cations with mono-heterocyclic donor ligands or cations: A review correlating chemical composition, connectivity and chain conformation. *Coordination Chemistry Reviews, 288*, 18-49.

Smith, D. W. (1977). Ionic hydration enthalpies. *Journal of Chemical Education, 54*(9), Article#540.

Soltanzadeh, N., & Morsali, A. (2010). Sonochemical synthesis of a new nano-structures bismuth (III) supramolecular compound: new precursor for the preparation of bismuth (III) oxide nano-rods and bismuth (III) iodide nano-wires. *Ultrasonics Sonochemistry, 17*(1), 139-144.

Song, X., Jeong, S., Kim, D., & Lah, M. S. (2012). Transmetalations in two metal–organic frameworks with different framework flexibilities: Kinetics and core–shell heterostructure. *Crystengcomm, 14*(18), 5753-5756.

Song, X., Kim, T. K., Kim, H., Kim, D., Jeong, S., Moon, H. R., & Lah, M. S. (2012). Post-synthetic modifications of framework metal ions in isostructural metal–organic frameworks: Core–shell heterostructures via selective transmetalations. *Chemistry of Materials, 24*(15), 3065-3073.

Song, Y. M., Luo, F., Luo, M. B., Liao, Z. W., Sun, G. M., Tian, X. Z., Zhu, Y., Yuan, Z. J., Liu, S. J., Xu, W. Y., & Feng, X. F. (2012). The application of single-crystal-to-single-crystal transformation towards adjustable SMM properties. *Chemical Communications, 48*(7), 1006-1008.

Sonoyama, N., Takagi, K., Yoshida, S., Ota, T., Kimilita, P. D., & Ogasawara, Y. (2020). Optical properties of the europium (II) and (III) ions doped metal oxides obtained from sintering layered double hydroxides, and their fine structures. *Applied Clay Science, 186*, Article#105440.

Steed, J. W., & Atwood, J. L. (2009). *Supramolecular Chemistry*. UK: John Wiley & Sons, Ltd.

Steemers, F. J., Verboom, W., Reinhoudt, D. N., van der Tol, E. B., & Verhoeven, J. W. (1995). New Sensitizer-Modified Calix[4]arenes Enabling Near-UV Excitation of Complexed Luminescent Lanthanide Ions. *Journal of the American Chemical Society, 117*(37), 9408-9414.

Suh, M. P., Cheon, Y. E., & Lee, E. Y. (2008). Syntheses and functions of porous metallosupramolecular networks. *Coordination Chemistry Reviews, 252*(8-9), 1007-1026.

Suh, M. P., Park, H. J., Prasad, T. K., & Lim, D.-W. (2012). Hydrogen Storage in Metal–Organic Frameworks. *Chemical reviews, 112*(2), 782-835.

Sumida, K., Rogow, D. L., Mason, J. A., McDonald, T. M., Bloch, E. D., Herm, Z. R., Bae, T.-H., & Long, J. R. (2011). Carbon dioxide capture in metal–organic frameworks. *Chemical Reviews, 112*(2), 724-781.

Sumida, K., Stück, D., Mino, L., Chai, J.-D., Bloch, E. D., Zavorotynska, O., Murray, L. J., Dincă, M., Chavan, S., Bordiga, S., Head-Gordon, M., & Long, J. R. (2013). Impact of metal and anion substitutions on the hydrogen storage properties of M-BTT metal–organic frameworks. *Journal of the American Chemical Society, 135*(3), 1083-1091.

Sun, C.-Y., Wang, X.-L., Zhang, X., Qin, C., Li, P., Su, Z.-M., Zhu, D.-X., Shan, G.-G., Shao, K.-Z., Wu, H., & Li, J. (2013). Efficient and tunable white-light emission of metal–organic frameworks by iridium-complex encapsulation. *Nature Communications, 4*(1), 1-8.

Sun, D., Liu, W., Qiu, M., Zhang, Y., & Li, Z. (2015). Introduction of a mediator for enhancing photocatalytic performance via post-synthetic metal exchange in metal–organic frameworks (MOFs). *Chemical Communications, 51*(11), 2056-2059.

Sun, L., Campbell, M. G., & Dinca, M. (2016). Electrically conductive porous metal-organic frameworks. *Angewandte Chemie International Edition, 55*(11), 3566-3579.

Sun, Y.-Q., Zhang, J., & Yang, G.-Y. (2006). A series of luminescent lanthanide–cadmium–organic frameworks with helical channels and tubes. *Chemical Communications*(45), 4700-4702.

Sundberg, J., Cameron, L. J., Southon, P. D., Kepert, C. J., & McKenzie, C. J. (2014). Oxygen chemisorption/desorption in a reversible single-crystal-to-single-crystal transformation. *Chemical Science, 5*(10), 4017-4025.

Suyetin, M., Peskov, M. V., & Schwingenschlögl, U. (2020). Methane sorption in a family of qzd-MOFs: A multiscale computational study. *Chemical Engineering Journal, 384*, Article#123296.

T. L. Che, Q. C. Gao, W. P. Zhang, Z. X. Nan, H. X. Li, Y. G. Cai, & Zhao, J. S. (2009). Two novel coordination polymers [Sm2(Pzdc)3(H2O)]x·2xH2O and [Nd2(Pzdc)3(H2O)]x·2xH2O: synthesis, structure, and photoluminescent properties. *Russian Journal of Coordination Chemistry, 35*(10), 723-720.

Tan, Y.-X., He, Y.-P., & Zhang, J. (2012). Tuning MOF stability and porosity via adding rigid pillars. *Inorganic Chemistry, 51*(18), 9649-9654.

Taylor, J. M., Dekura, S., Ikeda, R., & Kitagawa, H. (2015). Defect control to enhance proton conductivity in a metal–organic framework. *Chemistry of Materials, 27*(7), 2286-2289.

Thirumurugan, A., & Rao, C. (2005). 1, 2-, 1, 3-and 1, 4-Benzenedicarboxylates of Cd and Zn of different dimensionalities: Process of formation of the three-dimensional structure. *Journal of Materials Chemistry, 15*(35-36), 3852-3858.

Thirumurugan, A., Sanguramath, R. A., & Rao, C. N. (2008). Hybrid structures formed by lead 1,3-cyclohexanedicarboxylates. *Inorganic Chemistry, 47*(3), 823-831.

Tonigold, M., Lu, Y., Bredenkötter, B., Rieger, B., Bahnmüller, S., Hitzbleck, J., Langstein, G., & Volkmer, D. (2009). Heterogeneous catalytic oxidation by MFU-1: A Cobalt (II)-containing metal–organic framework. *Angewandte Chemie International Edition, 48*(41), 7546-7550.

Tran, V. H., & Świątek-Tran, B. (2008). Spin-glass behaviour in the coordination polymer [Co (C 3 H 3 N 2) 2] n. *Dalton Transactions*(36), 4860-4865.

Tranchemontagne, D. J., Mendoza-Cortés, J. L., O'Keeffe, M., & Yaghi, O. M. (2009). Secondary building units, nets and bonding in the chemistry of metal–organic frameworks. *Chemical Society Reviews, 38*(5), 1257-1283.

Trickett, C. A., Gagnon, K. J., Lee, S., Gandara, F., Burgi, H. B., & Yaghi, O. M. (2015). Definitive molecular level characterization of defects in UiO-66 crystals. *Angewandte Chemie International Edition, 54*(38), 11162-11167.

Tsuboi, T., & Silfsten, P. (1991). Time-resolved spectroscopy of the luminescence in KBr:Sn2+ crystals. *Physical Review B, 43*(2-15).

Tsuruoka, T., Furukawa, S., Takashima, Y., Yoshida, K., Isoda, S., & Kitagawa, S. (2009). Nanoporous nanorods fabricated by coordination modulation and oriented attachment growth. *Angewandte Chemie International Edition, 48*(26), 4739-4743.

Tu, B., Pang, Q., Wu, D., Song, Y., Weng, L., & Li, Q. (2014). Ordered vacancies and their chemistry in metal-organic frameworks. *Journal of the American Chemical Society, 136*(41), 14465-14471.

Tu, J., Zeng, X., Xu, F., Wu, X., Tian, Y., Hou, X., & Long, Z. (2017). Microwave-induced fast incorporation of titanium into UiO-66 metal–organic frameworks for enhanced photocatalytic properties. *Chemical Communications, 53*(23), 3361-3364.

Vaesen, S., Guillerm, V., Yang, Q., Wiersum, A. D., Marszalek, B., Gil, B., Vimont, A., Daturi, M., Devic, T., & Llewellyn, P. L. (2013). A robust amino-functionalized titanium (IV) based MOF for improved separation of acid gases. *Chemical Communications, 49*(86), 10082-10084.

Van Aert, S., Batenburg, K. J., Rossell, M. D., Erni, R., & Van Tendeloo, G. (2011). Three-dimensional atomic imaging of crystalline nanoparticles. *Nature, 470*(7334), 374-377.

Vuong, G. T., Pham, M. H., & Do, T. O. (2013). Synthesis and engineering porosity of a mixed metal Fe2Ni MIL-88B metal-organic framework. *Dalton Transactions, 42*(2), 550-557.

Walsh, A., & Watson, G. W. (2005). The origin of the stereochemically active Pb(II) lone pair: DFT calculations on PbO and PbS. *Journal of Solid State Chemistry, 178*(5), 1422-1428.

Wang, C., Liu, X., Demir, N. K., Chen, J. P., & Li, K. (2016). Applications of water stable metal–organic frameworks. *Chemical Society Reviews, 45*(18), 5107-5134.

Wang, G.-H., Li, Z.-G., Jia, H.-Q., Hu, N.-H., & Xu, J.-W. (2009). Metal–organic frameworks based on the pyridine-2, 3-dicarboxylate and a flexible bispyridyl ligand: syntheses, structures, and photoluminescence. *CrystEngComm, 11*(2), 292-297.

Wang, H., Zhu, Q.-L., Zou, R., & Xu, Q. (2017). Metal-organic frameworks for energy applications. *Chem, 2*(1), 52-80.

Wang, H. L., Zhu, Q. L., Zou, R. Q., & Xu, Q. (2017). Metal-Organic Frameworks for Energy Applications. *CHEM, 2*(1), 52-80.

Wang, J. H., Zhang, Y., Li, M., Yan, S., Li, D., & Zhang, X. M. (2017). Solvent-assisted metal metathesis: A highly efficient and versatile route towards synthetically demanding chromium metal–organic frameworks. *Angewandte Chemie International Edition, 56*(23), 6478-6482.

Wang, L. J., Deng, H., Furukawa, H., Gándara, F., Cordova, K. E., Peri, D., & Yaghi, O. M. (2014). Synthesis and characterization of metal–organic framework-74 containing 2, 4, 6, 8, and 10 different metals. *Inorganic Chemistry, 53*(12), 5881-5883.

Wang, P., Ma, J.-P., Dong, Y.-B., & Huang, R.-Q. (2007). Tunable luminescent lanthanide coordination polymers based on reversible solid-state ion-exchange monitored by ion-dependent photoinduced emission spectra. *Journal of the American Chemical Society, 129*(35), 10620-10621.

Wang, X., Gao, W.-Y., Luan, J., Wojtas, L., & Ma, S. (2016). An effective strategy to boost the robustness of metal–organic frameworks via introduction of size-matching ligand braces. *Chemical Communications, 52*(9), 1971-1974.

Wang, X.-J., Li, P.-Z., Liu, L., Zhang, Q., Borah, P., Wong, J. D., Chan, X. X., Rakesh, G., Li, Y., & Zhao, Y. (2012). Significant gas uptake enhancement by post-exchange of zinc(ii) with copper(ii) within a metal–organic framework. *Chemical Communications, 48*(83), 10286-10288.

Wardana, F. Y., Ng, S.-W., & Wibowo, A. C. (2015). The lead coordination polymers containing pyrazine-2,3-dicarboxylic acid: Rapid structural transformations and cation exchange. *Crystal Growth & Design, 15*(12), 5930-5938.

Wei, F. X., Deng, Z. Y., Sun, S. J., Xie, F., Kieslich, G., Evans, D. M., Carpenter, M. A., Bristowe, P. D., & Cheetham, A. K. (2016). The synthesis, structure and electronic properties of a lead-free hybrid inorganic-organic double perovskite (MA)(2)KBiCl6 (MA = methylammonium). *Materials Horizons, 3*(4), 328-332.

Wei, R., Huo, Q., Tao, J., Huang, R., & Zheng, N. (2011). Spin-crossover FeII 4 squares: Two-step complete spin transition and reversible single-crystal-to-single-crystal transformation. *Angewandte Chemie International Edition, 50*, 8940-8943.

Wei, Y., Yu, Y., & Wu, K. (2008). Highly stable five-coordinated Mn (II) polymer [Mn (Hbidc)] n (Hbidc= 1 H-Benzimidazole-5, 6-dicarboxylate): Crystal structure, antiferromegnetic property, and strong long-lived luminescence. *Crystal Growth and Design, 8*(7), 2087-2089.

West, A. R. (2014). *Solid state chemistry and its applications*: John Wiley & Sons.

Wibowo, A. C., Vaughn, S. A., Smith, M. D., & zur Loye, H.-C. (2010). Novel bismuth and lead coordination polymers synthesized with pyridine-2, 5-dicarboxylates: two single component “white” light emitting phosphors. *Inorganic Chemistry, 49*(23), 11001-11008.

Wieme, J., Lejaeghere, K., Kresse, G., & Van Speybroeck, V. (2018). Tuning the balance between dispersion and entropy to design temperature-responsive flexible metal-organic frameworks. *Nature Communications, 9(1)*, 1-10.

Woodward, S. (2002). HSAB matching and mismatching in selective catalysis and synthesis. *Tetrahedron, 58*(6), 1017-1050.

Xia, Q. C., Li, Z. J., Tan, C. X., Liu, Y., Gong, W., & Cui, Y. (2017). Multivariate metal-organic frameworks as multifunctional heterogeneous asymmetric catalysts for sequential reactions. *Journal of the American Chemical Society, 139*(24), 8259-8266.

Xiang, S.-C., Zhang, Z., Zhao, C.-G., Hong, K., Zhao, X., Ding, D.-R., Xie, M.-H., Wu, C.-D., Das, M. C., & Gill, R. (2011). Rationally tuned micropores within enantiopure metal-organic frameworks for highly selective separation of acetylene and ethylene. *Nature Communications, 2*, Article#204.

Xiao, Z., Wang, Y., Zhang, S., Fan, W., Xin, X., Pan, X., Zhang, L., & Sun, D. (2017). Stepwise synthesis of diverse isomer MOFs via metal-ion metathesis in a controlled single-crystal-to-single-crystal transformation. *Crystal Growth & Design, 17*(8), 4084-4089.

Xu, C. Y., Wang, X. J., Ding, D. A., Hou, H. W., & Fan, Y. T. (2011). Tunable structures aroused by cation exchange reaction of solvent-mediated mechanism. *Inorganic Chemistry Communications, 14*(9), 1410-1413.

Xu, T., Jiang, Z., He, M., Gao, X., & He, Y. (2019). Effect of arrangement of functional groups on stability and gas adsorption properties in two regioisomeric copper bent diisophthalate frameworks. *CrystEngComm, 21*(32), 4820-4827.

Xu, X.-Y., & Yan, B. (2015). Eu(III)-functionalized MIL-124 as fluorescent probe for highly selectively sensing ions and organic small molecules especially for Fe(III) and Fe(II). *ACS Applied Materials & Interfaces, 7*(1), 721-729.

Xu, Y., Vermeulen, N. A., Liu, Y., Hupp, J. T., & Farha, O. K. (2016). SALE-Ing a MOF-based "ship of theseus." sequential building-block replacement for complete reformulation of a pillared-paddlewheel metal-organic framework. *European Journal of Inorganic Chemistry, 2016*(27), 4345-4348.

Yaghi, O. M. (2014). Multivariate metal-organic frameworks for carbon dioxide capture in the presence of water. *Abstracts of Papers of the American Chemical Society,* (Vol. 248). 1155 16th St, NW, Washington, DC 20036 USA: American Chemical Society.

Yaghi, O. M., Li, G., & Li, H. (1995). Selective binding and removal of guests in a microporous metal–organic framework. *Nature, 378*(6558), 703-706.

Yaghi, O. M., & Li, H. L. (1996). T-shaped molecular building units in the porous structure of Ag(4,4'-bpy)center dot NO3. *Journal of the American Chemical Society, 118*(1), 295-296.

Yaghi, O. M., O'Keeffe, M., Ockwig, N. W., Chae, H. K., M., E., & Kim , J. (2003). Reticular synthesis and the design of new materials. *Nature, 423*, 705-714.

Yang, C.-X., Ren, H.-B., & Yan, X.-P. (2013). Fluorescent metal–organic framework MIL-53 (Al) for highly selective and sensitive detection of Fe3+ in aqueous solution. *Analytical Chemistry, 85*(15), 7441-7446.

Yang, E.-C., Liu, Z.-Y., Shi, X.-J., Liang, Q.-Q., & Zhao, X.-J. (2010). Two 3D triazolate− tricarboxylate-bridged CuII/I frameworks by one-pot hydrothermal synthesis exhibiting spin-canted antiferromagnetism and strong antiferromagnetic couplings. *Inorganic Chemistry, 49*(17), 7969-7975.

Yang, J., Li, G. D., Cao, J. J., Yue, Q., Li, G. H., & Chen, J. S. (2007). Structural variation from 1D to 3D: Effects of ligands and solvents on the construction of lead(II)-organic coordination polymers. *Chemistry – A European Journal, 13*(11), 3248-3261.

Yang, J., Ma, J.-F., Liu, Y.-Y., Ma, J.-C., & Batten, S. R. (2009). A series of lead(II) complexes with π−π stackings: Structural diversities by varying the ligands. *Crystal Growth & Design, 9*(4), 1894-1911.

Yang, L.-R., Song, S., Zhang, W., Zhang, H.-M., Bu, Z.-W., & Ren, T.-G. (2011). Synthesis, structure and luminescent properties of neodymium (III) coordination polymers with 2, 3-pyrazinedicarboxylic acid. *Synthetic Metals, 161*(9-10), 647-654.

Yang, Q.-Y., Pan, M., Wei, S.-C., Li, K., Du, B.-B., & Su, C.-Y. (2015). Linear dependence of photoluminescence in mixed Ln-MOFs for color tunability and barcode application. *Inorganic Chemistry, 54*(12), 5707-5716.

Yang, T.-H., Liao, Y., Zheng, L.-M., Dinnebier, R. E., Su, Y.-H., & Ma, J. (2009). Tuning the field-induced magnetic transition in a layered cobalt phosphonate by reversible dehydration-hydration process. *Chemical Communications*(21), 3023-3025.

Yao, Q., Sun, J., Li, K., Su, J., Peskov, M. V., & Zou, X. (2012). A series of isostructural mesoporous metal–organic frameworks obtained by ion-exchange induced single-crystal to single-crystal transformation. *Dalton Transactions, 41*(14), 3953-3955.

Yazaki, R., Kumagai, N., & Shibasaki, M. (2010). Direct catalytic asymmetric addition of allyl cyanide to ketones via soft Lewis acid/hard Brønsted base/hard lewis base catalysis. *Journal of the American Chemical Society, 132*(15), 5522-5531.

Yoon, M., Srirambalaji, R., & Kim, K. (2012). Homochiral metal–organic frameworks for asymmetric heterogeneous catalysis. *Chemical Reviews, 112*(2), 1196-1231.

Yuan, C. Z., Wu, H. B., Xie, Y., & Lou, X. W. (2014). Mixed transition-metal oxides: Design, synthesis, and energy-related applications. *Angewandte Chemie-International Edition, 53*(6), 1488-1504.

Yuan, S., Feng, L., Wang, K., Pang, J., Bosch, M., Lollar, C., Sun, Y., Qin, J., Yang, X., & Zhang, P. (2018). Stable metal–organic frameworks: design, synthesis, and applications. *Advanced Materials, 30*(37), Article#1704303.

Yuan, S., Feng, L., Wang, K. C., Pang, J. D., Bosch, M., Lollar, C., Sun, Y. J., Qin, J. S., Yang, X. Y., Zhang, P., Wang, Q., Zou, L. F., Zhang, Y. M., Zhang, L. L., Fang, Y., Li, J. L., & Zhou, H. C. (2018). Stable metal-organic frameworks: Design, synthesis, and applications. *Advanced Materials, 30*(37), Article#1704303.

Yuan, S., Lu, W. G., Chen, Y. P., Zhang, Q., Liu, T. F., Feng, D. W., Wang, X., Qin, J. S., & Zhou, H. C. (2015). Sequential linker installation: Precise placement of functional groups in multivariate metal-organic frameworks. *Journal of the American Chemical Society, 137*(9), 3177-3180.

Zaworotko, M. J. (2007). Molecules to crystals, crystals to molecules ... and back again? *Crystal Growth & Design, 7*(1), 4-9.

Zhang, H. B., Nai, J. W., Yu, L., & Lou, X. W. (2017). Metal-organic-framework-based materials as platforms for renewable energy and environmental applications. *Joule, 1*(1), 77-107.

Zhang, J., Ren, M., Li, X., Hao, Q., Chen, H., & Ma, X. (2020). Ni-based catalysts prepared for CO2 reforming and decomposition of methane. *Energy Conversion and Management, 205*, Article#112419.

Zhang, J. J., Zhao, Y., Gamboa, S. A., Munoz, M., & Lachgar, A. (2008). Solvent-mediated ion exchange and structural transformations of cluster-based coordination polymers. *European Journal of Inorganic Chemistry*(19), 2982-2990.

Zhang, Q., Geng, A., Zhang, H., Hu, F., Lu, Z.-H., Sun, D., Wei, X., & Ma, C. (2014). An independent 1D Single-walled metal–organic nanotube transformed from a 2D layer exhibits highly selective and reversible sensing of nitroaromatic compounds. *Chemistry – a European Journal, 20*(17), 4885-4890.

Zhang, S., Wei, Q., Xie, G., Yang, Q., & Chen, S. P. (2012). In situ hydrothermal syntheses, structures and photoluminescent properties of three coordination polymers based on 3-amidecarbonylpyrazine-2-carboxylic acid. *Inorganica Chimica Acta, 387*, 52-57.

Zhang, W., Chen, Z., Al-Naji, M., Guo, P., Cwik, S., Halbherr, O., Wang, Y., Muhler, M., Wilde, N., Glaser, R., & Fischer, R. A. (2016). Simultaneous introduction of various palladium active sites into MOF via one-pot synthesis: Pd@[Cu3-xPdx(BTC)2]n. *Dalton Transactions, 45*(38), 14883-14887.

Zhang, X.-P., Wang, D.-G., Su, Y., Tian, H.-R., Lin, J.-J., Feng, Y.-L., & Cheng, J.-W. (2013). Luminescent 2D bismuth–cadmium–organic frameworks with tunable and white light emission by doping different lanthanide ions. *Dalton Transactions, 42*(29), 10384-10387.

Zhang, X. F., Yan, T., Wang, T., Feng, J., Wang, Q., Wang, X., Du, L., & Zhao, Q. H. (2018). Single-crystal-to-single-crystal (SCSC) transformation and dissolution-recrystallization structural transformation (DRST) among three new copper(II) coordination polymers. *Crystengcomm, 20*(5), 570-577.

Zhang, X. H., Hao, Z. M., & Zhang, X. M. (2011). Spin canting and metamagnetism in the first hybrid cobalt–hypoxanthine open framework with umr topology. *Chemistry–A European Journal, 17*(20), 5588-5594.

Zhang, Y., Yuan, S., Day, G., Wang, X., Yang, X., & Zhou, H.-C. (2018). Luminescent sensors based on metal-organic frameworks. *Coordination Chemistry Reviews, 354*, 28-45.

Zhang, Y. B., Furukawa, H., Ko, N., Nie, W. X., Park, H. J., Okajima, S., Cordova, K. E., Deng, H. X., Kim, J., & Yaghi, O. M. (2015). Introduction of functionality, selection of topology, and enhancement of gas adsorption in multivariate metal organic framework-177. *Journal of the American Chemical Society, 137*(7), 2641-2650.

Zhang, Z., Wojtas, L., Eddaoudi, M., & Zaworotko, M. J. (2013). Stepwise transformation of the molecular building blocks in a porphyrin-encapsulating metal–organic material. *Journal of the American Chemical Society, 135*(16), 5982-5985.

Zhang, Z., Xiao, Y., Cui, M., Tang, J., Fei, Z., Liu, Q., Chen, X., & Qiao, X. (2019). Modulating the basicity of Zn-MOF-74 via cation exchange with calcium ions. *Dalton Transactions, 48*(40), 14971-14974.

Zhang, Z., Zhang, L., Wojtas, L., Nugent, P., Eddaoudi, M., & Zaworotko, M. J. (2011). Templated synthesis, postsynthetic metal exchange, and properties of a porphyrin-encapsulating metal–organic material. *Journal of the American Chemical Society, 134*(2), 924-927.

Zhao, J. a., Mi, L., Hu, J., Hou, H., & Fan, Y. (2008). Cation exchange induced tunable properties of a nanoporous octanuclear Cu (II) wheel with double-helical structure. *Journal of the American Chemical Society, 130*(46), 15222-15223.

Zhao, X., Bu, X., Wu, T., Zheng, S.-T., Wang, L., & Feng, P. (2013). Selective anion exchange with nanogated isoreticular positive metal-organic frameworks. *Nature Communications, 4*, Article#2344.

Zhao, X.-Q., Zhao, B., Shi, W., & Cheng, P. (2009). Structures and luminescent properties of a series of Ln–Ag heterometallic coordination polymers. *Crystengcomm, 11*(7), 1261-1269.

Zhao, Y. H., Xu, H. B., Fu, Y. M., Shao, K. Z., Yang, S. Y., Su, Z. M., Hao, X. R., Zhu, D. X., & Wang, E. B. (2008). A series of lead(ii)-organic frameworks based on pyridyl carboxylate acid N-oxide derivatives: Syntheses, structures, and luminescent properties. *Crystal Growth & Design, 8*(10), 3566-3576.

Zhou, H. C., & Kitagawa, S. (2014). Metal-organic frameworks (MOFs). *Chemical Society Reviews, 43*(16), 5415-5418.

Zhou, Y., Yan, B., & Lei, F. (2014). Postsynthetic lanthanide functionalization of nanosized metal–organic frameworks for highly sensitive ratiometric luminescent thermometry. *Chemical Communications, 50*(96), 15235-15238.

Zou, L., Feng, D., Liu, T.-F., Chen, Y.-P., Yuan, S., Wang, K., Wang, X., Fordham, S., & Zhou, H.-C. (2016). A versatile synthetic route for the preparation of titanium metal–organic frameworks. *Chemical Science, 7*(2), 1063-1069.

LIST OF PUBLICATIONS AND PAPERS PRESENTED

List of publications

1. **Hamisu**, **A. M.,** Wardana, F.Y., Ariffin, A., Baig, I., Malliakas, C.D., Wibowo, A.C. (2019). A new synthetic approach for substitutional solid solutions in a 3D Pb-based coordination polymer: Cation vacancy and tunable photoluminescence. *Journal of Solid State Chemistry*, 279 Article#120948.

2. **Hamisu**, **A. M.,** Ariffin, A., Wibowo, A.C. (2020). Cation exchange in metal-organic frameworks (MOFs): The Hard-Soft Acid-Base (HSAB) principle appraisal. *Inorginica Chimica Acta,*511 Article#119801.

List of papers presented

1. **Hamisu**, **A. M.,** Ariffin, A., Wibowo, A.C. (2017). *Mixed valent and multiple doping in a dynamic metal-organic coordination polymer:* Oral presentation at the 4th International Conference on Science, Computing, Chemistry and Management (ICSCCM-2017). 7-8 December, 2017, Langkawi, Malaysia.

2. **Hamisu**, **A. M.,** Ariffin, A., Wibowo, A.C. (2018). *Substitutional defects in dynamic Pb-based Coordination Polymer: Hetero-valence, cation vacancy, and dual colour luminescence.* Conference Paper Presented at 2nd South East Asia conference on Crystal Engineering, (SEACCE-2 2018). 6 – 8 August, 2018, Sunway University, Kuala Lumpur, Malaysia.

3. **Hamisu**, **A. M.,** Ariffin, A., Wibowo, A.C. (2020). *A new synthetic approach for substitutional solid solutions in a 3D coordination polymer: cation vacancy, and tunable photoluminescence*. International Conference on Advances in Material Science and Chemistry (ICAMSC-2020). 10th -12th August 2020, Kerala, India.

4. **Hamisu**, **A. M.,** Ariffin, A., Wibowo, A.C. (2020). *Cation exchange in metal-organic frameworks (MOFs): The Hard-Soft Acid-Base (HSAB) principle appraisal*. International Conference on Advances in Material Science and Chemistry (ICAMSC-2020). 10th -12th August 2020, Kerala, India.